SMART POLYMERIC PRODRUGS FOR TARGETED DRUG DELIVERY AND FUNCTIONALIZABLE HYDROGELS FOR BIOSENSING APPLICATIONS

by

Sadık Kağa

M.S., Chemistry, Afyon Kocatepe University

B.S., Chemistry, Atatürk University

Submitted to the Institute for Graduate Studies in
Science and Engineering in partial fulfillment of
the requirements for the degree of
Doctor of Philosophy

Graduate Program in Chemistry

Boğaziçi University

2016

Dedicated to my beloved family

ACKNOWLEDGEMENTS

I would like to express my deepest appreciation to my PhD advisors, Assoc. Prof. Rana SANYAL and Prof. Amitav SANYAL. Without their guidance and persistent help this dissertation would have not been possible. Their comments and discussions are valuable on both an academic and a personal level, for which I am extremely grateful.

It is great pleasure to acknowledge my special thanks to Dr. Lisa Kaminskas for sharing her inestimable experiences in pharmacokinetic and drug delivery studies and to Dr. Michael Whittaker and Prof. Thomas P. Davis for allowing me to benefit from all the facilities in Monash University during my research visit in Australia. I also want to thank Prof. Rene Roy for supply of reactive carbohydrates.

I would like to extend my thanks to PhD thesis committee members, Prof. İlknur Doğan, Assoc. Prof. Mert Erkan, Prof. Sedat Hakan Orer and Prof. Ümit Tunca for their careful and constructive review of the final manuscript and for their care and help during my PhD program.

I want to thank to Burcu Sümer Bolu, Özgül Gök, Elif Kağa, Ahmet Genç, Merve Karaçivi, Yavuz Öz and Tuğçe Nihal Gevrek for their contribution to my projects and their patience.

I would like to express my thanks to present and former labmates, Mehmet Arslan, Nergiz Cengiz, Sebla Onbulak, Serap Yapar, Sezin Yiğit, Saltuk Buğra Hanay, Eun Ju Park, Emine Ece Manavoğlu Geçici, Kader Merve Türksoy, Rabia Kolat Arslan, Nazlı Böke, Melike Eceoğlu, Ülkü Güler, Duygu Aydın, Elif İyilik, Gamze Tanrıver, Sedef Günday, Özlem Kalaoğlu Altan, Filiz Emlik Çalık, İsmail Altınbaşak, H. Utku Aksoy, Yavuz Öz, Janset Yener, Evrim Arslan, Sesil Genç, Yasemin Üzüm, Buğra Aktan, Hasan Can Helvacı, Hazal İpek, Laura Chambre, Azize Kıraç, Büşra Karagöz and Gizem Baş for their companion, help and friendship.

I would like to thank all the members of the faculty in the Chemistry Department.

I want to thank to Scientific and Technological Research Council of Turkey (TUBITAK), 2211-D and 2214-A programs for financial support.

I want to express my deepest gratitude to administrators of Afyon Kocatepe University for giving me the permission to complete my PhD in Boğaziçi University.

Finally and the most importantly I would like to express my deepest thanks to my dear wife Elif for her endless patience, support and encouragement throughout years passed together.

Tuna, my son, meaning of my life, I want to notice my excuses for the days when I left you alone in the games during these years.

This research has been supported by The Scientific and Technological Research Council of Turkey (TUBİTAK) (Project No. 108T898), Ministry of Development of Turkey (Grants, 2009K120520 and 2012K120480), Ministry of Science Industry and Technology of Turkey (Grant, STZ.2010-1.00589) and Boğaziçi University Research Fund (BAP Project No. 5521).

ABSTRACT

SMART POLYMERIC PRODRUGS FOR TARGETED DRUG DELIVERY AND FUNCTIONALIZABLE HYDROGELS FOR BIOSENSING APPLICATIONS

Biosensing applications have an enormous place for diagnosis of numerous diseases. New platforms and materials have been developed to detect markers for several diseases. However, well defined materials are required for specific and sensitive detection of biological compounds. Dendrons and dendrimers with multifunctional properties possess several advantages for designing such materials. The first part of this dissertation focuses on designing well-defined hydrogel systems by introducing functionalizable dendrons into the network as 3-D platforms for biosensing applications. Two different approaches were described for the formation of functionalizable hydrogels and control over the degree of hydrogel functionalization was successfully demonstrated. The discovery of enhanced permeability and retention (EPR) effect, anti-angiogenic therapy and new targeting strategies have prompted researchers for designing prodrugs for cancer therapy. Although investigations have focused on various drawbacks and obtained promising developments in macromolecular prodrug design, better pharmacokinetic and biodistribution parameters and more effective strategies are required to achieve better therapeutic results. Stealth and inactivity of anti-cancer drugs in blood and healthy tissues is desired to decrease systemic side effects. Effective transport and release of the active agent at the target tissue is an attractive approach to improve therapeutic effect. The second part of this dissertation includes design and *in vitro* and *in vivo* evaluations of smart polymeric prodrugs for drug delivery applications. Polymer drug conjugates and polymeric micellar type prodrugs were designed to increase solubility and improve pharmacokinetic and therapeutic properties of the anti-mitotic and anti-angiogenic drugs. Targeting and controlled drug release properties were introduced by covalent attachment of a targeting ligand and using enzymatically cleavable or pH sensitive linkers. Stealth of the active agents was enhanced by branching strategy obtained by oligo ethylene glycol side chains on the polymer backbone and/or by encapsulation into the hydrophobic core of the micelles.

ÖZET

HEDEFLİ İLAÇ TAŞIMA VE BİYOALGILAMA UYGULAMALARI İÇİN AKILLI POLİMERİK ÖN İLAÇLAR VE FONKSİYONELLEŞTİRİLEBİLİR HİDROJELLER

Biyoalgılama uygulamaları birçok hastalığın teşhisinde oldukça fazla yer almaktadır. Çeşitli hastalıkların belirteçlerini tespit etmek için yeni platform ve malzemeler geliştirilmiştir. Ancak, spesifik ve hassas algılama için iyi tanımlanmış malzemelere gerek duyulmaktadır. Dendron ve dendrimerler bu tarz malzemelerin tasarımında çeşitli avantajlar sunmaktadır. Tezin ilk kısmı, biyoalgılama uygulamaları için üç boyutlu platformlar olarak, fonksiyonelleştirilebilir dendronların entegrasyonu ile iyi tanımlanmış hidrojellerin tasarımına odaklanmaktadır. Fonksiyonelleştirilebilir hidrojellerin hazırlanmasında iki farklı yaklaşım açıklanmış ve hidrojel fonksiyonelleştirilme derecesinin kontrolu başarılı bir şekilde gösterilmiştir. Gelişmiş geçirgenlik ve alıkonma etkisi (EPR), anti-anjiogenik tedavi ve yeni hedefleme stratejilerinin keşfedilmesi, araştımacıları kanser tedavisi için ön ilaçların tasarımına yönlendirmiştir. Her ne kadar, araştırmalar ön ilaç tasarımdaki problemler üzerine yoğunlaşmış ve umut verici ilerlemeler elde edilmiş olsa da, daha etkin tedavi edici sonuçlara ulaşmak için, daha iyi farmakokinetik ve biyodağılım parametrelerine ve daha etkili stratejilere ihtiyaç duyulmaktadır. Sistemik yan etkileri azaltmak için, kanser ilaçlarının kanda ve sağlıklı dokularda gizliliği ve etkisizliği istenmektedir. Hedeflenen dokuya aktif ajanın etkili bir şekilde taşınması ve salımı tedavi etkisini arttıracak bir yaklaşımdır. Tezin ikinci kısmı, akıllı polimerik ön ilaçların tasarımı ve *in vitro* ve *in vivo* değerlendirmelerini kapsamaktadır. Anti-mitotik ve anti-anjiogenetik ilaçların çözünürlüğünü arttırmak, farmakokinetik ve tedavi edici özelliklerini geliştirmek için, polimerik ilaç konjugatları ve polimerik misel tipi ön ilaçlar tasarlanmıştır. Hedefleme ve kontrollu salım özellikleri, hedefleyici bir ligandın kovalent bağlanmasıyla ve enzimatik olarak kırılabilir veya pH ya duyarlı bağlayıcılar kullanılarak sağlanmıştır. Akfif ajanların gizliliği, polimer omurgasındaki oligo etilen glikol yan dalları ve/veya misellerin hidrofobik merkezine kapsülleme ile arttırılmıştır.

TABLE OF CONTENTS

ACKNOWLEDGEMENTS iv
ABSTRACT vi
ÖZET vii
LIST OF TABLES xv
LIST OF FIGURES xvi
LIST OF ACRONYMS/ABBREVIATIONS xxv
1. INTRODUCTION 1
1.1. Formation of Hydrogels Using Dendritic Building Blocks 1
1.1.1. Chemically Cross-linked Hydrogels Using Dendritic Building Block ...3
1.1.2. Physically Cross-linked Hydrogels Using Dendritic Building Blocks..21
1.2. Water Soluble Constructs for Delivery of Anti-cancer Drugs 29
1.2.1. Cancer 29
1.2.2. Polymer Therapeutics in Cancer Treatment 36
1.2.3. Polymer Drug Conjugates 39
1.2.4. Polymeric Micellar Type Nanoparticles 47
2. RESEARCH OVERVIEW 56
3. FABRICATION AND FUNCTIONALIZATION OF ABA TYPE DENDRON-POLYMER CONJUGATE BASED HYDROGELS VIA SEQUENTIAL THIOL-ENE 'CLICK' REACTIONS 58
3.1. Introduction 58
3.2. Experimental 59
3.2.1. Materials 59
3.2.2. Synthesis of Dendron [G2]4OR (4) 60
3.2.3. Synthesis of Dendron [G3]8OR (5) 60
3.2.4. Synthesis of Compound G2PEG6K (8) 61
3.2.5. Synthesis of Compound G3PEG6K (9) 61
3.2.6. Synthesis of Compound G3PEG20K 61
3.2.7. Synthesis of Bulk Hydrogels via Thiol-ene Chemistry 62
3.2.8. Synthesis of Hydrogel Micropatterns via Thiol-ene Chemistry 62

3.2.9. Scanning Electron Microscopy (SEM) Images of Hydrogel Samples . 62
3.2.10. Water Uptake Analysis 63
3.2.11. Functionalization of Micropatterns with BODIPY Thiol 63
3.3. Results and Discussion 63
3.3.1. Synthesis and Characterization of ABA Type Dendron Polymer Conjugates..... 63
3.3.2. Hydrogel Formation..... 65
3.3.3. Physical Properties of Hydrogels 67
3.3.4. Hydrogel Functionalization..... 68
3.4. Conclusion 70
4. FORMATION OF WELL-DEFINED CARBOHYDRATE FUNCTIONALIZED HYDROGELS AS MULTIVALENT 3D MATERIALS FOR BIOIMMOBILIZATION OF LECTINS..... 71
4.1. Introduction..... 71
4.2. Experimental..... 72
4.2.1. Materials..... 72
4.2.2. Synthesis of G2[4 alkyne]-G0[1 OH] Dendron 73
4.2.3. Synthesis of G2[4 alkyne]-G0[1 alkene] Dendron..... 73
4.2.4. Synthesis of G2[4 alkyne]-G1[2 alkene] Dendron..... 74
4.2.5. Synthesis of G2[4 alkyne]-G2[4 alkene] Dendron..... 75
4.2.6. Hydrogel Formation..... 76
4.2.7. Water Uptake Studies 77
4.2.8. Morphology of the Hydrogels 77
4.2.9. Hydrogel Functionalization with BODIPY-thiol 77
4.2.10. Hydrogel Functionalization with Thiol Bearing D-mannose..... 78
4.2.11. Immobilization of Con A into Hydrogel Network 78
4.3. Results and Discussion 78
4.3.1. Synthesis of G2[4 alkyne]-G0[1 OH] Dendron 78
4.3.2. Synthesis of G2[4 alkyne]-G0[1 alkene], G2[4 alkyne]-G1[2 alkene] and G2[4 alkyne]-G2[4 alkene] Dendrons..... 79
4.3.3. Hydrogel Formation..... 82
4.3.4. Swelling Studies 85
4.3.5. Morphology of Hydrogel Samples 85

4.3.6. Hydrogel Functionalization with Thiol Functionalized D-Mannose.... 86
4.3.7. Hydrogel Functionalization with BODIPY-thiol 87
4.3.8. Immobilization of Con A-Texas Red Conjugate into Hydrogel Network..... 90
4.4. Conclusion 93
5. PHARMACOKINETIC EVALUATION OF LINEAR AND BRANCHED POLYMER DOCETAXEL CONJUGATES..... 95
5.1. Introduction..... 95
5.2. Experimental..... 97
5.2.1. Materials..... 97
5.2.2. Synthesis of POEGMEMA-DTX and PHPMA-DTX Conjugates..... 97
5.2.3. Enzymatic Release Study..... 98
5.2.4. Cell Lines 98
5.2.5. In Vitro Cell Viability Assay..... 98
5.2.6. Animals 99
5.2.7. Pharmacokinetic Procedure..... 99
5.2.8. Quantification of DTX in Plasma Samples..... 100
5.2.9. Procedure for Biodistribution Study..... 100
5.2.10. Quantification of DTX in Organ and Tissue Samples..... 100
5.2.11. Maximum Tolerated Dose (MTD) Study..... 101
5.2.12. Statistics 101
5.3. Results and Discussion 101
5.3.1. Synthesis of MA-GFLG-DTX..... 101
5.3.2. Synthesis of POEGMEMA-DTX Conjugates..... 102
5.3.3. Synthesis of HPMA-DTX Conjugates..... 104
5.3.4. Enzymatic Release Profiles of POEGMEMA-DTX and PHPMA-DTX conjugates..... 107
5.3.5. Cytotoxicity of POEGMEMA-DTX, PHPMA-DTX Conjugates..... 108
5.3.6. Blood Toxicity of POEGMEMA-DTX, PHPMA-DTX Conjugates and Free DTX..... 109
5.3.7. Body Weight Change..... 110
5.3.8. Plasma Free DTX Concentration Values of POEGMEMA-DTX, PHPMA-DTX Conjugates and DTX..... 110

5.3.9. Plasma Total DTX Concentration Values of POEGMEMA-DTX, PHPMA-DTX Conjugates and DTX 112
5.3.10. Free and Total DTX Biodistribution of POEGMEMA-DTX, PHPMA-DTX Conjugates and DTX 114
5.3.11. Maximum Tolerated Dose (MTD) Study for POEGMEMA-DTX (50 kDa)..... 116
5.4. Conclusion 119
6. ANTI-TUMOR EFFECT OF POEGMEMA BASED POLYMER DRUG CONJUGATES 120
6.1. Introduction 120
6.2. Experimental 120
6.2.1. Materials 120
6.2.2. Synthesis of POEGMEMA-DTX-NHS Conjugate 121
6.2.3. cRGDfK Conjugation for Targeted Polymer Drug Conjugate 121
6.2.4. Inactivation of NHS Groups for Non-targeted Polymer Drug Conjugate.. 122
6.2.5. Plasma Release Study 122
6.2.6. Enzymatic Release Study 122
6.2.7. Cell Lines 123
6.2.8. In Vitro Cell Viability Assay 123
6.2.9. Animals 123
6.2.10. Tolerability Study for Polymer Drug Conjugates at 40 mg/kg DTX Equivalent Dose 124
6.2.11. Tumor Study 124
6.2.12. Statistics 125
6.3. Results and Discussion 125
6.3.1. Synthesis of POEGMEMA-DTX-NHS Conjugate 125
6.3.2. Synthesis of POEGMEMA-DTX-cRGDfK Polymer Drug Conjugate. 126
6.3.3. Synthesis of POEGMEMA-DTX Polymer Drug Conjugate 128
6.3.4. Enzymatic and Plasma Release profiles of Polymer Drug Conjugates. 128
6.3.5. Cytotoxicity of Polymer Drug Conjugates 129

6.3.6. Tolerability of POEGMEMA-DTX and POEGMEMA-DTX-cRGDfK Conjugates at 40 mg/kg DTX Equivalent Dose 130
6.3.7. Anti-tumor Efficacy of Polymer Drug Conjugates in Human Lung Carcinoma Model 132
6.4. Conclusion 133
7. BIODISTRIBUTION OF POLYMERIC NANOPARTICLES WITH DIFFERENT SIZE AND MORPHOLOGY GENERATED BY POLYMERIZATION INDUCED SELF ASSEMBLY (PISA) 135
7.1. Introduction 135
7.2. Experimental 136
7.2.1. Materials 136
7.2.2. Cell Culture Conditions 137
7.2.3. Animals 137
7.2.4. Synthesis of PGMA 137
7.2.5. Synthesis of PGMA-*b*-POEGMEMA 137
7.2.6. Nanoparticle Formation by Polymerization Induced Self-Assembly (PISA) 138
7.2.7. Radiolabelling of Nanoparticles via Tiritiated 2-amino ethane-1-ol and Inactivation Remaining Epoxide Groups for Biodistribution Study 138
7.2.8. Inactivation of Epoxide Groups for Cytotoxicity Assays 139
7.2.9. Cytotoxicity of Nanoparticles on HT1080 cells 139
7.2.10. Biodistribution of Nanoparticles in HT080 Xenografts Tumor Model 139
7.2.11. Statistics 140
7.3. Results and Discussion 140
7.3.1. Nanoparticle Formation with Different Sizes and Morphologies by PISA 140
7.3.2. Cytotoxicity of Nanoparticles 145
7.3.3. Biodistribution of Nanoparticles 145
7.4. Conclusions 148

8. FORMATION OF TARGETED POLYMERIC NANOPARTICLES USING DIBLOCK COPOLYMERS COMPOSED OF POEGMEMA AND POLYMERIC DRUG SEGMENT…. 150
8.1. Introduction 150
8.2. Experimental 151
8.2.1. Materials 151
8.2.2. Synthesis of Polymerizable Combretastatin-A4 Monomer (CombMA) 152
8.2.3. Synthesis of SCPDB 152
8.2.4. Synthesis of POEGMEMA and NHS-POEGMEMA Homopolymers 153
8.2.5. Synthesis of POEGMEMA-co-CombMA and NHS-POEGMEMA-co-CombMA Block Copolymers 153
8.2.6. Synthesis of cRGDfK-POEGMEMA-*b*-PCombMA Block Copolymer 154
8.2.7. Formation of Targeted and Non-targeted Polymeric Nanoparticles 154
8.2.8. Critical Micelle Concentration (CMC) Measurements 154
8.2.9. Nile Red Internalization in HUVECs. 155
8.2.10. Endothelial Cell Tube Formation Assay on HUVECs 155
8.2.11. Animals 155
8.2.12. Fluorescence Based Biodistribution of Targeted and Non-targeted Nanoparticles 156
8.3. Results and Discussion 156
8.3.1. Synthesis of POEGMEMA and NHS-POEGMEMA Homopolymers 157
8.3.2. Synthesis of POEGMEMA-*b*-PCombMA and NHS-POEGMEMA-*b*-PCombMA Block Copolymers 158
8.3.3. Synthesis of cRGDfK-POEGMEMA-*b*-PCombMA Block Copolymer 160
8.3.4. Formation of Targeted and Non-targeted Polymeric Nanoparticles 162
8.3.5. Critical Micelle Concentration (CMC) Values for Block Copolymers 164

8.3.6. Stability of Nanoparticles upon Addition of Organic Solvent and Serial Dilution with Water 167
8.3.7. Morphology of the Polymeric Nanoparticles 169
8.3.8. Nile Red Internalization in HUVECs. 170
8.3.9. Endothelial Cell Tube Formation Assay on HUVECs 170
8.3.10. Fluorescence Based Biodistribution of Targeted and Non-targeted Nanoparticles 171
8.4. Conclusion 175
9. CONCLUSIONS 177
REFERENCES 181
APPENDIX A: SPECTROSCOPY DATA 207
APPENDIX B: PERMISSIONS FOR FIGURES 222

LIST OF TABLES

Table 1.1. Chemotherapy agents that target DNA replication..... 32
Table 1.2. Chemotherapy agents that target microtubules 33
Table 1.3. Anti-angiogenic drugs in cancer treatment.. 35
Table 1.4. Anti-angiogenic drugs in cancer treatment.. 39
Table 1.5. Polymer drug conjugates available in the market..... 40
Table 1.6. Polymer drug conjugates in clinical trials..... 41
Table 1.7. Clinically approved nanoparticles in cancer therapy..... 47
Table 1.8. Polymeric nanoparticles in clinical trials for cancer therapy 48
Table 3.1. Properties of hydrogels and average available functional groups on one DPD unit..... 66
Table 4.1. Nomenclature and precursor ratios of the hydrogel samples 77
Table 5.1. Polymerization conditions for POEGMEMA-DTX and PHPMA-DTX Conjugates.....106
Table 5.2. Pharmacokinetic parameters of free DTX for polymer drug conjugates and DTX.....111
Table 5.3. Pharmacokinetic parameters of total DTX for polymer drug conjugates and DTX.....113
Table 7.1. Characterization of PGMA-*b*-POEGMEMA-*b*-PST copolymers 143
Table 7.2. Characterization of PGMA-*b*-POEGMA-*b*-PST copolymer nanoparticles. 144
Table 8.1. Repeating unit numbers and molecular weight values of synthesized polymers..... 162
Table 8.2. Properties of targeted and non-targeted nanoparticles..... 167

LIST OF FIGURES

Figure 1.1. Non-covalent encapsulation and physical absorption for hydrogel functionalization 1
Figure 1.2. Employing reactive monomers or polymers to obtain modified hydrogels 2
Figure 1.3. Divergent and convergent synthesis of dendrons 2
Figure 1.4. Schematic illustration of ABA type dendron-polymer conjugate synthesis and hydrogel formation. 4
Figure 1.5. Dendritic scaffolds having three alkene and six azide groups (left) and six alkene and three azide groups (right). 5
Figure 1.6. Physical and functional properties of dendron polymer conjugates 6
Figure 1.7. Synthesis of the dendron polymer conjugates and hydrogel formation 7
Figure 1.8. Photo-crosslinkable methacrylated dendron PEG ester conjugate 8
Figure 1.9. Photo-crosslinkable ABA type dendron-polymer conjugate and the hydrogel image 8
Figure 1.10. Dendron modification and fluorescent microscope images of hydrogels 10
Figure 1.11. Synthesis of photoreactive PAMAM-PEG conjugate and photo-initiated cross-linking for hydrogel formation. 11
Figure 1.12. Formation of hydrogel-dendrimer-nanoparticle system (HDNP) 12
Figure 1.13. Schematic illustration for hydrogel formation. 13
Figure 1.14. Chemical structure of lysine-based dendrons obtained hydrogels. 14
Figure 1.15. Hydrogel formation and pseudoproline ligation. 14
Figure 1.16. Native chemical ligation and hydrogel dissolution via thiol-thioester exchange. 16
Figure 1.17. Stability and degradation of hydrogels. 166
Figure 1.18. Hydrogel formation by amide bond for sealing corneal incisions. 17
Figure 1.19. Formation, physical properties of the hydrogels. 188
Figure 1.20. Hydrogel formation and physical properties of the hydrogel. 20
Figure 1.21. Bolaamphiphile structures 22
Figure 1.22. Structure of bolaamphiphile with a tetrathiafulvalene spacer. 22
Figure 1.23. Ammonium functionalized phosphorus based dendrimers as hydrogelators 23
Figure 1.24. Chemical structure of hydrogelator and gelation properties. 24

Figure 1.25. Gel-to-sol mechanism of amphiphilic dendron and azobenzene components. 25
Figure 1.26. Janus type dendrimers and self-assembly. 26
Figure 1.27. Dendron-polymer conjugates and hydrogel formation. 27
Figure 1.28. Structure of hydrogel precursors and physical cross-linking. 28
Figure 1.29. World estimated age-standardized cancer incidence and mortality rates (ASR) per 100 000, by major cancer types, in men and women. 30
Figure 1.30. Normal and cancer cell divisions. 31
Figure 1.31. Morphological changes in microtubules during cell cycle. 33
Figure 1.32. Effect of microtubule-stabilizing and microtubule-destabilizing factors and agents on spindle microtubules. 34
Figure 1.33. The action principle of anti-angiogenic factors. 35
Figure 1.34. Commonly used water soluble polymers in polymer therapeutics. 36
Figure 1.35. EPR effect for polymer therapeutics. 37
Figure 1.36. Commonly used extracellular and intracellular stimuli-labile linkers in polymer therapeutics. 38
Figure 1.37. Molecular weight dependent plasma concentration profiles of PEG polymers with molecular weights ranging from 6 - 170 kDA. 42
Figure 1.38. Structure of the PEG doxorubicin conjugate with a peptide linker 42
Figure 1.39. Four-armed PEG-SN38 polymer drug conjugate. 43
Figure 1.40. Synthesis of HPMA-Docetaxel polymer drug conjugate with GFLG linker cRGDfK targeting moiety. 433
Figure 1.41. Molecular weight and targeting effect on anti-tumor efficacy of HPMA-Docetaxel conjugates at different dose administration. 44
Figure 1.42. Structure of HPMA-Docetaxel conjugates with a pH sensitive linker 45
Figure 1.43. Drug release profile (panel A) and anti-tumor efficacy (panel B) of HPMA-Docetaxel conjugates at different dose administration (20 mg/kg and 40 mg/kg). 45
Figure 1.44. Structure of PGA-Paclitaxel Conjugate. 46
Figure 1.45. Plasma concentration of taxanes and free paclitaxel after administration of PGA-Paclitaxel and free paclitaxel in four representative patients. 46
Figure 1.46. General scheme for formation of block copolymer micelles through self-assembly in aqueous solutions. 49

Figure 1.47. Formation of ligand introduced micellar type diblock polymer micelles..... 50
Figure 1.48. Anti-tumor effect of targeted polymeric particle..... 51
Figure 1.49. Combretastatin–A4 attached flower type triblock micelles and their cell internalization. 52
Figure 1.50. Formation of polymeric micelles with combined drug approach and release diagram. 53
Figure 1.51. Schematic illustration of polymeric nanoparticle formation with different morphologies using PISA approach. 54
Figure 1.52. Obtained nanoparticles with different morphologies via PISA approach.. 55
Figure 3.1. Schematic illustration of formation and functionalization of hydrogels using sequential thiol-ene click reactions. 59
Figure 3.2. Synthesis of alkene functionalized ABA type dendron polymer conjugates . 64
Figure 3.3. Synthesis of hydrogels with different functional group densities. 65
Figure 3.4. Water uptake results of hydrogels.. 67
Figure 3.5. Scanning Electron Microscopy (SEM) images of dry hydrogels. 68
Figure 3.6. Hydrogel functionalization using radical thiol-ene conjugation. 69
Figure 3.7. Hydrogel micropatterns and functionalization.. 69
Figure 4.1. Synthesis of G2[4 alkyne]-G0[1 OH] dendron. 79
Figure 4.2. ^{1}H NMR spectra of G2[4 alkyne]-G0[1 OH] dendron..... 79
Figure 4.3. G2[4 alkyne]-G0[1 alkene], G2[4 alkyne]-G1[2 alkene] and G2[4 alkyne]-G2[4 alkene] dendrons. 80
Figure 4.4. ^{1}H NMR spectra of G2[4 alkyne]-G0[1 alkene] dendron. 81
Figure 4.5. ^{1}H NMR spectra of G2[4 alkyne]-G1[2 alkene] dendron. 81
Figure 4.6. ^{1}H NMR spectra of G2[4 alkyne]-G2[4 alkene] dendron. 82
Figure 4.7. Cross-linking of hydrogel precursor via Huisgen type of [3+2] cycloaddition 82
Figure 4.8. General scheme for formation of hydrogels..... 83
Figure 4.9. The chemical structures of hydrogel precursors..... 84
Figure 4.10. FTIR spectra of hydrogel precursors (PEG diazides and dendrons) and hydrogels. 84
Figure 4.11. Water uptake values of the hydrogel samples. 85
Figure 4.12. SEM images of the hydrogel samples. 86
Figure 4.13. D-mannose functionalization of the hydrogels..... 86

Figure 4.14. Fluorescence microscope images of hydrogel samples. 88
Figure 4.15. Fluorescence intensity values of hydrogel samples prepared by PEG 2kDa diazide. 89
Figure 4.16. Fluorescence intensity values of hydrogel samples prepared by PEG 6kDa diazide. 89
Figure 4.17. Schematic illustration of expected fluorescence intensities following BODIPY-thiol conjugation and Con A immobilization. 90
Figure 4.18. Fluorescence microscope images of hydrogel samples 91
Figure 4.19. Fluorescence intensity values of hydrogel samples prepared by PEG 2kDa diazide. 91
Figure 4.20. Fluorescence intensity values of hydrogel samples prepared by PEG 2kDa diazide. 92
Figure 4.21. Normalized intensity values of the hydrogels prepared by PEG 2kDa diazide (left) and PEG 6kDa diazide (right) following immobilization of Con A. 93
Figure 5.1. ^{1}H NMR spectrum and characterization of MA-GFLG-DTX..... 102
Figure 5.2. Synthesis of POEGMEMA-DTX polymer drug conjugates. 102
Figure 5.3. ^{1}H NMR spectrum of POEGMEMA-DTX (50 kDa). 103
Figure 5.4. ^{1}H NMR spectrum of POEGMEMA-DTX (85 kDa). 104
Figure 5.5. Synthesis of PHPMA-DTX polymer drug conjugates..... 104
Figure 5.6. ^{1}H NMR spectrum of PHPMA-DTX (52 kDa). 105
Figure 5.7. ^{1}H NMR spectrum of PHPMA-DTX (85 kDa). 106
Figure 5.8. Schematic illustration of polymer drug conjugates with drug contents..... 107
Figure 5.9. Enzymatic release profiles of conjugates with low molecular weights. 107
Figure 5.10. Enzymatic release profiles of conjugates with high molecular weights. 108
Figure 5.11. Cytotoxicity of polymer drug conjugates and free DTX for MDA-MB-231 cell line. 108
Figure 5.12. Cytotoxicity of polymer drug conjugates and free DTX for BxPC3 cell line..... 109
Figure 5.13. Percent change in hemogram values of the rats treated with polymer drug conjugates and DTX. 109
Figure 5.14. Body weight change values of polymer drug conjugates and DTX. 110
Figure 5.15. Plasma free DTX concentrations of polymer drug conjugates..... 111

Figure 5.16. Plasma total DTX concentrations of polymer drug conjugates..... 112
Figure 5.17. Free DTX biodistribution values of polymer drug conjugates and DTX. ... 114
Figure 5.18. Total DTX biodistribution values of polymer drug conjugates and DTX. .. 115
Figure 5.19. Normalized body weight change of POEGMEMA-DTX (50 kDa) injected mice with different dosages..... 116
Figure 5.20. Changes in liver/body weight and spleen/body weight ratio of the mice injected with POEGMEMA-DTX (50 kDa). 117
Figure 5.21. Normalized WBC and RBC count change values of the mice injected with POEGMEMA-DTX (50 kDa) polymer drug conjugate..... 118
Figure 6.1. ^{1}H NMR spectra of POEGMEMA-DTX-NHS conjugate. 125
Figure 6.2. ^{1}H NMR spectra of POEGMEMA-DTX-cRGDfK conjugate. 126
Figure 6.3. BCA protein assay for polymer drug conjugates..... 127
Figure 6.4. ^{1}H NMR spectra of POEGMEMA-DTX-cRGDfK conjugate after NHS deactivation. 127
Figure 6.5. ^{1}H NMR spectra of POEGMEMA-DTX conjugate after NHS deactivation. 128
Figure 6.6. Enzymatic and plasma release profiles of DTX..... 129
Figure 6.7. Cytotoxicity of polymer drug conjugates and free DTX for A-549 cell line 129
Figure 6.8. Normalized body weight change of mice injected with polymer drug conjugates at dose of 40 mg/kg DTX equivalent. 130
Figure 6.9. Liver/body weight and spleen/body weight ratios of the mice injected with polymer drug conjugates at dose of 40 mg/kg at fifth day..... 131
Figure 6.10. Normalized WBC and RBC count change values of the mice injected with polymer drug conjugate at dose of 40 mg/kg DTX equivalent. 131
Figure 6.11. Body weight changes of mice at each group during anti-tumor study. 132
Figure 6.12. Changes in tumor volume of mice at each group during anti-tumor study.. 133
Figure 7.1. Chemical structures and ^{1}H NMR spectra of PGMA and PGMA-*b*-POEGMEMA polymers..... 141
Figure 7.2. Characterization of PGMA-*b*-POEGMEMA-*b*-PST triblock copolymers. . 142
Figure 7.3. Confirmation of successful epoxide inactivation by ^{1}H NMR..... 143
Figure 7.4. TEM images of nanoparticles before and after epoxide inactivation. 144

Figure 7.5. Cytotoxicity of polymeric nanoparticles on HT1080 (human adenocarcinoma cell line) cells at different nanoparticle concentrations. ... 145
Figure 7.6. Biodistribution of nanoparticles in HT1080 tumor xenografts after sacrifice at 48 h. ... 146
Figure 8.1. Overall scheme for the synthesis of the polymers. ... 156
Figure 8.2. ^{1}H NMR spectrum of POEGMEMA. ... 157
Figure 8.3. ^{1}H NMR spectrum of NHS-POEGMEMA. ... 158
Figure 8.4. ^{1}H NMR spectrum of POEGMEMA-*b*-PCombMA. ... 159
Figure 8.5. ^{1}H NMR spectrum of NHS-POEGMEMA-*b*-PCombMA. ... 159
Figure 8.6. ^{1}NMR spectrum of cRGDfK-POEGMEMA-*b*-PCombMA. ... 160
Figure 8.7. Protein content difference due to cRGDfK conjugation. ... 161
Figure 8.8. GPC traces of obtained homopolymers, block copolymers and copolymer cRGDfK conjugate. ... 161
Figure 8.9. Non-targeted polymeric nanoparticle formation. ... 162
Figure 8.10. Targeted polymeric nanoparticle formation. ... 163
Figure 8.11. Size distribution of targeted (top) and non-targeted (bottom) nanoparticles by volume, average size and PDI values. ... 163
Figure 8.12. CMC analysis samples for non-targeted nanoparticles after THF evaporation ... 164
Figure 8.13. CMC analysis samples for targeted nanoparticles after THF evaporation. . 164
Figure 8.14. Fluorescence emission spectra of Nile Red in non-targeted nanoparticles.. 165
Figure 8.15. Fluorescence emission spectra of Nile Red in targeted nanoparticles. ... 165
Figure 8.16. Plot of the emission intensity at 612 nm versus the log of POEGMEMA-*b*-PCombMA concentration. ... 166
Figure 8.17. Plot of the emission intensity at 612 nm versus the log of total POEGMEMA-*b*-PCombMA and cRGDfK-POEGMEMA-*b*-PCombMA concentration. ... 166
Figure 8.18. Stability of non-targeted particles upon THF addition and ultra-dilution.... 167
Figure 8.19. Stability of targeted particles upon THF addition and ultra-dilution. ... 168
Figure 8.20. TEM images of polymeric nanoparticles. ... 169
Figure 8.21. Cell internalization of Nile Red doped polymeric nanoparticles and Nile Red dye only into the HUVECs. ... 170
Figure 8.22. Anti-angiogenic assay using HUVECs on Matrigel. ... 171

Figure 8.23. Count based lateral IVIS images of mice bearing tumor tissue at right flank site after systemic Cy5.5 doped targeted and non-targeted nanoparticle administration. ... 172
Figure 8.24. *Ex vivo* fluorescence images of tumor, tissue, organ and blood samples. ... 174
Figure 8.25. Relative fluorescence intensity values belonging to the *ex vivo* images. ... 174
Figure 8.26. Count based ventral IVIS images of mice bearing tumor tissue at right flank site after systemic Cy5.5 doped targeted and non-targeted nanoparticle administration. ... 175
Figure A.1. ^{1}H NMR spectra of alkene functionalized G2 dendron 4. ... 174
Figure A.2. ^{1}H NMR spectra of alkene functionalized G3 dendron 5 ... 174
Figure A.3. FTIR spectra of alkene functionalized G2 dendron 4, PEG-6K bis-azide 6, dendron-polymer conjugate G2PEG6K 8. ... 174
Figure A.4. FTIR spectra of alkene functionalized G3 dendron 5, PEG-6K bis-azide 6, dendron-polymer conjugate G3PEG6K 9 ... 208
Figure A.5. FTIR spectra of alkene functionalized G3 dendron 5 (purple), PEG-20K bis-azide 7 (red), dendron-polymer conjugate G3PEG20K 10 (green) ... 209
Figure A.6. ^{1}H NMR spectra of dendron-polymer conjugate G2PEG6K 8 ... 209
Figure A.7. ^{1}H NMR spectra of dendron-polymer conjugate G3PEG6K 9. ... 210
Figure A.8. ^{1}H NMR spectra of dendron-polymer conjugate G3PEG20K 10. ... 210
Figure A.9. ^{13}C NMR spectra G2[4 alkyne]-G0[1 OH] ... 211
Figure A.10. ^{13}C NMR spectra G2[4 alkyne]-G0[1 alkene] ... 211
Figure A.11. ^{13}C NMR spectra G2[4 alkyne]-G1[2 alkene] ... 212
Figure A.12. ^{13}C NMR spectra G2[4 alkyne]-G2[4 alkene] ... 212
Figure A.13. FTIR spectra of PHPMA-DTX (52 kDa). ... 213
Figure A.14. FTIR spectra of PHPMA-DTX (85 kDa) ... 213
Figure A.15. FTIR spectra of POEGMEMA-DTX (50 kDa) ... 214
Figure A.16. FTIR spectra of POEGMEMA-DTX (85 kDa). ... 214
Figure A.17. FTIR spectra of POEGMEMA-DTX-NHS (43 kDa) ... 215
Figure A.18. FTIR spectra of POEGMEMA-DTX-RGDfK (43 kDa) ... 215
Figure A.19. FTIR spectra of POEGMEMA-DTX (43 kDa) ... 216
Figure A.20. ^{1}H NMR spectra of CombMA ... 216
Figure A.21. ^{13}C NMR spectra of CombMA ... 217
Figure A.22. FTIR spectra of CombMA ... 217

Figure A.23. ^{1}H NMR spectra of SCPDB 218
Figure A.24. FTIR spectra of SCPDB 218
Figure A.25. FTIR spectra of POEGMEMA (7.7 kDa) 219
Figure A.26. FTIR spectra of NHS-POEGMEMA (7.1 kDa) 219
Figure A.27. FTIR spectra of POEGMEMA-*b*-PCombMA (11.2 kDa) 220
Figure A.28. FTIR spectra of NHS-POEGMEMA-*b*-PCombMA (11.7 kDa) 220
Figure A.29. FTIR spectra of cRGDfK-POEGMEMA-*b*-PCombMA (12.5 kDa) 221
Figure A.30. Cell internalization of Nile Red doped polymeric nanoparticles and Nile Red dye only into the HUVECs 221
Figure B.1. Permission for Figure 1.4 222
Figure B.2. Permission for Figure 1.5 222
Figure B.3. Permission for Figure 1.6 223
Figure B.4. Permission for Figure 1.7 224
Figure B.5. Permission for Figure 1.8 224
Figure B.6. Permission for Figure 1.9 225
Figure B.7. Permission for Figure 1.10 225
Figure B.8. Permission for Figure 1.11 226
Figure B.9. Permission for Figure 1.12 226
Figure B.10. Permission for Figure 1.13 227
Figure B.11. Permission for Figure 1.14 228
Figure B.12. Permission for Figure 1.15 228
Figure B.13. Permission for Figure 1.16 and Figure 1.17 229
Figure B.14. Permission for Figure 1.18 230
Figure B.15. Permission for Figure 1.19 230
Figure B.16. Permission for Figure 1.20 231
Figure B.17. Permission for Figure 1.21 232
Figure B.18. Permission for Figure 1.22 232
Figure B.19. Permission for Figure 1.23 233
Figure B.20. Permission for Figure 1.24 234
Figure B.21. Permission for Figure 1.25 235
Figure B.22. Permission for Figure 1.26 236
Figure B.23. Permission for Figure 1.27 237
Figure B.24. Permission for Figure 1.28 238

Figure B.25. Permission for Figure 1.31 and Figure 1.32 239
Figure B.26. Permission for Figure 1.33 240
Figure B.27. Permission for Figure 1.38 241
Figure B.28. Permission for Figure 1.39 242
Figure B.29. Permission for Figure 1.40 and Figure 1.41 243
Figure B.30. Permission for Figure 1.42 and Figure 1.43 243
Figure B.31. Permission for Figure 1.44 and Figure 1.45 244
Figure B.32. Permission for Figure 1.47 and Figure 1.48 245
Figure B.33. Permission for Figure 1.49 245
Figure B.34. Permission for Figure 1.50 246
Figure B.35. Permission for Figure 1.51 and Figure 1.52 247

LIST OF ACRONYMS/ABBREVIATIONS

A-549	Human lung carcinoma cell line
AIBN	2,2′-Azobis(2-methylpropionitrile)
AUC	Area under the curve
bis-MPA	2,2-bis(-hydroxymethyl) propionic acid
BODIPY	Boron-dipyrromethene
CA4	Combretastatine-A4
CCK-8	Cell Counting Kit-8
$CDCl_3$	Deuterated chloroform
CL	Clearance
Cy5.5	Cyanine 5.5
Cmax	Maximum concentration
CMC	Critical micelle concentration
CPADB	4-Cyanopentanoic acid dithiobenzoate
CuAAC	Copper-catalyzed azide-alkyne cycloaddition
cRGDfK	Cyclo (Arg-Gly-Asp-D-Phe-Lys)
DAPI	4',6-Diamidino-2-phenylindole
DCM	Dichloromethane
DIPEA	*N*,*N*-Diisopropylethylamine
DMAc	*N*,*N*-Dimethylacetamide
DMAP	4-Dimethylaminopyridine
DMF	Dimethyl formamide
DMPA	2,2-Dimethoxy-2-phenylacetophenone
DMSO	Dimethyl sulfoxide
DPM	Disintegration per minute
DTX	Docetaxel
d-$CDCl_3$	Deuterated chloroform
d-CD_3OD	Deuterated methanol
EC_{50}	Half maximal effective concentration
EDTA	Ethylenediaminetetraacetic acid
EMA	European medicines agency

EPR	Enhanced permeability and retention
EtOAc	Ethyl acetate
FBS	Fetal bovine serum
FDA	Food and drug administration
FTIR	Fourier transform infrared
GFLG	Gly-Phe-Leu-Gly
GMA	Glycidyl methacrylate
GPC	Gel permeation chromotography
HCT	Hematocrit
HGB	Hemoglobin
HPLC	High pressure liquid chromatogrphy
HPMA	*N*-(2-hydroxypropyl)methacrylamide
HT1080	Human adenocarcinoma cell line
HUVECs	Human umbilical vein endothelial cells
DCC	Dicyclohexylcarbodiimide
DLS	Dynamic light scattering
kDa	Kilo dalton
LCMS	Liquid chromatography mass spectroscopy
MDA-MB-231	Human breast adenocarcinoma cell line
MeOH	Methanol
MHz	Mega hertz
MTD	Maximum tolerated dose
MTT	3-(4,5-dimethylthiazol-2-yl)-2,5-diphenyltetrazolium bromide
MWCO	Molecular weight cut-off
NMR	Nuclear magnetic resonance
NHS	*N*-Hydroxysuccinimide
NHSMA	Methacrylic acid *N*-hydroxysuccinimide ester
OEGMEMA	Oligo (ethylene glycol) methyl ether methacrylate
PBS	Phosphate buffer solution
PDI	Poly dispersity index
PEG	Poly (ethylene glycol)
PGA	Poly glycolic acid
PGMA	Poly glycidyl methacrylate

PHPMA	Poly (*N*-(2-hydroxypropyl) methacrylamide)
PISA	Polymerization induced self-assembly
POEGMEMA	Poly oligo (ethylene glycol) methyl ether methacrylate
PST	Poly styrene
BxPC3	Human pancreas adenocarcinoma cell line
RAFT	Reversible-addition fragmentation chain transfer polymerization
RBC	Red blood cell
RES	Reticulo endothelial system
RID	Refractive index detector
SCPDB	4-Cyano-4-((thiobenzoyl)sulfanyl) pentanoic succinimide ester
SEC	Size-Exclusion Chromatography
SEM	Scanning Electron Microscopy
ST	Styrene
TEA	Triethylamine
TEM	Transmission electron microscopy
THF	Tetrahydrofuran
$V_D\beta$	Volume of distribution
WBC	White blood cell

1. INTRODUCTION

1.1. Formation of Hydrogels Using Dendritic Building Blocks

The judicious design and formation of polymeric materials with functional properties allow developments in wide range of biomedical applications. Recent years have witnessed innovations in the area of cross-linked polymeric networks. Hydrogels, resembling soft tissues in terms of physical structures and characteristics, have become widely used materials towards various applications such as tissue engineering [1,2], drug delivery [3], regenerative medicine [4] and biological sensing [5]. Besides the physical and chemical characteristics of the hydrogels, formation and functionalization efficiencies for desired applications are also need to be considered for the final material to achieve intended results. Several biological applications of hydrogels usually need incorporating ligands and biologically active moieties to provide them with functional properties. Generally physical modification techniques such as non-covalent encapsulation and physical absorption are used to incorporate small molecules, peptides, and large biomolecules into hydrogel matrix (Figure 1.1). However, controlled retention and release of encapsulated compound can be challenging in such strategies.

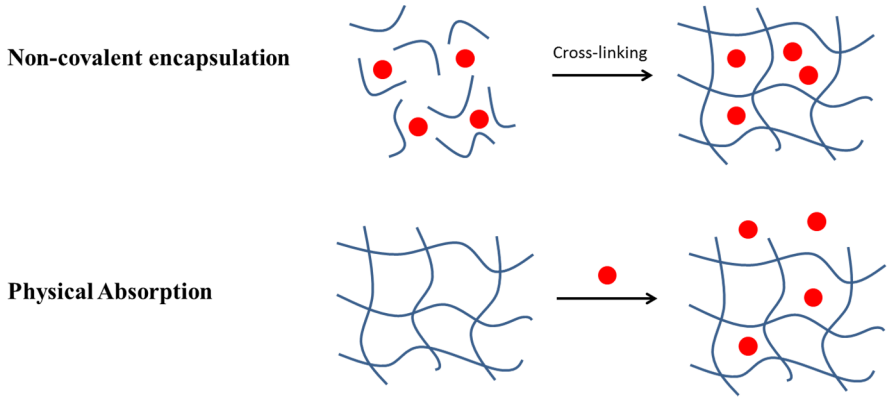


Figure 1.1. Non-covalent encapsulation and physical absorption for hydrogel functionalization.

There are also chemical modification techniques to achieve functional hydrogels such as employing reactive monomers or polymers, but the controlled degree of

functionalization can be challenging due to polydisperse nature of the polymers (Figure 1.2).

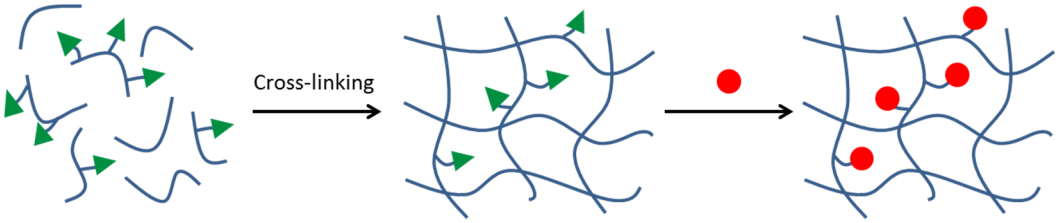


Figure 1.2. Employing reactive monomers or polymers to obtain modified hydrogels.

Dendrimers and dendrons with multivalent and multifunctional properties present advantages in either formation or post-gelation modification of the hydrogels through chemical or physical cross-linking techniques. These molecules can be synthesized using divergent and convergent approaches (Figure 1.3). In the divergent synthesis of dendrons, the dendron is derived from a multi-functional core, and the dendron generations raised outward by consecutive reactions. For the convergent synthesis of dendrons, dendrons are constructed from small molecules which form peripheral groups, and the reactions proceed inward to increase the generation.

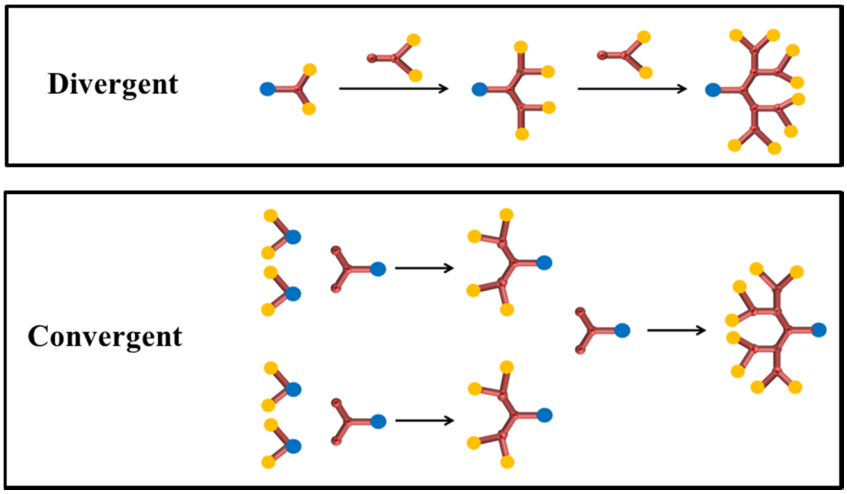


Figure 1.3. Divergent and convergent synthesis of dendrons.

Synthesis of multivalent polymeric compounds by attaching dendrons or dendrimers to chain-ends or backbones of polymers for hydrogel formation brings multivalent and multifunctional nature to hydrogels to use either in formation or post-gelation functionalization. This multifunctional character of dendron/dendrimer- polymer

conjugates also provides enhancing the number of cross-linking interactions to obtain robust materials with high efficiency.

The first scope of this dissertation is to show formation of functional hydrogels using dendron-polymer conjugates as building blocks and to prove the control over the functionalization. For better understanding the formation strategies and applications of hydrogels, recent examples of functional hydrogels, fabricated using dendritic building blocks, were discussed. These recent literature examples were classified into two groups according to hydrogel formation strategies; chemically and physically cross-linked hydrogels.

1.1.1. Chemically Cross-linked Hydrogels Using Dendritic Building Blocks

Chemical cross-linking reactions are commonly used in formation of hydrogels since providing robust and stable networks in the biological conditions. Click reactions, photo-cross-linking, chemical ligation, amide and thioester linkages, epoxy-amine reaction and various alternative chemical cross-linking reactions have been widely utilized on the formation of functional hydrogels through cross-linking of dendrimer or dendron containing building blocks.

Since the advent of “click” chemistries, many research groups have employed most of these efficient reactions, such as thiol-ene, thiol-yne and Huisgen-type copper-catalyzed azide-alkyne cycloaddition (CuAAC), for *in situ* hydrogel formation using dendritic structures and functional polymers [6]. Sanyal and co-workers reported a small library of functionalizable hydrogels based on dendron-polymer conjugates obtained by polyester dendrons and linear PEG diazides in 2010 [7]. ABA type triblock copolymers were synthesized by coupling second and third generation (G2 and G3) 2,2-bis(-hydroxymethyl) propionic acid (bis-MPA)-based polyester dendrons containing an alkyne group at their core with PEG diazides via the CuAAC reaction [8,9]. The hydroxyl groups on the dendron peripheries were reacted with 4-pentynoic anhydride to obtain alkyne groups. Hydrogels were formed by cross-linking the alkyne terminated ABA type, dendron-linear polymer-dendron, copolymer with tetra (ethylene glycol) diazide via the CuAAC reaction (Figure 1.4). They showed control over the degree of residual alkyne functionalities by stoichiometric adjustment of the alkyne-azide ratio in the gel precursor formulation.

Tunable cross-linking and degree of functionalization were justified by covalently attached fluorescent dyes. They also proved degree of functionalization by immobilization of streptavidin after attachment of biotin azide onto functionalizable hydrogels.

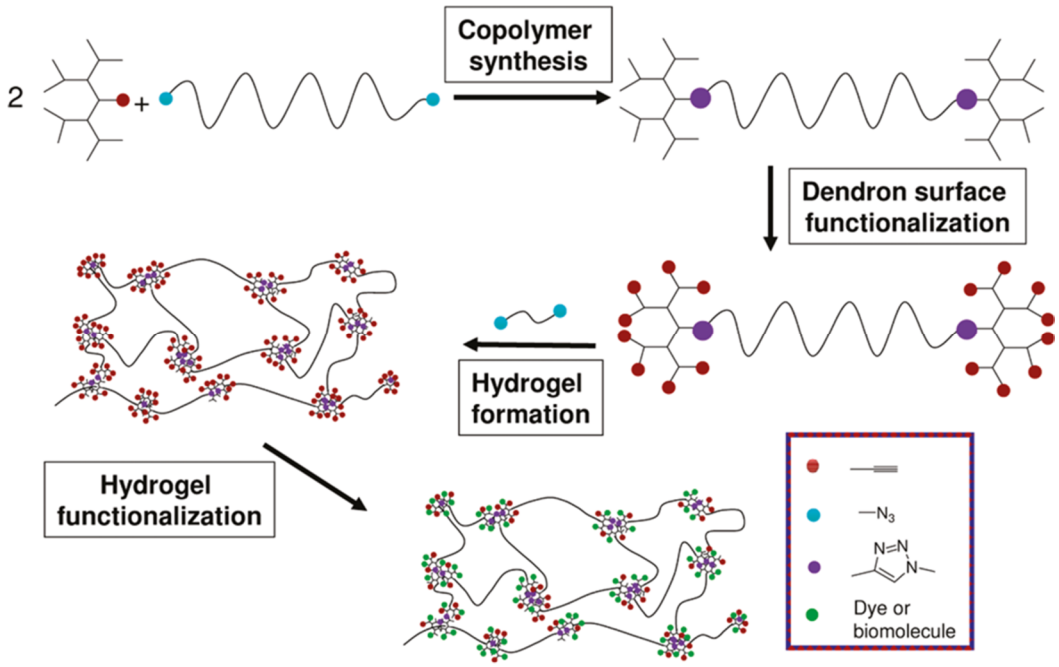


Figure 1.4. Schematic illustration of ABA type dendron-polymer conjugate synthesis and hydrogel formation. Reprinted with permission from [7], Copyright © 2010 American Chemical Society.

Recently, Malkoch and co-workers used orthogonally functionalized dendrimers and PEG dithiol for formation of functional hydrogels [10]. Firstly, two sets of polyester dendritic scaffolds were synthesized. While one of them was designed to have three alkene and six azide groups, the other one was designed to have six alkene and three azide groups (Figure 1.5). Hydrogels were formed by crosslinking of alkene groups with PEG dithiol (M_w = 6 kDa) via UV-initiated thiol-ene click reaction. Functionalization of these cross-linked networks was demonstrated by modification with D-mannose, L-DOPA and carboxylic acid bearing alkyne groups via the CuAAC reaction.

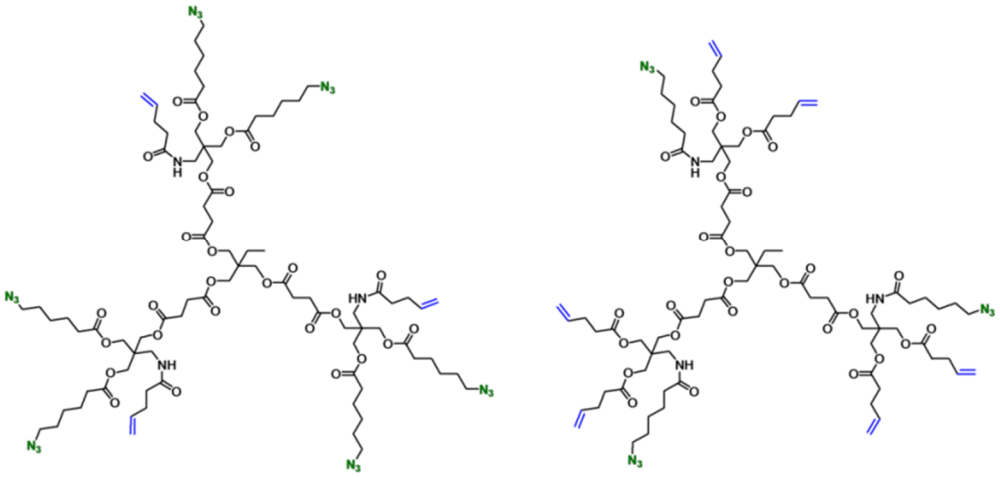


Figure 1.5. Dendritic scaffolds having three alkene and six azide groups (left) and six alkene and three azide groups (right). Adapted from [10], with permission by The Royal Society of Chemistry.

Wang and co-workers showed a rapid hydrogel formation using a thiol-ene click reaction between a poly(amido amine) (PAMAM) dendrimer bearing vinyl sulfone groups on the periphery and thiolated hyaluronic acid [11]. A fifth generation (G5) PAMAM dendrimer bearing 75 acetyl and the 35 residual amine groups were reacted with Traut's reagent to achieve thiol groups. These thiol functionalities on the dendrimer periphery were reacted with divinyl sulfone (DVS) to obtain vinyl sulfone groups on the periphery. Partial functionalization of vinyl sulfone groups with arginine-glycine-aspartic acid (RGD) gave G5 PAMAM Ac (75)-DVS (30)-RGD (5) dendrimer. Hydrogels were formed by the hydrogel precursor composed of this dendrimer and thiolated hyaluronic acid.

Malkoch and co-workers synthesized a series of homo-functional dendron-polymer conjugates and cross-linking methodologies for designing functional hydrogels [12]. They prepared ABA type dendron-linear polymer-dendron conjugates by a divergent approach using PEG diol and a bis-MPA dendron to obtain G3 polyester dendrons. The periphery of the dendrons was functionalized with allyl, alkynyl and *N*-hydroxy succinimide (NHS) groups. For the formation of the hydrogels they used thiol-ene, thiol-yne, CuAAC or NHS ester coupling reactions with complementary telechelic PEG polymers. They varied the ratio between dendron-linear polymer-dendron (DLD) and the linear telechelic PEG polymers to get tunable mechanical properties. Thiol-yne hydrogels were than

functionalized through conjugation of an azide-containing rhodamine dye with the residual alkynes groups via CuAAC reaction (Figure 1.6).

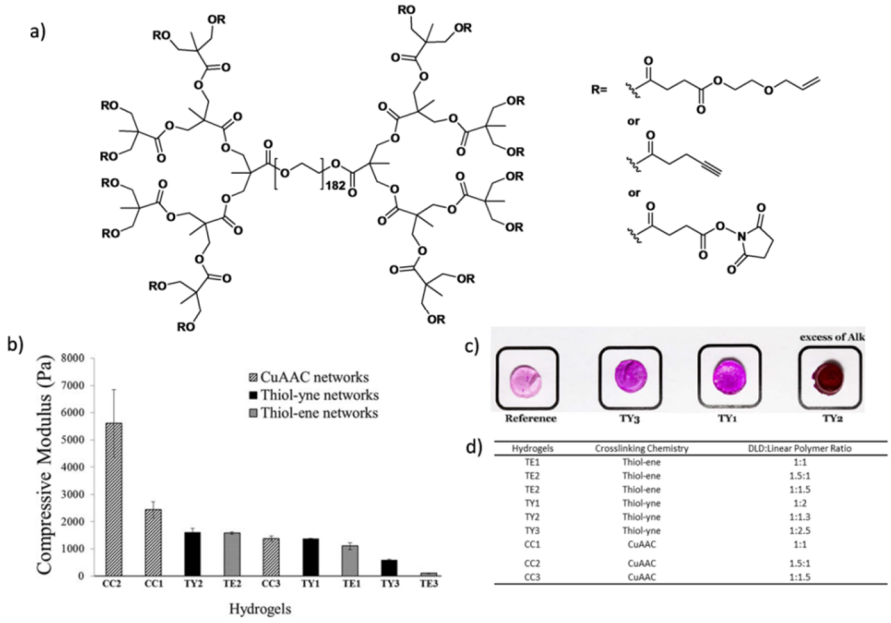


Figure 1.6. Physical and functional properties of dendron polymer conjugates. (a) allyl, acetylene or N-hydroxy succinimide (NHS) functionalities; (b) compressive modulus values of the hydrogels; (c) post-modification functionalization of thiol-yne (TY) hydrogels with azide functional rhodamine (reference sample prepared without catalyst); (d) Hydrogel definitions. From [12]. Copyright © 2015 by John Wiley & Sons, Inc. Adapted by permission of John Wiley & Sons, Inc.

This research group also employed UV-initiated thiol-ene click chemistry (TEC) for the formation of degradable and non-toxic hydrogels using orthogonally-functionalized ABA type dendron-linear polymer-dendron conjugates [13]. They used a special monomer for the synthesis of polyester dendrons over PEG-diol polymer to end up with orthogonal functionality at periphery of the dendrons (Figure 1.7). The cross-linking was achieved by TEC between alkenes groups on the dendron periphery and the thiol groups on a PEG 2-kDa dithiol. The azide groups on the dendron surface used for attachment of several bio-molecules, such as an alkyne bearing biotin, l-dopamine and D-mannose using the CuAAC reaction. They proposed the potential of these hydrogels as an artificial extra cellular matrix for the tissue engineering applications.

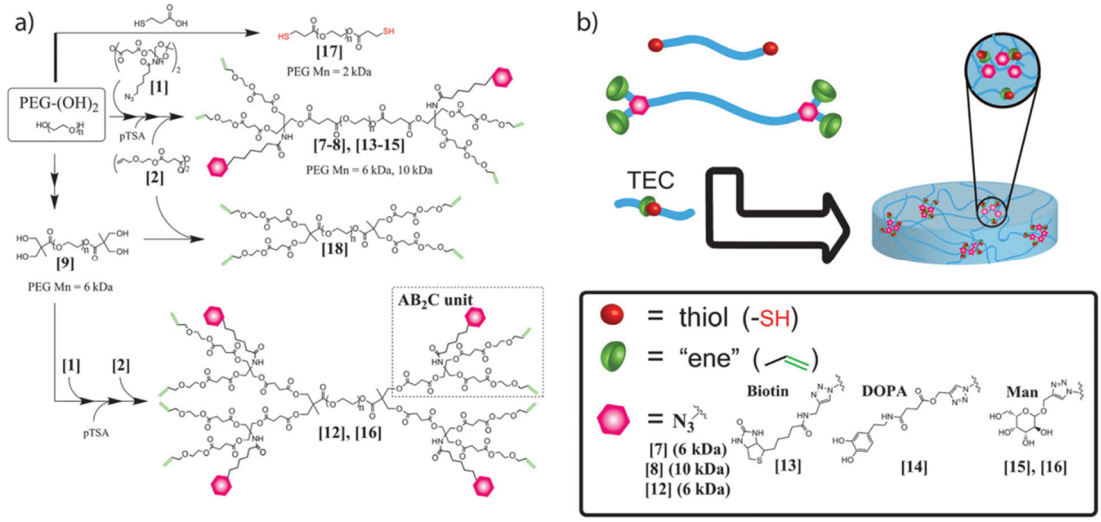


Figure 1.7. Synthesis of the dendron polymer conjugates and hydrogel formation. Adapted from [13]; with permission by The Royal Society of Chemistry.

Besides these click reactions there are also various photo-crosslinking strategies for the formation of chemically cross-linked hydrogels using dendritic structures as building blocks. Grinstaff and co-workers used biocompatible dendritic units composed glycerol and succinic acid to synthesize ABA type dendron-linear polymer-dendron conjugates [14,15]. They used PEG 3.4-kDa as the linear polymer part. The dendron peripheries of the conjugates were functionalized with methacrylate groups for photo-crosslinking. *In situ* gel sealants were prepared for the repairmen of corneal incisions using these dendron-polymer conjugates with an eosin-Y photo-initiation system, including n-vinyl pyrrolidinone under laser irradiation. They showed that the dendron generation of the copolymer has a significant role on the cross-linking density and solubility of the conjugates. The conjugate with the G1 dendron showed best sealing property. In another study, they used the same ABA type conjugate with the G1 dendron for the formation of a hydrogel for cartilage repair [16]. Methacrylate groups at the dendron periphery provided photo-crosslinking with the eosin-Y-based photo-initiation system (Figure 1.8). They prepared a library of hydrogels with different mechanical properties and swelling rates by using different gelation concentrations. These hydrogels showed insignificant volume changes during *in situ* cross-linking at the cartilage trauma site. They proposed the feasibility of these hydrogels as bone regeneration materials.

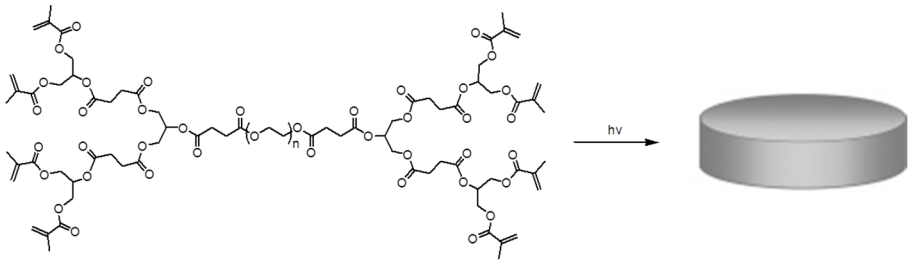


Figure 1.8. Photo-crosslinkable methacrylated dendron PEG ester conjugate. Adapted with permission from [16], Copyright 2006 American Chemical Society.

This group, in a following study, synthesized a series of ABA type dendron-linear polymer-dendron conjugates using the same strategy previously described with some differences [17]. They used glycerol (GL) together with other two biocompatible compounds, succinic acid (SA) and β-alanine (BA) for the synthesis of the first-generation dendrons by divergent approach over PEG. The surface of the dendrons was functionalized with methacrylate groups. Hydrogels were prepared using copolymers composed of glycerol (GL) and β-alanine (BA); glycerol and succinic acid (SA); glycerol, β-alanine and succinic acid by an eosin-Y-based photo-initiation system (Figure 1.9). Although all hydrogels showed low swelling rates, they displayed different mechanical properties due to the varieties in their composition, generation size and concentration. The hydrogel composed of GL and BA with G1 dendron prepared by the concentration of 20 *w/v*% displayed similar physical parameters with native articular cartilage. They tested this hydrogel in a pilot study for the cartilage repair on a damaged rabbit knee model and achieved encouraging results.

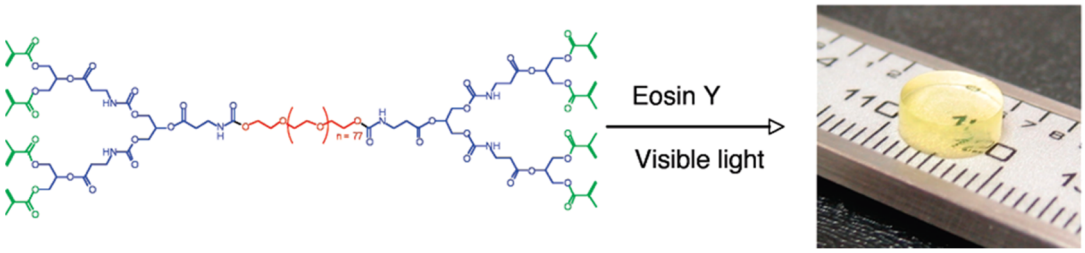


Figure 1.9. Photo-crosslinkable ABA type dendron-polymer conjugate and the hydrogel image. Reprinted with permission from [17], Copyright © 2008 American Chemical Society.

The same research group designed double-layered hydrogel corneal implants by sequential injection of gel precursors in the same mold to achieve improved adhesion properties of the hydrogels [18]. A 2-hydroxyethylmethacrylate and methacrylic acid (HEMA-*co*-MAA)-based hydrogel was used as the upper layer, and the glycerol and succinic acid based hydrogel composed of ABA type dendron-polymer conjugate was used as the bottom layer of the implant. (HEMA-*co*-MAA) hydrogels were covalently modified with type I collagen to achieve corneal epithelial cell adhesion and dendrimer-based hydrogels were modified with arginine-glycine-aspartic acid (RGD) for corneal fibroblast adhesion. The hydrogel network was formed by ammonium persulfate-tetramethylethylenediamine (APS-TEMED)-based initiation in the presence of arginine-glycine-aspartic acid-cysteine (RGDC)-PEG-acrylamide to give an RGD-modified hydrogel. Tunable physical properties were obtained by changing the concentration for double-layered corneal implants. The results showed successful epithelialization of implanted material and integration into tissue.

Sanyal and co-workers reported the fabrication of functionalizable hydrogels using orthogonally functionalized ABA type dendron- linear polymer- dendron conjugates [19]. In the hydrogel formation, instead of using the CuAAC reaction, they used photo-crosslinking of the dendron-polymer conjugate to eliminate the use of copper. The periphery of the dendrons was conjugated with methacrylate groups for photo-crosslinking and alkyne groups for post-gelation functionalization. Stoichiometric design of the orthogonally-reactive methacrylate and alkyne groups on the dendron surfaces provided tunable cross-linking levels, as well as number of alkyne functionalities (Figure 1.10). Successful and controlled covalent modification the hydrogels were demonstrated by the attachment of BODIPY azide and biotin azide. Biotin azide modified hydrogels were further employed to show immobilization of FITC-labelled streptavidin. Fluorescence microscopy analysis of functionalized hydrogels showed that the increase in the alkyne units on the dendrons resulted in more biotin azide ligand attachment onto the hydrogels and, thus, to dictate the extent of immobilization of the streptavidin. This approach allows the modification of biomaterials with biomolecules in a controlled manner, and that may be useful in tissue engineering or sensing applications.

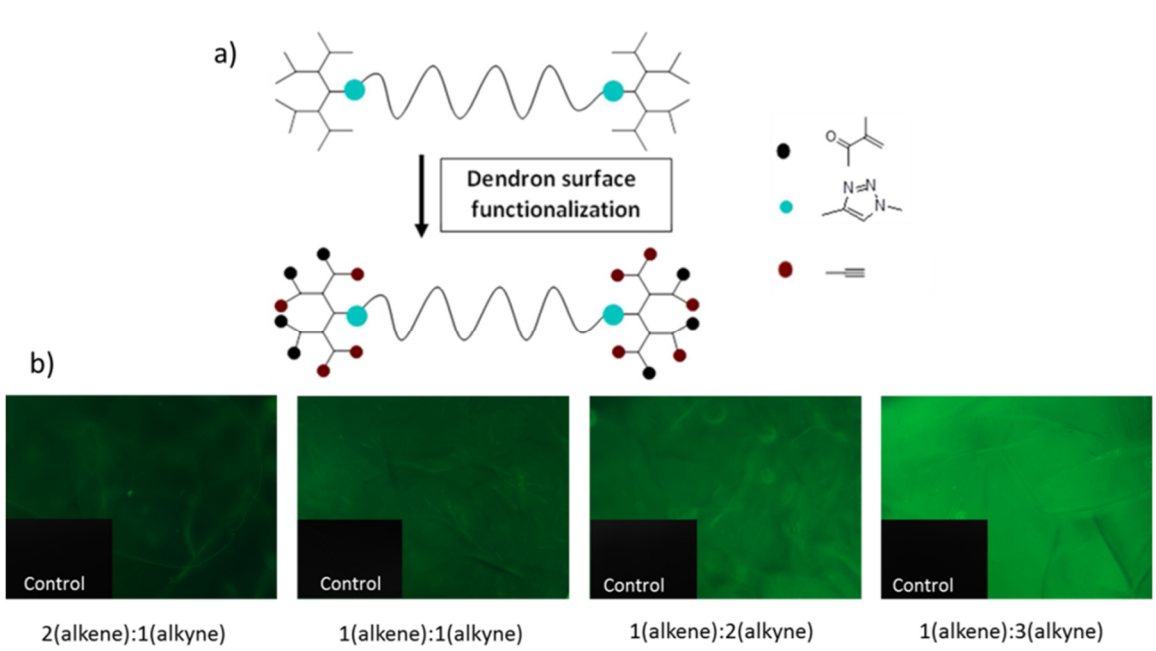


Figure 1.10. Dendron modification and fluorescent microscope images of hydrogels. (a) Dendron modification; (b) increasing fluorescence intensity upon the increase in alkyne quantity. Adapted with permission from [19], Copyright © 2015 American Chemical Society.

Yang and co-workers reported fabrication of hydrogels using photo-curable polymer conjugates of poly(amido amine) (PAMAM) dendrimers (Figure 1.11) [20]. They conjugated the G3 PAMAM dendrimer with PEG chains after the activation of PEG diols in the presence of 4-nitrophenyl chloroformate (NPC) and triethylamine (TEA). Photo-reactive dendrimer polymer conjugates were synthesized by attachment of acryloyl groups to remaining amine groups of the PAMAM dendrimer and the hydroxyl group of PEG segments. Hydrogels were formed using an eosin-Y-based photo-initiating system. The degree of PEGylation, PEG chain length and acrylate distribution affected the gelation and swelling properties. They proposed the potential tissue engineering and drug delivery applications of these hydrogels due to their cyto-compatibility and structural characteristics. However, the reactivity of acryloyl chloride towards free amine groups on the dendrimer periphery disabled the selective acrylation of PEG hydroxyl group. They also concluded that efficient cross-linking was also probably avoided due to shielding effect of PEG on the acrylate groups of the dendrimer surface.

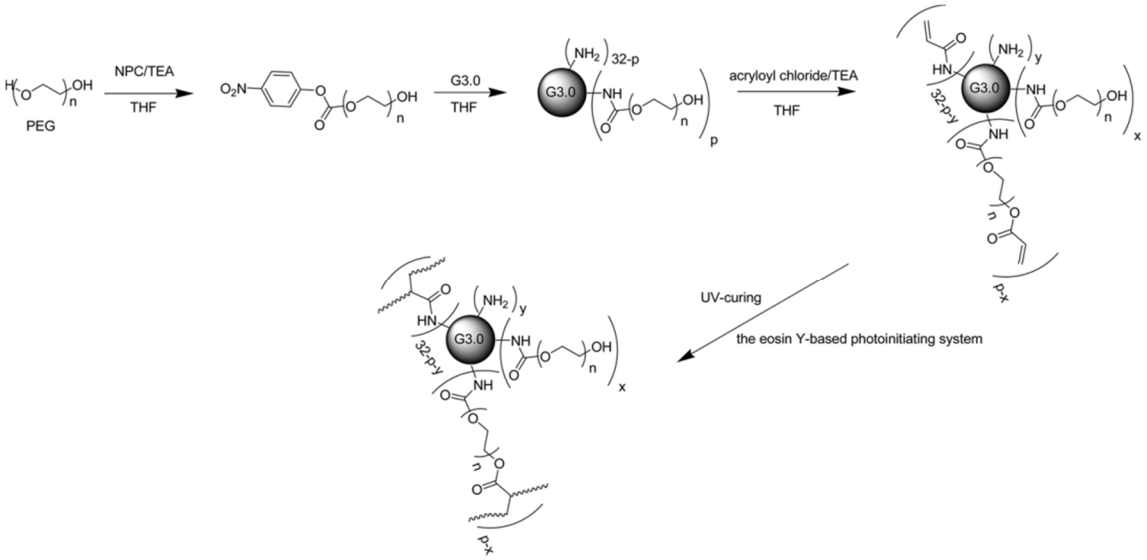


Figure 1.11. Synthesis of photoreactive PAMAM-PEG conjugate and photo-initiated cross-linking for hydrogel formation. Reprinted with permission from [20], Copyright © 2010 American Chemical Society.

They used a slightly different approach for the synthesis of PEGylated PAMAM dendrimers to obtain efficient cross-linking [21]. PEG diol was acrylated before the conjugation with PAMAM dendrimer. They used the G3 PAMAM dendrimer and PEG (12 kDa)-acrylate to obtain the PEGylated dendrimer. They prepared drug formulations to obtain hydrogels in the presence of one or both of the two anti-glaucoma drugs, brimonidine and timolol maleate in PBS using same initiation system. The interior hydrophobic core of the PAMAM dendrimer and the hydrophilic nature of PEG provided encapsulation of the hydrophobic drug brimonidine and the hydrophilic drug timolol maleate within the hydrogel matrix. The water solubility of brimonidine increased dramatically, and intracellular uptake and sustained release of the two anti-glaucoma drugs were demonstrated by *in vitro* and *ex vivo* studies.

Yang and co-workers also formulated a hybrid dendrimer hydrogel/poly(lactic-co-glycolic acid) (PLGA) nanoparticle system to obtain better controlled drug release, with these two anti-glaucoma agents (Figure 1.12) [22]. The dendrimer hydrogel drug formulation was prepared as previously mentioned, and they prepared nanoparticle drug formulation according to the literature procedure [23]. The drug-loaded PLGA nanoparticles were encapsulated into the hydrogel matrix during the cross-linking of the PEG-PAMAM dendrimer conjugate.

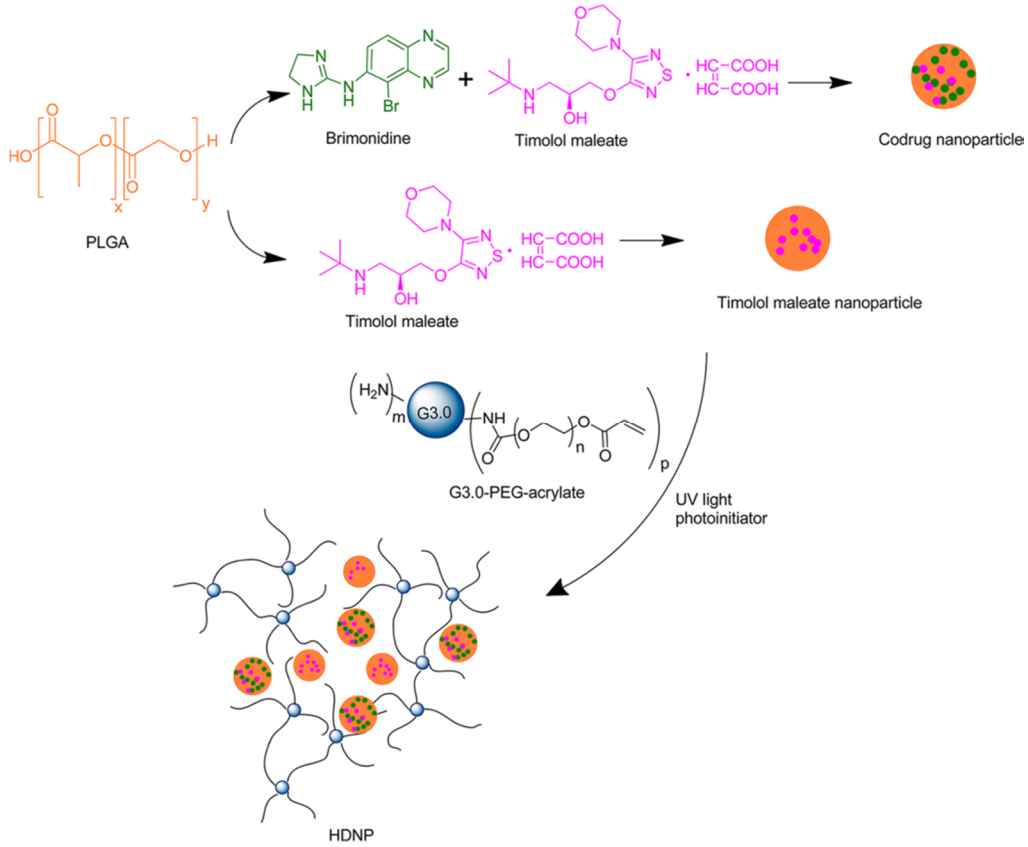


Figure 1.12. Formation of hydrogel-dendrimer-nanoparticle system (HDNP). Reprinted with permission from [22], Copyright © 2012 American Chemical Society. PLGA, poly (lactic-co-glycolic acid).

They performed *in vitro* and *in vivo* experiments and the results showed that this hybrid formulation provided combined drug delivery properties of both hydrogel and nanoparticle system and improved the drug release profiles. The dendrimer-based hydrogel also improved the muco-adhesive behavior of the PLGA nanoparticles due to the amine functionalities on the dendrimer periphery.

Jia, Yang and co-workers designed a novel hydrogel by *in situ* photo-crosslinking for tissue engineering applications [24]. They prepared hydrogels through cross-linking of a diacrylate-terminated poly (lactic acid)-*b*-poly (ethylene glycol)-*b*-poly (lactic acid) (PEG-PLA-DA) triblock copolymer and a PAMAM dendrimer having PEGs with acryloyl groups. A G4 PAMAM dendrimer was modified with acryloyl-terminated PEG segments and arginine-glycine-(aspartic acid)-(d-tyrosine)-cysteine (RGDyC) groups. A series of hydrogels with different ratios of the PEG-PLA-DA and PAMAM dendrimer were

obtained under UV-irradiation (Figure 1.13). They performed *in vitro* experiments to evaluate the similarity of these hydrogels with the extracellular matrix, and they concluded that introducing RGDyC to the hydrogel matrix enhanced cell attachment and proliferation.

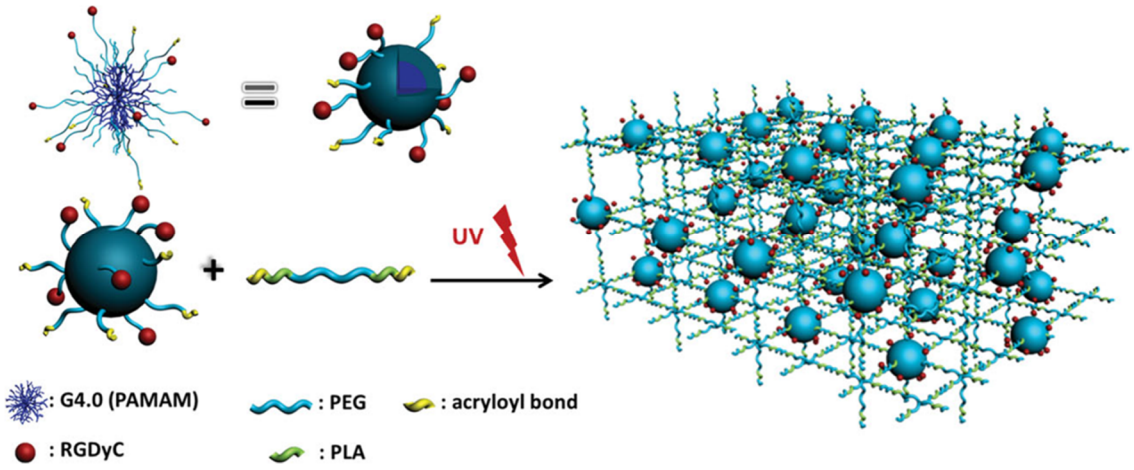


Figure 1.13. Schematic illustration for hydrogel formation. From [24], Copyright © 2014 by John Wiley & Sons, Inc. Reprinted by permission of John Wiley & Sons, Inc. RGDyC, arginine-glycine-(aspartic acid)-(d-tyrosine)-cysteine.

Several ligation strategies were also used in the formation hydrogels using dendritic building blocks. Grinstaff and co-workers designed hydrogel-based sealants for small corneal incisions for cataract operations by using native chemical ligation between peptide-based dendrons and linear PEGs. Cysteine-containing peptide dendrons and PEG-bearing propionaldehyde (P-Ald PEG) were used for formation of *in situ* cross-linked hydrogels by chemical ligation [25]. Four or eight N-terminal cysteine groups bearing lysine-based peptide dendrons were synthesized. A thiazolidine linkage was formed between cysteine and aldehyde groups under mild aqueous conditions (in HEPES buffer, pH: 7.4) upon mixing the homobifunctional aldehyde containing PEG and the lysine-based dendrons (Figure 1.14). Following preparation of hydrogels by using different dendron generations and macromer concentrations, mechanical properties and the refractive index values of the hydrogels were measured. The *ex vivo* results on enucleated eyes showed that these hydrogels possess improved parameters compared to suture and unassisted healing.

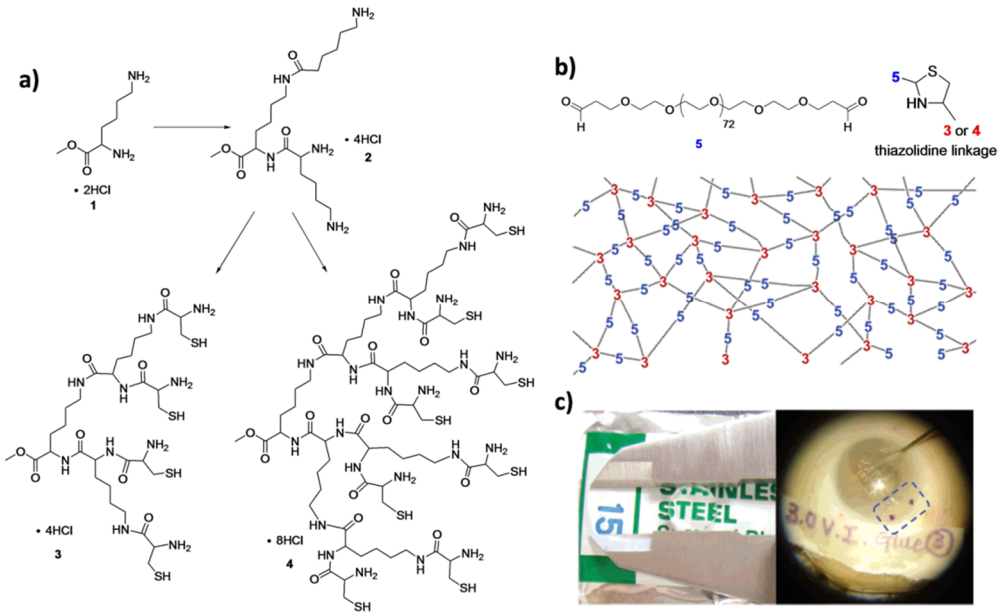


Figure 1.14. Chemical structure of lysine-based dendrons obtained hydrogels. (a) Synthesis of lysine-based dendrons; (b) thiazolidine linkage and hydrogel network; (c) hydrogel transparency (left) and hydrogel sealant for corneal incision. Adapted with permission from [25], Copyright © 2004 American Chemical Society.

In a following study, they employed pseudoproline formation toward the formation of these hydrogels to accelerate the cross-linking and prolong their stability [26]. The same peptide-based dendrons reacted with PEG-ester aldehyde (E-Ald PEG) for the formation of thiazolidine linkage. The reversibility of this thiazolidine structure and ester group on the E-Ald PEG led to an irreversible pseudoproline linkage formation via O, N acyl migration (Figure 1.15).

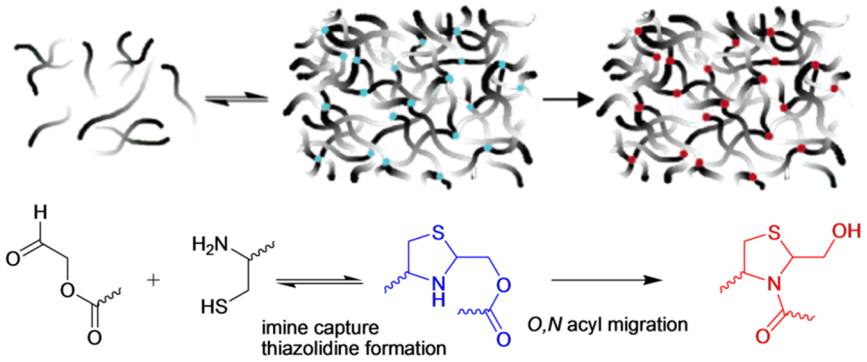


Figure 1.15. Hydrogel formation and pseudoproline ligation. Reprinted with permission from [26], Copyright © 2006 American Chemical Society.

These hydrogels were formed in seconds after mixing hydrogel precursors and prepared hydrogels remained stable for more than six months with a small mass change (less than 10 %). Performed *ex vivo* results on an enucleated eye showed that these hydrogels reduced the number of sutures required for securing corneal transplants, but adhesivity of the hydrogels remained insufficient to secure the incision without using suture.

Grinstaff and co-workers also performed a study to understand the adhesive, physical and mechanical properties of hydrogels based on peptide-based dendrons [27]. Tunable mechanical properties were obtained by changing the hydrogel precursor and gelation concentrations. Hydrogels prepared by P-Ald PEG, B-Ald PEG and PEG-bearing butyraldehyde (E-Ald PEG) showed different degradation times; six days, 1.5 and 24 weeks, respectively. B-Ald hydrogel showed the best adhesive behavior on an enucleated eye model. They suggested that these materials would be useful for wound-healing applications requiring different healing times.

Besides these click, photo-initiation and ligation chemistries, Grinstaff and co-workers used thioester and amide linkages for formation of hydrogels based on peptide-based dendron polymer conjugates and PEG disuccinimidyl valerate (SVA-PEG-SVA) [28]. A dendron-polymer conjugate bearing four terminal amines (PEG-Lys-NH_2) was synthesized and used for the preparation of amide-linked hydrogels as the control hydrogel material to compare with the ones having thioester linkage. They also synthesized dendron-polymer conjugate containing four peripheral SH (thiol) groups (PEG-Lys-SH) to form thioester linkage. Dendron-polymer conjugates with four terminal amines and thiols were mixed PEG disuccinimidyl valerate (M_w = 3.4 kDa), and hydrogels were formed via amide or thioester linkages. The thiol-thioester exchange chemistry was used for the dissolution of the prepared hydrogel (Figure 1.16). These hydrogels were tested by *ex vivo* experiments to understand the adherence and dissolubility properties on human skin tissues. Stability of the hydrogels proved upon applied mechanical stress. Dissolubility of the hydrogels was tested by a solution of l-cysteine methyl ester for thiol-thioester exchange chemistry.

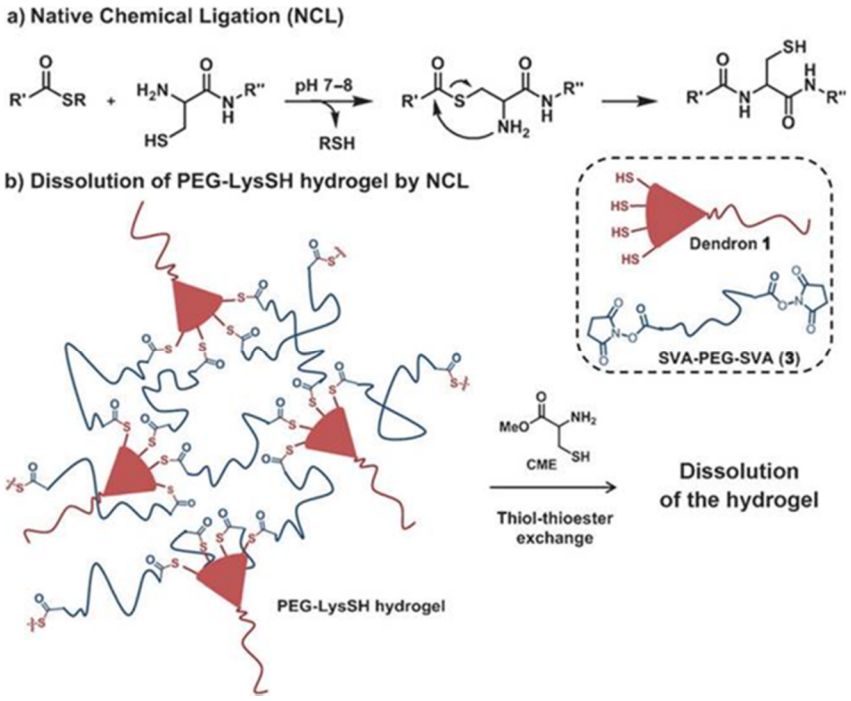


Figure 1.16. Native chemical ligation and hydrogel dissolution via thiol-thioester exchange. From [28], Copyright © 2013 by John Wiley & Sons, Inc. Reprinted by permission of John Wiley & Sons, Inc.

The results showed that the hydrogel formed by the thioester bond was degraded in 30 min, whereas the hydrogel formed by the amide bond remained stable (Figure 1.17). The authors underlined the feasibility of these hydrogels in cases requiring emergency intervention and subsequent operation.

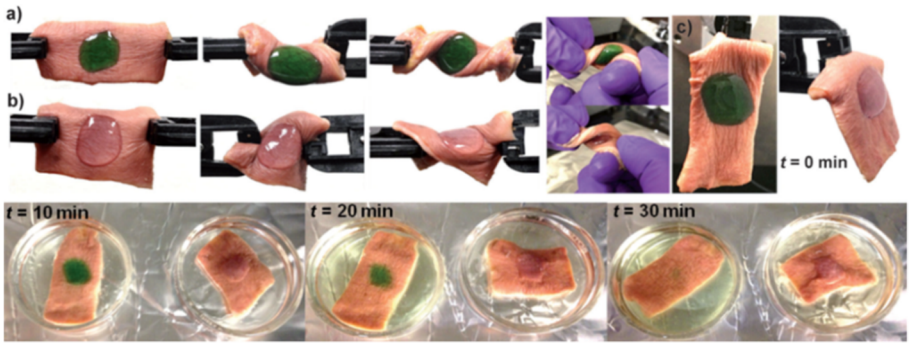


Figure 1.17. Stability and degradation of hydrogels. (a) Mechanical stability of hydrogels formed by thio-ester (green) bond; (b) mechanical stability of hydrogels formed by amide (pink) bond; (c) degradation of the hydrogels by l-cysteine methyl ester solution. From [28], Copyright © 2013 by John Wiley & Sons, Inc. Reprinted by permission of John Wiley & Sons, Inc.

In a more recent study, Grinstaff and co-workers compared the hydrogel formed by amide bond with a commercially available tissue sealant and adhesive products (Figure 1.18) [29]. The *ex vivo* experiments on bovine aorta or murine skin tissue samples showed that this hydrogel showed the same sealing performance as tested products when sealing small incisions.

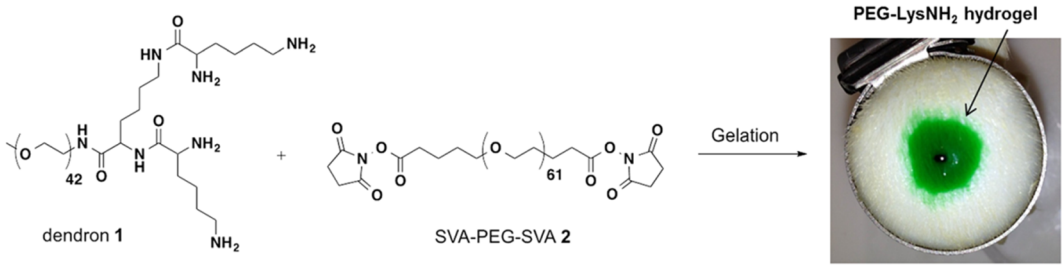


Figure 1.18. Hydrogel formation by amide bond for sealing corneal incisions. Reproduced from [29]; published by the BioMed Central.

Gitsov and co-workers reported formation of hydrogels using cross-linking between isocyanate or epoxy-terminated telechelic PEGs (M_w = 3.4 kDa) and poly(benzyl ether) dendrimers having amine groups [30]. High reactivity of isocyanate groups towards amines resulted in fast cross-linking when using PEG diisocyanate. They reported that this fast cross-linking caused physical entanglement of PEG segments and low cross-link ratio. However, in the case of diepoxy PEG, highly cross-linked hydrogels were obtained due to the stability of epoxides under cross-linking conditions. They showed that varying PEG content and dendrimer generation affected the water uptake properties of the hydrogels. In a following study, the environmental response and feasibility for bioanalytical and biomedical applications of these hydrogels were investigated by the group [31].

Hedden and Unal used epoxy-amine reaction for the construction of hydrogels using amine-terminated PAMAM dendrimers and epoxy-terminated telechelic PEG (4 kDa) [32]. Hydrogels were prepared using G0, G2 and G4 PAMAM dendrimers by altering polymer concentrations and dendrimer/PEG ratios to understand the effect of these changes on cross-linking and water uptake properties. Hydrogels showed a wide range of water uptake ratios (from 15–1000 folds), the authors reported that these behavior was mostly influenced by the mole ratio between amine and epoxide groups. They suggested that

superabsorbent hydrogels can be obtained by using a large excess of dendrimers over PEG and the role of the dendrimer generation on swelling behavior was negligible.

Alternatively, pyridyl disulfide-thiol exchange reaction, enzymatic and oxidation reactions have been utilized in formation of hydrogel using dendrimers and polymers as building blocks. Kannan and co-workers constructed biodegradable hydrogels for sustained drug release in treatment of genital infections [33]. The hydrogels were formed by using, a G4 PAMAM dendrimer having pyridyl disulfide groups and an eight-arm PEG containing peripheral thiol groups. Hydrogels were formed in seconds by mixing dendrimer and PEG solutions (Figure 1.19).

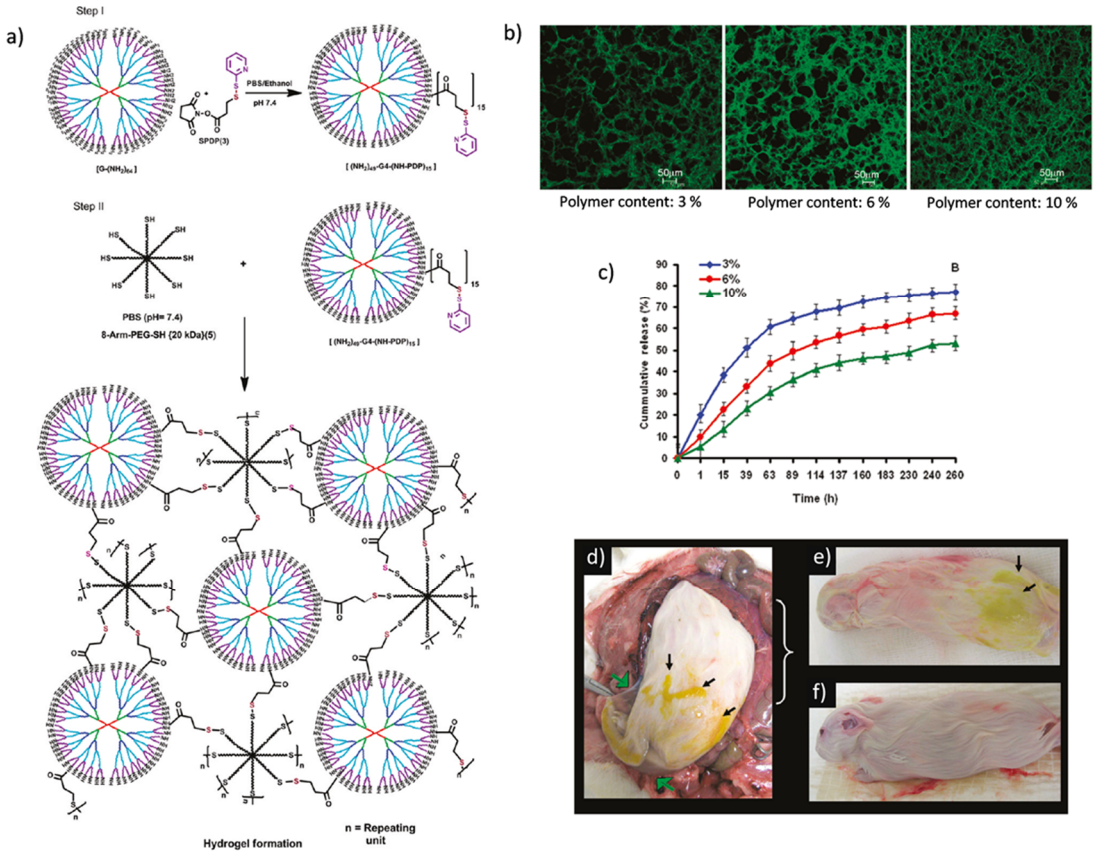


Figure 1.19. Formation, physical properties of the hydrogels. (a) Disulfide formation; (b) network changes using different polymer content; (c) drug release profiles of the hydrogels prepared by different polymer ratio; (d,e) hydrogel degradation on fetal membrane; (f) hydrogels remained outside of the fetal membrane. Adapted with permission from [33], Copyright © 2011 American Chemical Society.

Fluorescence microscopy images showed that the pore size in the hydrogel network decreased and cross-linking ratio increased by increasing the polymer content. The time to reach equilibrium swelling state and drug loading efficiency of the hydrogels decreased upon increasing polymer content due to high cross-linking ratio. Drug loaded hydrogels were prepared by dissolving amoxicillin in the eight-arm PEG solution followed by mixing this solution with dendrimer solution.

These hydrogels were tested by *in vitro* drug release and *in vivo* experiments in a pregnant guinea pig model. *In vitro* experiments showed that the decrease in cross-linking density caused an increase in cumulative drug release and sustained release was achieved for more than 10 days. They reported that degradation of the hydrogels started after 3 days and *in vivo* experiments showed that degraded hydrogels were retained in the maternal tissues and could not transfer across the fetal membrane (Figure 1.19). They suggested that these hydrogels can be used to achieve localized and selective treatment for genital infections during pregnancy without affecting the fetus.

Tran and co-workers used an enzymatic reaction in fabrication of biocompatible hydrogels derived from cationic PAMAM dendrimers and tetronic, a non-toxic surfactant [34]. The G3 PAMAM dendrimer was functionalized with p-hydroxyphenyl acetic acid (HPA) via carbodiimide coupling. Tetronic was modified with tyramine by activation of terminal hydroxyl groups via substitution of nitrophenyl chloroformate and tyramine. Hydrogels were formed by the reaction between phenol groups of HPA functionalized dendrimer and tyramine groups of tetronic. This reaction was catalyzed by horseradish peroxidase enzyme (HRP) and hydrogen peroxide. Heparin-loaded dendrimer-tetronic hydrogels showed better sustained heparin release (over 30 days) compared to heparin-loaded tetronic hydrogel. They reported that the increase in dendrimer ratio caused a lower degree of cumulative heparin release.

As one another alternative strategy, Jia, Yang and co-workers utilized oxidation-induced cross-linking for the fabrication of hydrogels formation using a dendrimer-polymer conjugate and a hyper-branched PEG as building blocks for tissue engineering applications (Figure 1.20) [35].

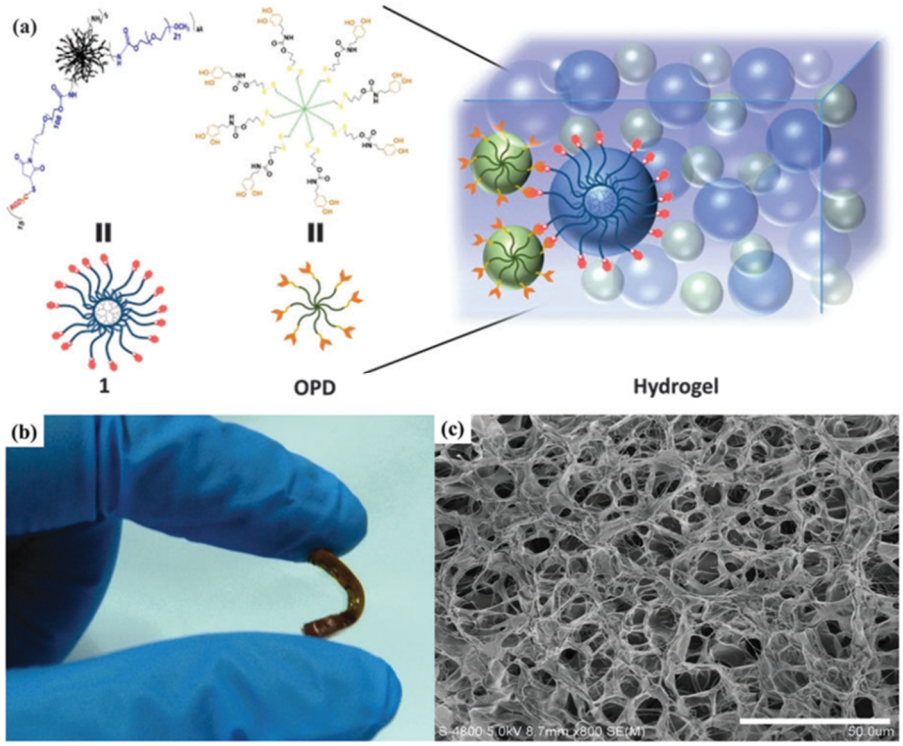


Figure 1.20. Hydrogel formation and physical properties of the hydrogel. (a) Formation of hydrogel using RGDyC-modified PEGylated PAMAM dendrimer and DOPA-terminated eight-armed PEG (OPD); the photograph (b) and SEM image (c) of the hydrogel. Reproduced from [35] with permission of The Royal Society of Chemistry.

Cross-linking was achieved between DOPA and phenol groups by the oxidation-induced reaction in the presence of $NaIO_4$ and bioactive peptide of arginine-glycine-(aspartic acid)-(D-tyrosine)-cysteine (RGDyC). They used the PAMAM dendrimer to benefit from its multifunctional structure to increase the cross-linking density and DOPA to benefit from its strong adhesion property to enhance the adhesion to tissue. RGDyC was used to increase the success of the implanted material due to its bioactivity. This biodegradable hydrogel showed high mechanical properties and a low swelling behavior, which are desirable characteristics for bone tissue engineering materials. Additionally, *in vivo* studies on the mouse calvarial critical size defect model demonstrated that this material enhanced the bone tissue formation when it was implanted in the defected region. They underlined the possibility to use this material in different tissue engineering and clinical applications.

1.1.2. Physically Cross-linked Hydrogels Using Dendritic Building Blocks

Dendrons and dendrimers have been used alone or together with polymers as building blocks in the formation of physically cross-linked hydrogels in recent years. Physically cross-linked hydrogels based on dendritic structures have been evaluated as medium-sensitive matrices and as promising candidates for drug delivery applications [36]. In the formation of such cross-linked networks, macromolecules with dendritic architectures usually resulting in supramolecular hydrogels using different strategies. Adjustment of the sol-gel dynamics by changing the conditions for network formation is possible to achieve such materials. This also enables to fabricate physically cross-linked networks with tunable mechanical and morphological characteristics. The gelation mechanisms of these materials usually include the self-assembly of hydrogel precursors in aqueous mediums via several non-covalent interactions. The main non-covalent intermolecular interactions which are resulted in physically cross-linked networks include hydrogen bonding, π-π stacking and van der Waals interactions. These kinds of strategies have been also utilized for the design of stimuli-responsive supramolecular hydrogels that can be used in various sensing applications.

Newkome and co-workers demonstrated the synthesis of effective hydrogelators based on dendritic molecules. Newkome-type arborols were synthesized as bolaamphiphiles which have two water-soluble hydroxyl groups linked by a hydrophobic spacer. These structures were used in formation of thermally-reversible hydrogels. It was shown that the length of hydrophobic spacer and dendron generation affected the hydrogelation reaction kinetics [37]. Formation of the gels is explained by an aggregation model where the polar hydroxyl groups provide solubility in aqueous media and the hydrophobic alkyl spacer causes aggregation. As a model dendrimer containing 9 hydroxyl groups at sides and 10 methylene spacer units, gelation reaction was induced when aqueous solutions were heated to 80 ºC and cooled back to 25 ºC. The authors demonstrated the mechanical and morphological properties of the hydrogels by various methods, including light scattering, optical microscopy, TEM and viscometry. They reported that the viscosity increased rapidly during gelation reaction and showed formation of rod-shaped aggregates with uniform diameters, but variable lengths by TEM analysis. They explained this observation by the interlocking network of dumbbell-shaped arborols

where intermolecular lipophilic and hydrophilic interactions resulted in rod-shaped aggregates. Newkome and co-workers reported the gelation of a bolaamphiphile with a central triple bond to achieve a polyacetylene covalent structure from pre-organized stacked cores (Figure 1.21) [38,39]. Following gel formation, a novel morphology of a helical supramolecular structure was demonstrated by TEM analysis. This was attributed to the rigid nature of the alkyne units of the arborol which was resulted in non-orthogonal stacking.

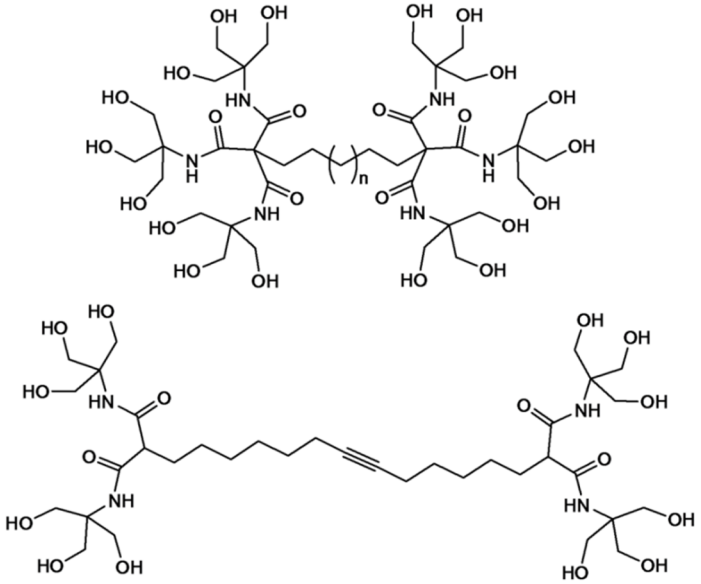


Figure 1.21. Bolaamphiphile structures. Adapted with permission from [39], Copyright © 1997 American Chemical Society.

Self-assembly of arborol in hydrogel formation was thereafter exploited by Jorgensen and co-workers using a bolaamphiphile which has a tetrathiafulvalene spacer (Figure 1.22) [40].

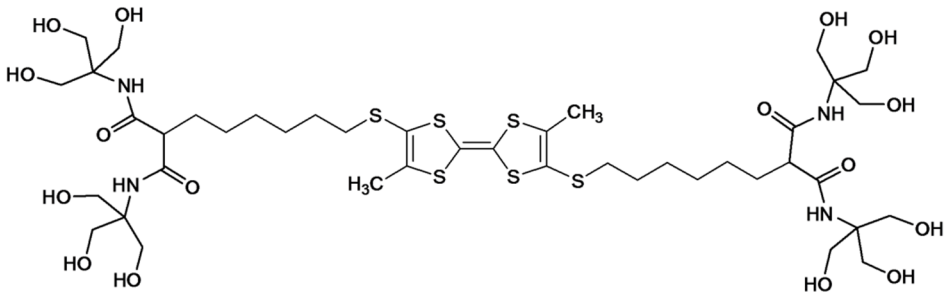


Figure 1.22. Structure of bolaamphiphile with a tetrathiafulvalene spacer. Adapted with permission from [40], Copyright © 1994 American Chemical Society.

The tetrathiafulvalene structure was installed to promote electrical conductivity in conjunction with a proper dopant to end up with self-assembling molecular wire. A hot dendrimer solution in ethanol-water or DMF-water mixture was cooled to induce gelation. String-like superstructures with lengths in microns and diameters from thirty to several hundred nanometers were observed by phase contrast optical microscopy and atomic force microscopy (AFM). UV-VIS analysis showed characteristic absorption bands of tetrathiafulvalene oligomers after iodine oxidation.

After these early examples, a wide range of dendritic structures have been used as potential hydrogelators in the formation of physically cross-linked hydrogels. Boons and co-workers investigated the self-assembly of glycodendrons to understand the hydrogelation behavior [41]. They reported that glycodendrons with different branch lengths and the 1,3-dicarboxy-5-hydroxybenzene-based core moiety formed thermally-reversible aqueous networks. Structural variations, such as the length of the branches significantly changed the hydrogelation behavior.

Another thermally induced hydrogel formation using the surface-modified organophosphorus dendrimers reported by Majoral and co-workers (Figure 1.23) [42].

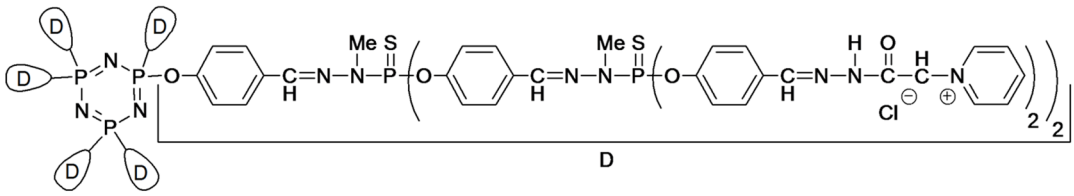


Figure 1.23. Ammonium functionalized phosphorus based dendrimers as hydrogelators. From [43], Copyright © 2001 by John Wiley & Sons, Inc. Adapted by permission of John Wiley & Sons, Inc.

The dendrimers with peripheral alkylammonium or pyridinium functional groups were utilized in formation of physically cross-linked hydrogels through heating the solution at 60–65 ºC for 11–13 days, but this gelation mechanism could be accelerated by using several water-soluble additives such as buffers, metal salts, and acids. The gelation mechanism was explained by supramolecular interactions, such as hydrogen bonds, π-stacking and hydrophilic/hydrophobic interactions of dendrimer peripheral groups. In

another study, the same group obtained physically cross-linked hydrogels and macroscopic fibers through salt-induced self-assembly using water-soluble, poly-cationic phosphorus dendrimers [43]. Thermally-reversible hydrogels with tunable sol-gel transition temperatures were affected by the salt type, dendrimer generation, precursor concentration and temperature.

Secondary-, tertiary- and quaternary-level structures of peptides provide appropriate conditions in physically cross-linked hydrogel design which are not provided with organic molecules or polymers [44]. Liu and co-workers used G1 and G2 generations of l-glutamic acid-based amphiphilic dendrons that form a physically cross-linked hydrogel over a wide pH-range from 2–13 [45]. These dendrons having long alkyl cores self-assemble into nanofibers or helical nanotubes. The authors reported that various types of chiral nanostructures were obtained by variations of pH values. In a following study, they used the peptide based dendrons for metal ion-triggered shrinkable supramolecular hydrogel formation [46]. It was revealed that the gelation was significantly influenced by the presence of certain metal ions such as Mg^{2+}, Cu^{2+} (Figure 1.24).

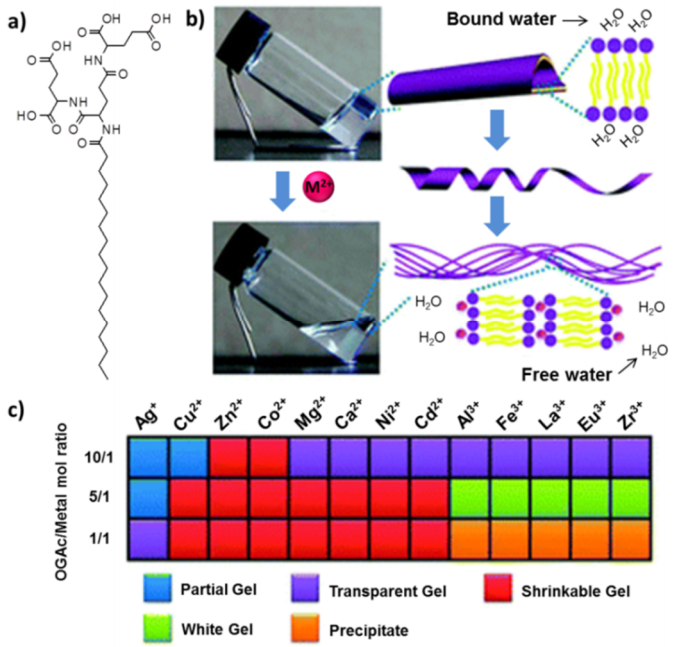


Figure 1.24. Chemical structure of hydrogelator and gelation properties. (a) The hydrogelator (OGAc); (b) metal ion-triggered shrinkage of the supramolecular hydrogel; (c) effect of metal ions on the gelation properties. Adapted from [46] with permission of The Royal Society of Chemistry.

The critical gelation concentration was directly affected by the type and the ratio of metal ions. Hydrogels triggered by divalent metal ions showed continuous shrinkage. They showed that upon heating of the shrunken gel it turned into a solution, and then, the gel was formed again by cooling. They used this reversibly-shrinkable hydrogel in controlled release of vitamin B1 and showed that, addition of divalent ions allowed the release of vitamin B1, and the release of vitamin B1 increased by hydrogel shrinkage. The reversible volume-phase transitions of these peptide-dendron based metallo-hydrogels were also regulated by pH change [47].

Another example of stimuli-responsive hydrogel was reported by Sako and Takaguchi [48]. They utilized a dendron with an anthracene core and gluconamide peripheral units as a photo-responsive hydrogelator. The macroscopic volume phase transitions or shrinking/swelling of photo-responsive hydrogels was explained by photoisomerization of chromophores in the gel matrix. The gel-to-sol transition of the hydrogel was shown to be forced by photodimerization of the anthracene moieties. Liu and co-workers recently reported another photo-responsive system by using co-assembly of an l-glutamic acid-terminated amphiphilic dendron and a positively-charged azobenzene [49]. The formation of the multi-bilayer structure through electrostatic interaction of these two compounds resulted in an initial gel phase. The shrinkage of the gel matrix was explained by the aggregation of azobenzene moieties upon resting at room temperature. Cis-trans isomerization of the azobenzene groups induced by photo-irradiation of the shrunken gel allowed the expansion of distances between layers and resulted in swelling of the gel network (Figure 1.25).

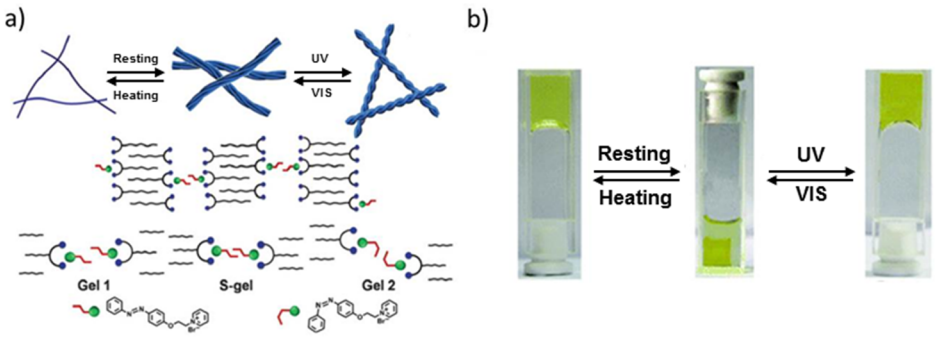


Figure 1.25. Gel-to-sol mechanism of amphiphilic dendron and azobenzene components. (a) The hierarchical co-assembly; (b) thermal and photo-responsive reversible control on hydrogel network. Adapted from [49] with permission of The Royal Society of Chemistry.

This technique enabled both thermal and photo-responsive control on hydrogel network and swelling/deswelling kinetics. The formation of physically cross-linked hydrogels based on amphiphilic Janus type dendrimers was recently reported by Nummelin and co-workers [50]. Dendrimers having *O*-alkylated benzyl and hydroxyl-terminated bis-MPA-based hydrophilic segments were synthesized by using CuAAC reaction (Figure 1.26).

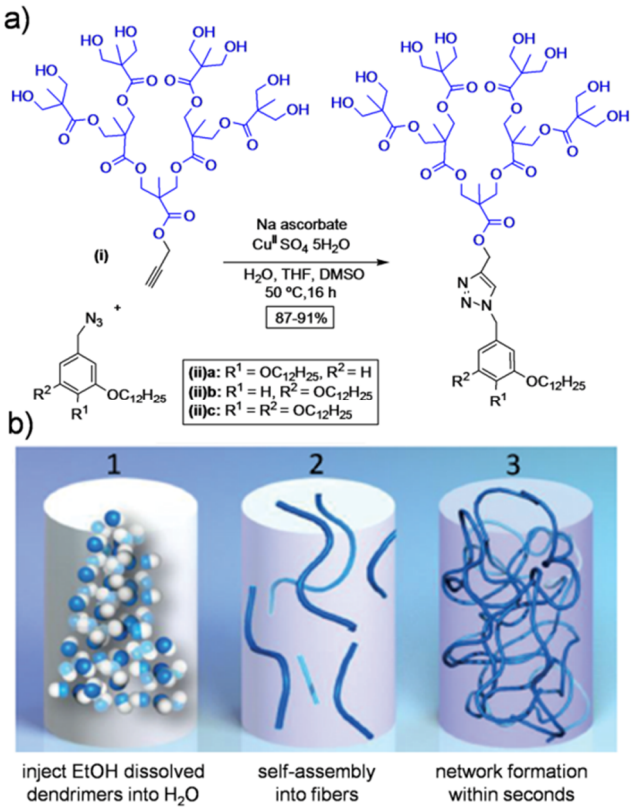


Figure 1.26. Janus type dendrimers and self-assembly. (a) Synthesis dendrimers; (b) self-assembly of dendrimers to form fibers and hydrogel network. From [50], Copyright © 2015 by John Wiley & Sons, Inc. Adapted by permission of John Wiley & Sons, Inc.

These dendrimers formed fibrous structures in aqueous conditions leading to formation of physically cross-linked hydrogels. They reported that the storage moduli and melting temperature of hydrogels were regulated by the position or number of alkyl chains. The controlled release of small-molecule drug, nadolol; a decapeptide, gonadorelin; and an enzyme, HRP evaluated using these hydrogels.

Besides these dendron dendrimer based examples, there are also various strategies in formation of physically cross-linked hydrogels using dendron polymer conjugates as building blocks. Namazi and Adeli synthesized ABA type dendron-linear polymer-dendrons having linear PEG and citric acid-based polyester dendron segments for thermo-reversible hydrogel formation [51]. In the preparation step of the hydrogels dendron polymer solutions with different concentrations in hot water cooled below the transition temperature. They prepared drug/dendron-polymer formulations in hot ethanol/water and obtained drug loaded hydrogels to understand the host-guest behavior of the dendron polymer conjugates. In a following study, they tested the feasibility of these hydrogels in drug-delivery platforms using several dendron polymer conjugates having different dendron generations [52].

In a remarkable study Aida and co-workers prepared physically cross-linked hydrogels using guanidinium ion-terminated ABA type dendron polymer conjugates and clay nanosheets [53]. They prepared the dendron polymer conjugates using a linear PEG segment and polyester dendrons having guanidinium ions. Sodium polyacrylate was used for dispersion of clay nanosheets prior to the hydrogel formation (Figure 1.27).

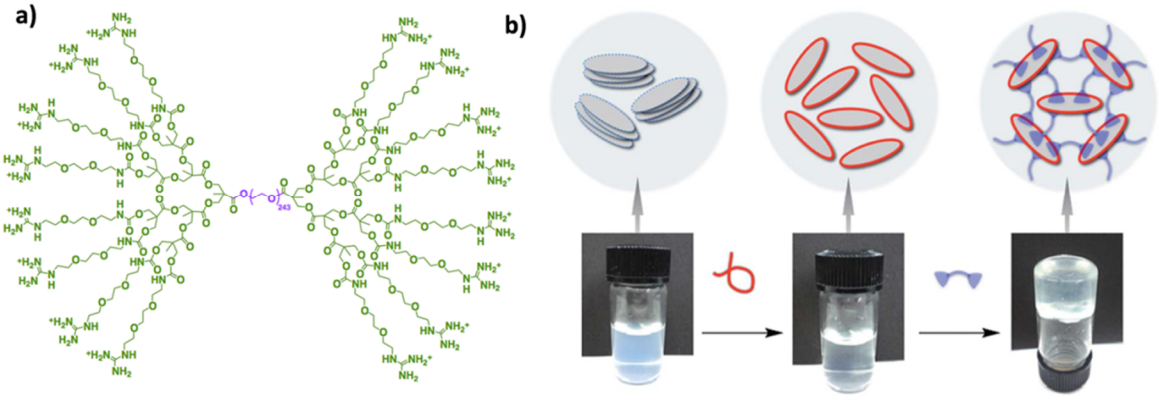


Figure 1.27. Dendron-polymer conjugates and hydrogel formation. (a) Structure of the conjugates with guanidinium ions; (b) physical cross-linking. Adapted by permission from Macmillan Publishers Ltd: Nature [53], Copyright © 2010.

Dispersed clay nanosheets and guanidinium ions on the periphery of the dendron polymer conjugates strongly interacted to obtain hydrogels with great mechanical and self-healing properties compared to ones prepared by conventional approaches [54,55]. They

showed the stability and activity of these myoglobin loaded hydrogels and the compatibility of these networks for biomedical science.

The multi-step synthesis of these dendritic hydrogelators can cause some practical challenges in applications which require large scale production. To understand the efficiency of linear molecular hydrogelators compared to dendritic ones, Aida and co-workers also designed linear polymeric hydrogelators having same guanidinium groups [56]. They prepared hydrogels in the same manner as described above and compared self-healing behaviors of linear and dendritic binders (Figure 1.28). The results showed that the hydrogels obtained by linear binders showed similar self-healing properties as dendritic binders, however dendritic binders exhibited faster hydrogel formation compared to linear ones. They suggested that multiple functionalities of dendritic binders enabled faster hydrogelation.

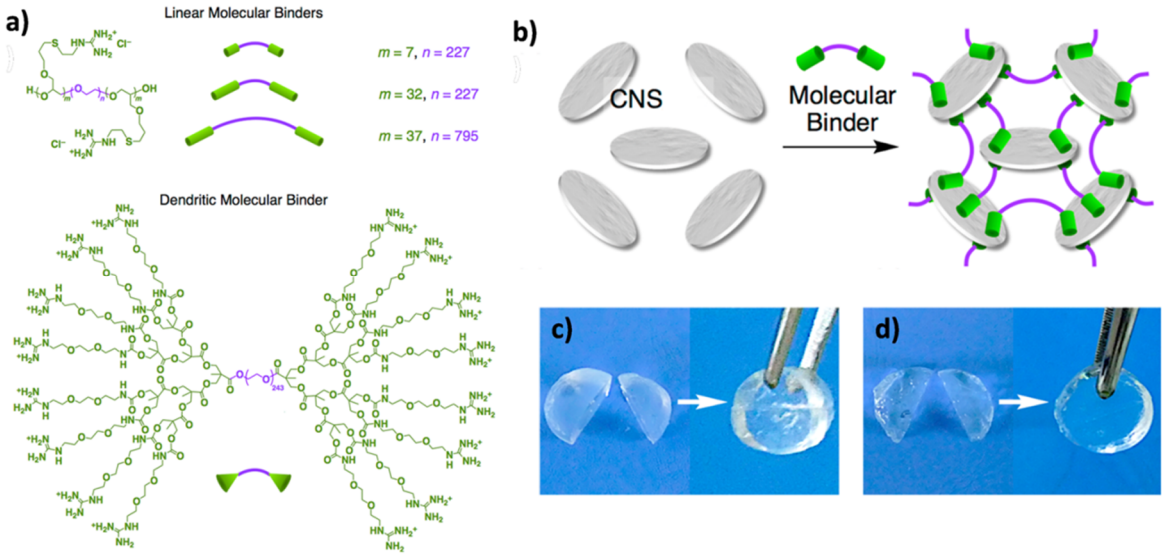


Figure 1.28. Structure of hydrogel precursors and physical cross-linking. (a) Linear and dendritic polymeric binders; (b) hydrogel formation by linear dendritic binder. Self-healing behaviors of hydrogels formed by linear (c) and dendritic (d) polymeric binders. Adapted with permission from [56], Copyright © 2013 American Chemical Society.

Seelbach and co-workers used a dendron-polymer conjugate for *in situ* injectable and thermo-responsive hydrogel to be used in cell-based regenerative medicine applications. They used hyaluronic acid and peptide-based dendron conjugate and a thermo-gelling unit

for hydrogel formation [57]. Firstly, they conjugated integrin-binding sequences, RGDS (Arg-Gly-Asp-Ser) and DGRS (Asp-Gly-Arg-Ser) peptides to mono-azide-bearing diethylenetriamine pentaacetic acid bearing four oligo (ethylene glycol) aminoethyl groups to obtain peptide-based dendrons. Then, these dendrons were covalently grafted with propargylamine-derived hyaluronic acid using the CuAAC reaction. Poly (*N*-isopropy lacrylamide) and hyaluronan conjugate was used as a thermo-gelling unit. The hydrogels were formed by mixing these two different conjugates in aseptic conditions. The *in vitro* experiments performed with human mesenchymal stromal cells showed the feasibility of these hydrogels in musculoskeletal repair.

Zhuo and co-workers formulated physically cross-linked hydrogels using poly(vinyl alcohol) and amine-terminated G6 PAMAM dendrimer [58]. The aim of introducing the PAMAM dendrimer into the hydrogel matrix was described was to improve the drug release and loading properties of poly (vinyl alcohol) hydrogels. Hydrogel formation was obtained by the process of freeze/thaw cycles which cause hydrogen bonding between hydroxyl groups of poly (vinyl alcohol) and amine and the amide groups of the PAMAM dendrimer. The increase in the number of freeze/thaw cycles raised the polymer crystallite formation expressing hydrogen bonds. They showed that the hydrogels prepared with higher PAMAM dendrimer content demonstrated a faster swelling rate and higher swelling ratios.

1.2. Water Soluble Constructs for Delivery of Anti-cancer Drugs

1.2.1. Cancer

In the 21st century, cancer has still maintained its position as the biggest health problem and cancer-related deaths have the highest proportion of all deaths. In 2012, 14.1 million new cancer cases and 8.2 million cancer-related deaths affected the people all around world [59]. The highest incidence rates are associated with the developed countries of North America and Western Europe. More than 60 % of cancer cases and 70% of cancer-related deaths occur in Africa, Asia, and Central and South America [60]. Lung cancer and prostate cancer had the two highest incidences among men. Among women, breast cancer and colorectal cancer had the two highest incidence numbers (Figure 1.29).

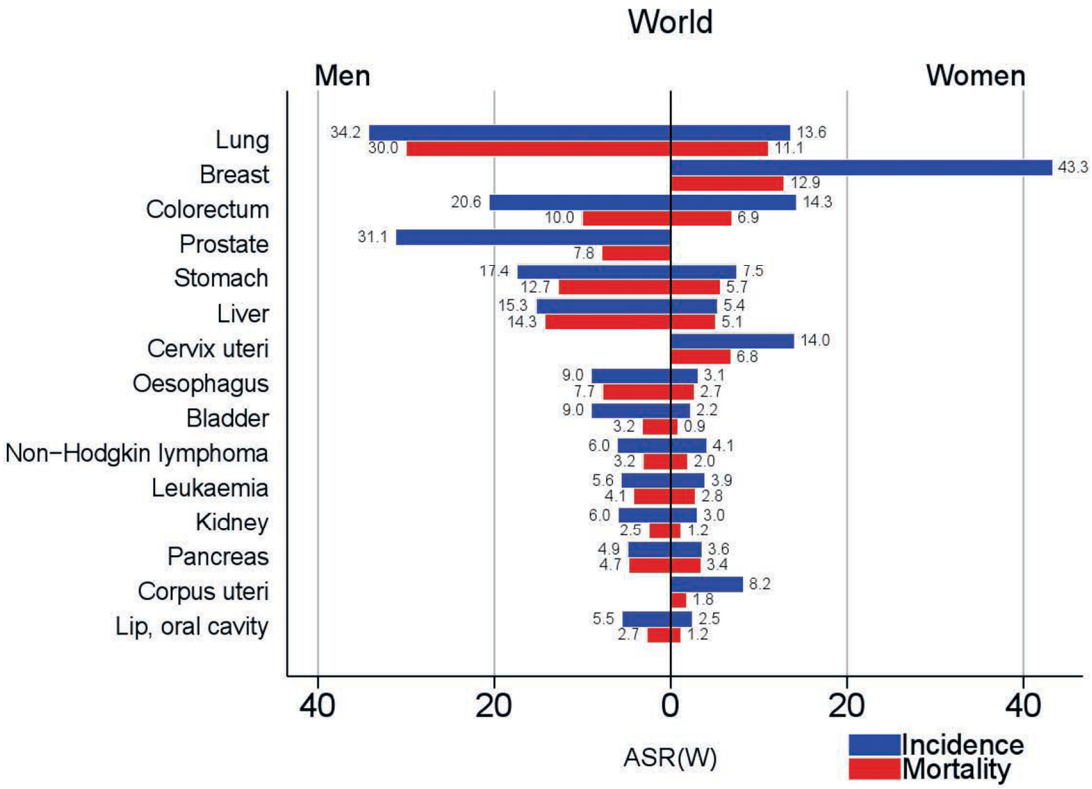


Figure 1.29. World estimated age-standardized cancer incidence and mortality rates (ASR) per 100 000, by major cancer types, in men and women [60].

Cancer is essentially a group of diseases characterized by uncontrolled proliferation and neoplastic transformation of the cells with the potential to invade or spread to other tissues of the body. Normal metabolic activities and environmental factors such as radiation, chemical and biological carcinogens can cause DNA damage, resulting in around 1 million individual molecular lesions per cell in a day [61]. Mostly minor damage in DNA is repaired by DNA repair systems. High levels of damage lead cell death by inducing apoptosis. Thus, organisms would have to protect themselves. The accumulation of DNA damage in the medium level can cause mutations. In the case of cells with damaged DNA cannot control themselves by apoptosis or failed DNA repair processes, irreparable DNA damage may occur, including double-strand breaks and DNA cross-linkages. This can eventually leads rapid and uncontrolled proliferation of cancer cells and formation of tumor tissues (Figure 1.30). During the multistep development of tumors cancer cells acquire six biological capabilities including sustaining proliferative signaling, evading growth suppressors, resisting cell death, enabling replicative immortality, inducing angiogenesis, and activating invasion and metastasis [62].

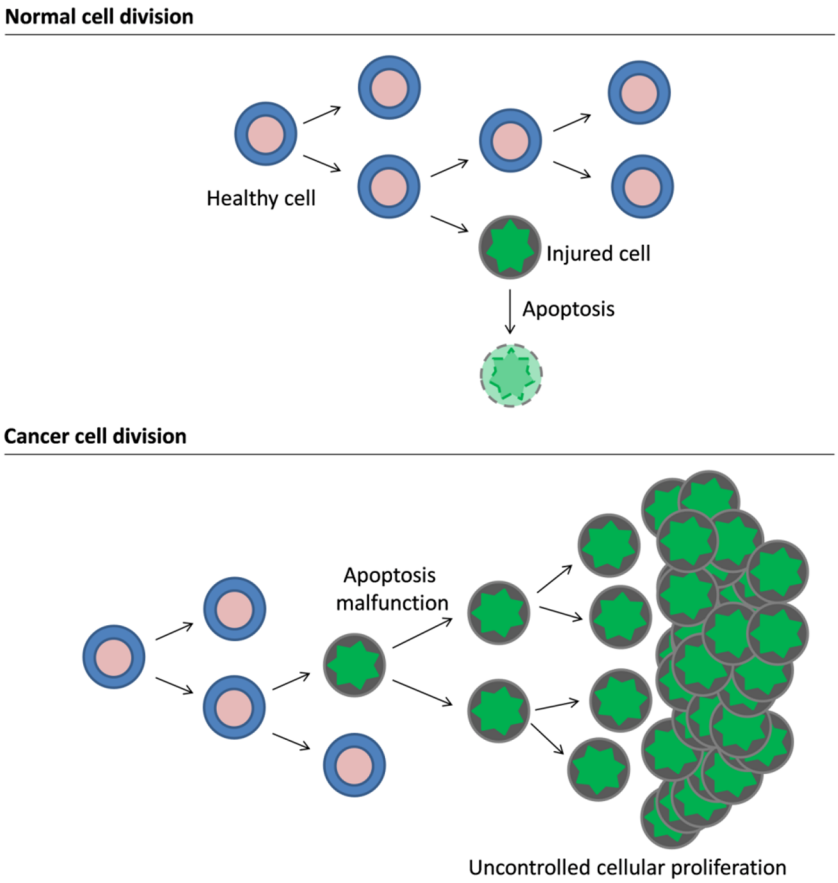


Figure 1.30. Normal and cancer cell divisions.

There are various types of curative treatment modalities for cancer in clinical medicine. Surgery, chemotherapy, radio therapy, hormonal therapy, targeted therapy and immunotherapy are the common treatment methods. There are also other techniques and procedures such as bone marrow transplantation, hyperthermia, photodynamic therapy, laser applications and blood product donation and transfusion. In most cases some of these methods are applied together or consecutively to increase the success of the treatment.

Of all these cancer treatments, chemotherapy has still been an indispensable one which works by killing the cancer cells that divide quickly. Cell division specific chemotherapy agents act on different targets in the process of cell division. These targets are mainly DNA replication and microtubules. Common chemotherapy agents that target DNA replication is given in Table 1.1.

Table 1.1. Chemotherapy agents that target DNA replication [63].

Drug	Therapeutic Applications
Inhibitors of Nucleotide Synthesis	
Methotrexate	Childhood acute lymphoblastic leukemia; Choriocarcinoma; Some lymphomas and solid tumors
Hydroxyurea	Chronic myelogenous leukemia
5-Fluorouracil	gastrointestinal, breast and head and neck carcinomas
DNA Polymerase Inhibitors	
Cytosine Arabinoside	Acute myleocytic leukemia; Childhood leukemia
Gemcitabine	Pancreatic, lung and bladder cancers
DNA-Template Damaging Agents	
Cyclophosphamide	Breast cancer and other carcinomas; Burkitt's lymphoma and other non-Hodgkin's lymphomas
Bleomycin	Testicular and ovarian cancer
Doxorubicin	Carcinomas including breast; Sarcomas including osteogenic; Hodgkin's and non-Hodgkin's lymphomas
Mitomycin C	Cervical, stomach, breast, head and neck, and lung carcinomas
Cisplatin	Testicular and ovarian cancers; Lung, gastric, and bladder carcinomas
DNA Topoisomerase Inhibitors	
Camptothecin	Colon, lung and ovarian carcinomas; Leukemia and gastric cancer
Etoposide	Testicular, lung and gastric cancers; Leukemia and sarcomas
Doxorubicin	Carcinomas including breast; Sarcomas including osteogenic; Hodgkin's and non-Hodgkin's lymphomas
Daunorubicin	Leukemia

Common chemotherapy agents that target microtubules for cancer therapy is given in Table 1.2.

Table 1.2. Chemotherapy agents that target microtubules [64].

Drug	Therapeutic Applications
Microtubule-stabilizing Agents (Taxanes and Epothilones)	
Paclitaxel	Breast cancer, non-small cell lung cancer, ovarian cancer, AIDS-related Kaposi sarcoma
Docetaxel	Breast cancer, non-small cell lung cancer, head and neck cancer, prostate cancer and gastric adenocarcinoma
Cabazitaxel	Metastatic, hormone-resistant prostate cancer
Ixabepilone	Metastatic or locally advanced breast cancer
Microtubule-destabilizing Agents (Vinca alkaloids)	
Eribulin	Recurrent metastatic breast cancer (pre-treated with taxanes and anthracycline)
Vintafolide	In clinical phase II trials as sole treatment for ovarian and lung cancer

Microtubules undergo morphological changes throughout the cell cycle, making them important targets for cancer therapy (Figure 1.31).

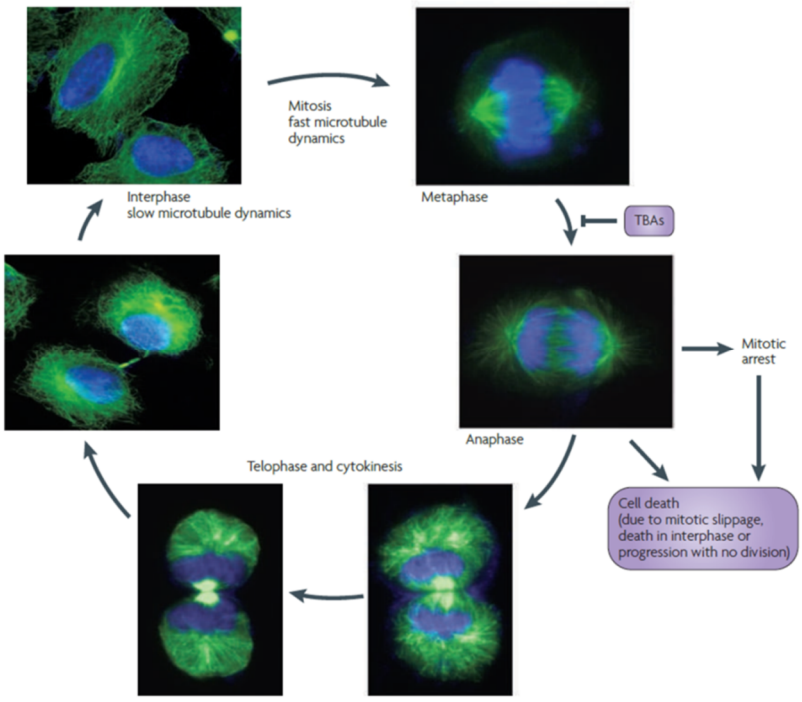


Figure 1.31. Morphological changes in microtubules during cell cycle. DNA is shown in blue, microtubules shown in green. Reprinted by permission from Macmillan Publishers Ltd: Nature [65], Copyright © 2010.

Spindle microtubule dynamics are important factors for cell cycle. Microtubule-destabilizing agents disrupt spindle microtubules by binging to the interface between β- and α-tubulin which results in mitotic arrest and causes cell death. Microtubule-stabilizing agents enhance microtubule polymerization by binding to β-tubulin and prevent depolymerization of spindle microtubules and lead to cell death [64]. The action mechanisms of agents that target microtubules are complex, but their effects on spindle microtubules are similar with stathmin (a destabilizing factor) and microtubule associated proteins (MAPs, stabilizing factors) (Figure 1.32).

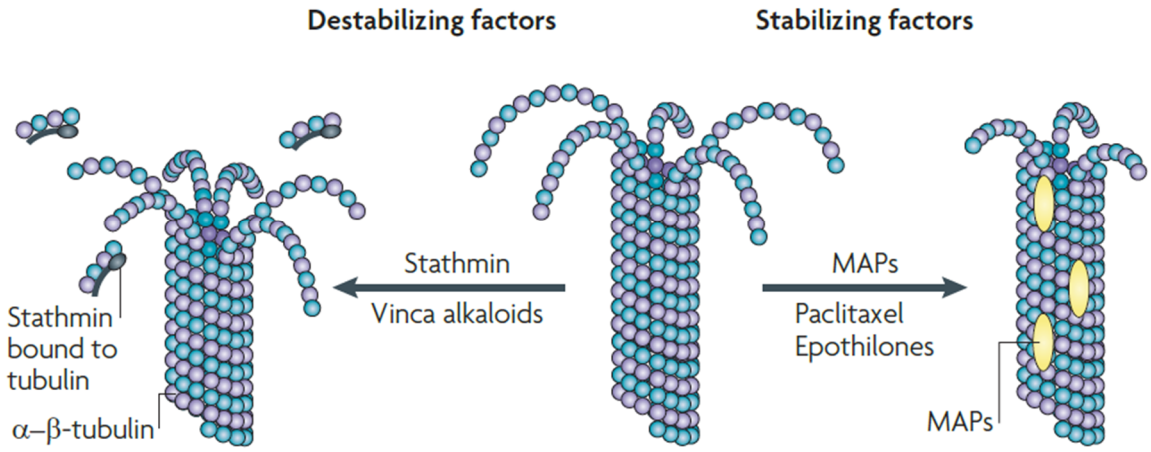


Figure 1.32. Effect of microtubule-stabilizing and microtubule-destabilizing factors and agents on spindle microtubules. Reprinted by permission from Macmillan Publishers Ltd: Nature [65], Copyright © 2010.

Anti-angiogenic drugs possess another strategy for tumor regression. Angiogenesis is formation of new blood capillaries from preexisting ones and have crucial effect on tumor progression and metastasis. Oxygen and nutrients can reach into non-angiogenic solid tumors (1-2 mm^3) by simple diffusion. Oxygen deficiency (cellular hypoxia) begins when the size of a solid tumor reaches 2 mm^3. In the case of cellular hypoxia, cancer cells release pro-angiogenic factors and tumor necrosis factor or stimulate surrounding normal cells to produce angiogenic signaling factors in formation of new blood vessels. This process results in tumor growth and spread of cancer cells to nearby tissues (metastates) [66]. Hence, inhibition of angiogenic factors is a major approach for treatment of various types of cancers which is firstly suggested by Folkman in 1971 [67] (Figure 1.33). The list of FDA approved anti-angiogenic drugs in cancer therapy is given in Table 1.3.

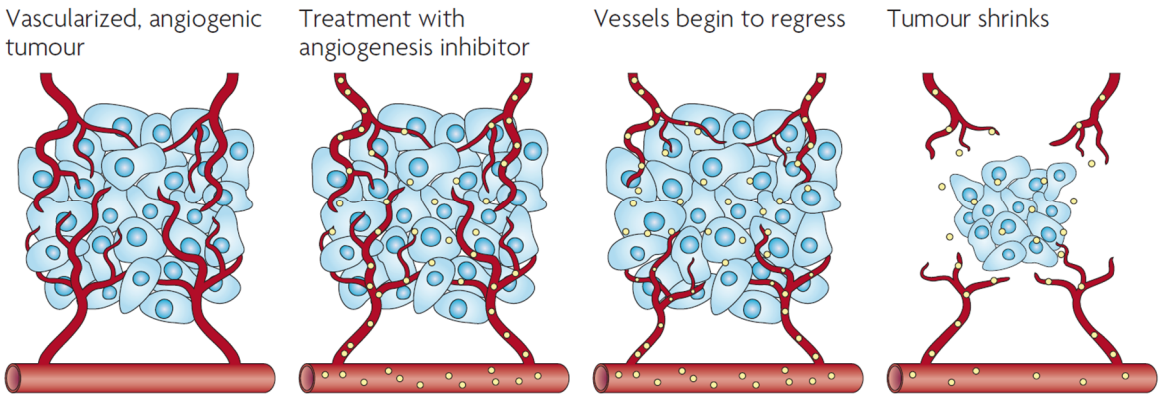


Figure 1.33. The action principle of anti-angiogenic factors. Reprinted by permission from Macmillan Publishers Ltd: Nature [68], Copyright © 2008.

Table 1.3. Anti-angiogenic drugs in cancer treatment [69,70].

Drug	**Therapeutic Applications**
Axitinib (Inlyta)	Kidney cancer
Bevacizumab (Avastin)	Colorectal cancer, kidney cancer, and lung cancer
Bortezomib (Velcade)	Myeloma
Cabozantinib (Cometriq)	Medullary thyroid cancer
Cetuximab (Erbitux)	Metastatic colorectal cancer
Everolimus (Afinitor)	Kidney and breast cancer, and pancreatic carcinoma
Erlotinib (Tarceva)	Unresectable or metastatic pancreatic carcinoma
Lenalidomide (Revlimid)	Multiple myeloma, Hodgkin's lymphoma
Panitumumab (Vectibix)	Metastatic colorectal carcinoma
Pazopanib (Votrient)	Kidney cancer and advanced soft tissue sarcoma
Ramucirumab (Cyramza)	Stomach cancer, colorectal and non-small cell lung cancers
Regorafenib (Stivarga)	Colorectal cancer and gastrointestinal stromal tumor
Sorafenib (Nexavar)	Kidney cancer, liver cancer, and thyroid cancer
Sunitinib (Sutent)	Kidney cancer, PNET, and gastrointestinal stromal tumor
Thalidomide (Synovir)	Multiple myeloma
Trastuzumab (Herceptin)	Breast cancer
Vandetanib (Caprelsa)	Medullary thyroid cancer
Ziv-aflibercept (Zaltrap)	Colorectal cancer

1.2.2. Polymer Therapeutics in Cancer Treatment

Traditional chemotherapy is considered a systemic therapy and it can affect entire body. Therefore, damaging also healthy cells is an ineluctable consequence of traditional chemotherapy. Mainly white and red blood cells, platelets and the cells that lining mouth, heart, intestines, stomach and hair follicles are predominantly affected by the chemotherapy agents. Thus, chemotherapy agents can cause several systemic side effects such as neutropenia, anemia, thrombocytopenia, diarrhea, nausea, alopecia and cardiotoxicity. Such drawbacks limit the dose amount of chemotherapy agents in clinical use. Moreover, having hydrophobic nature, many chemotherapy drugs need to be dosed to the patients with some chemicals having side effects, to facilitate the dissolution by creating the water complex, resulting in certain restrictions on the exercise of these drugs [71,72].

Conjugation of chemotherapy drugs with high molecular weight water soluble polymers is commonly used to eliminate drawbacks and to increase the efficacy of the active agent. This strategy helps to increase the solubility of hydrophobic drugs and to improve the pharmacokinetic profile of the agent. Moreover, surrounding polymer chains provide protection against enzymatic degradation due to steric hindrance and prevention of immunogenicity. Commonly used water soluble polymers in polymer therapeutics are poly(ethylene glycol) (PEG), poly(hydroxypropyl methacrylate) (HPMA) and poly(glycolic acid) (PGA) (Figure 1.34).

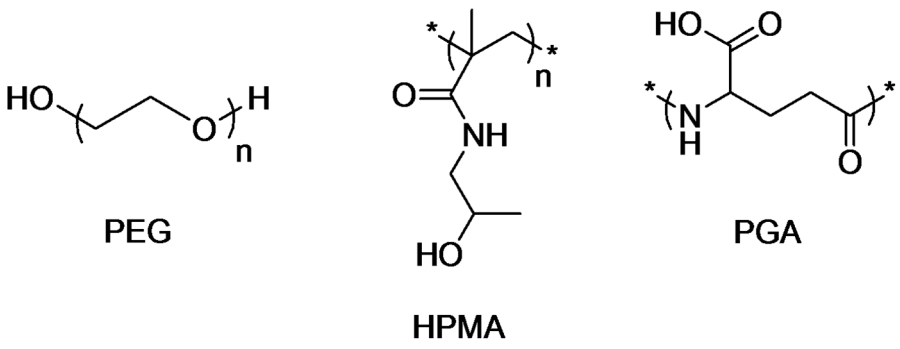


Figure 1.34. Commonly used water soluble polymers in polymer therapeutics.

Chemotherapy agents are relatively small molecules as compared with the macromolecular therapeutics. They can move in the tumor tissue in scattered layout, as well as through endothelial cells of healthy tissues. However, progress towards healthy cells into the tissue of large molecules such as polymers, above a certain molecular weight, is very difficult. Since tumor vessels are defective, permeability of such macromolecules is enhanced through newly formed vasculature in tumor mass. This fact is known as the "Enhanced Permeability and Retention Effect" (EPR effect) [73]. This effect provides a passive targeting of macromolecules to the tumor tissue. The general scheme for EPR effect was illustrated in Figure 1.35.

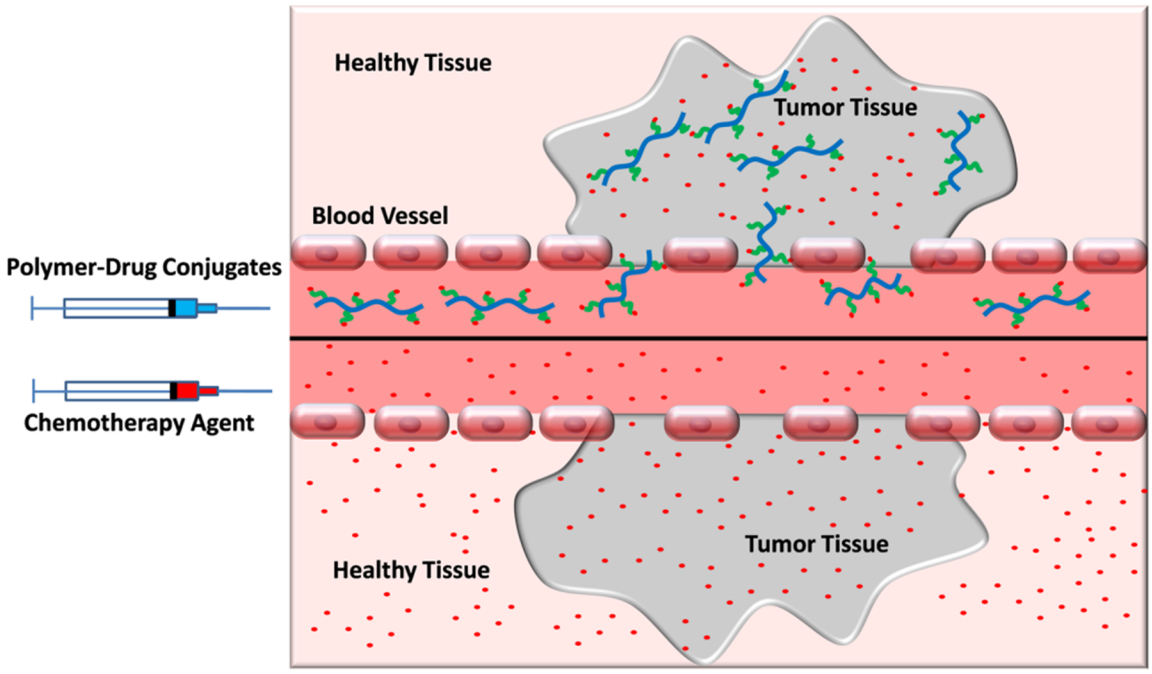


Figure 1.35. EPR effect for polymer therapeutics.

Chemotherapy agents are biologically inactive in the bloodstream when they covalently attached to the polymer backbone. This strategy helps to avoid the several side effects of the active agent. The linker between polymer backbone and the chemotherapy agent has a significant role to release the agent in its active structure at the target tissue [74]. Enzymatically cleavable [75] or pH-sensitive [76,77] linkers are preferred in polymer based drug carrier systems due to the acidic microenvironment and some over expressed enzymes in the tumor tissue. [75,78]. The list of commonly used labile linkers for polymer therapeutics is given in Figure 1.36.

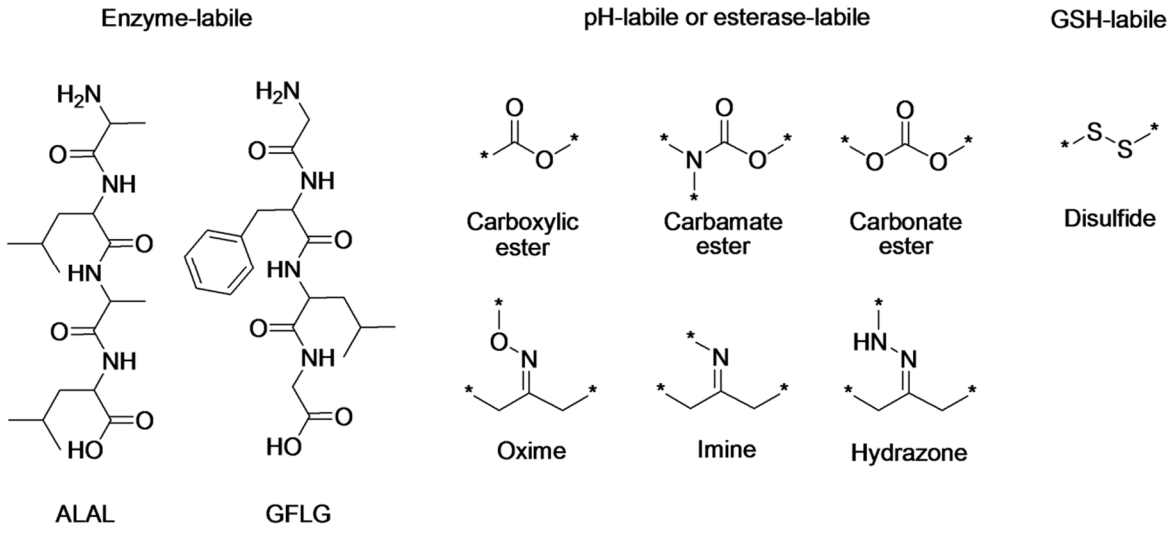


Figure 1.36. Commonly used extracellular and intracellular stimuli-labile linkers in polymer therapeutics [79].

Upregulation of several receptors in tumor tissue inspired scientist to design ligand type of constructs for the delivery of chemotherapy agents. Using targeting moieties which have high affinity to specific receptors in tumor tissue is an attractive approach to increase the targeting efficiency of the passive targeting provided by EPR effect [80]. As an example, a tripeptide RDG (Arg-Gly-Asp) sequence selectively binds to α_v-β_3 integrin receptors overexpressed in tumor tissues [81]. Researchers suggested that cyclized RGD binds to α_v-β_3 integrin receptors about 40-fold more avidly.

There are various studies which benefits from the strong and selective binding nature of these kinds of specific ligands for active targeting of drug delivery systems [82,83]. Most of the upregulated integrins in tumor tissue are also responsible for the cell to cell or cell to extracellular matrix adhesion mechanisms which is an important step for the growth of the tumor tissue. Therefore, integrin binding (signaling) inhibitors have a crucial role in anti-cancer therapy. There are different integrin targeted compounds for various tumor types in clinical trials (Table 1.4).

Table 1.4. Integrin binding ligands for anti-cancer therapy in clinical trials [84].

Compound	Target	Cancer Type
Vitaxin/etaracizumab	αvβ3	Solid tumors, melanoma, colorectal cancer, small intestine cancer, lymphoma, prostate cancer
CTNO 95	αv integrins	Solid tumors, lymphoma, prostate cancer
Cilengitide (cRGD)	αvβ3, αvβ5	Lung cancer, prostate cancer, melanoma
Volociximab	αvβ1	Solid tumors, melanoma, ovarian cancer, renal cancer, pancreatic cancer, lung cancer
ATN-161 PHSRN mimetic	αvβ1 and other fibronectin-binding	Solid tumors, renal cell carcinoma, brain and CNS tumors
PF-00562271	FAK, Pyk2	Pancreatic cancer, prostate cancer, head and neck cancer
GSK22566098	FAK, Pyk2	Solid tumors
PF-04554878	FAK, Pyk2	Metastatic nonhematologic tumors
VS-4718	FAK, Pyk2	Metastatic nonhematologic tumors
VS-6063	FAK, Pyk2	ovarian cancer

1.2.3. Polymer Drug Conjugates

Anti-tumor agents are rapidly distributed in the body due to their relatively small size as compared with polymers. As a result of the small size, they also exhibit fast renal clearance which results in short durations of activity and considerable dissipation. Only a very small amount of injected drug can reach to the cancer cells. By conjugating anti-tumor agents with water soluble polymers having high molecular weights, solubility, bioavailability and pharmacokinetic profiles can be improved. An additional contribution of conjugation with water soluble polymers is providing a passive targeting through EPR effect due to the physiology of the tumor tissues with disorganized vasculature and poor lymphatic drainage.

The first covalent conjugation approach of drug molecules to a polymer backbone was performed by Ringsdorf in 1975 [85,86]. He successfully showed the release of the attached drug molecules through cleavable linker. Then, this approach received immediate attention and first synthetic N-(2-hydroxypropyl)methacrylamide (HPMA) based polymer drug conjugate was developed by Kopecek and Duncan in the late 1970s [87,88]. Over the last two decades, the interest in conjugation strategy of biologically active agents with polymers has increased remarkably due to the passive accumulation of such conjugates in tumor tissues and reduced systemic side effects. There are various types of polymer drug conjugates on the market (Table 1.5) and clinical trials (Table 1.6) thanks to the efforts of the scientist.

Table 1.5. Polymer drug conjugates available in the market [89].

Conjugate	**Indication**	**Marketing year**	**Company**
PEG-adenosine deaminase (Adagen)	SCID syndrome	1990	Enzon
PEG-asparaginase (Oncaspar)	Acute lymphplastic leukaemia	1994	Enzon
SMANCS (Zinostatin Stimalamer)	Hepatocellular carsinoma	1993	Yamanouchi Pharmaceutical
Linear PEG-interferon a2b (PEG-intron)	Hepatitis C, clinical evaluation on cancer, multiple sclerosis and	2000	Schering Plough/Enzon
Branched PEG-interferon a2a (Pegasys)	Hepatitis C	2002	Roche/Nektar
PEG–growth hormone receptor antagonist	Acromegaly	2002	Pfizer (Pharmacia)
PEG–G-CSF (Pegfilgrastim, Neulasta)	Prevention of neutropenia associated with cancer chemotherapy	2002	Amgen
Branched PEG–anti-VEGF aptamer	Age-related macular degeneration	2004	OSI Pharmaceutical/Pfizer
PEG–anti-TNF Fab	Rheumatoid arthritis and Crohn's disease	2008	UCB (formerly Celltech)

Table 1.6. Polymer drug conjugates in clinical trials [90].

Conjugates	Drug name	Company	Indication	Status
PEG-naloxol	NKTR-118	Nektar	Opioid-induced constipation	Phase III
PEG-irinotecan	NKTR-102	Nektar	Solid tumor	Phase III/II
PEG-SN38	EZN-2208	Enzon	Solid tumor	Phase II
PEG-docetaxel	NKTR-105	Nektar	Solid tumor	Phase I
PHPMA-doxorubicin	PK1 (FCE28068)	Pfizer	Breast cancer, lung cancer, colorectal cancer	Phase II
PHPMA-platinum	AP5280	Access Pharmaceuticals	Various malignancies	Phase II
PHPMA-DACH-oxaliplatin	ProLindac™ (AP5346)	Access Pharmaceuticals	Ovarian cancer	Phase II
Fleximer®-camptothecin	XMT-1001	Mersana	Gastric cancer, lung cancer	Phase I
Carboxymethyl dextran-T2513	Delimotecan (MEN 4901/T-0128)	Daiichi Pharmaceuticals	Various malignancies	Phase I
Cyclodextrin-camptothecin	CRLX101	Cerulean	Advance solid tumor	Phase IIa
Polyglutamic acid-paclitaxel	Xyotax™, Opaxio™, CT-2103	Cell Therapeutics	Lung cancer, ovarian cancer	Phase III
Polyglutamic acid-camptothecin	CT-2106	Cell Therapeutics	Colon cancer, ovarian cancer	Phase I/II

Molecular weight of a polymer is the most important feature that determines the half-life of the polymer in the blood stream. Ikada and co-workers reported the effect of molecular weight of PEG on pharmacokinetic profile via an *in vivo* study. The results showed that polymers with higher molecular weights were able to circulate longer in blood stream due to the delayed renal clearance [91] (Figure 1.37).

Plasma half-life values of the polymers were also improved at least 1000-fold through the increase in molecular weight [91]. It was reported that accumulation through EPR effect with polymers having molecular weights around their renal clearance threshold (40–45 kDa) is as effective as their higher molecular weight analogues [73,93].

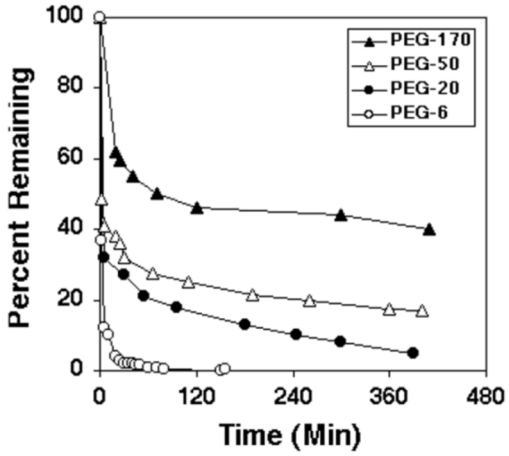


Figure 1.37. Molecular weight dependent plasma concentration profiles of PEG polymers with molecular weights ranging from 6 - 170 kDA [91,92].

As a consequence of conjugating hydrophobic drug molecules to water soluble polymers, drug loading capacity versus and water solubility has become an inherent dilemma in the design of polymer drug conjugates. Above certain drug content the stealth capability of the conjugates were also affected because of exceeding the limits of the required polymer ratio necessary to surround the active agents. Therefore, in most polymer drug conjugates the drug ratio is less than 10 % by weight [94]. For example, Veronese, Duncan and co-workers have conjugated PEG and doxorubicin via various enzymatically cleavable linkers using PEG with different molecular weights ranging from 5 to 20 kDA (Figure 1.38). The doxorubicin contents of the conjugates lied between 2.7–8.0 % by weight [95].

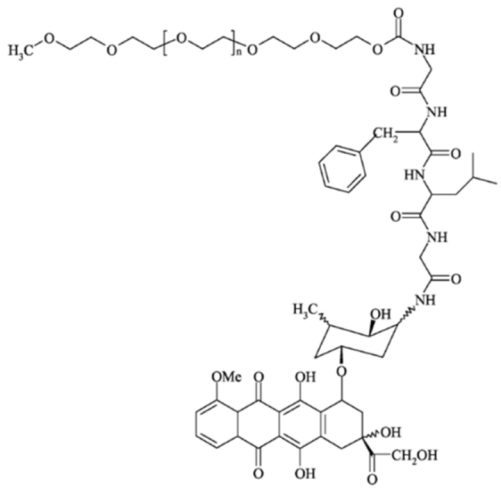


Figure 1.38. Structure of the PEG doxorubicin conjugate with a peptide linker. Reprinted with permission from [95], Copyright © 2005 American Chemical Society.

In another study, instead of linear PEG, Pasut and Veronese designed four-armed PEG-SN38 polymer drug conjugates using different architecture by coupling SN38 to four-armed PEGs with molecular weight of 40 kDa (Figure 1.39). The drug content of the conjugates was but only of 3.7 % by weight [96].

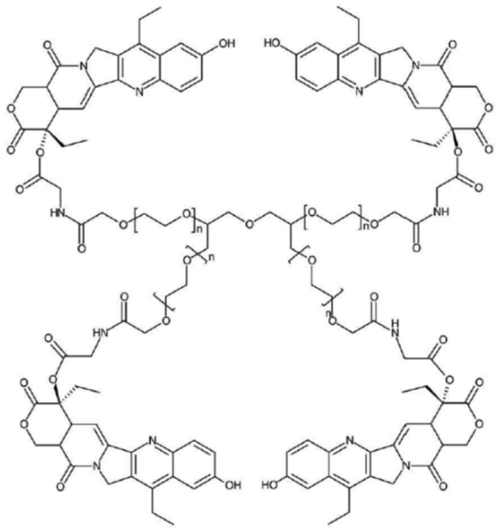


Figure 1.39. Four-armed PEG-SN38 polymer drug conjugate. Reprinted with permission from [96], Copyright © 2009 Elsevier B. V.

Ghandehari and co-workers designed a small library of HPMA-Docetaxel polymer drug conjugates with an enzymatically cleavable GFLG linker (Figure 1.40).

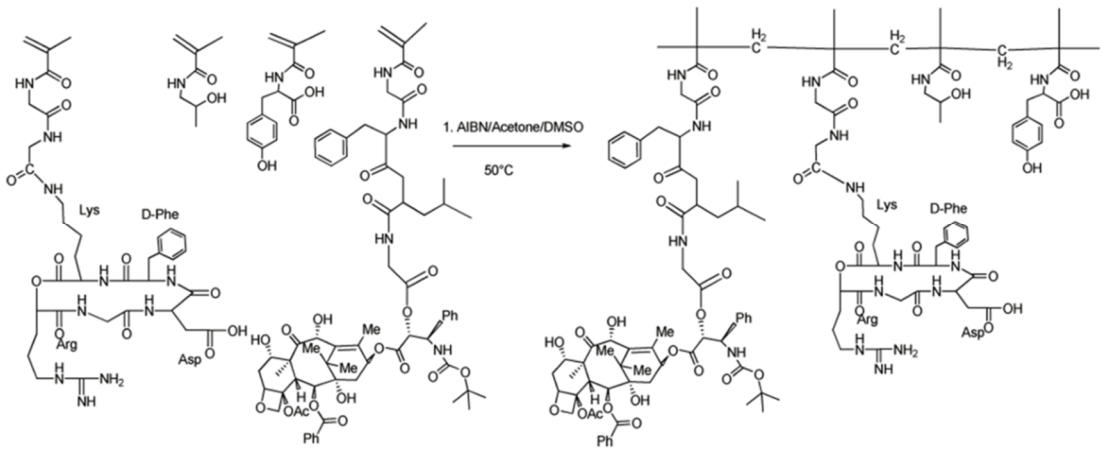


Figure 1.40. Synthesis of HPMA-Docetaxel polymer drug conjugate with GFLG linker cRGDfK targeting moiety. Reprinted with permission from [97], Copyright © 2011 American Chemical Society.

They prepared polymer drug conjugates with different molecular weights and with/without a targeting moiety (cRDGfK) to compare anti-tumor effect of molecular weight and contribution of targeting group on DU145 prostate tumor xenografts [97]. The drug contents of the conjugates were recorded between 6.80 - 7.15 % by weight. They reported that non-targeted conjugate with high molecular weight (87.1 kDa) and targeted conjugate with low molecular weight (26.9 kDa) showed improved anti-tumor efficacy compared to free Docetaxel. Although non-targeted conjugate with low molecular weight (32.6 kDa) exhibited an anti-tumor efficacy when compared with saline group, its effect was not superior to free Docetaxel at tested doses of 20 and 40 mg/kg (Figure 1.41).

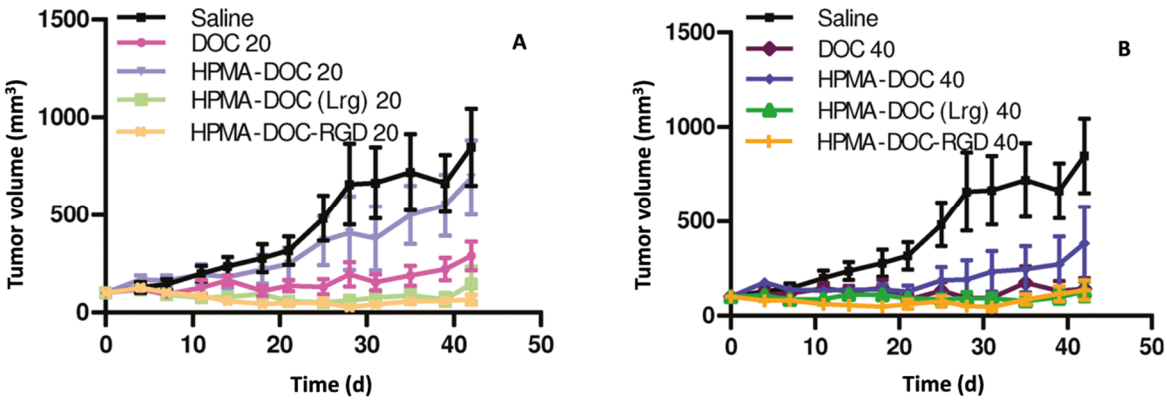


Figure 1.41. Molecular weight and targeting effect on anti-tumor efficacy of HPMA-Docetaxel conjugates at different dose administration (Panel A, 20 mg/kg; panel B, 40 mg/kg). Adapted with permission from [97], Copyright © 2011 American Chemical Society.

Etrych and co-workers were synthesized HPMA-Docetaxel conjugates with pH-labile spacer stable under physiological conditions (pH 7.4) and degradable in mild acidic environments (pH 5.0) [98]. They designed polymer drug conjugates to achieve prolonged blood circulation and sustained release of the drug molecules in tumor tissue. Hydrolytic cleavage of the spacer was provided by the carbonyl group of the drug derivative and the hydrazine group on the side chains of the polymer (Figure 1.42). They reported faster release of the drug molecules from the polymer backbone at pH 5.0 than at pH 7.4. HPMA-Docetaxel conjugates containing acylated with levulic acid (LEV) linker were tested for their anti-tumor activity over EL4 T cell lymphoma *in vivo* model. HPMA-Docetaxel conjugate demonstrated high anti-tumor activity (Figure 1.43).

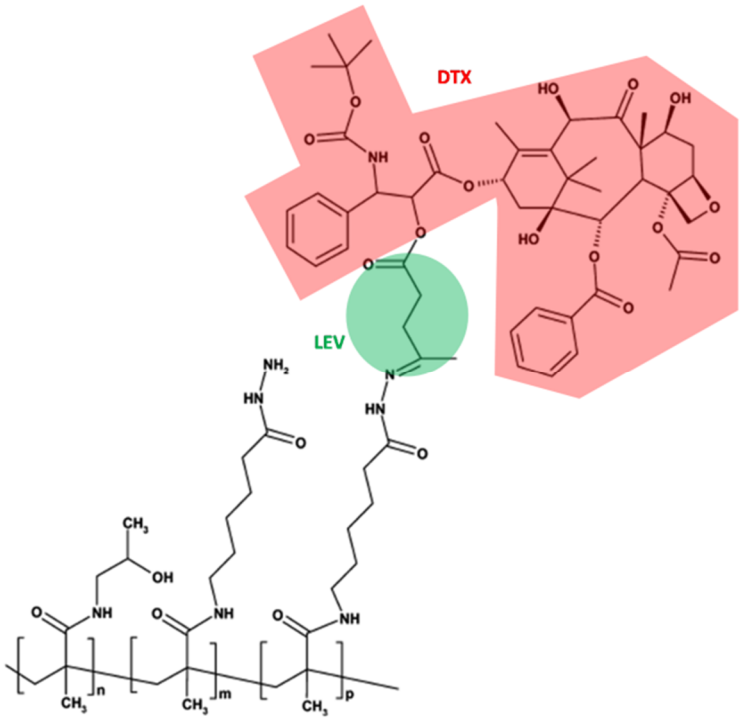


Figure 1.42. Structure of HPMA-Docetaxel conjugates with a pH sensitive linker. Adapted with permission from [98], Copyright © 2010 American Chemical Society.

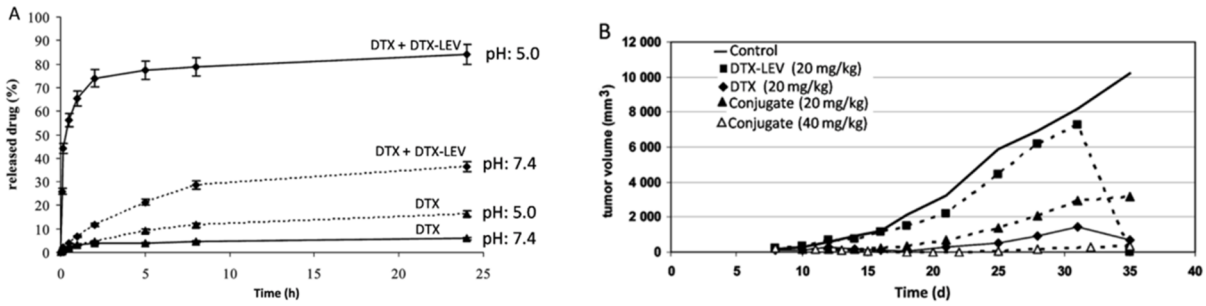


Figure 1.43. Drug release profile (panel A) and anti-tumor efficacy (panel B) of HPMA-Docetaxel conjugates at different dose administration (20 mg/kg and 40 mg/kg). Adapted with permission from [98], Copyright © 2010 American Chemical Society.

Some polymer drug conjugates have high drug contents. For instance, researchers developed L-glutamic acid based PGA-Paclitaxel polymer drug conjugate (XYOTAX^{TM}) with a drug content of approximately 37 % by weight [99]. The chemical structure of the conjugate is given in Figure 1.44.

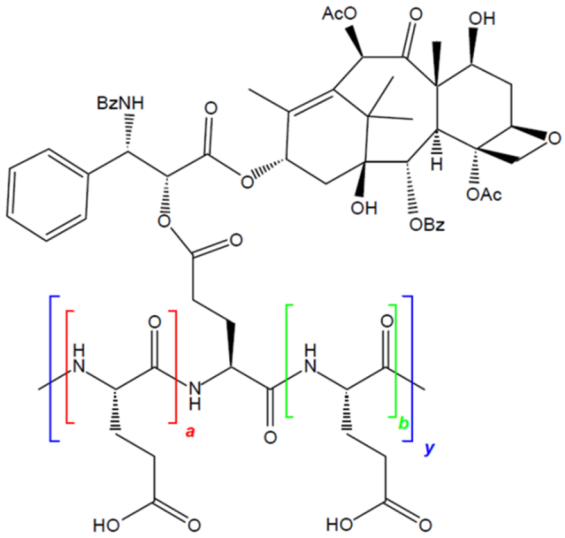


Figure 1.44. Structure of PGA-Paclitaxel Conjugate. Adapted with permission from [99], Copyright © 2005 Elsevier B. V.

It was reported that the conjugate is highly water-soluble although the high drug content. Unlike traditional non-degradable polymers such as PEG and HPMA, its breakdown product L-glutamic acid is not excreted by the kidney and enters cellular metabolism. Preclinical studies demonstrated that anti-tumor activity of PGA-Paclitaxel conjugate is superior to standard paclitaxel. The pharmacokinetic studies showed that PGA-Paclitaxel conjugate prolonged the half-life of free paclitaxel (Figure 1.45, Panel A).

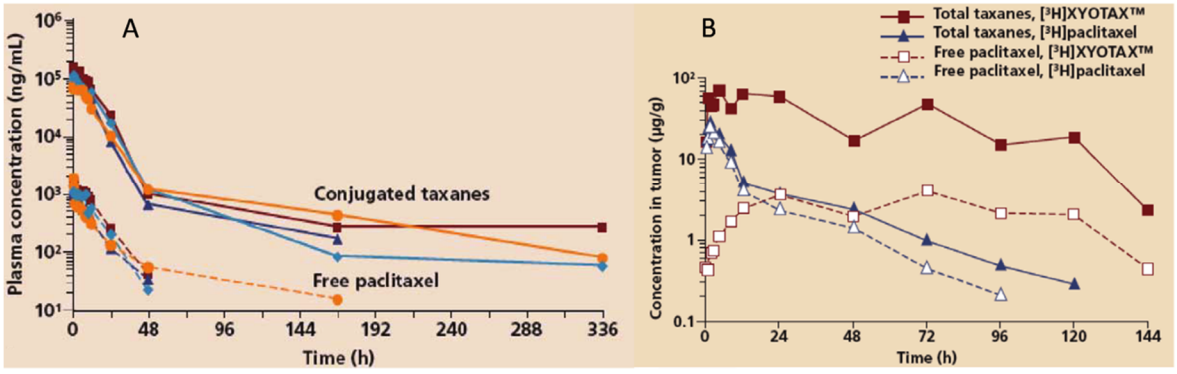


Figure 1.45. Plasma concentration of taxanes and free paclitaxel after administration of PGA-Paclitaxel and free paclitaxel in four representative patients (Panel A). Tumor concentration of total taxanes and free paclitaxel after the administration of tritium-labeled PGA-Paclitaxel or free paclitaxel (Panel B). Adapted with permission from [99], Copyright © 2005 Elsevier B. V.

The conjugate also showed a volume of distribution approximately equal to blood volume. Preclinical data showed the accumulation of PGA-Paclitaxel conjugate in tumor tissue through EPR effect and slow and progressive release of paclitaxel (Figure 1.45, Panel B). Phase I and II clinical studies showed that PGA-Paclitaxel conjugate reduced systemic side effects of standard taxanes such as neutropenia and alopecia and allowed more convenient administration schedule.

1.2.4. Polymeric Micellar Type Nanoparticles

Since the discovery of the enhanced permeability and retention (EPR) effect, macromolecules with long blood circulation have become the primary substances for drug delivery due to improved accumulation in tumors through fenestrated blood vessels [100].

Table 1.7. Clinically approved nanoparticles in cancer therapy [103].

Name	Particle type/drug	Indication	Approval (year)	Company
Doxil/Caelyx	Liposomal doxorubicin (PEGylated)	Ovarian cancer HIV-associated Kaposi's sarcoma Multiple myeloma	FDA (1995) EMA (1996)	Janssen
DaunoXome	Liposomal daunorubicin (non-PEGylated)	HIV-associated Kaposi's sarcoma	FDA (1996)	Galen
Myocet	Liposomal doxorubicin (non-PEGylated)	Treatment of metastatic breast cancer	EMA (2000)	Teva UK
Abraxane	Albumin-particle bound paclitaxel	Advanced nonsmall cell lung cancer Metastatic breast cancer Metastatic pancreatic cancer	FDA (2005) EMA (2008)	Celgene
Marqibo	Liposomal vincristine (non-PEGylated)	Philadelphia chromosome-negative acute lymphoblastic leukemia	FDA (2012)	Spectrum
MEPACT	Liposomal mifamurtide (non-PEGylated)	Treatment for osteosarcoma	EMA (2009)	Millennium
Onivyde MM-398	Liposomal irinotecan (PEGylated)	Metastatic pancreatic cancer	FDA (2015)	Merrimack

Likewise other biocompatible macromolecules, there have been great interest on nanoparticles in drug delivery systems for cancer disease mainly due to their body distribution properties [101,102]. There have been several nanoparticle drug formulations approved by authorized institutions for cancer therapy (Table 1.7).

Table 1.8. Polymeric nanoparticles in clinical trials for cancer therapy [103].

Name	Particle type/drug	Indication	Company	Status
AZD2811	Aurora B kinase inhibitor polymer particle accurin	Advanced solid tumors	AstraZeneca with BIND Therapeutics	Phase I
BIND-014	PSMA targeted docetaxel PEG-PLGA or PLA-PEG particle	Prostate, metastatic, nonsmall cell lung, cervical, head and neck, or KRAS	BIND Therapeutics	Phase I/II
Cynviloq IG-001	Paclitaxel polymeric micelle nanoparticle	Breast cancer	Sorrento	Phase I
Genexol-PM	Paclitaxel polymeric micelle nanoparticle	Head and neck or breast cancer	Samyang Biopharmaceuticals	Phase II/IV
NC-6004 Nanoplatin	Polyamino acid, PEG, and cisplatin derivative micellar nanoparticle	Advanced solid tumors, lung, biliary, bladder, or pancreatic cancers	Nanocarrier	Phase I/II/III
NC-4016 DACH-Platin micelle	Polyamino acid, PEG, and oxaliplatin nanoparticle	Advanced solid tumors or lymphomas	Nanocarrier	Phase I
NK105	Paclitaxel micelle	Breast cancer	Nippon Kayaku	Phase III
Docetaxel-PM DOPNP201	Docetaxel micelle	Head and neck cancer and advanced solid tumors	Samyang Biopharmaceuticals	Phase I/II
CriPec	Docetaxel micelle	Solid tumors	Cristal Therapeutics	Phase I
CRLX101	Cyclodextrin based nanoparticle camptothecin conjugate	Ovarian, renal cell, small cell lung, or rectal cancers	Cerulean	Phase I/II
CRLX301	Cyclodextrin based nanoparticle docetaxel conjugate	Dose escalation study in advanced solid tumors	Cerulean	Phase I/II

Eisenberg and coworkers demonstrated the first example of self-assembly of asymmetric copolymers in solutions in the 1990s [104,105]. Then, there have been focused attention on amphiphilic block copolymers having polymer blocks with different physical and chemical properties to generate polymeric nanoparticles via self-assembly [106,107]. There are various types of polymeric nanoparticle drug formulations in clinical trials for cancer therapy (Table 1.8).

There are different types of techniques for the preparation of polymeric nanoparticles [108,109]. Self-assembly of polymeric compounds is an attractive method for micellar type polymeric nanoparticle formation.

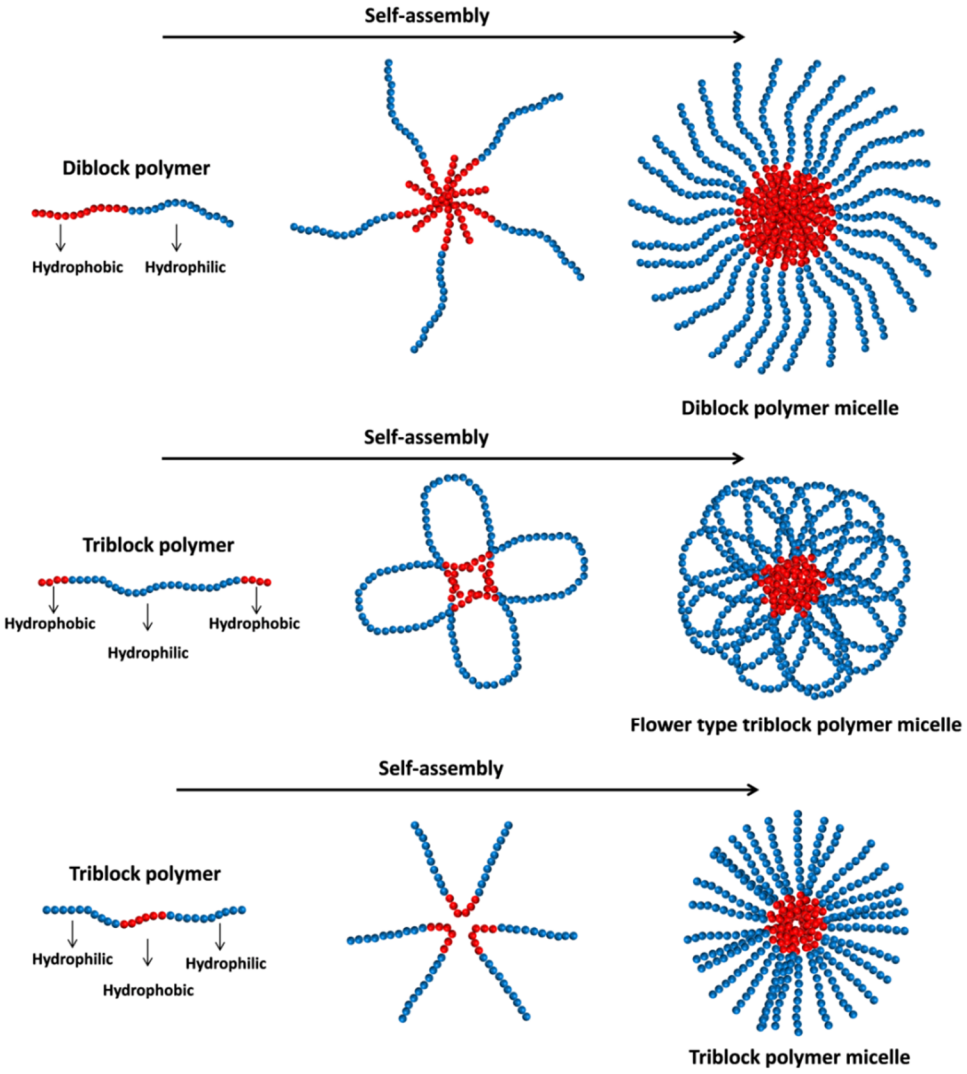


Figure 1.46. General scheme for formation of block copolymer micelles through self-assembly in aqueous solutions.

Polymeric micelles are composed of two different domains, a drug loading hydrophobic core and hydrophilic shell. As seen in Figure 1.44 amphiphilic diblock or triblock copolymers having hydrophilic and hydrophobic domains form micellar type polymeric nanoparticles through self-assembly due to hydrophobic interactions in aqueous solutions. Water-insoluble drug loading into hydrophobic core of polymeric micelles can be achieved during or after formation of self-assembly. Although, significant advances in overcoming cellular barriers such as specific targeting to cancer cells, enhanced cellular uptake, endosome escapes, and controlled drug release have been made, many challenges still remains. For example, the nanoparticles generally accumulate in the major organs such as liver, spleens and kidney. Only a small percentage can accumulate in tumor tissue. Therefore, high tumor accumulation is arguably the most challenging barrier in cancer drug delivery. There have been great efforts to provide high tumor accumulation of polymeric nanoparticles. For example, Nishiyama, Kataoka and co-workers designed a series of diblock polymer micelles via self-assembly of PEG-b-poly-(L-glutamic acid) and oxaliplatin in treatment of brain tumors [83].

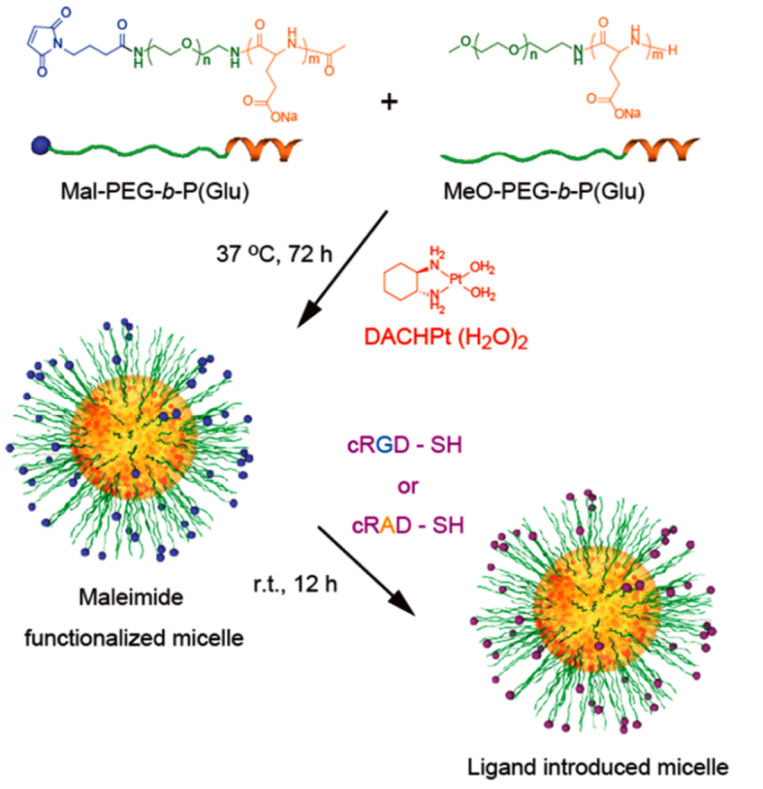


Figure 1.47. Formation of ligand introduced micellar type diblock polymer micelles. Adapted with permission from [83]. Copyright © 2013 American Chemical Society.

Modification of particles for active targeting was obtained by partial using of maleimide functionalized PEG-b-poly-(L-glutamic acid) in nanoparticle precursor mixture and attachment of thiol modified targeting unit (cRGD-SH) (Figure 1.47). To evaluate the targeting efficiency of the particles they also prepared particles with non-targetable cRAD-SH. They showed that cRGD introduced micelles exhibited anti-tumor effect compared to the ones with non-targetable cRAD. They concluded that this strategy is an efficient targeted therapy of glioblastoma beyond the blood-brain tumor barrier (Figure 1.48).

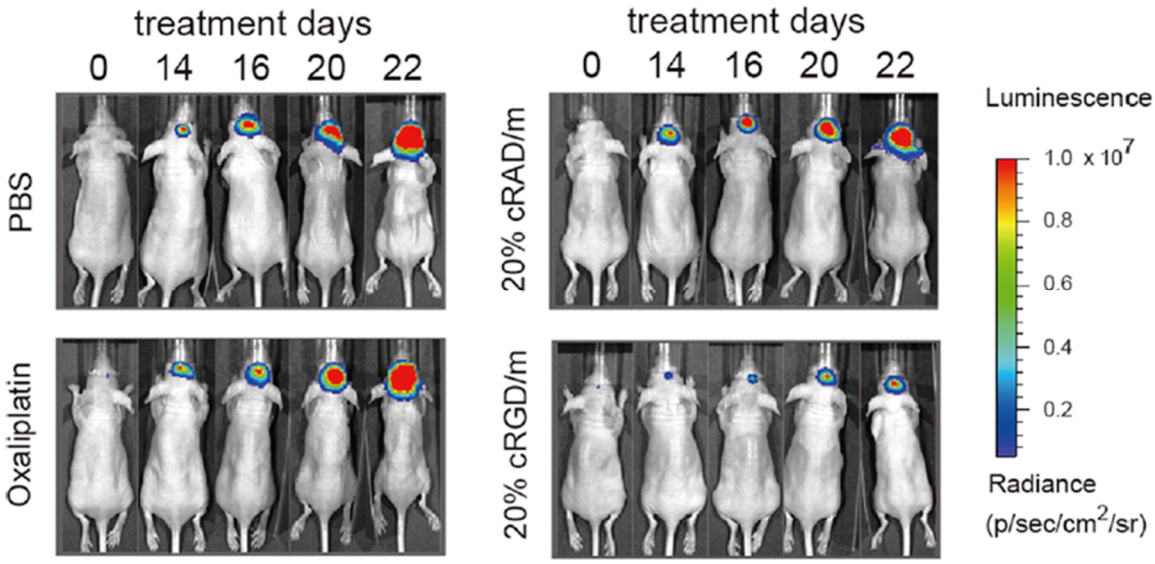


Figure 1.48. Anti-tumor effect of targeted polymeric particles. Luminescence intensity shows tumor regression. Adapted with permission from [83]. Copyright © 2013 American Chemical Society.

Controlled and sustained release of the drug molecules is also an important issue for polymeric nanoparticle drug formulations. Covalent attachment of drug molecules into the core of the particles via cleavable linkers is an approach response to this need. This concept can be useful most of anti-cancer drugs. In a recent study, Sanyal and co-workers prepared flower type triblock polymer micelles composed of dendron-linear polymer-dendron conjugates [110]. Dendron segment at both side of the block copolymer provided attachment of multiple drug molecules via an ester linker to reach high drug content. Covalent attachment combretastatine-A4 (an anti-angiogenic small drug molecule in clinical trials) was achieved by copper-catalyzed azide-alkyne cycloaddition (CuAAC) reaction between alkyne groups at the periphery of the dendron segments and azide

functionalized combretastatine-A4. They successfully showed internalization of the drug molecules into human umbilical vein endothelial cells (HUVECs) and sustained release of the drug molecules via *in vitro* experiments (Figure 1.49).

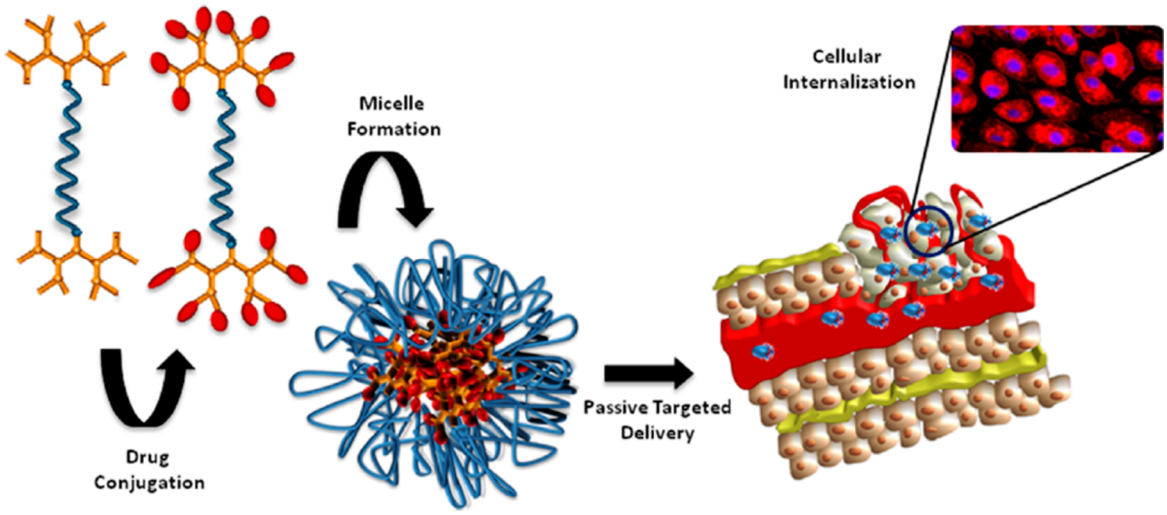


Figure 1.49. Combretastatin–A4 attached flower type triblock micelles and their cell internalization. Reprinted with permission from [110]. Copyright © 2016 American Chemical Society.

Combined therapy or in other words dual therapy is another approach for designing anti-cancer drug formulations using different drug molecules having different or synergistic effects over tumor regression. Polymeric nanoparticles are ideal materials when designed accordingly for this kind of approaches. A recent example was published by Xiao, Zhang and co-workers [111]. They developed hypoxia responsive prodrug micelles for the release of anti-angiogenic (Combretastatin-A4) and anti-mitotic (doxorubicin) drug molecules to hypoxic tumor cells in a combined way. Combretastatin-A4 was attached to a linear PEG-maleimide via a azobenzene (AZO) linker conjugated with 1,6-hexanedithiol. Obtained polymer drug conjugate (PEG–C6–AZO–CA4) was used formation of polymeric micelles. Doxorubicin solution in DMSO was introduced to micelle precursor solution in water and as a result of self-assembly in aqueous conditions doxorubicin was encapsulated into the hydrophobic core of the micelles via hydrophobic interactions. They examined release kinetics of the drug molecules introduced in hypoxic tumor cells. Results showed successful hypoxy trigger release of Combretastatin-A4 thanks to the AZO linker and release of doxorubicin under hypoxic conditions (Figure 1.50). They concluded that this

hypoxy trigger release mechanism would be a useful approach for nanomedicinal cancer treatment.

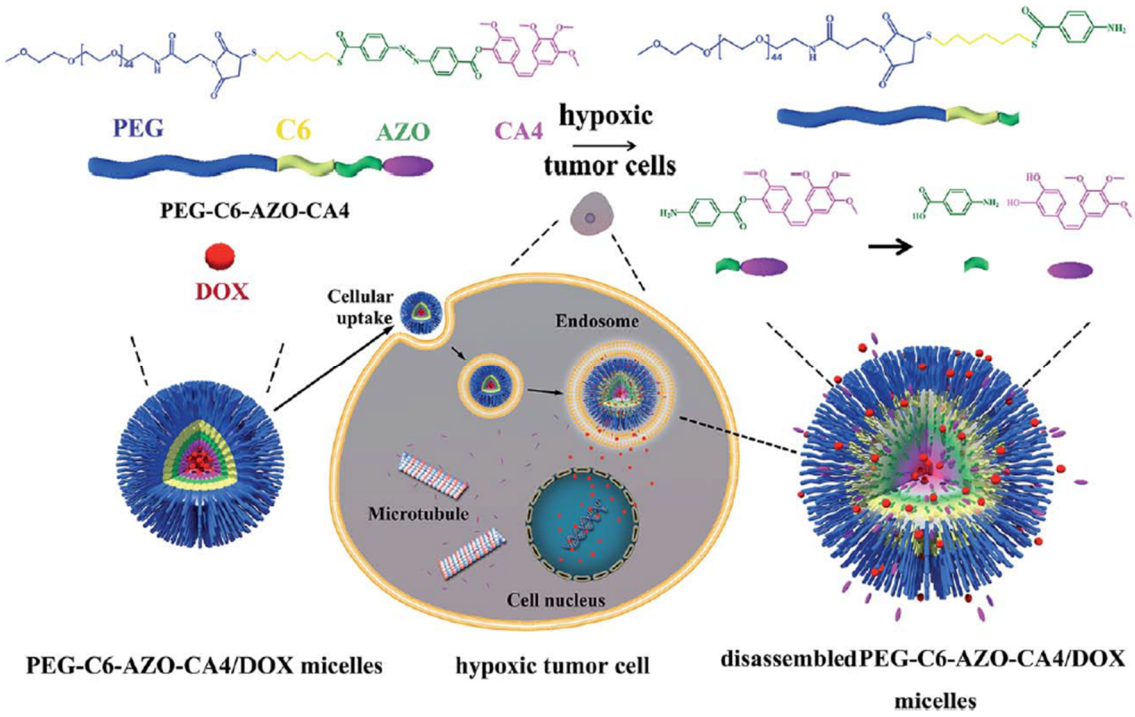


Figure 1.50. Formation of polymeric micelles with combined drug approach and release diagram. Reprinted from [111], with permission by The Royal Society of Chemistry.

Biological route of a nanoparticle have full of challenges to reach to tumor cells. Besides the size and surface modifications, morphology of the nanoparticles has also a crucial effect on biodistribution patterns [112]. Polymerization induced self-assembly (PISA) is a useful technique for preparation of polymeric nanoparticles with different morphologies, among the techniques used for different nanoparticle formation. This technique enables one to form highly concentrated polymeric nanoparticle suspensions. Controlled and efficient polymerization techniques are required to achieve particles with low dispersities. Generally, chain extension of a hydrophilic polymer with a monomer in a solvent in which resultant extended chain is insoluble results in formation of micellar type polymeric nanoparticles. Continuous chain extension induces reorganization dynamics and worm-like, rod-like and vesicle type nanoparticles are formed. A representative illustration of polymeric nanoparticle formations with different morphologies using PISA approach is given in Figure 1.51.

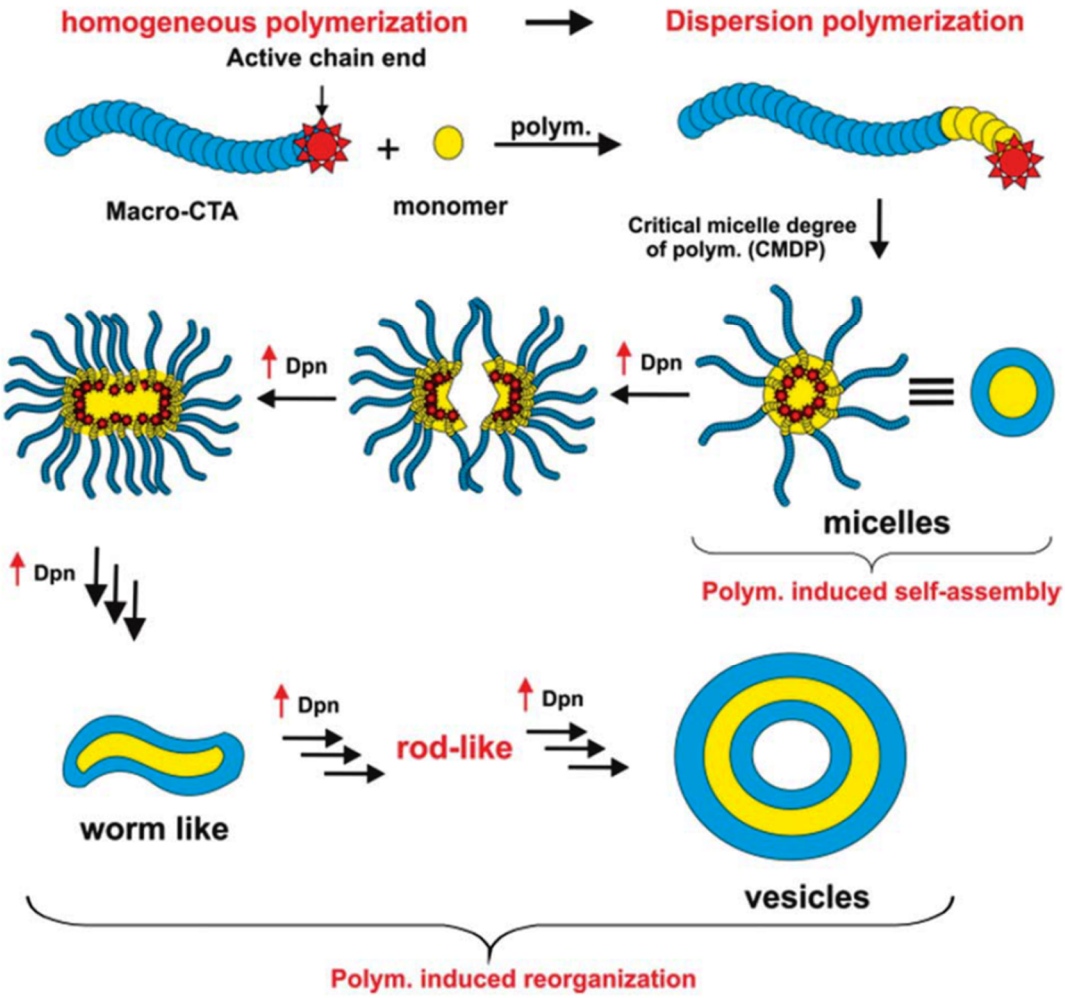


Figure 1.51. Schematic illustration of polymeric nanoparticle formation with different morphologies using PISA approach. Reprinted from [113], with permission by The Royal Society of Chemistry.

Boyer, Davis and co-workers used PISA approach in formation of polymeric nanoparticles with different morphologies [113]. Firstly, they synthesized poly (olygoethyleneglycol) methacrylate (POEGMEMA) homopolymer using reversible addition-fragmentation chain transfer (RAFT) polymerization as a macro chain transfer agent. Chain extension of second block was achieved by using styrene (S) and vinyl benzaldehyde (VBA) monomers in methanol via RAFT polymerization. Resulting POEGMEMA-*b*-P(S-*co*-VBA) amphiphilic block copolymer enabled formationof micellar type, worm-like, rod-like and vesicle type polymeric nanoparticles thanks to the insolubility of the second block in methanol at different polymerization durations. (Figure 1.52). Benzaldehyde group was used for both conjugation of an anti-mitotic drug

(doxorubicin) and cross-linking with 1,3-diaminopropane. They demonstrated significant effect of nanoparticle morphology on cellular uptake using MCF-7 cell line. The cytotoxicity results of doxorubicin loaded polymeric nanoparticles were also found to be correlated with cell uptake results.

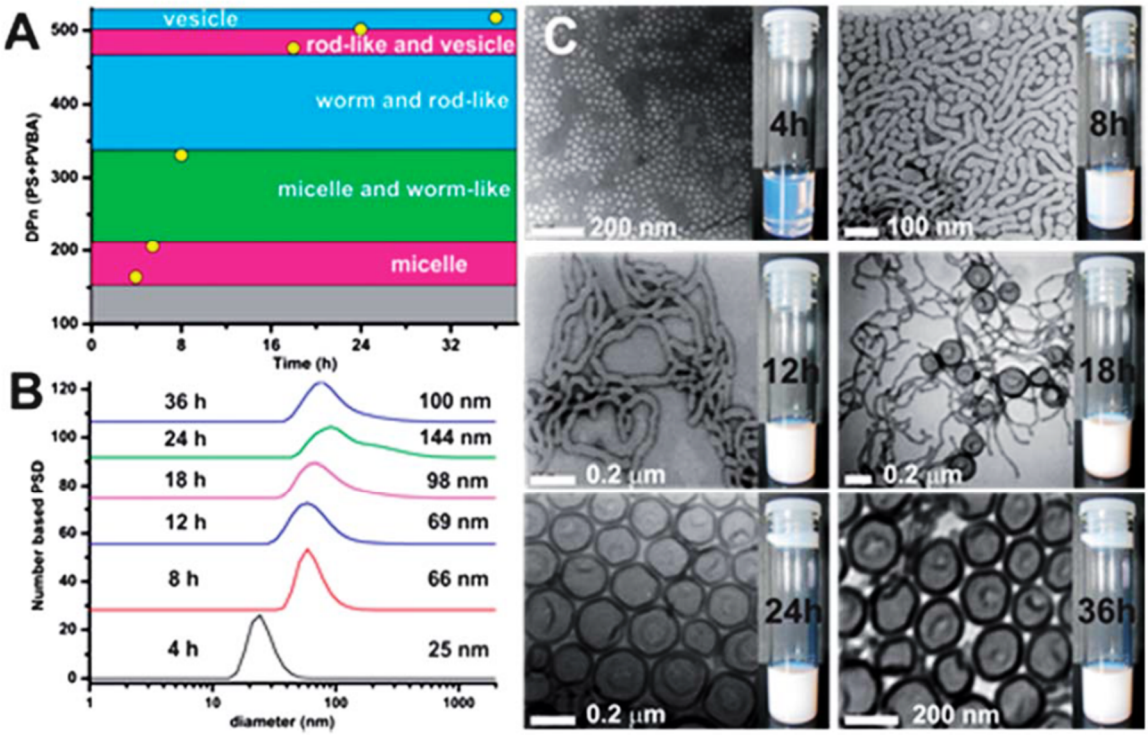


Figure 1.52. Obtained nanoparticles with different morphologies via PISA approach. Polymerization degree of second block (Panel A), molecular weight changes during chain extension (Panel B), morphology of obtained nanoparticles (Panel C). Reprinted from [113], with permission by The Royal Society of Chemistry.

2. RESEARCH OVERVIEW

Investigations reported in this dissertation can be grouped under two main parts. The first part is focused on fabrication of functionalizable hydrogels using polymeric and dendritic building blocks with control over the location and degree of functionalization to obtain effective biosensing platforms. Different strategies were designed to obtain such hydrogels and these materials were evaluated in post-gelation modification techniques to demonstrate their potential use for intended applications. The first two projects in this dissertation are related to the formation of functionalizable hydrogels. ABA type dendron-polymer conjugates, bow-tie dendrons and bifunctional linear biocompatible polymers were designed as building blocks for fabrication of these functionalizable hydrogels. Dendritic structures were synthesized using divergent approach and different chemistries were utilized for the synthesis of dendron polymer conjugates and bow-tie dendrons. In the first project, ABA type dendron-polymer conjugates were utilized in formation of such hydrogels using sequential radical thiol-ene reaction. The degree of functionalization was controlled by tailoring the dendron generation and the length of linear polymer segment. In the second project hetero-functional bow-tie dendrons having groups for both cross-linking and functionalization, and bifunctional linear polymers was used to fabricate hydrogels that can be further functionalized. Cluster effect of dendrons into these hydrogels with various functional dendron generations and length of linear polymer segment were investigated by sugar-based immobilization of Concanavalin A, an enzyme with specific binding abilities to certain biological compounds.

The second part of this dissertation is related to designing smart polymeric prodrugs for drug delivery applications. Polymer drug conjugates and polymeric nanoparticles were constructed and evaluated for the potential use in drug delivery applications. This part of the dissertation includes four projects. In the first two projects, poly oligo (ethylene) glycol methyl ether methacrylate (POEGMEMA) based polymer drug conjugates bearing drug molecules with an enzymatically degradable linker at side chains were synthesized using free radical and reversible addition–fragmentation chain transfer (RAFT) polymerization techniques. Following the synthesis, *in vitro* and *in vivo* experiments were performed to evaluate cytotoxicity, release, pharmacokinetic, biodistribution and anti-tumor growth

properties of these polymeric prodrugs. In the last two projects, polymeric nanoparticles were constructed using different techniques. Polymerization induced self-assembly (PISA) technique was used to form polymeric nanoparticles with different morphology including spherical, rod-like and worm-like nanoparticles using RAFT polymerization. Nanoparticles were formed during chain extension of POEGMEMA block with styrene monomer thanks to the insolubility of styrene block in methanol. Biodistribution of radio-labeled nanoparticles were investigated to understand effect of diameter size and morphology of nanoparticles. In the last project, polymeric micelles were obtained using block polymers having hydrophilic POEGMEMA segment and hydrophobic segment derived from drug monomer. Micelle formation was achieved by co-solvent evaporation in water. Characterization of micelles was followed by *in vitro* experiments to understand the cell internalization behavior, antiangiogenic effect of micelles compared to free drug. To evaluate biodistribution profile of the polymeric micellar nanoparticles an *in vivo* fluorescence based biodistribution study was performed.

3. FABRICATION AND FUNCTIONALIZATION OF ABA TYPE DENDRON-POLYMER CONJUGATE BASED HYDROGELS VIA SEQUENTIAL THIOL-ENE 'CLICK' REACTIONS

3.1. Introduction

Hydrogels as polymeric networks can swell in aqueous environment several times of their dry weights without fragmentation. Since the adjustable porous network and mechanical properties of the hydrogels, they can be designed having very similar physical properties with soft tissues. Moreover, physical and chemical modifications in hydrogel matrix provide a huge application area in biomedical science such as tissue engineering, drug delivery and biological sensing platforms. Besides conventional physical and chemical modifications, post-gelation modification of the hydrogels is an efficient approach to covalently attach functional moieties into the hydrogel matrix [6,114]. Tailoring the amount of functional groups in the hydrogel network provides an ideal platform for well-designed biomedical applications. Dendrons and dendrimers with precise and multi-functional structures are feasible materials for this purpose and have been widely used in hydrogel fabrication as building blocks.

Efficient chemical reactions are required to fabricate chemically cross-linked hydrogels using well-defined polymeric precursors. Since the advent of 'click' reactions, they have been widely utilized in construction of functionalize hydrogels [6-8]. Copper-based Huisgen type cycloaddition chemistry is one of the widely used click reaction to formulate these kinds of hydrogels. However, the potential toxicity and difficulties in purification of metal based click reactions limit their usage in biomedical applications. Metal-free 'click' reactions such as strain-promoted azide-alkyne cycloaddition reaction [115], the Diels-Alder reactions [116,117], tetrazine-norbornene chemistry [118], thiol-epoxy [119], thiol-maleimide [120,121], and the radical thiol-ene reactions [122-127] are alternative efficient reactions to obtain such cross-linked polymeric network. The use of such metal-free reactions eliminates the presence of trapped metal impurities in the hydrogel matrix which can interfere with intended biological compounds. In this regard, the radical thiol-ene reaction has been widely utilized in formation of various types of

polymeric materials, including hydrogels. The radical thiol-ene reaction usually is realized under photo-irradiation at ambient conditions.

Herein, we used the photo-chemical radical thiol-ene reaction in fabrication of hydrogels and this reaction was also used to functionalize thus obtained hydrogels. ABA type dendron-polymer conjugates having alkene functionalized biodegradable polyester dendrons as A blocks and biocompatible hydrophilic linear PEG polymers as B block were designed as hydrogel precursors. While some of these alkene groups were utilized in hydrogel formation via thiol-ene click reaction, the remaining alkene groups were expected to allow covalent functionalization of the hydrogel matrix with desired molecules via a consecutive thiol-ene click reaction (Figure 3.1).

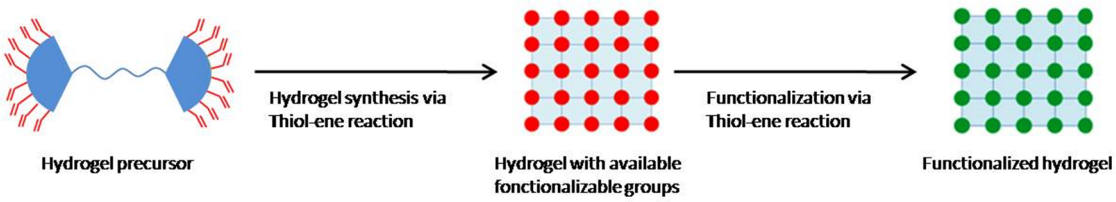


Figure 3.1. Schematic illustration of formation and functionalization of hydrogels using sequential thiol-ene click reactions.

3.2. Experimental

3.2.1. Materials

2,2-Bis(hydroxymethyl)propionic acid (BMPA), 2,2-Dimethoxypropane, p-Toluene sulfonic acid, Dowex X50WX2, propargyl alcohol, 4-pentenoic anhydride and pentaerythritol tetrakis (3-mercaptopropionate) were purchased from Alfa Aesar. 2,2-Dimethoxy-2-phenylacetophenone (DMPA) was purchased from Aldrich. All poly (ethylene glycol) polymers were obtained from Fluka. All solvents were purchased from Merck and used as obtained unless otherwise noted. BODIPY thiol were synthesized according to literature procedures [128]. Polyester dendrons [G2]-4OH (1) and [G3]-8OH (2) were obtained using literature protocols [8]. The dendron and dendron-polymer conjugate characterizations involved ^{1}HNMR spectroscopy (Varian 400 MHz) and ATR-FTIR spectroscopy (Thermo Fisher Scientific Inc. Nicolet 380). Microstructures of

hydrogels were analyzed using an ESEM-FEG/ EDAX Philips XL-30 (Philips, Eindhoven, The Netherlands) instrument at an accelerating voltage of 10kV. Hydrogels were visualized after functionalization with fluorescent dyes using Zeiss Observer.Z1 inverted fluorescent microscope.

3.2.2. Synthesis of Dendron [G2]4OR (4)

Dendron [G2]4OH (1) (0.200 g, 0.495 mmol), pyridine (0.24 mL), and DMAP (0.0602 g, 0.494 mmol) were dissolved in anhydrous CH_2Cl_2 (5 mL) in a 25 mL round bottom flask. To the stirring reaction mixture was added pentenoic anhydride (0.540 g, 2.96 mmol) and stirring was continued for 24 h at room temperature under nitrogen atmosphere. H_2O (0.25 mL) was added to the reaction mixture and stirring was continued for 4 h. The reaction mixture was diluted with CH_2Cl_2 (30 mL) and then extracted with 1M $NaHSO_4$ (3 x 30 mL), 10 % Na_2CO_3 (3 x 30 mL), and then with brine (2 x 30 mL). Combined organic layers were dried over anhydrous Na_2SO_4, and the residue was concentrated *in vacuo* to give 280 mg of [G2]4OR (4) as a yellowish-brown viscous liquid (78 % yield). ^{1}H NMR ($CDCl_3$,δ, ppm) 5.82-5.72 (m, 4H), 5.07-4.98 (m, 8H), 4.72 (d, 2H, J = 2.3 Hz), 4.30-4.17 (m, 12H), 2.51 (t, 1H, J = 2.3 Hz), 2.44-2.32 (m, 16H), 1.28 (s, 3H),1.23 (s, 6H). FTIR (cm^{-1}): 3273, 2981, 1734, 1641.

3.2.3. Synthesis of Dendron [G3]8OR (5)

Dendron [G3]8OH (2) (0.211 g, 0.183 mmol), pyridine (0.20 mL), and DMAP (0.0223 g, 0.183 mmol) were dissolved in dry CH_2Cl_2 (5 mL) in a 25 mL round bottom flask. To the stirring reaction mixture was added pentenoic anhydride (0.400 g, 2.197 mmol) and continued stirring for 24 h at room temperature under N_2. 0.20 mL H_2O was added to the reaction mixture and stirred at room temperature for 4 h. The reaction mixture was diluted with CH_2Cl_2 (30 mL) and then extracted with 1M $NaHSO_4$ (3 x 30 mL), 10% Na_2CO_3 (3 x 30 mL), and then with brine (2 x 30 mL). Combined organic layers were dried over anhydrous Na_2SO_4, and the residue was concentrated *in vacuo* to give 299 mg of [G3]8OR (5) as a yellowish-brown viscous liquid (87 % yield). ^{1}H NMR ($CDCl_3$,δ, ppm) 5.84-5.74 (m, 8H), 5.06-4.98 (m, 16H), 4.72 (d, 2H, J = 2.3 Hz), 4.31-4.16 (m, 28H), 2.53 (t, 1H, J = 2.3 Hz), 2.43-2.32 (m, 32H), 1.31 (s, 3H),1.24 (s, 6H), 1.22 (s, 12H). FTIR (cm^{-1}): 3273, 2981, 1734, 1641.

3.2.4. Synthesis of Compound G2PEG6K (8)

PEG-6K-diazide (6) (400 mg, 0.065 mmol) and propargyl [G2]8OR (4) (150 mg, 0.197 mmol) were dissolved in THF (4 mL). In a separate flask CuBr (1.8 mg, 0.013 mmol) and N,N,N',N'',N''-pentamethyldiethylenetriamine (PMDETA, 2.7 µL, 0.013 mmol) were dissolved in THF (2 mL) and purged with N_2. The mixture was then transferred onto azide-propargyl alcohol solution and stirred at room temperature for 24 h. The solvent was then evaporated, and the crude product was dissolved in CH_2Cl_2 (100 mL) and extracted with water (2 x25 mL). The solvent was concentrated by rotary evaporator, and crude product was precipitated with Et_2O, filtered, and dried *in vacuo*, to give compound G2PEG6K (8) (405 mg, 83 %) as a white solid. ^{1}H NMR ($CDCl_3$,δ, ppm) 7.83 (s, 2H), 5.84-5.74 (m, 8H), 5.25 (s, 4H), 5.06-4.98 (m, 16H), 4.56 (t, 4H, J = 2.3 Hz), 4.27-4.12 (m, 24H), 3.90-3.45 (m, 544H) 2.43-2.32 (m, 32H), 1.23 (s, 6H),1.19 (s, 12H). FTIR (cm^{-1}): 2882, 1739, 1642.

3.2.5. Synthesis of Compound G3PEG6K (9)

Synthesized via the same procedure as compound G2PEG6K using PEG-6K-diazide (6) (400 mg, 0.065 mmol), propargyl [G3]8[OR] (5) (300 mg, 0.197 mmol), CuBr (1.8 mg, 0.013 mmol) and N,N,N',N'',N''-pentamethyldiethylenetriamine (PMDETA, 2.7 µL, 0.013 mmol) to give compound G3PEG6K (9) (448 mg, 76 %) as a white solid. ^{1}H NMR ($CDCl_3$,δ, ppm) 7.81(s, 2H), 5.84-5.74(m, 16H), 5.24 (s, 4H), 5.06-4.98 (m, 32H), 4.54 (t, 4H, J = 2.3 Hz), 4.25-4.16 (m, 56H), 3.89-3.45 (m, 544H), 2,42-2.33 (m, 64H), 1.25-1.20 (m, 42H). FTIR (cm^{-1}): 2884, 1739, 1642.

3.2.6. Synthesis of Compound G3PEG20K

Synthesized via the same procedure as compound [G3]8[OR] (5) using PEG-20K-diazide (7) (702 mg, 0.034 mmol), propargyl [G3]8[OR] (5) (160 mg, 0.104 mmol), CuBr (1.6 mg, 0.011 mmol), and PMDETA (2.3 µL, 0.011 mmol), yielding compound G3PEG20K (10) (0.701 g, 89 %) as a white solid. ^{1}H NMR ($CDCl_3$,δ, ppm) 7.81(s, 2H), 5.84-5.74 (m, 16H), 5.24 (s, 4H), 5.06-4.97 (m, 32H), 4.54 (t, 4H, J = 2.3 Hz), 4.25-4.15 (m, 56H), 3.89-3.44 (m, 1816H), 2,43-2.33 (m, 64H), 1.25-1.20 (m, 42H). FTIR (cm^{-1}): 2880, 1740, 1641.

3.2.7. Synthesis of Bulk Hydrogels via Thiol-ene Chemistry

To a small vial was added G2PEG6K (20 mg, 2,6 μmol) and pentaerythritol tetrakis(3-mercaptopropionate) as cross-linker (0,5 or 1.0 or 2.0 eq.) in water (20 μL) and ethanol (60 μL). The mixture was mixed under ultrasound to give a clear solution. The vial was added DMPA (photoinitiator) (0.2 mg, 0.79 μmol). The mixture was exposed 4 watt UV light (365 nm) from 3 cm distance for 10 min. Hydrogels were incubated in 2 mL ethanol for 2 h and taken into another vial. H_2O (3 mL) was added into the vial and hydrogels were kept for 2 days in the vial during which the aqueous phase was refreshed several times. Finally, H_2O was removed. Hydrogels were obtained by using G3PEG6K (20 mg, 2 μmol) and G3PEG20K (20 mg, 0.86 μmol) as same above with pentaerythritol tetrakis(3-mercaptopropionate) (1.0 or 2.0 or 4.0 eq). The hydrogel samples were freeze-dried *in vacuo* until the solvent was sublimed, yielding transparent hydrogels with high conversions (> 90 %).

3.2.8. Synthesis of Hydrogel Micropatterns via Thiol-ene Chemistry

Hydrogel patterns were synthesized via the same procedure as bulk hydrogels using G2PEG6K (10 mg, 1.3 μmol) and cross-linker (2:1) in H_2O (10 μL) and ethanol (30 μL) and DMPA (0.1 mg, 0.39 μmol). 10 μL of the mixture applied by capillary effect between Polydimethylsiloxane (PDMS) mold (60-40 μm) and silyl functionalized glass surfaces. The mixture in PDMS mold was exposed 4 watt UV light (365 nm) from 3 cm distance for 10 min. PDMS mold was removed carefully and hydrogel patterns were washed with THF (2 mL). Hydrogels were obtained by using G3PEG6K (10 mg, 1 μmol) and G3PEG20K (10 mg, 0.43 μmol) as above with 2:1 DPD:cross-linker ratio.

3.2.9. Scanning Electron Microscopy (SEM) Images of Hydrogel Samples

The bulk hydrogel samples were equilibrated in deionized water at room temperature for 16 h. The equilibrated hydrogel samples were frozen and then freeze-dried in vacuo 24 h. The images of the freeze-dried hydrogel samples were obtained by a scanning electron microscope.

3.2.10. Water Uptake Analysis

The swelling profiles of the hydrogel samples were obtained as a function of time. The weight gain was measured at each immersion time period in 25 mL of deionized water. At the measuring times the hydrogel samples were removed from the water, blotted with wet filter paper to eliminate the water adsorbed by the hydrogel surface, and weighed. Measurements were taken until swelling degree was reached equilibrium, considered when three consecutive measurements gave the similar results (0.001 g). Water uptake analysis was done for a minimum of three samples of a particular hydrogel. The swelling profile was expressed as the swelling ratio percent (*W)*, where *Mw* represents weight of swollen equilibrated hydrogel and *Md* represents weight of dry hydrogel.

$$W = (Mw - Md)/Md \; x100$$

3.2.11. Functionalization of Micropatterns with BODIPY Thiol

Hydrogel patterns containing residual alkene groups were obtained using G2(2:1)PEG6K, G3(2:1)PEG6K and G3(2:1)PEG20K. Prior to functionalization, the hydrogel patterns were washed with THF to remove any excipient water. Micropatterns were exposed to excess BODIPY thiol (1.5 eqv of available alkene groups (calculated for 2 mg hydrogel patterns), (1.0 mg, 2.4 μmol; 2.0 mg, 4.6 μmol and 0.8 mg, 1.8 μmol respectively) in THF solution (25 μL) including DMPA (0.1 mg, 0.39 μmol). The patterns were exposed to UV-irradiation (365 nm, 4 watt) from a distance of 3 cm for 10 min. Hydrogel micropatterns were rinsed with copious amounts of THF to remove unreacted BODIPY thiol.

3.3. Results and Discussion

3.3.1. Synthesis and Characterization of ABA Type Dendron Polymer Conjugates

The dendron polymer conjugates were synthesized using Huisgen type [3+2] azide-alkyne cycloaddition reaction between linear PEG-bisazides and orthogonally functionalized dendrons bearing alkene units at their periphery and an alkyne group at their focal point. Utilization of such dendron provides facile conjugation of different molecules at different sites of the dendrons [129,130]. This strategy provided the synthesis of dendron

bearing thiol functionalized hydrogel precursors in a single step. The alcohol groups on dendrons were functionalized with pentenoic anhydride via the acylation reaction to obtain orthogonally functionalized G2 and G3 dendrons. The purity and precise chemical structure of the dendrons were confirmed by ^{1}H NMR spectroscopy. Proton resonances due to methyl groups of the polyester dendron backbone around 1.22 - 1.31 ppm as well as proton resonances due to alkyne group around 2.50 - 2.53 ppm proton resonances due to and alkene units around 4.98 – 5.06 and 5.74 – 5.84 ppm were present in expected ratios (Figure A.1 and Figure A.2). The synthesis of triblock copolymers (G2PEG6K, G3PEG6K and G3PEG20K) was achieved in the presence of CuBr and PMDETA in THF (Figure 3.2).

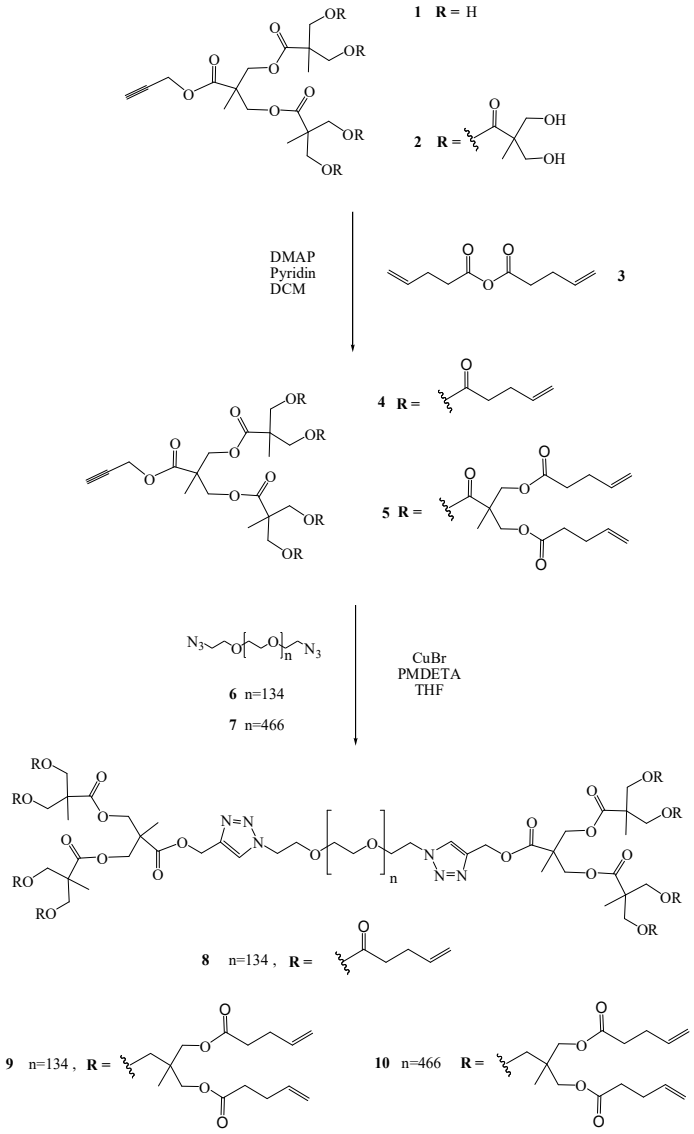


Figure 3.2. Synthesis of alkene functionalized ABA type dendron polymer conjugates.

Azide bearing linear PEG polymers PEG6K and PEG20K were synthesized according to literature procedures to form the hydrophilic section of the hydrogel precursors with different PEG lengths, 6K and 20K, respectively [131]. These ABA type conjugates are named according to length of PEG and dendron generation used: i.e., G2PEG6K represents a PEG 6KDa polymer flanked with two G2 dendrons bearing alkene units on their peripheral sphere.

Purity of the dendron polymer conjugates were analyzed using infrared (IR) and ^{1}HNMR spectra. Comparison of the FTIR spectra of purified conjugates, the alkene functionalized dendrons and the bisazido PEG polymers (Figure A.3, Figure A.4 and Figure A.5) shows the disappearance of the azide stretching near 2100 cm^{-1} for the conjugates. The purity and the precise chemical composition of dendron-polymer conjugates were also proved from the ^{1}HNMR spectra. Expected resonances due to the triazole proton around 7.8 ppm, the vinylic protons on the dendron peripheries near 5.8 and 5.0 ppm, and the ethylene repeat units from the linear PEG fragment between 3.4 to 3.9 ppm with appropriate ratios confirmed the purity of these hydrogel precursors (Figure A.6, Figure A.7 and Figure A.8).

3.3.2. Hydrogel Formation

Hydrogels were formed via the photo-chemically promoted radical thiol-ene “click” reaction (Figure 3.3).

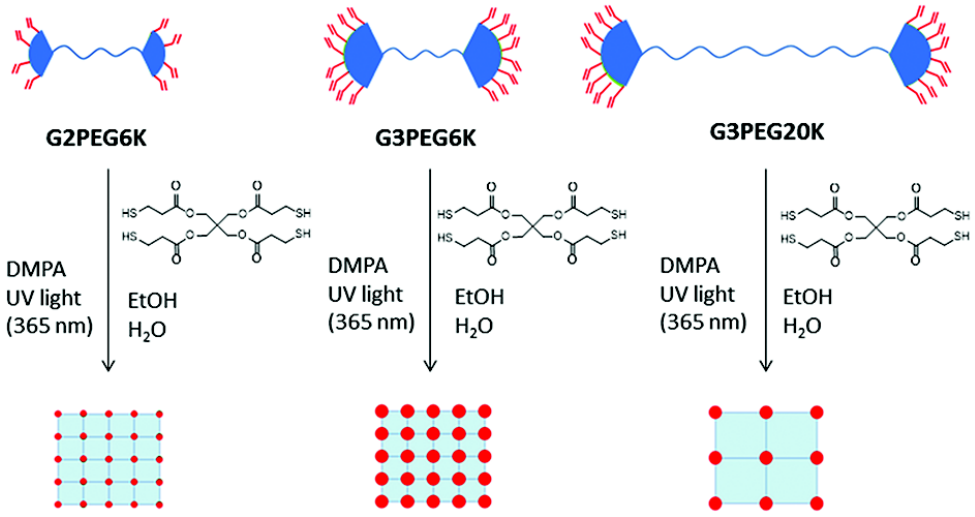


Figure 3.3. Synthesis of hydrogels with different functional group densities.

Alkene containing triblock copolymers G2PEG6K, G3PEG6K and G3PEG20K, pentaerythritoltetrakis (3-mercaptopropionate) and a tetra-thiol containing cross-linker used as hydrogel precursors. 2,2-dimethoxy-2-phenylacetophenone (DMPA) used as a photo-initiator. Clear and transparent hydrogels were achieved by dissolving all components in ethanol-water mixture and exposing UV-irradiation for 10 min, followed by washing with ethanol and water sequentially to remove any unreacted components.

Gelation of dendron-polymer conjugates G2PEG6K and G3PEG6K which have same PEG lengths but different dendron generations, with the same dendron-polymer-dendron (DPD):cross-linker mole ratio allowed to form hydrogels with different number of residual alkene groups for one DPD unit. G2PEG6K and G3PEG6K have eight and sixteen alkenes on the periphery, respectively. Since the cross-linker has four thiol groups, 2 : 1 DPD : cross-linker mole ratio results in six left-over alkenes for G2PEG6K and fourteen left-over alkenes for G3PEG6K for further functionalization (Table 1, item 1 and 4).

Table 3.1. Properties of hydrogels and average available functional groups on one DPD unit.

Item	DPD	PEG	Hydrogel	DPD : cross-linker ratio	Average available functional groups on one DPD unit
1	8	6000	6KG2 (2:1)	2:1	6
2	8	6000	6KG2 (1:1)	1:1	4
3	8	6000	6KG2 (1:2)	1:2	-
4	9	6000	6KG3 (2:1)	2:1	14
5	9	6000	6KG3 (1:1)	1:1	12
6	9	6000	6KG3 (1:2)	1:2	8
7	9	6000	6KG3 (1:4)	1:4	-
8	10	20000	20KG3 (2:1)	2:1	14
9	10	20000	20KG3 (1:1)	1:1	12
10	10	20000	20KG3 (1:2)	1:2	8
11	10	20000	20KG3 (1:4)	1:4	-

Gelation of G3PEG6K and G3PEG20K which have same dendrons but different PEG lengths, with the same DPD : cross-linker mole ratio allowed to obtain hydrogels with the same number of left-over alkene groups for one DPD unit. 2 : 1 DPD : cross-linker mole ratio results in fourteen residual alkenes for both G3PEG6K and G3PEG20K (Table 3.1, item 4 and 8). The reaction of cross-linker with alkene groups on the same dendron is

also possible, but this would not change the average number of left-over alkene groups for one DPD unit.

3.3.3. Physical Properties of Hydrogels

The water-uptake properties of the hydrogels formed by using ABA type copolymers G2PEG6K, G3PEG6K and G3PEG20K in which the dendron generations and cross-linker ratio were varied are shown in Figure 3. The water uptake measurements showed that using higher dendron generation does not significantly affect the water uptake of the hydrogels, but increasing the length of the PEG segment cause a dramatic increase in water uptake ratio of hydrogels due to hydrophilic nature of the PEG block. The water uptake of hydrogels slightly decreased for all hydrogels by increasing the cross-linker mole ratio (Figure 3.4).

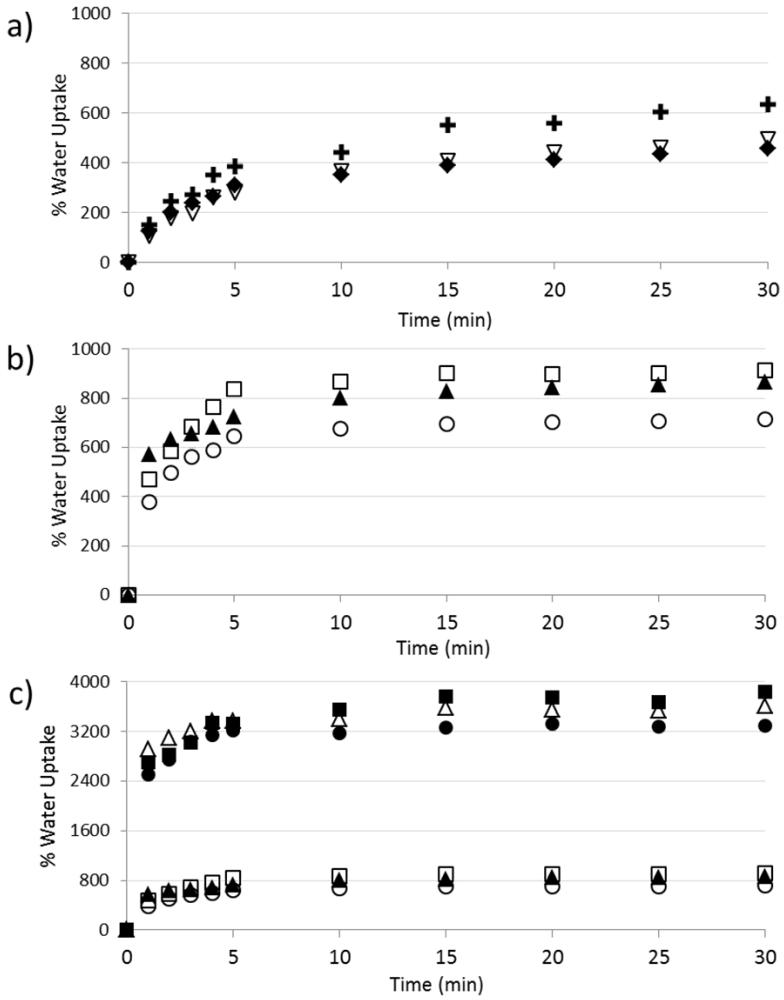


Figure 3.4. Water uptake results of hydrogels. (a) 6KG2, (b) 6KG3, (c) comparison of 6KG3 and 20KG3 hydrogels.

The hydrogel samples were allowed to reach equilibrated swollen state in deionized water, frozen, and then lyophilized to compare the morphological properties the hydrogels. SEM micrographs of dry hydrogel samples revealed their porous structures (Figure 3.5). As expected, the hydrogels formed using longer PEG length have enhanced porosity compared to hydrogels formed with short PEG chains. No significant difference was observed between the hydrogels formed with different dendron generations while keeping the same PEG length. The increase in cross-linker mole ratio in the feed caused a decrease in porosity and resulted in hydrogels with dense structure. Morphological structure and water uptake results were complementary to each other in terms of hydrophilic linear PEG segment amount.

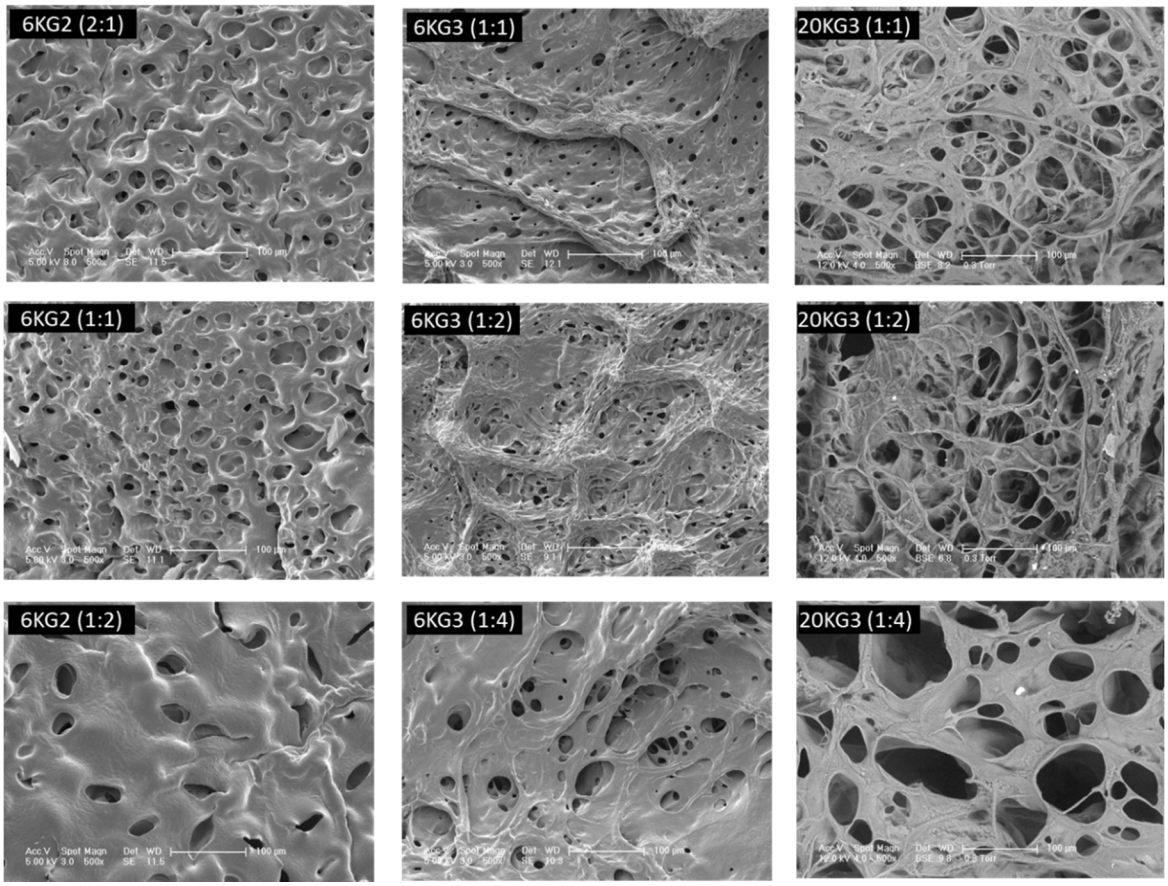


Figure 3.5. Scanning Electron Microscopy (SEM) images of dry hydrogels.

3.3.4. Hydrogel Functionalization

After obtaining the hydrogels with residual alkene groups at cross-linking region, functionalization of these hydrogels were investigated using subsequent thiol-ene conjugation reaction. The presence and the reactivity of residual alkene groups were

evaluated by reaction of these groups with thiol-containing molecule (BODIPY thiol) (Figure 3.6). BODIPY thiol has an emission at green-shifted wavelengths. It was attached to micropatterned hydrogels using photo-induced radical thiol-ene reaction.

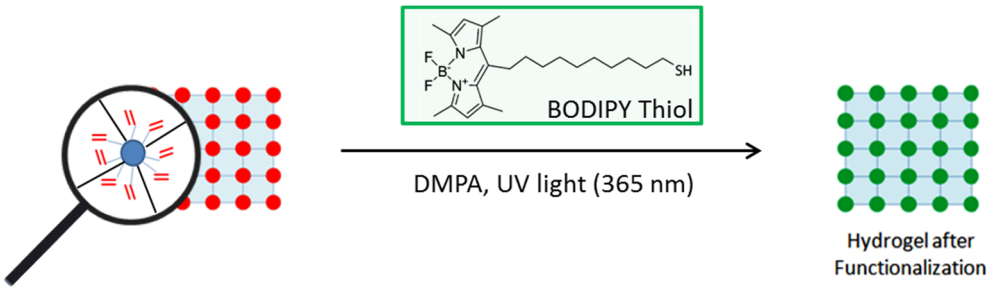


Figure 3.6. Hydrogel functionalization using radical thiol-ene conjugation.

Patterned hydrogel samples were prepared on glass slides coated with a thin layer of 3-(trimethoxysilyl)propyl methacrylate providing the adhesion of the hydrogel micropatterns on the surface (Figure 3.7).

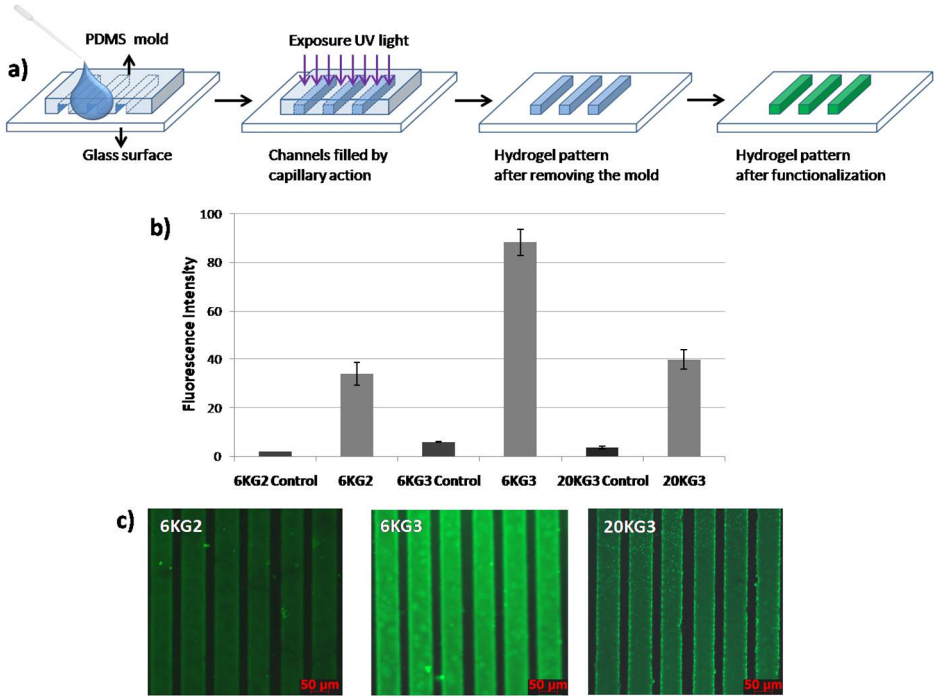


Figure 3.7. Hydrogel micropatterns and functionalization. (a) Formation and functionalization of micropatterned hydrogels. (b) Fluorescence intensity graph and (c) fluorescence microscope images of hydrogels functionalized with BODIPY thiol. In graph, control refers to BODIPY thiol treatment without DMPA and UV-irradiation.

Hydrogel micropatterns prepared using 2 : 1 DPD : cross-linker ratio. 6KG2, 6KG3 and 20KG3 were treated with BODIPY thiol via thiol-ene chemistry in the presence of UV-irradiation and DMPA. As control experiments, samples were treated with BODIPY thiol in the absence of DMPA and UV-irradiation. Thus functionalized hydrogels were visualized under a fluorescence microscope. Comparison of 6KG2 and 6KG3 hydrogel samples demonstrated the effect of using different dendron generation on post-gelation functionalization. 6KG3 hydrogel patterns showed higher fluorescent intensity due to presence of more residual alkene groups compared to 6KG2 hydrogel patterns. Comparison of 6KG3 and 20KG3 hydrogel patterns having different PEG segment length and same number of alkene groups showed that using a shorter PEG segment resulted in higher fluorescent intensity due to higher density of available functional groups into hydrogel matrix.

3.4. Conclusion

Clear and transparent hydrogels were constructed and functionalized with thiol-containing dye molecule using sequential thiol-ene 'click' reaction. Formation of the hydrogels bearing available alkene functional groups was achieved by using well-defined ABA type dendron-polymer conjugates. Following gelation, physical characteristics of the hydrogels such as swelling and morphology were evaluated. Hydrogel micropatterns were obtained by using micromolding technique for further functionalization. The available alkenes allowed efficient post-gelation modification of the hydrogel matrix with thiol-containing dye molecule using the radical thiol-ene reaction. Using different length of the PEG block and dendron generations enabled formation of hydrogels with tunable degree of functionalization. The photochemical nature of gelation technique is combined with micromolding in capillaries to form hydrogel micropatterns that can undergo facile functionalization in a controlled manner.

4. FORMATION OF WELL-DEFINED CARBOHYDRATE FUNCTIONALIZED HYDROGELS AS MULTIVALENT 3D MATERIALS FOR BIOIMMOBILIZATION OF LECTINS

4.1. Introduction

Lectin and carbohydrate interactions are mainly derived from hydrophobic interactions and hydrogen bonds between the amino-acid residues of the lectins and the hydroxyl groups of the carbohydrates. The carbohydrate binding sites of lectins are present on the surface of the protein in the form of grooves [132]. One of the crucial features of this interaction is that their binding affinities are highly enhances when the carbohydrates are displayed in a multivalent fashion. It was reported that the binding affinity of methyl-α-mannoside significantly increased in case of polymerized forms of this saccharide which display multiple mannose moieties [133]. The increased local ligand density mechanism was firstly explained by Lee and co-workers as a result of clustering effect [134]. Tunable topological and local proximities can be designed by clustering intended ligands to achieve optimal molecular properties leading to improved binding affinities [135].

Mannose is a monosaccharide of the aldohexose series of carbohydrates and a C-2 epimer of glucose. It is responsible for glycosylation of certain proteins [136]. Protein binding affinity of mannose has been shown increase when presented in a multivalent design [137]. While there is a wide range of applications and investigations including lectins, Concanavalin A (Con A) has been the most investigated carbohydrate binding protein, especially for α-D-mannoside ligands. It also has binding affinity towards α-D-glucosyl residues. Con A is a member of the legume lectin family and exists in the form of a tetramer subunits each having one binding site.

Dendritic structures, mainly dendrons and dendrimers have been widely used to create ligand clusters due to their monodisperse and multivalent nature. For example, Cloninger et al. have designed a small library of mannose functionalized PAMAM dendrimers ranging from G1 to G6 generations. They showed that binding affinities of the mannose functionalized dendrimers towards Con A increased upon the increase in size and

multivalency of the glycodendrimers [138]. In another study, they also showed tunable degree of lectin clustering and overall activity by changing the mannose/hydroxyl ratios on the dendrimer surfaces [139]. Moreover, orthogonal design of the dendritic macromolecules their synthesis using effective 'click' type reactions enables introducing these ligand clusters for bio-immobilization applications. Peiters and co-workers synthesized alkyne functionalized dendrimers based on 3,5-di-(2-aminoethoxy) benzoic acid repeating units and conjugated these dendrimers with azide-terminal mannose via a copper-catalyzed alkyne-azide cycloaddition "click" reaction to obtain glycodendrimers. Amine functionalized core of the glycodendrimers was deprotected for coupling to a chip surface to fabricate a microarray [140]. Malkoch and co-workers synthesized mannosylated G5 polyester dendron on a cellulose surface and compared its Con A binding affinity with another surface which has monomeric mannose residue. They reported that a 10-fold higher binding affinity was obtained in the case of dendronized substrates compared to monomeric one [141]. However, there are no examples related to application of cluster glycoside effect in a well-defined 3D environment like a hydrogel.

In this project we synthesized well-defined network hydrogels that possess clusters of carbohydrate ligands using orthogonally functionalizable bow-tie dendrons and Huisgen type of [3+2] cycloaddition. Utilization of orthogonal nature of the dendrons allowed efficient cross-linking of alkyne groups with PEG diazides as well as post-gelation functionalization with alkene functionalities. Hydrogel samples designed to display different alkene cluster motifs were modified with D-mannose to evaluate the binding affinities of Con A in such 3D networks.

4.2. Experimental

4.2.1. Materials

2,2-Bis(hydroxymethyl)propionic acid (BMPA), 2,2-Dimethoxypropane, p-Toluene sulfonic acid, Dowex X50WX2, propargyl alcohol, 4-pentenoic anhydride, 4-pentynoic acid and mercapto ethanol were purchased from Alfa Aesar. 2,2-Dimethoxy-2-phenylacetophenone (DMPA) was purchased from Aldrich. All poly(ethylene glycol) polymers were obtained from Fluka. Con A-Texas red conjugate was obtained from Life Technologies-Molecular Probes. (BMPA-Anhydride) derived from BMPA and 2,2-

Dimethoxypropane was synthesized according to literature procedure [8]. All solvents were purchased from Merck and used as obtained unless otherwise noted. Azide functionalized PEGs [131], BODIPY azide [7], and polyester G2 dendron bearing maleimide core and four alkyne groups at periphery, G2M[4 alkyne] [129], were synthesized according to literature procedures. Acetyl protected D-mannose bearing thioacetate group ($C_{18}H_{26}O_{11}S$) supplied by Rene Roy, University of Quebec, 8888, Montreal, Canada. The dendron characterizations involved ^{1}HNMR spectroscopy (Varian 400 MHz) and ATR-FTIR spectroscopy (Thermo Fisher Scientific Inc. Nicolet 380). Microstructures of hydrogels were analyzed using an ESEM-FEG/ EDAX Philips XL-30 (Philips, Eindhoven, The Netherlands) instrument at an accelerating voltage of 10kV. Hydrogels were visualized after functionalization with fluorescent dyes using Zeiss Observer.Z1 inverted fluorescent microscope.

4.2.2. Synthesis of G2[4 alkyne]-G0[1 OH] Dendron

G2M[4 alkyne] (660 mg, 0.75 mmol), mercapto ethanol (71 mg, 0.90 mmol) and triethyl amine (8 mg, 0.0075 mmol) were dissolved in dry THF (5 mL) under N_2 in a 25 mL round bottom flask. Reaction was allowed for 6 h. The solvent was then evaporated and the crude product was purified by column chromatography on silica with hexane and EtOAc (5:1) to give final product. (488 mg, 68 %). ^{1}H NMR ($CDCl_3$) δ (ppm): 4.21-4.32 (m, 12H); 4.10 (t, 2H, *J* = 6.1 Hz); 3.87-3.92 (m, 3H); 3.62 (t, 2H, *J* = 6.8 Hz); 3.20 (dd, 1H, *J* = 18.7, 9.1 Hz); 3.12 (dt, 1H, *J* = 14.5, 5.5 Hz); 2.90 (dt, 1H, *J* = 14.0, 5.4 Hz); 2.46-2.61 (m, 17H); 1.94-2.01 (m, 6H); 1.29 (s, 3H); 1.26 (s, 6H). ^{13}C NMR ($CDCl_3$) δ (ppm): 174.6, 172.1, 171.4, 82.5, 69.4, 65.9, 65.5, 62.3, 62.1, 46.8, 46.5, 39.7, 36.5, 35.8, 33.3, 26.8, 18.0, 17.7, 14.5. Anal. Calcd. [$C_{44}H_{55}NO_{17}S$]: C, 58.59; H, 6.15; N, 1.55; O, 30.16; S, 3.56. Exact mass: 901.32, molecular weight: 901.97. FTIR (cm^{-1}): 3533, 3283, 2936, 1733, 1702.

4.2.3. Synthesis of G2[4 alkyne]-G0[1 alkene] Dendron

G2[4 alkyne]-G0[1 OH] (50 mg, 0.055 mmol), pyridine (6 µL), and DMAP (6.8 mg 0.055 mmol) were dissolved in anhydrous CH_2Cl_2 (2 mL) in a 10 mL round bottom flask. Pentenoic anhydride (15.5 mg, 0.083 mmol) was dissolved in anhydrous CH_2Cl_2 (0.5 mL) in separate vial. To the stirring reaction mixture was added pentenoic anhydride solution and stirring was continued for 24 h at room temperature under nitrogen atmosphere. H_2O

(20 µL) was added to the reaction mixture and stirring was continued for 4 h. The reaction mixture was diluted with CH_2Cl_2 (10 mL) and then extracted with 1M $NaHSO_4$ (3 x 5 mL), 10% Na_2CO_3 (3 x 5 mL), and then with brine (2 x 5 mL). Combined organic layers were dried over anhydrous Na_2SO_4, and the residue was concentrated in vacuo to give 46 mg of G2[4 alkyne]-G0[1 alkene] as a yellowish viscous liquid (85 % yield). ^{1}H NMR ($CDCl_3$) δ (ppm): 5.77-5.87 (m, 1H); 5.00-5.09 (m, 2H); 4.41 (dt, 1H, *J* = 11.5, 6.4 Hz); 4.21-4.34 (m, 13H); 4.09 (t, 2H, *J* = 6.3 Hz); 3.84 (dd, 1H, *J* = 9.0, 3.5 Hz); 3.61 (t, 2H, *J* = 6.7 Hz); 3.26 (dt, 1H, *J* = 13.6, 6.1 Hz); 3.17 (dd, 1H, *J* = 18.6, 8.9 Hz); 2.94 (dt, 1H, *J* = 14.3, 6.7 Hz); 2.44-2.58 (m, 17H); 2.35-2.42 (m, 4H); 1.94-2.00 (m, 6H);1.29 (s, 3H); 1.25 (s, 6H). ^{13}C NMR ($CDCl_3$) δ (ppm): 176.7, 174.5, 172.1, 171.3, 136.6, 115.8, 82.5, 69.4, 65.8, 63.5, 62.6, 62.3, 46.8, 46.5, 38.7, 35.9, 33.5, 33.3, 30.8, 28.9, 26.8, 18.0, 17.7, 14.5. Anal. Calcd. [$C_{49}H_{61}NO_{18}S$]: C, 59.81; H, 6.25; N, 1.42; O, 29.27; S, 3.26. Exact mass: 983.36, molecular weight: 984.07. FTIR (cm^{-1}): 3284, 2960, 1732, 1703, 1642.

4.2.4. Synthesis of G2[4 alkyne]-G1[2 alkene] Dendron

G2[4 alkyne]-G0[1 OH] (200 mg, 0.22 mmol), pyridine (25 µL), and DMAP (27.5 mg 0.22 mmol) were dissolved in anhydrous CH_2Cl_2 (4 mL) in a 25 mL round bottom flask. BMPA anhydride (110 mg, 0.33 mmol) was dissolved with in anhydrous CH_2Cl_2 (1 mL) in separate vial. To the stirring reaction mixture was added BMPA anhydride solution and stirring was continued for 24 h at room temperature under nitrogen atmosphere. H_2O (50 µL) was added to the reaction mixture and stirring was continued for 4 h. The reaction mixture was diluted with CH_2Cl_2 (15 mL) and then extracted with 1M $NaHSO_4$ (3 x 10 mL), 10 % Na_2CO_3 (3 x 10 mL), and then with brine (2 x 10 mL). Combined organic layers were dried over anhydrous Na_2SO_4. Then the residue was concentrated in vacuo and dissolved in 10 mL MeOH. The solution mixture was added 50 mg Dowex and stirred for 4 h. The solution mixture was filtered and the residue was concentrated in vacuo. 40 mg of this intermediate product having two alcohol group (0.039 mmol), pyridine (8.8 µL), and DMAP (4.8 mg 0.039 mmol) were dissolved in anhydrous CH_2Cl_2 (2 mL) in a 10 mL round bottom flask. Pentenoic anhydride (21.5 mg, 0.118 mmol) was dissolved in anhydrous CH_2Cl_2 (0.5 mL) in separate vial. To the stirring reaction mixture was added pentenoic anhydride solution and stirring was continued for 24 h at room temperature under nitrogen atmosphere. H_2O (50 µL) was added to the reaction mixture and stirring was continued for 4 h. The reaction mixture was diluted with CH_2Cl_2 (10 mL) and then

extracted with 1M $NaHSO_4$ (3 x 5 mL), 10% Na_2CO_3 (3 x 5 mL), and then with brine (2 x 5 mL). Combined organic layers were dried over anhydrous Na_2SO_4, and the residue was concentrated in vacuo to give 36 mg of G2[4 alkyne]-G1[2 alkene] as a yellowish viscous liquid (78 % yield). ^{1}H NMR ($CDCl_3$) δ (ppm): 5.75-5.85 (m, 2H); 4.99-5.08 (m, 4H); 4.45 (dt, 1H, *J* = 12.1, 6.1 Hz); 4.20-4.33 (m, 17H); 4.10 (t, 2H, *J* = 6.2 Hz); 3.81 (dd, 1H, *J* = 9.0, 3.6 Hz); 3.61 (t, 2H, *J* = 7.1 Hz); 3.27 (dt, 1H, *J* = 14.1, 6.2 Hz); 3.18 (dd, 1H, *J* = 18.6, 9.2 Hz); 2.97 (dt, 1H, *J* = 14.0, 6.8 Hz); 2.46-2.58 (m, 17H); 2.34-2.40 (m, 8H); 1.94-2.00 (m, 6H);1.29 (s, 3H); 1.24-1.27 (m, 9H). ^{13}C NMR ($CDCl_3$) δ (ppm): 176.7, 174.4, 172.7, 172.6, 172.1, 171.3, 136.6, 115.8, 82.5, 69.4, 65.8, 65.5, 65.4, 63.1, 62.3, 46.8, 46.5, 38.6, 35.7, 33.5, 33.3, 30.7, 28.9, 26.8, 18.0, 17.7, 14.5. Anal. Calcd. [$C_{59}H_{75}NO_{22}S$]: C, 59.94; H, 6.39; N, 1.18; O, 29.77; S, 2.71. Exact mass: 1181.45, molecular weight: 1182.29. FTIR (cm^{-1}): 3288, 2931, 1733, 1705, 1637.

4.2.5. Synthesis of G2[4 alkyne]-G2[4 alkene] Dendron

The intermediate product having two alcohol group described in 4.2.4 (100 mg, 0.098 mmol), pyridine (21.5 µL), and DMAP (12.0 mg, 0.098 mmol) were dissolved in anhydrous CH_2Cl_2 (4 mL) in a 25 mL round bottom flask. BMPA anhydride (97 mg, 0.29 mmol) was dissolved with in anhydrous CH_2Cl_2 (1 mL) in separate vial. To the stirring reaction mixture was added BMPA anhydride solution and stirring was continued for 24 h at room temperature under nitrogen atmosphere. H_2O (50 µL) was added to the reaction mixture and stirring was continued for 4 h. The reaction mixture was diluted with CH_2Cl_2 (15 mL) and then extracted with 1M $NaHSO_4$ (3 x 10 mL), 10 % Na_2CO_3 (3 x 10 mL), and then with brine (2 x 10 mL). Combined organic layers were dried over anhydrous Na_2SO_4. Then the residue was concentrated in vacuo and dissolved in 10 mL MeOH. The solution mixture was added 50 mg Dowex and stirred for 4 h. The solution mixture was filtered and the residue was concentrated in vacuo. 105 mg of the product having four alcohol group (0.088 mmol), pyridine (39 µL), and DMAP (10.8 mg 0.088 mmol) were dissolved in anhydrous CH_2Cl_2 (4 mL) in a 10 mL round bottom flask. Pentenoic anhydride (96.5 mg, 0.530 mmol) was dissolved in anhydrous CH_2Cl_2 (1 mL) in separate vial. To the stirring reaction mixture was added pentenoic anhydride solution and stirring was continued for 24 h at room temperature under nitrogen atmosphere. H_2O (50 µL) was added to the reaction mixture and stirring was continued for 4 h. The reaction mixture was diluted with CH_2Cl_2 (10 mL) and then extracted with 1M $NaHSO_4$ (3 x 5 mL), 10% Na_2CO_3 (3 x 5 mL), and

then with brine (2 x 5 mL). Combined organic layers were dried over anhydrous Na_2SO_4, and the residue was concentrated in vacuo to give 101 mg of G2[4 alkyne]-G2[4 alkene] as a yellowish viscous liquid (73 % yield). ^{1}H NMR ($CDCl_3$) δ (ppm): 5.74-5.84 (m, 4H); 4.98-5.07 (m, 8H); 4.45 (dt, 1H, *J* = 12.0, 6.4 Hz); 4.16-4.33 (m, 25H); 4.09 (t, 2H, *J* = 6.1 Hz); 3.84 (dd, 1H, *J* = 9.1, 3.6 Hz); 3.61 (t, 2H, *J* = 7.0 Hz); 3.29 (dt, 1H, *J* = 13.9, 6.1 Hz); 3.19 (dd, 1H, *J* = 18.6, 9.0 Hz); 2.99 (dt, 1H, *J* = 14.0, 7.4 Hz); 2.43-2.58 (m, 17H); 2.32-2.42 (m, 16H); 1.93-2.00 (m, 6H);1.29 (s, 3H); 1.24-1.26 (m, 9H); 1.23 (s, 6H). ^{13}C NMR ($CDCl_3$) δ (ppm): 176.7, 174.5, 172.6, 172.2, 172.1, 171.3, 136.6, 115.8, 82.5, 69.4, 65.8, 65.7, 65.5, 65.3, 63.2, 62.3, 46.9, 46.8, 46.5, 38.6, 35.8, 35.7, 33.4, 33.3, 30.7, 28.8, 18.0, 17.7, 14.4. Anal. Calcd. [$C_{79}H_{103}NO_{30}S$]: C, 60.10; H, 6.58; N, 0.89; O, 30.40; S, 2.03. Exact mass: 1577.63, molecular weight: 1578.72. FTIR (cm^{-1}): 3281, 2980, 1733, 1705, 1642.

4.2.6. Hydrogel Formation

As a representative hydrogel formation, to a small vial, G2[4 alkyne]-G0[1 alkene] Dendron (8.68 mg, 0.0088 mmol) and PEG 6 kDa diazide (110 mg, 0.018 mmol) were added and dissolved in 75 µL ethanol and 75 µL THF mixture. To this solution 5 µL deionized H_2O containing sodium ascorbate (2 mg, 10.1 µmol) was added and the mixture was sonicated till a clear solution was obtained. Copper sulfate (3.7 mg, 0.015 mmol) in water (50 µL) was added and placed either at at 50 ºC in an oil bath for 2 h. The formed gel was taken out from the vial and left for stir in EDTA solution (5 %, pH 7-8) to get rid of trapped $CuSO_4$, ethanol to remove unreacted dendron and finally with deionized water. Then, the hydrogel was frozen and freeze-dried in vacuo. To equalize the double bond content in the hydrogel network G2[4 alkyne]-G0[1 OH] dendron was introduced to the gel mixtures where needed. The number of alkene groups in alkene bearing dendrons and the length of the PEG diazide was used in the nomenclature of the hydrogel samples. For example, the hydrogel in which the dendron having 2 alkene groups and PEG 6 kDa were utilized as precursors was named as H-2A-6K. Nomenclature of the hydrogels, the mole ratios of the precursor used and the conversion values are given in Table 4.1.

Table 4.1. Nomenclature and precursor ratios of the hydrogel samples.

	Mole ratios of hydrogel precursors						
Hydrogel	G2[4 alkyne]-G0[1 OH]	G2[4 alkyne]-G0[1 alkene]	G2[4 alkyne]-G1[2 alkene]	G2[4 alkyne]-G2[4 alkene]	PEG 2 kDa diazide	PEG 6 kDa diazide	Yield %
H-1A-2K	-	1.00	-	-	2.05	-	98
H-2A-2K	0.50	-	0.50	-	2.05	-	95
H-4A-2K	0.75	-	-	0.25	2.05	-	96
H-1A-6K	-	1.00	-	-	-	2.05	97
H-2A-6K	0.50	-	0.50	-	-	2.05	95
H-4A-6K	0.75	-	-	0.25	-	2.05	98

4.2.7. Water Uptake Studies

Water uptake values of the hydrogels were investigated by transferring a piece of lyophilized and purified hydrogel sample to a flask containing deionized water. Increase in the weight of hydrogel samples was recorded as a function of time after immersing the gel into the water for a given period of time and drying it on the surface of a wet filter paper. These experiments were repeated at least three times with different pieces of a particular hydrogel samples. The water uptake ratio percent W was calculated via equation the equation below where Mw and Md are the weights of wet and dry samples.[57]

$$W = (Mw - Md) / Md \times 100$$

4.2.8. Morphology of the Hydrogels

Hydrogel samples were placed in deionized water for one day at room temperature in order to reach to the equilibrium state. Then, swollen hydrogels were frozen and freeze-dried in lyophilizer. The morphology of the gels was observed with Jeol Neoscope JCM-5000 scanning electron microscopy (SEM).

4.2.9. Hydrogel Functionalization with BODIPY-thiol

As a representative hydrogel functionalization, a piece of H-1A-2K hydrogel sample (6 mg, 0.0012 mmol alkene) was added to a degassed solution of BODIPY-thiol (0.99 mg, 0.0024 mmol) in THF (50 μL) consisting DPMA (0.12 mg, 0,00048 mmol) as photo-initiator and the mixture was exposed UV light (365 nm, 4 watt) from 3 cm distance for 10 min. Hydrogel was washed with THF to remove unbound BODIPY-thiol. In addition, two control experiments were performed. In the first control experiment same amount of

hydrogel sample were reacted with BODIPY-azide (1.00 mg, 0.0024 mmol) according to literature procedure [7] to evaluate the presence of alkyne groups. For the second control experiment, same amount of hydrogel sample was treated with BODIPY-thiol (0.99 mg, 0.0024 mmol) in THF (50 µL) in the absence of catalyst and UV light for 10 min. and washed with THF to remove BODIPY-thiol. The second control experiment was performed to evaluate presence of unbound BODIPY-thiol in the hydrogel network. Described functionalization and control experiments were applied for all hydrogel samples.

4.2.10. Hydrogel Functionalization with Thiol Bearing D-mannose

Acetyl protected D-mannose thioacetate was deprotected according to literature procedure [142] prior to the functionalization step. For the functionalization of alkene groups with thiol modified D-mannose, as a representative example, a piece of H-1A-2K hydrogel sample (6 mg, 0,0012 mmol alkene) was added to a degassed solution of thiol modified D-mannose (0.57 mg, 0.0024 mmol) in DMF/H_2O (1:1 v/v, 50 µL) consisting DPMA (0.12 mg, 0,00048) as photo-initiator and the mixture was exposed UV light (365 nm, 4 watt) from 3 cm distance for 30 min. Hydrogel was washed with MeOH and H_2O to remove unbound thiol modified D-mannose. All hydrogel samples were functionalized in the same manner.

4.2.11. Immobilization of Con A into Hydrogel Network

D-mannose functionalized hydrogel samples were then treated with 50 µL Con A-Texas red conjugate solution in PBS buffer (0.5 mg/mL) for 30 min and washed with excess amount of PBS buffer. To evaluate presence of unbound Con A-Texas red conjugate in the hydrogel network, alkene functionalized hydrogel samples were also treated with Con A-Texas red conjugate in the same manner.

4.3. Results and Discussion

4.3.1. Synthesis of G2[4 alkyne]-G0[1 OH] Dendron

Synthesis of G2[4 alkyne]-G0[1 OH] dendron was performed using thiol-maleimide Michael addition click reaction in the presence of Et_3N in THF. Synthesis and chemical structure of the dendron are given in Figure 4.1.

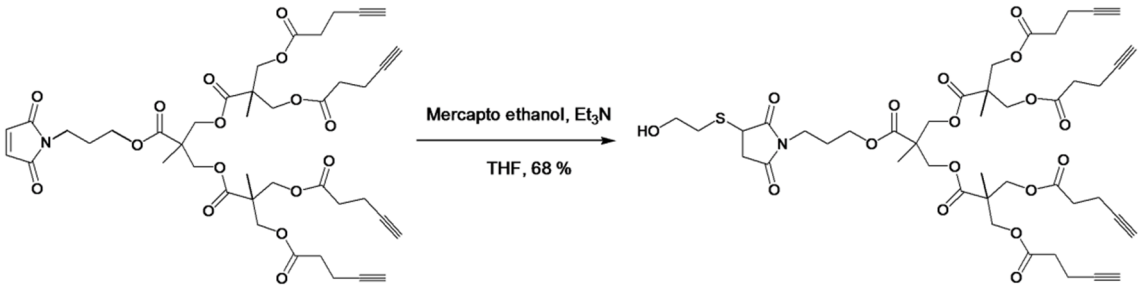


Figure 4.1. Synthesis of G2[4 alkyne]-G0[1 OH] dendron.

Analysis of the synthesized dendron using ^{1}H NMR revealed successful conjugation of mercapto ethanol and maleimide group of the G2 dendron via thiol-maleimide Michael addition click reaction. Full ^{1}H NMR characterization of the G2[4 alkyne]-G0[1 OH] dendron is given in Figure 4.2.

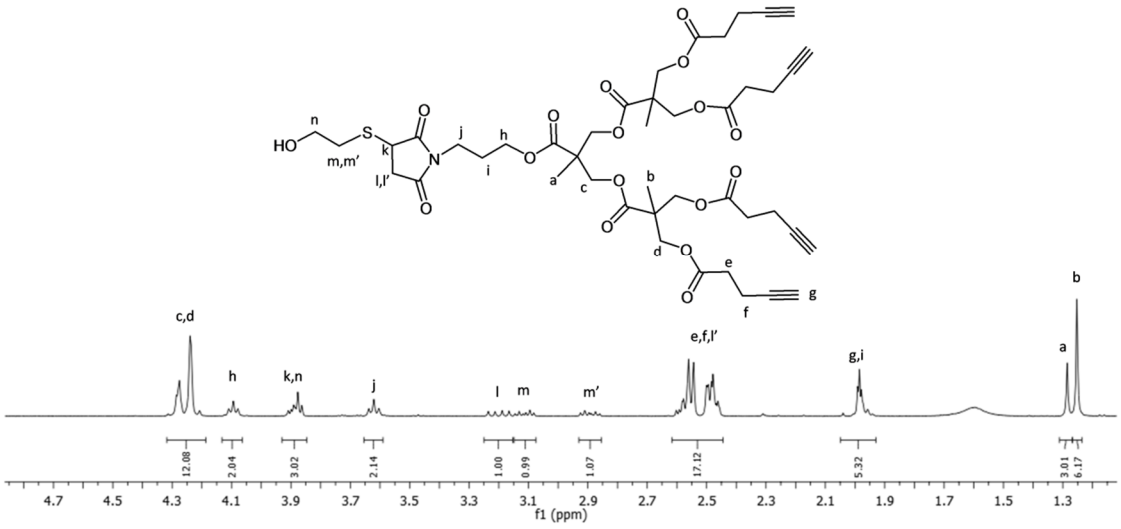


Figure 4.2. ^{1}H NMR spectra of G2[4 alkyne]-G0[1 OH] dendron.

4.3.2. Synthesis of G2[4 alkyne]-G0[1 alkene], G2[4 alkyne]-G1[2 alkene] and G2[4 alkyne]-G2[4 alkene] Dendrons

Synthesis and chemical structures of G2[4 alkyne]-G0[1 alkene], G2[4 alkyne]-G1[2 alkene] and G2[4 alkyne]-G2[4 alkene] dendrons are given in Figure 4.3. For the synthesis of orthogonally functionalized alkene and alkyne containing bow-tie dendrons, higher dendron generations were obtained using the OH group of the G2[4 alkyne]-G0[1 OH] dendron using literature procedures [7]. G2[4 alkyne]-G0[1 OH] and other two bow-tie

dendrons possessing 2 and 4 OH groups were reacted with pentenoic anhydride in the presence of DMAP and pyridine to yield G2[4 alkyne]-G0[1 alkene], G2[4 alkyne]-G1[2 alkene] and G2[4 alkyne]-G2[4 alkene] dendrons.

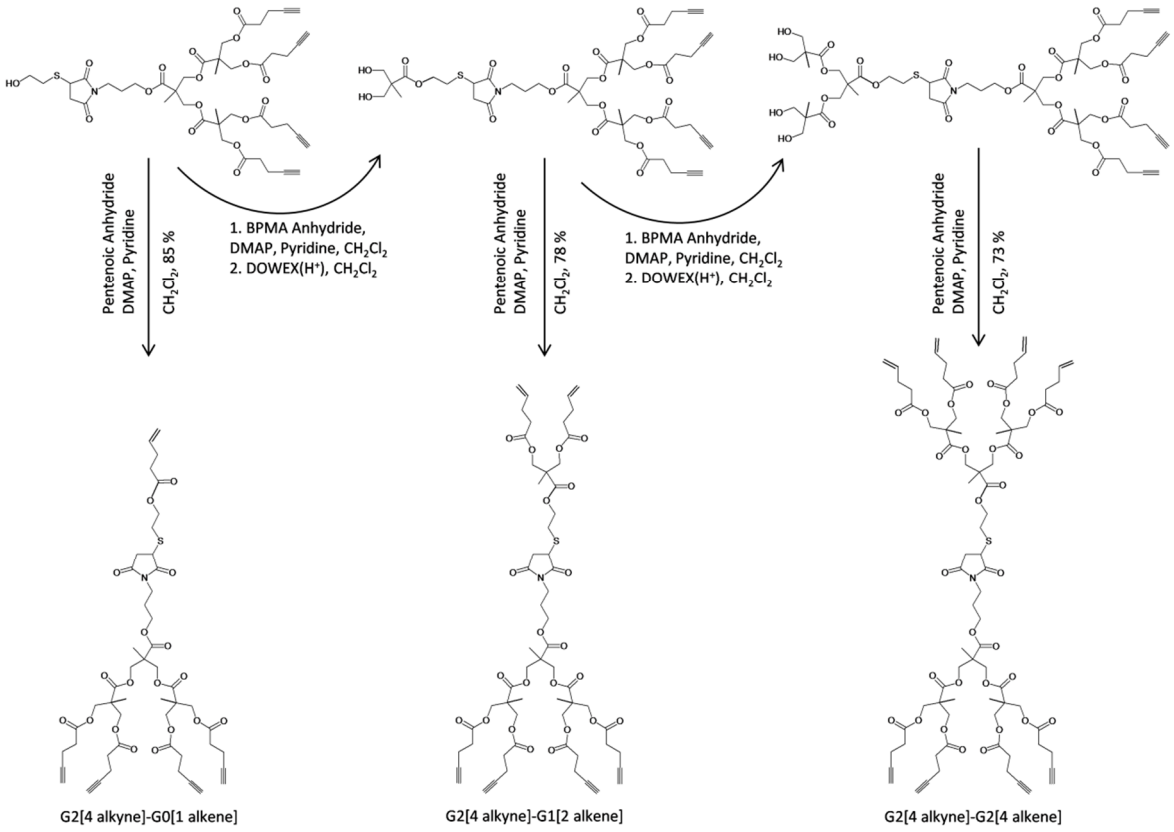


Figure 4.3. Synthesis of G2[4 alkyne]-G0[1 alkene], G2[4 alkyne]-G1[2 alkene] and G2[4 alkyne]-G2[4 alkene] dendrons.

Analysis of the synthesized dendrons using ^{1}H NMR spectroscopy revealed successful functionalization of the OH periphery of the dendrons with pentenoic anhydride. Full ^{1}H NMR characterizations of the G2[4 alkyne]-G0[1 alkene], G2[4 alkyne]-G1[2 alkene] and G2[4 alkyne]-G2[4 alkene] dendrons are given in Figure 4.4, Figure 4.5 and Figure 4.6, respectively.

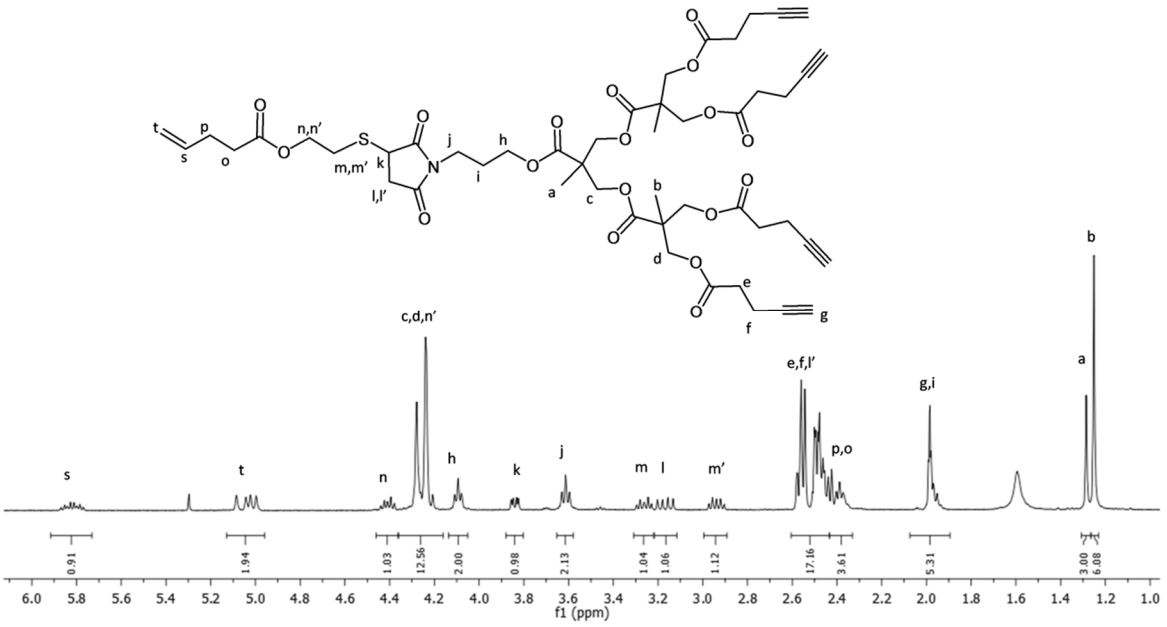


Figure 4.4. ^{1}H NMR spectra of G2[4 alkyne]-G0[1 alkene] dendron.

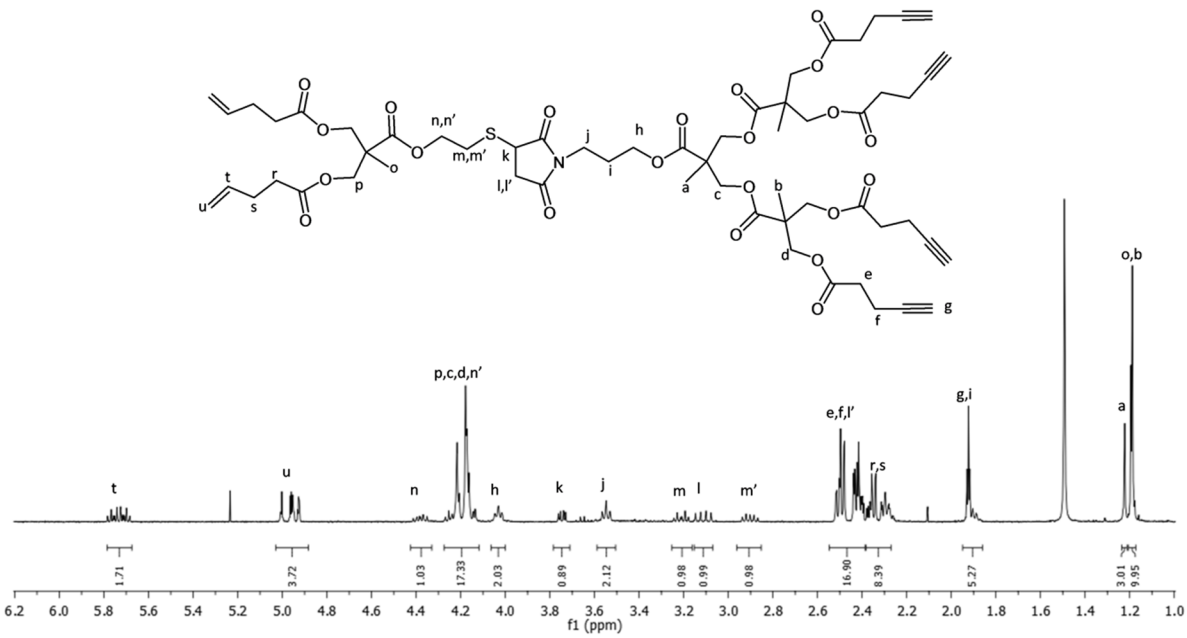


Figure 4.5. ^{1}H NMR spectra of G2[4 alkyne]-G1[2 alkene] dendron.

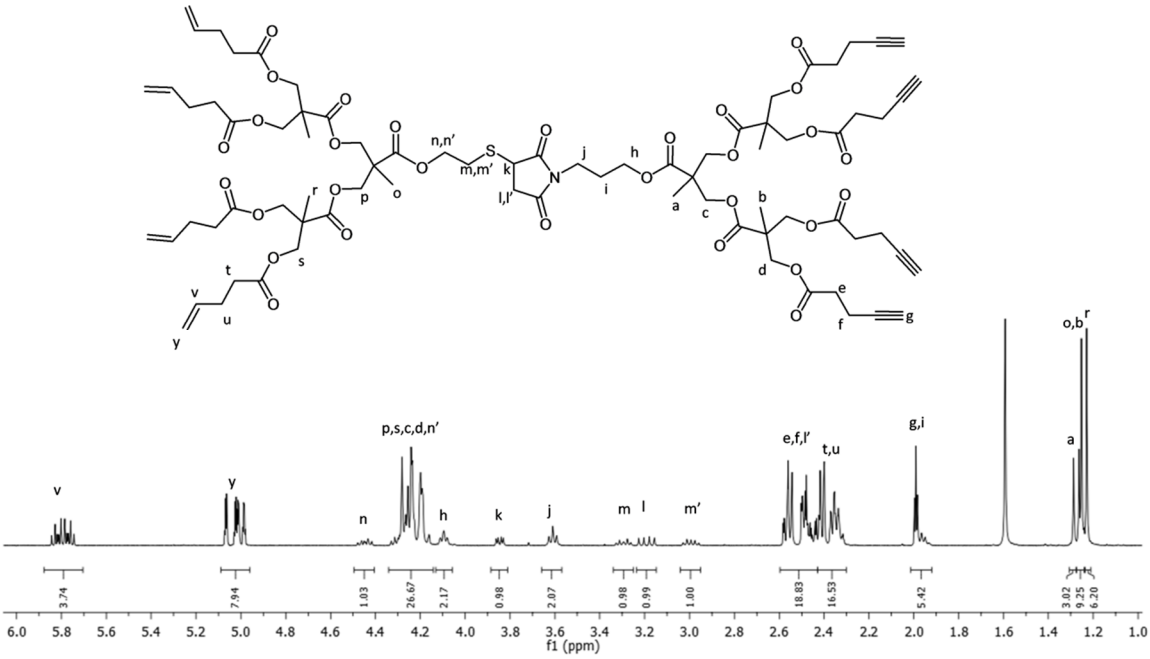


Figure 4.6. ^{1}H NMR spectra of G2[4 alkyne]-G2[4 alkene] dendron.

4.3.3. Hydrogel Formation

Six different hydrogel decorations were designed using synthesized dendrons and PEG diazides (PEG 2kDa and PEG 6kDa) to investigate cluster effect in hydrogel network. Cross-linking was achieved by Huisgen type of [3+2] cycloaddition between the alkyne groups of the dendrons and the azide groups of telechelic PEG diazides (Figure 4.7).

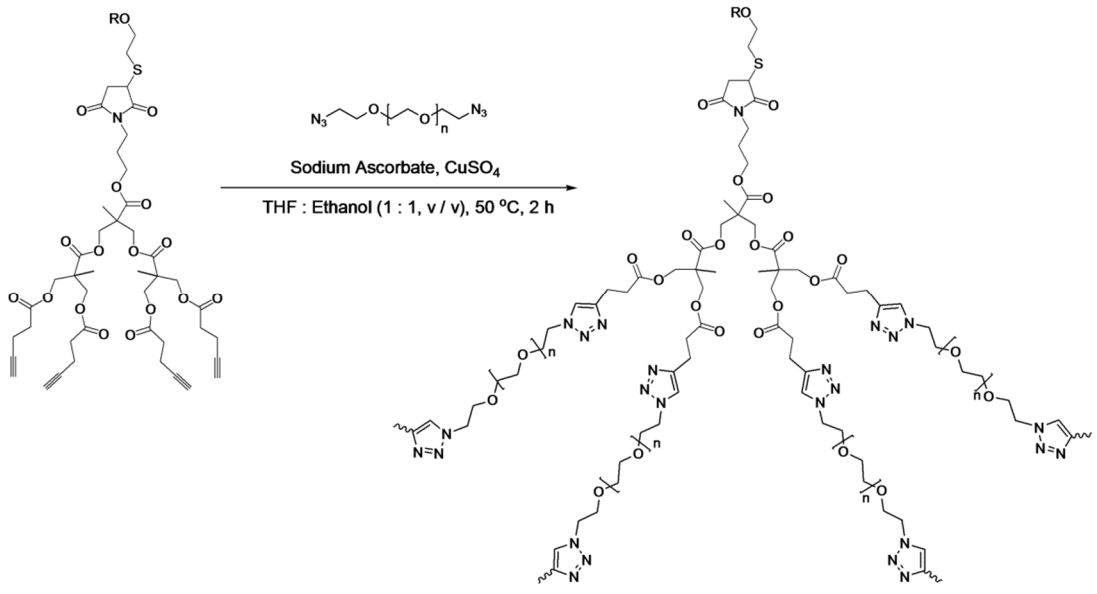


Figure 4.7. Cross-linking of hydrogel precursor via Huisgen type of [3+2] cycloaddition.

Hydrogels were designed to contain similar amount of alkene groups in the network but the locations of the alkene groups were varied in each hydrogel sample because of the dendritic structures containing either 1, 2 or 4 alkene groups in G2[4 alkyne]-G0[1 alkene], G2[4 alkyne]-G1[2 alkene] and G2[4 alkyne]-G2[4 alkene] dendrons, respectively.

To normalize the alkene content in the hydrogel network G2[4 alkyne]-G0[1 OH] dendron was also used as co-precursor in the formation of the hydrogels in the case of higher dendron generations. General scheme for hydrogel formation is given Figure 4.8. Efficient cross-linking is required for the formation of well-defined hydrogel network and to make an accurate comparison between samples in which cluster properties are examined. Gravimetrically determined conversions revealed that at least 95 % hydrogel precursors were incorporated into the hydrogel matrix.

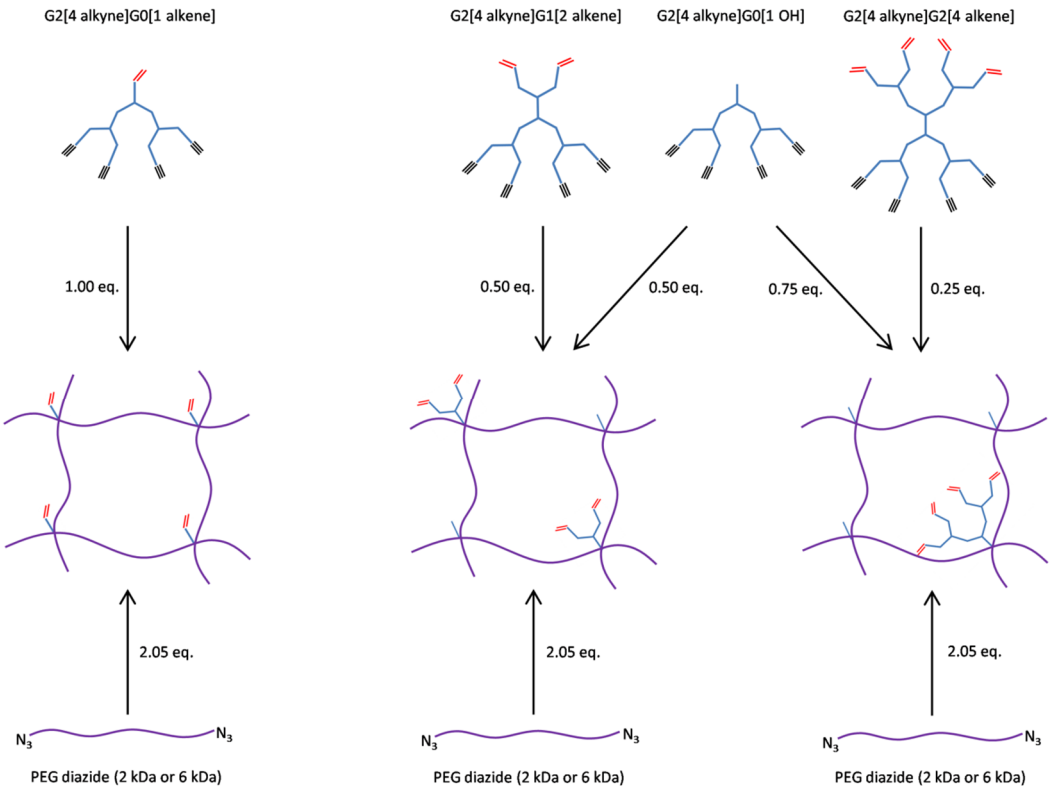


Figure 4.8. General scheme for formation of hydrogels.

The chemical structure of the hydrogel precursors, dendrons and PEG diazides, are given in Figure 4.9.

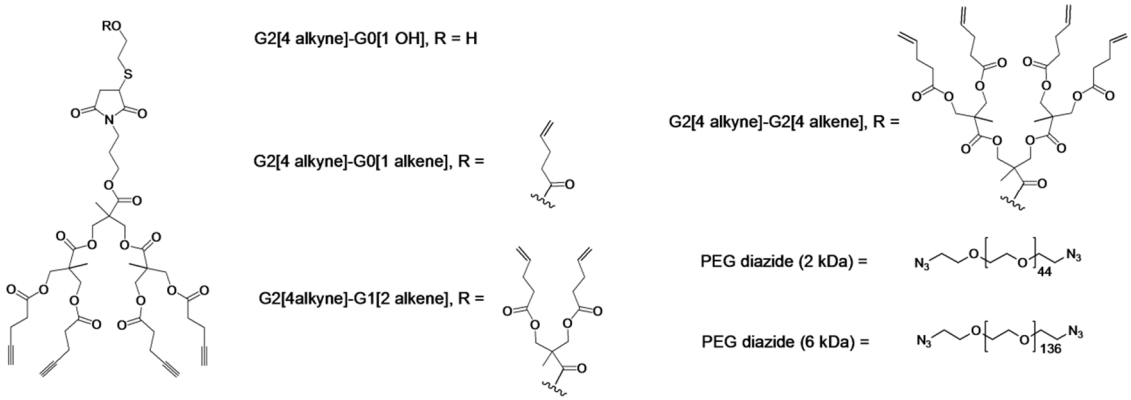


Figure 4.9. The chemical structures of hydrogel precursors.

As another proof of efficient cross-linking, FT-IR measurements showed complete disappearance of specific signals belonging to the azide groups of the PEGs and alkyne groups of the dendrons (Figure 4.10).

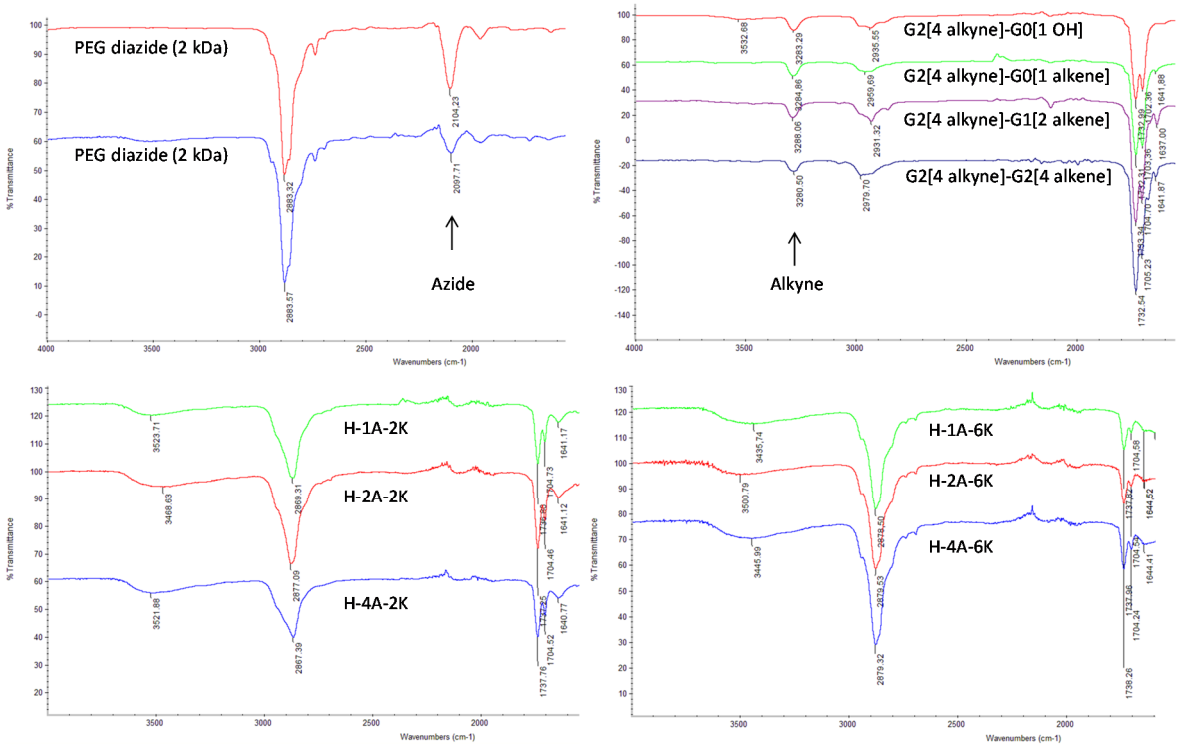


Figure 4.10. FTIR spectra of hydrogel precursors (PEG diazides and dendrons) and hydrogels.

4.3.4. Swelling Studies

Swelling behavior of the hydrogels was investigated by calculating water uptake % as a function of time until equilibrium was attained. It was observed that the increase in the water uptake of the hydrogel was directly proportional to the length of the PEG chains. As demonstrated in Figure 4.11, hydrogel samples prepared using PEG 6 kDa diazide have higher swelling compared to the ones prepared using a PEG 2 kDa diazide. The results also show that introducing G2[4 alkyne]-G0[1 OH] dendron bearing 1 OH group into hydrogel matrix caused a slight increase in water uptake ratio and was proportional to the amount used. All hydrogel samples reached their equilibrated swollen state in 40 min.

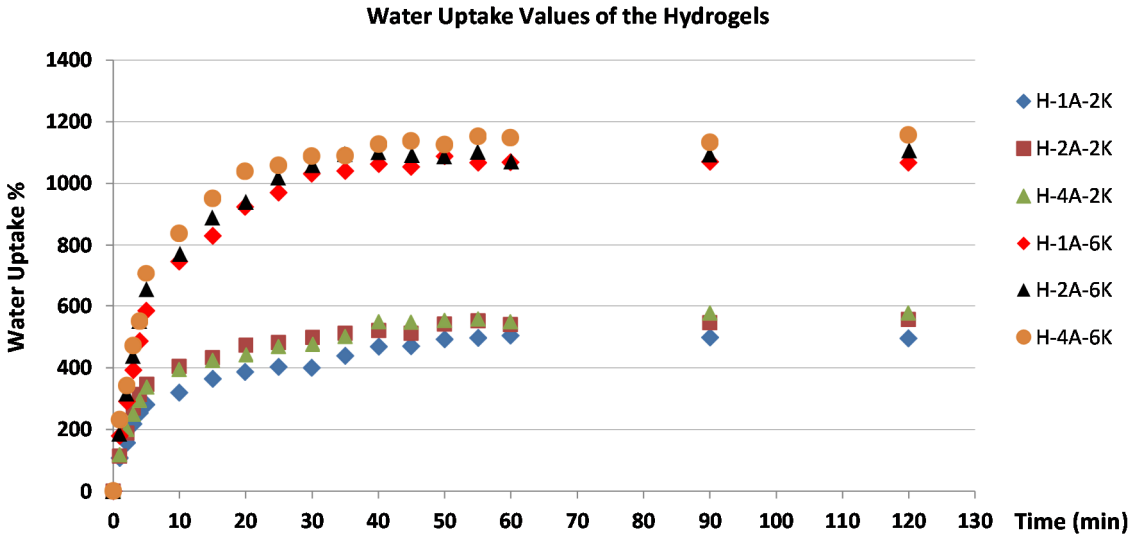


Figure 4.11. Water uptake values of the hydrogel samples.

4.3.5. Morphology of Hydrogel Samples

The obtained hydrogel samples were allowed to reach equilibrated swollen state in deionized water, frozen, and then lyophilized to compare the morphological characteristics of the hydrogels using scanning electron microscopy (SEM). Hydrogel samples where shorter PEG chains were used as one of the precursors together with dendrons resulted in a more densely packed structure compared to the ones prepared with longer PEG chains. More porous structures were obtained upon using longer PEG chains. Using different dendron formulations did not cause an important morphological change in terms of porosity and density while using both long and short chain PEGs. The SEM micrographs of the prepared hydrogels are given in Figure 4.12.

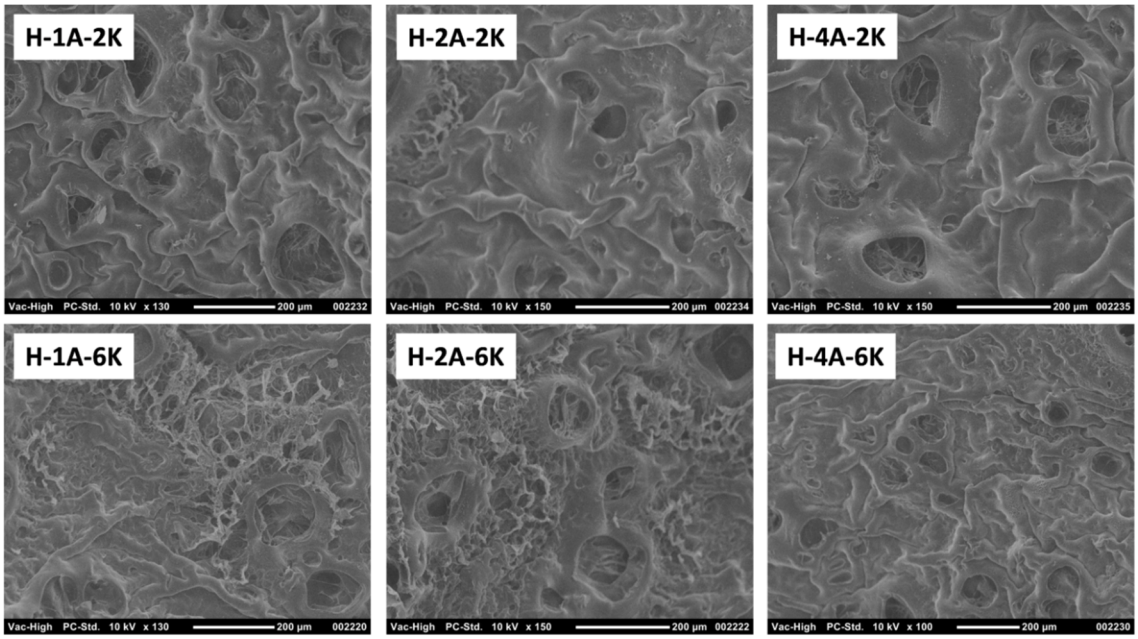


Figure 4.12. SEM images of the hydrogel samples.

4.3.6. Hydrogel Functionalization with Thiol Functionalized D-Mannose

D-mannose functionalization of dendrons bearing alkene groups at the junction points of hydrogel network is illustrated in Figure 4.13.

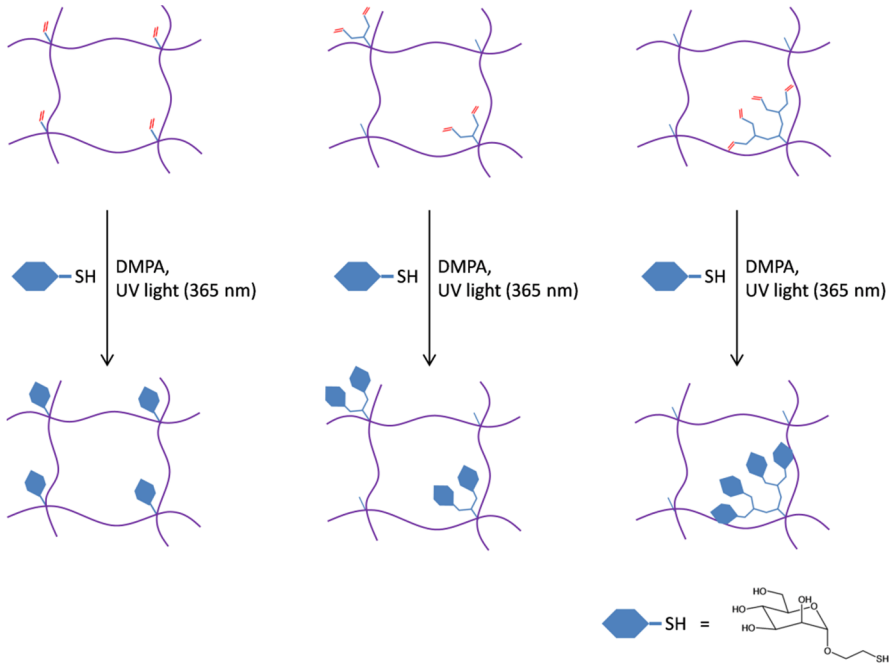


Figure 4.13. D-mannose functionalization of the hydrogels.

Hydrogel networks with different alkene decorations were functionalized with thiol group bearing D-mannose using the radical thiol-ene click reaction. Acetyl protected mannose bearing thioacetate group was deprotected according to the literature procedure [142] just before the functionalization. Lyophilized hydrogel samples were incubated with thiol functionalized D-mannose in DMF/H_2O (1:1, v/v) solution and exposed to UV irradiation in the presence of DMPA. For efficient functionalization within the hydrogel matrix UV exposure was maintained for 1 h. D-mannose functionalized hydrogel samples were then tested for immobilization of Texas red conjugated Con A protein.

4.3.7. Hydrogel Functionalization with BODIPY-thiol

It is important to ascertain that similar numbers of reactive groups are present within the various hydrogels while investigating the presence of a cluster effect. Hydrogel samples containing same amount of alkene groups located at junction points with different decorations were functionalized with a fluorescent dye, BODIPY-SH using radical thiol-ene click reaction. Lyophilized hydrogel samples were incubated with BODIPY-SH in a THF solution and exposed to UV irradiation in the presence of DMPA for 10 min. Following removal of unbound reagents with excess amount of THF, fluorescence images of hydrogel samples were obtained using a fluorescence microscope. The radical thiol-ene click reaction is an efficient chemistry even in hydrogel matrix when using small molecules. It was predicted that the hydrogels possessing same amount alkene groups would be adequately functionalized with thiol bearing small fluorescent dye molecules irrespective of differences in alkene decoration, because of the efficient and irreversible nature of this reaction.

We also performed two control experiments to understand whether there were unreacted alkyne moieties belonging to the dendrons and to evaluate the success of removing unreacted BODIPY-SH molecules. In the first control experiment we incubated hydrogel samples having same amount of alkene groups with BODIPY-azide according to literature procedure [7] to evaluate presence of alkyne groups. Hydrogel samples were also incubated with BODIPY-SH in the absence of DMPA and UV exposure as the second control experiment and hydrogel samples were washed with appropriate solvents in the same manner.

As expected and proved by the fluorescence microscope images, hydrogel samples in which same PEG length and same alkene quantity were established exhibited quite similar fluorescence intensity values with no dependence on the difference in dendron decorations. Lower fluorescence intensity values were obtained due to the decreased cross-linking density in the case of the hydrogel samples prepared from longer PEG units compared to their counterparts prepared using shorter PEGs. Fluorescence microscope images of the hydrogels with functionalizable alkene groups tested with functionalization and control experiments are shown in Figure 4.14.

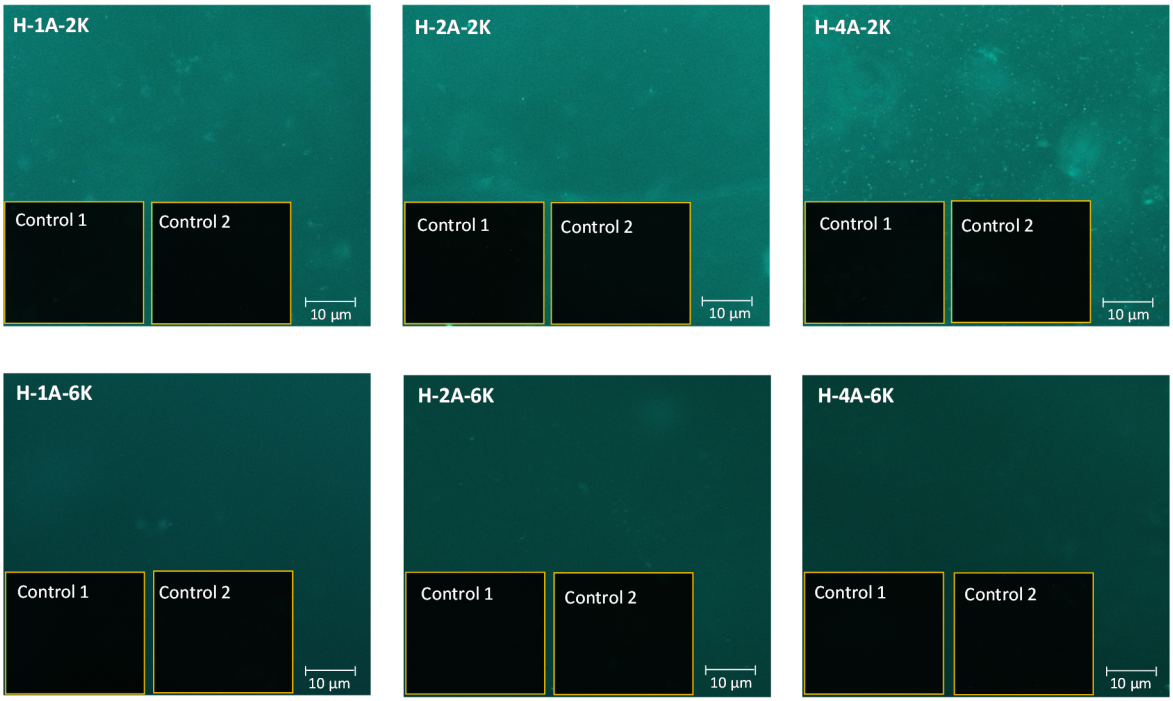


Figure 4.14. Fluorescence microscope images of hydrogel samples. Control 1: Samples were treated with BODIPY-azide, Control 2: Samples were treated with BODIPY-SH in the absence of catalyst and UV exposure.

Fluorescence intensity values of the hydrogel samples following functionalization and control experiments are shown in Figure 4.15 and Figure 4.16. Negligible degree of fluorescence intensity values were obtained in the two control experiments. When the findings obtained from control experiments were compared it can be concluded that the alkyne groups of the dendrons were entirely consumed which proves the efficiency of cross-linking during gelation. In both cases where PEG 2 kDa and PEG 6 kDa were used

as hydrophilic components of the hydrogel matrix, reasonably similar fluorescence intensities were observed when using similar amount of alkene groups.

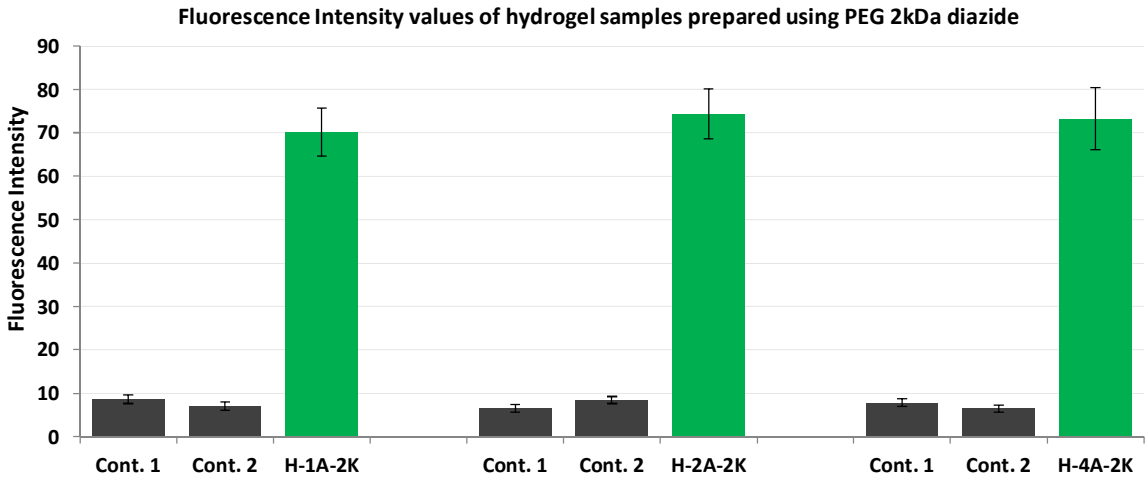


Figure 4.15. Fluorescence intensity values of hydrogel samples prepared by PEG 2kDa diazide. Control 1: samples were treated with BODIPY-azide, Control 2: samples were treated with BODIPY-SH in the absence of catalyst and UV exposure.

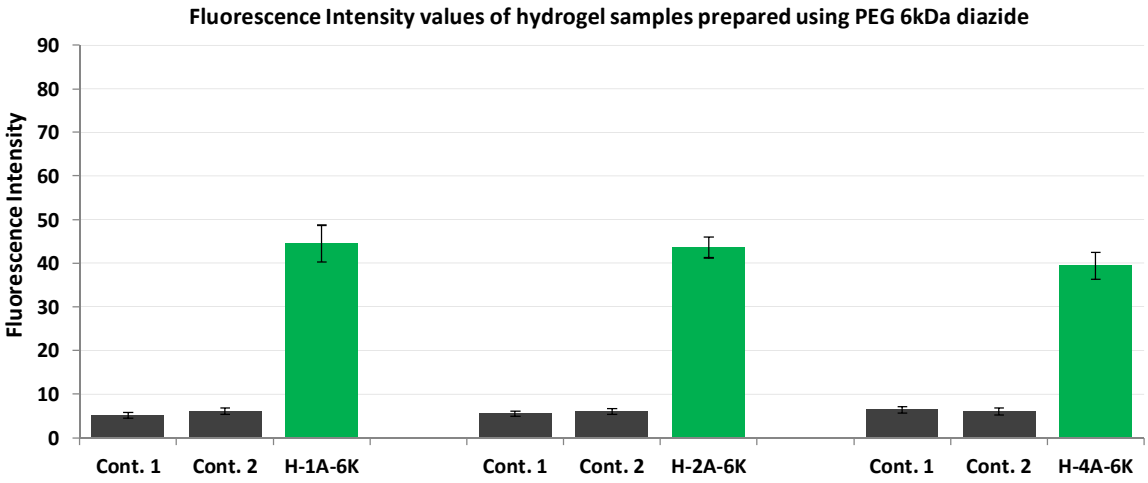


Figure 4.16. Fluorescence intensity values of hydrogel samples prepared by PEG 6kDa diazide. Control 1: samples were treated with BODIPY-azide, Control 2: samples were treated with BODIPY-SH in the absence of catalyst and UV exposure.

4.3.8. Immobilization of Con A-Texas Red Conjugate into Hydrogel Network

Following functionalization of dendron surface in the hydrogel network with thiol bearing D-mannose hydrogel samples were treated with Texas red conjugate of Con A which is a carbohydrate binding protein. Unlike the observations in the case of BODIPY-SH conjugation, we expected that immobilization of Con A would increase in the hydrogel network when higher dendron generations are used as a result of a cluster effect. These two different expected outcomes were explained with a cartoon in Figure 4.17.

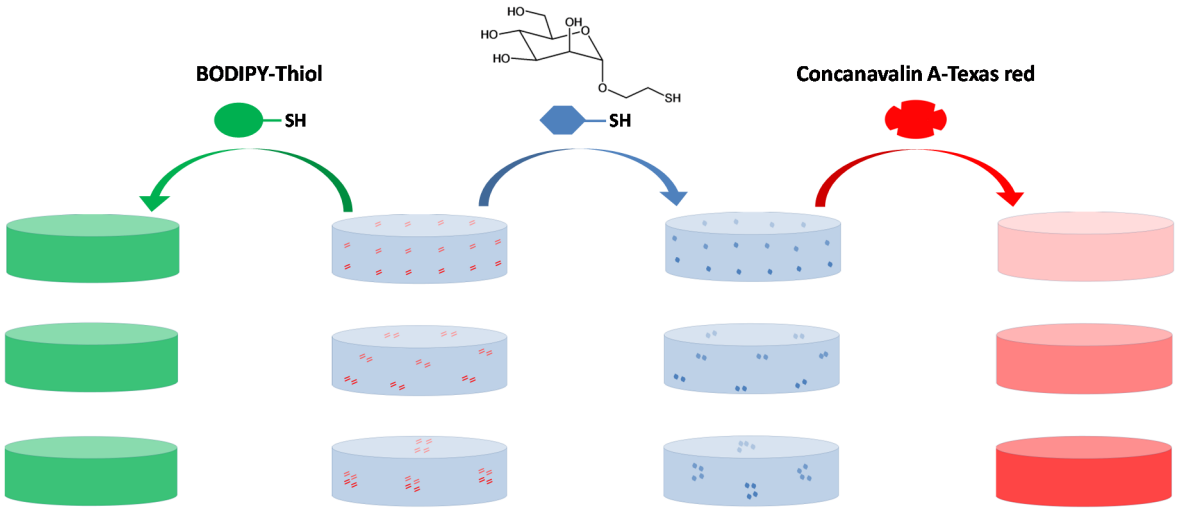


Figure 4.17. Schematic illustration of expected fluorescence intensities following BODIPY-thiol conjugation and Con A immobilization.

Following removal of unbound Con A with excess amount of PBS buffer, fluorescence images of hydrogel samples were obtained using fluorescence microscope. A control experiment was also performed to understand the presence of unbound Con A in the hydrogel matrix. For the control experiment, hydrogel samples possessing alkene functionalities were treated with Con A in the same manner.

The fluorescence microscope analysis showed that hydrogel samples in which D-mannose was decorated differently using different dendrons (G2[4 alkyne]-G0[1 alkene], G2[4 alkyne]-G1[2 alkene], G2[4 alkyne]-G2[4 alkene]) exhibited different fluorescence intensity values. It was observed that fluorescence intensities increased upon increasing the D-mannose conjugated dendron generation responsible for immobilization of Con A.

Fluorescence microscope images of the D-mannose conjugated hydrogels treated with the protein Con A and respective control experiments are shown in Figure 4.18.

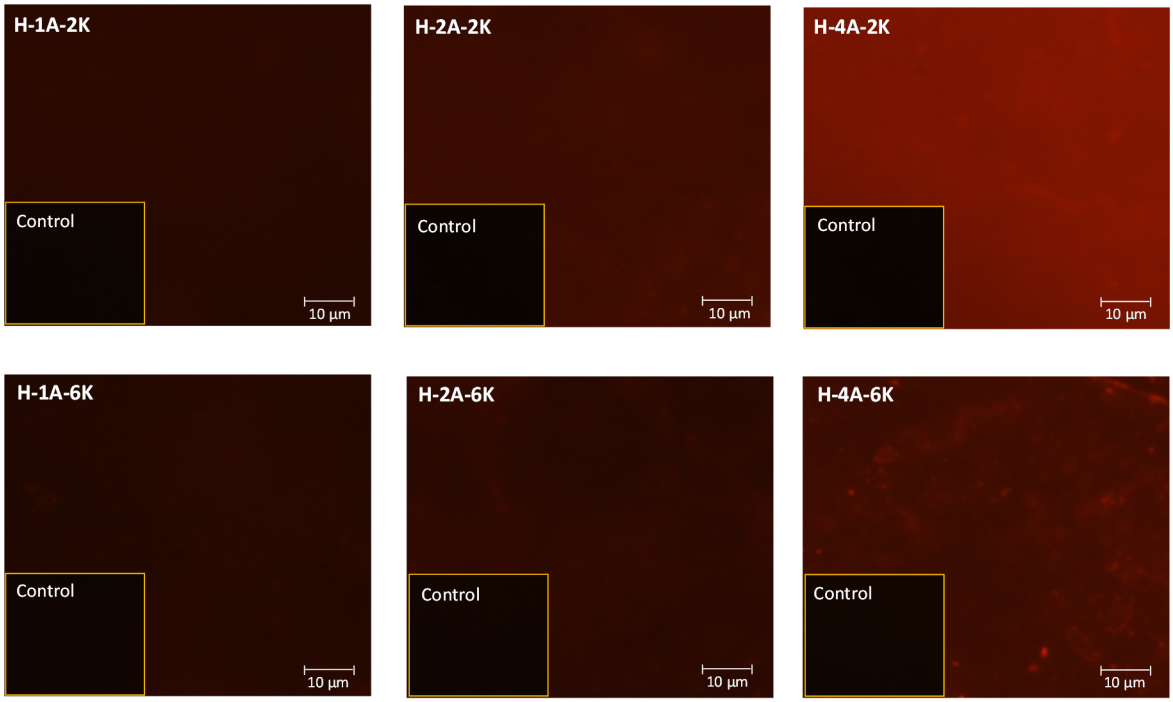


Figure 4.18. Fluorescence microscope images of hydrogel samples. Control: Hydrogel samples bearing alkene groups were treated with Con A in the same manner.

Fluorescence intensity values of the hydrogel samples following immobilization and control experiments are shown in Figure 4.19 and Figure 4.20.

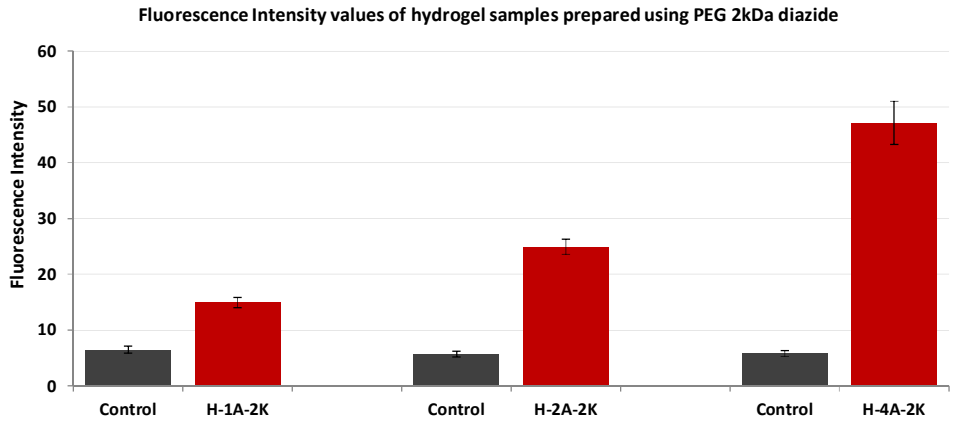


Figure 4.19. Fluorescence intensity values of hydrogel samples prepared by PEG 2kDa diazide. Control: Hydrogel samples bearing alkene groups were treated with Con A in the same manner.

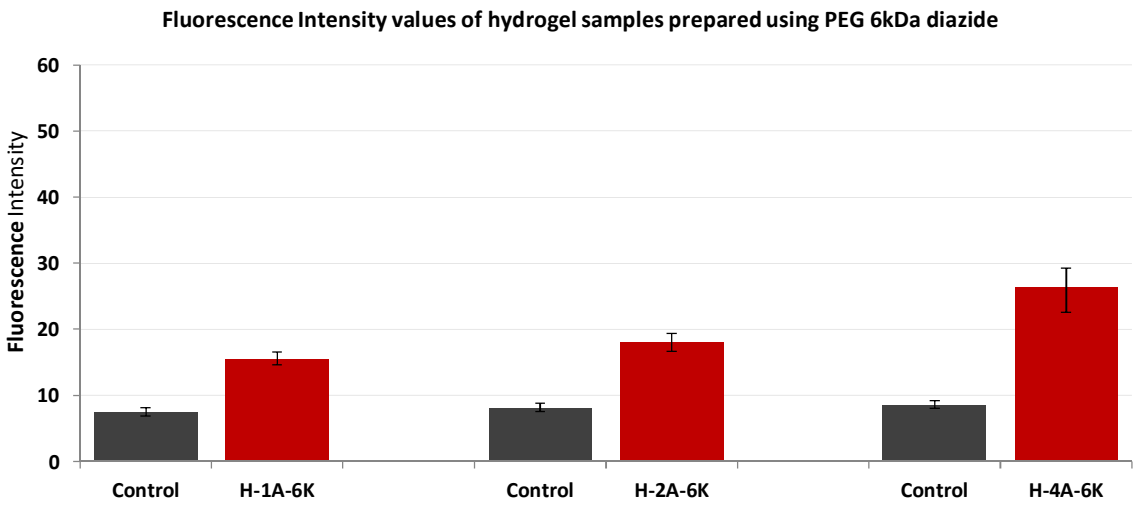


Figure 4.20. Fluorescence intensity values of hydrogel samples prepared by PEG 2kDa diazide. Control: Hydrogel samples bearing alkene groups were treated with Con A in the same manner.

Higher fluorescence intensities were obtained in the case of the hydrogel samples prepared by shorter PEG chains compared to the ones prepared by longer PEG chains, because of the increased cross-linking density. However, in both cases an obvious cluster effect was observed due to increased binding upon increasing the dendron generation.

We also consider the fluorescence intensities obtained by control experiments to evaluate the fold increase as a result of cluster effect upon the increase in dendron generation. Normalized fluorescence intensity values were obtained by subtracting intensity values of control experiments from the ones obtained upon immobilization of Con A protein. Normalized fluorescence intensity values are shown in Figure 4.21. As can be seen from the graphs, in the case of hydrogels prepared from PEG 2 kDa diazides, a 4.9 fold increment in fluorescence intensity was obtained upon using the G2 dendron bearing 4 D-mannose groups compared to the one containing only 1 D-mannose group. In the case of hydrogels prepared by PEG 6 kDa diazide, a 2.2 fold increase was found as a result of lower cross-linking density.

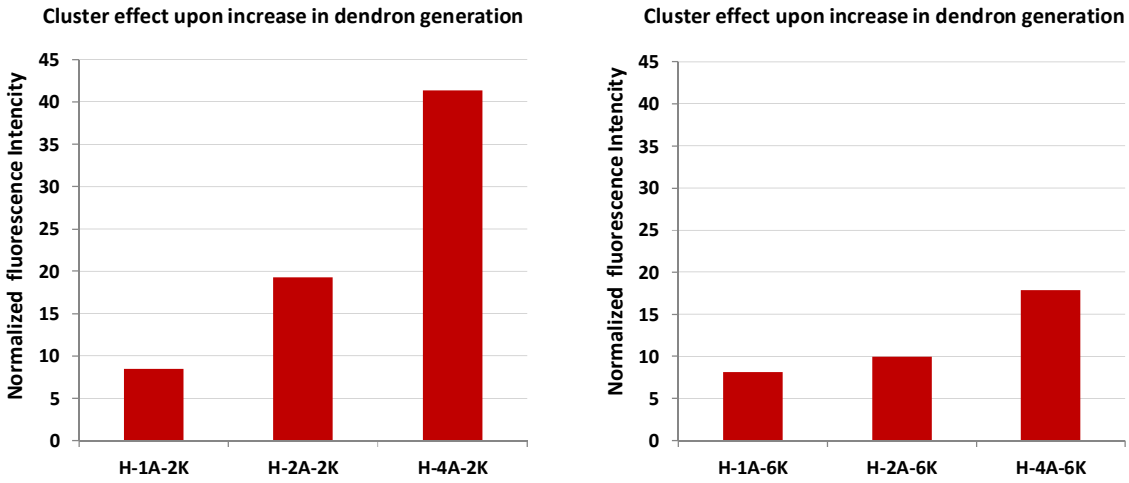


Figure 4.21. Normalized intensity values of the hydrogels prepared by PEG 2kDa diazide (left) and PEG 6kDa diazide (right) following immobilization of Con A.

4.4. Conclusion

Orthogonally functionalized bow-tie dendrons were successfully synthesized and utilized to yield multivalent thiol-reactive well-defined hydrogels. Owing to the orthogonal functionalities, these bow-tie dendrons allowed efficient cross-linking as well as post-gelation functionalization. While alkyne groups of these dendrons were cross-linked with azide containing PEG chains via CuAAC reaction, alkene groups were used to conjugate thiol containing small carbohydrate and dye molecules via radical thiol-ene reaction. Carbohydrate modified hydrogels were further used for immobilization of carbohydrate binding protein, Con A. Hydrogels were designed to possess same amount of alkene groups, but location of the alkene groups were displayed differently due to the hetero-functional nature of the dendrimers. Similar fluorescence intensity values were obtained in the case of functionalization of the hydrogels with small fluorescent dye molecule, BODIPY-SH. Because of the cluster effect in hydrogel network observed for the immobilization of Con A onto D-mannose modified hydrogel, an increased fluorescence was observed upon using higher generation dendrons. To evaluate the contribution of cross-linking density over cluster effect in such 3D environments we compared the hydrogels formed by different PEG lengths. Fluorescence microscope analysis revealed that shorter PEG usage in hydrogel formation contributed to the cluster effect and highly fluorescent images were obtained compared to the hydrogels prepared using longer PEG chains as result of increased density of alkene groups. We suggest that these 3D networks

when designed properly are feasible materials for the immobilization of biomolecules in which the cluster effect is possible. It can be expected that incorporation of such designs prevalent in nature will enhance the ability to detect biomolecules with higher specificity and sensitivity.

5. PHARMACOKINETIC EVALUATION OF LINEAR AND BRANCHED POLYMER DOCETAXEL CONJUGATES

5.1. Introduction

Docetaxel (DTX) is an anticancer agent, from the chemotherapy drug class of taxane. It is derived from Paclitaxel, an extract from the inner bark of Pacific yew tree Taxus brevifolia. DTX inhibits microtubule depolymerization by binding to microtubules [143]. It has a broad antitumor efficacy against a wide range of tumors and approved by FDA for the treatment of breast cancer, non-small cell lung cancer, head and neck cancer, prostate cancer and gastric adenocarcinoma [144]. However, drawbacks in its administration and side effects restrict its clinical use. DTX is poorly soluble in aqueous solutions, and so in its systemic administration a solvent system including polysorbate 80 and ethanol is used before being diluted in saline solutions [145]. The biological activity of DTX in the bloodstream also provides the occurrence of systemic side effects. It has been reported that polysorbate 80 contributes to the side effects of DTX such as acute hypersensitivity, peripheral neuropathy and fluid retention [146,147]. Besides having poor water solubility and systemic side effects, DTX has also very short half-life (β half-life; 38.3 min) [143]. Great effort has been made to eliminate systemic side effects, improve the pharmacokinetic profile and antitumor activity of chemotherapy drugs. Alternative formulations, including nanoparticles [148,149], micelles [150,151,152], liposomes [153,154,155], nanogels [156,157] and polymer drug conjugates [98,158,159] have been developed.

There are various type of polymer drug conjugates fabricated by using linear polymer chains such as poly ethyleneglycol (PEG) which have functional groups at the end of the polymer chains [160]. Mono or di functional linear polymer chains have limited functional groups for drug conjugation. That is resulted with low drug percentage of final polymer drug conjugate for high molecular weight linear polymers. On the other hand, aggregation is another phenomenon which is hard to deal with for this type polymer drug conjugates. Introducing drug monomers or drug attachable monomers to the polymer backbone is another common strategy to obtain polymer drug conjugates [98,158]. This

type polymer drug conjugates require a linker between drug and the polymer backbone. Enzymatically cleavable peptide linkers such as Gly-Phe-Leu-Gly (GFLG) were widely used in the area. DTX examples for this type conjugates were made up with small water soluble monomers such as N-(2-hydroxypropyl) methacrylamide (HPMA) to form backbone of the polymer drug conjugates. The enzymatically cleavable linkers between DTX and the backbone of the polymer conjugate are unstable in the blood stream due to lack of protection or steric hindrance for this type polymer drug conjugates.

This project was designed to reduce systemic side effects of DTX, while improving its pharmacokinetic and release profile for better antitumor activity. We synthesized the conjugate by free radical polymerization of poly(ethylene glycol) methyl ether methacrylate (POEGMEMA) monomer and the drug monomer having GFLG linker between DTX and the polymerizable part. Water soluble nature of the POEGMEMA monomer enabled us to provide a water soluble polymer drug conjugate for DTX. POEGMEMA-DTX conjugate does not require any additional solvents such as ethanol and polysorbate 80. It is soluble in saline, PBS buffer or any water based solution. The novelty of this polymer drug conjugate is having oligo (ethylene glycol) methyl ether methacrylate (OEGMEMA) monomer to provide branches on polymer backbone which increase stealth of linker and the drug. It was expected that this steric hindrance would provide a slow release compared to non-branched polymer drug conjugate systems. For better understanding the effect of branching we also synthesized HPMA based polymer drug conjugate (PHPMA-DTX).

HPMA has been widely used to obtain drug carriers over the last 30 years. These HPMA based drug carriers are biocompatible, water soluble, non-toxic, non-immunogenic copolymers and they were mostly designed for tumor treatment via site-specific delivery of anticancer agents into tumor tissues [161]. It was shown that, PHPMA copolymers accumulates in solid tumors due to EPR effect and the accumulation efficiency is depending on molecular weight of the copolymers [162]. Kidney and liver based clearance have great importance on biodistribution of macromolecules and it was shown that PHPMA copolymers with molecular weights less than ~ 45 kDa, like some other copolymers, are rapidly filtered by the kidney [163,164]. PHPMA-DTX conjugate was designed with similar strategy by using GFLG linker between polymer back bone and the

drug. POEGMEMA-DTX conjugate was designed as a prodrug for chemotherapy. Enzymatic release, cytotoxicity, pharmacokinetic and biodistribution profiles were investigated for better understanding the effect of branched structure.

5.2. Experimental

5.2.1. Materials

Oligo(ethylene glycol) monomethyl ether methacrylate (OEGMEMA, Mn= 300g/mol) and 2,2′-azobisisobutyronitrile (AIBN) were purchased from Aldrich. All other solvents were HPLC grade, obtained from Merck and used without further purification. N-(2-hydroxypropyl) methacrylamide (HPMA) [165], N-methacryloyl glycyl phenylalanyl leucyl glycine (MA-GFLG-OH) [166], and MA-GFLG-DTX monomer [158] were synthesized and characterized according to previously described methods. The monomer and copolymer characterizations involved ^{1}H NMR spectroscopy (Varian 400 MHz NMR spectrometer), fourier transform infrared (ATR-FTIR) spectroscopy (Nicolet 380, Thermo Scientific, USA) and gel permeation chromatography (GPC) (Shimadzu, Japan) with a mobile phase solution of 0.05 M lithium bromide in dimethylaceteamide (DMAc). GPC measurements of copolymers were carried out with PSS WinGPC Unity software. PSS Gram (length/ID 300 mm × 8 mm, 10 μm particle size) column was calibrated with polymethyl methacrylate standards, using refractive index detector (RID-10A). Docetaxel concentration in plasma was characterized by liquid chromatography-mass spectrometry (LC-MS) analysis using a LCMS-2020-Mass Spectrometer System (Shimadzu, Japan) equipped with an C-18 5 μm 150 × 4.6 mm column. Whole blood count analyses were performed using Mindray BC-2800 blood counter.

5.2.2. Synthesis of POEGMEMA-DTX and PHPMA-DTX Conjugates

POEGMEMA-DTX and PHPMA-DTX polymer drug conjugates were synthesized via free radical copolymerization of OEGMEMA and MA-GFLG-DTX monomers; and HPMA and MA-GFLG-DTX monomers, respectively, in anhydrous DMF using AIBN initiator. The feed composition of monomers for all polymerization reactions is given in Table 5.1. Firstly, OEGMEMA or HPMA monomer mixtures including AIBN in DMF were sealed in a round bottom flask under nitrogen and stirred at 80 ºC for 1 h. Then these

reaction mixtures were transferred into another oil bath at 50 ºC and MA-GFLG-DTX monomer in 500 μL anhydrous DMF was added under nitrogen and stirred for 47 h for POEGMEMA-DTX and 71 h for PHPMA-DTX conjugates. DMF was removed under reduced pressure. The crude product was dissolved in dichloromethane (DCM) and precipitated in diethyl ether. The precipitated copolymers were dried under vacuum and characterized using size exclusion chromatography (SEC) and ^{1}H NMR. FTIR spectra of PHPMA-DTX and POEGMEMA-DTX conjugates are given in Figure A.13, Figure A.14, Figure A.15 and Figure A.16.

5.2.3. Enzymatic Release Study

The released DTX amount from polymer drug conjugates was measured by LC-MS. Briefly, 0.25 mg polymer drug conjugates were dissolved in 10 μL DMSO separately. 100 μL buffer solution (0.1 M citric acid/0.2 M Na_2HPO_4, 2 mM EDTA, 10 mM GSH, pH: 5.0) was added to these polymer drug conjugate solutions. Finally 20 μL enzyme solution (0.1 M citric acid/0.2 M Na_2HPO_4, 0.2 mM papain, pH: 5.0) was added to the solution mixtures and final solution was shortly vortexed and incubated at 37 ºC. 370 μL acetonitrile was added at the end of incubation times (t_0, 30 m and 1, 2, 3, 4, 5, 6, 8, and 24 h) for each sample, and then samples were vortexed and spinned down. The DTX content in supernatant was evaluated by LC-MS to calibration standards of DTX prepared using serial dilutions.

5.2.4. Cell Lines

Human breast adenocarcinoma (MDA-MB-231) and human pancreas adenocarcinoma (BxPC3) cell lines were obtained from Lonza. Cells were grown in 75 cm^2 flasks in RPMI medium with with 10 % FBS and 1 % penicillin-streptomycin, 1 % sodium pyruvate, 1 % non-essential amino acids in a humidified atmosphere of 5 % CO_2 and at 37 °C. Cells were passaged 1:6 using 0.25 % trypsin-EDTA 3 times per week.

5.2.5. In Vitro Cell Viability Assay

Cell viabilities were determined by Cell Counting Kit-8 (CCK-8, Fluka). Cells were seeded in 100 μL of culture medium at a density of 5000 cells / well into 96-well plates in quadruplicates for each drug concentration. After overnight incubation to let cells to

adhere, cell media was replaced with fresh medium containing various concentrations of polymer drug conjugates, free drug, or controls. To increase the water solubility of Docetaxel, stock solution was prepared in 10 % dimethyl sulfoxide (DMSO) in growth medium (V/V) and subsequently diluted where the final DMSO concentration was below 0.5 % (V/V). Polymer drug conjugate solutions are prepared via sonication without any organic solvent addition. Cells were incubated continuously for 48 h in the presence of the polymer drug conjugates. Following the treatment, cell media containing the conjugates was removed, wells were washed with 1× PBS. For the determination the cell viability, 100 µL of culture medium together with 10 µL of CCK-8 solution was added into each well. After 4h incubation the absorbance values of three replicates per treatment at 450 nm were measured with a plate reader (Multiscan FC, Thermo Scientific, USA). Viability of treated cells was expressed as percentage of control cells (cell media only). Half maximal effective concentration (EC_{50}) values were obtained from concentration response curves by nonlinear regression analysis.

5.2.6. Animals

Male Wistar-Albino rats (270-320 g) were obtained from Boğazici University Experimental Animal Production and Maintenance Unit and maintained in a controlled environment with a 12 h light/dark cycle. Water was provided ad libitum. After internal jugular vein and carotid artery catheterization [167] rats were allowed to recover in individual cages for 24 h with harness jackets. Food was withheld 8 h for pre- and post-dosing but was provided ad libitum at all other times. Animal experimentation was approved by the Boğazici University Animal Experiments Local Ethics Committee (08.06.2015).

5.2.7. Pharmacokinetic Procedure

Free Docetaxel (DTX) in 125 µL polysorbate 80 was dissolved with 875 µL 13 % v/v solution of ethanol in saline to give 1 mL dosing solution for each rat. Dosing solutions for polymer drug conjugates were prepared by dissolving the conjugates with saline. After internal jugular vein and carotid artery catheterization, rats (n=4 for each group) were dosed with free DTX (5 mg/kg) and polymer drug conjugates (5 mg / kg DTX equivalent) via jugular vein cannulas with 2 min administration. Blank blood samples just before the dosing, and t_0 blood samples immediately following the infusion were collected in

heparinized tubes via the carotid artery cannula for all rats. Further blood samples were collected after 10 and 30 min and 1, 2, 4, 6, 8, 24, 27, 30 and 48 h for rats dosed with polymer drug conjugates and 5, 10, 20, 30 and 45 min and 1, 1.5, 2, 4, 6, 8 and 24 h for rats dosed with free DTX in heparinized tubes. Blood samples (200 μL) were collected at each data point. Blood samples were immediately centrifuged following collection and obtained plasma samples were kept in -20 ºC till the plasma drug concentration measurements.

5.2.8. Quantification of DTX in Plasma Samples

Rat plasma samples (50 μL) were added 450 μL acetonitrile in eppendorf tubes and vortexed for 1 min. Then tubes were centrifuged and the free DTX concentration in supernatant was measured with LC-MS using a free DTX calibration curve. For the quantification of total DTX, another 50 μL plasma samples were added 50 μL 1x phosphate buffered saline (PBS) and incubated 24 h at 37 ºC. Following incubation, samples were added 400 μL acetonitrile in eppendorf tubes and vortexed for 1 min. Then tubes were centrifuged and the free DTX concentration in supernatant was measured with LC-MS using a total DTX calibration curves prepared for each polymer drug conjugate. For the preparation of samples of total DTX calibration curves, polymer drug conjugates at different concentrations in 50 μL 1x PBS were incubated together with 50 μL rat plasma for 24 h at 37 ºC. Following addition of 400 μL and vortexing, samples were centrifuged and the measured free DTX concentration values in supernatant was adopted as standard total DTX concentration values.

5.2.9. Procedure for Biodistribution Study

All animals were sacrificed at 48 h and main organs liver, spleen, kidneys, heart, lung, kidneys and muscle tissue (about 1 g) were collected and kept at -80 ºC till the biodistribution measurements.

5.2.10. Quantification of DTX in Organ and Tissue Samples

Whole organ and tissue samples were homogenized with adequate amount of acetonitrile and centrifuged. The free DTX concentration in 500 μL supernatant measured with LC-MS using a free DTX calibration curve. For the quantification of total DTX,

another 500 µL supernatant samples were incubated for 24 h at 37 ºC. Following incubation, the total DTX concentration values were measured with LC-MS using calibration curve prepared before for the total DTX in plasma.

5.2.11. Maximum Tolerated Dose (MTD) Study

Male Balb-C mice separated into 3 groups (n=3). The mice in the first group were injected with POEGMEMA-DTX (50 kDa) (25 mg/kg DTX equivalent), the ones in the second group injected with POEGMEMA-DTX (50 kDa) (50 mg/kg DTX equivalent) and the last group was injected with POEGMEMA-DTX (50 kDa) (100 mg/kg DTX equivalent) via tail vein. Body weights were measured every day. Blood samples (50 µL) were collected at the dosing day (just prior dosing), after 48 h and the day mice were sacrificed from the orbital sinus or by cardiac puncture under anesthesia and blood count values were obtained using a whole blood counter. Major organs were collected after mice were sacrificed.

5.2.12. Statistics

One-way ANOVA test was used for the statistical analysis of pharmacokinetic and biodistribution results. Statistical significance was identified at a level of $p < 0.05$.

5.3. Results and Discussion

5.3.1. Synthesis of MA-GFLG-DTX

MA-GFLG-DTX monomer was synthesized as previously described methods [158] by coupling reaction of MA-GFLG-OH and DTX using diisopropylcarbodiimide (DIPC) as coupling reagent in anhydrous DMF. Analysis of MA-GFLG-DTX using ^{1}H NMR revealed successful coupling reaction of MA-GFLG-OH and DTX, as was evident from the proton resonances around 5.77 and 5.42 ppm due to the terminal alkenyl group of MA-GFLG-OH and the proton resonances around 8.12 and 8.14 ppm due to the phenyl group of DTX. Full ^{1}H NMR (CD_3OD) spectrum and characterization of MA-GFLG-DTX is given in Figure 5.1.

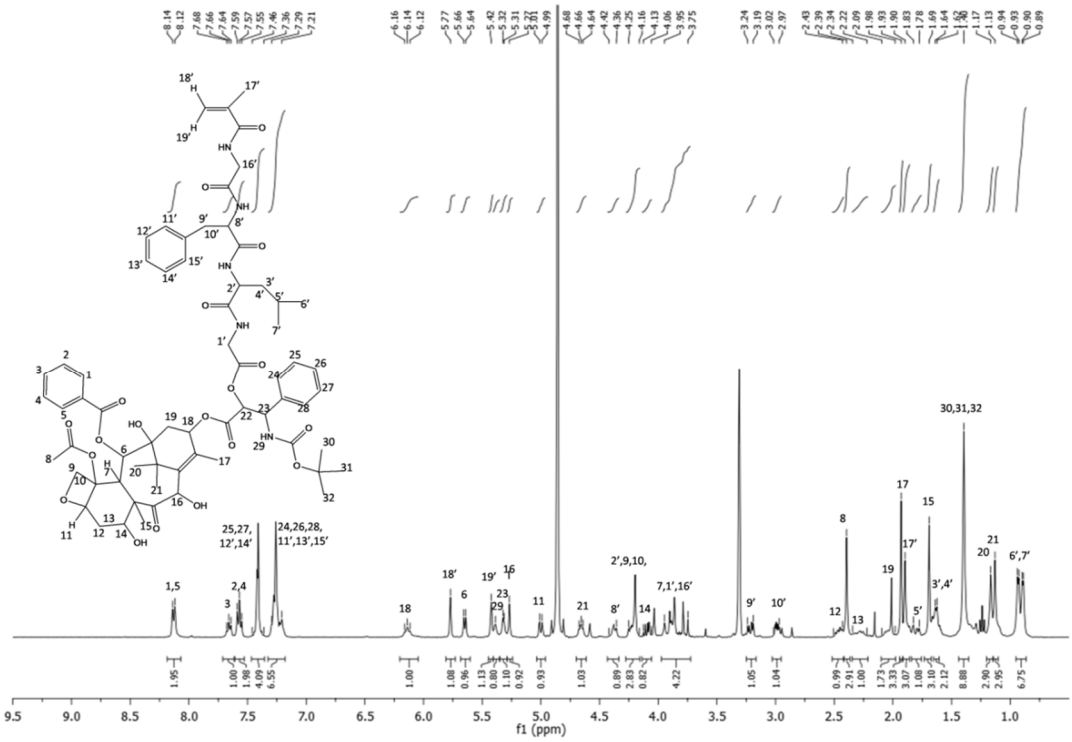


Figure 5.1. ^{1}H NMR spectrum and characterization of MA-GFLG-DTX.

5.3.2. Synthesis of POEGMEMA-DTX Conjugates

OEGMEMA and MA-GFLG-DTX monomers were polymerized via free radical copolymerization using AIBN as initiator in anhydrous DMF. Polymerization reaction is shown in Figure 5.2.

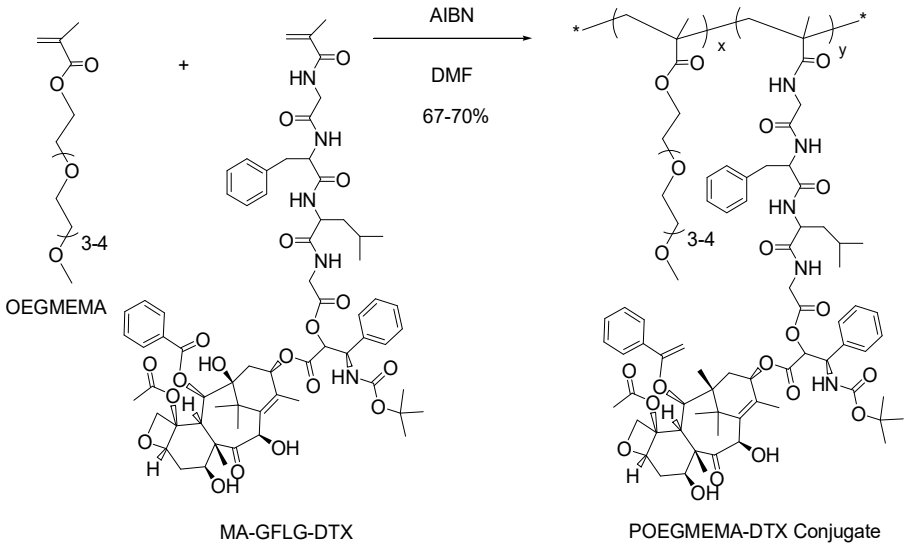


Figure 5.2. Synthesis of POEGMEMA-DTX polymer drug conjugates.

Analysis of POEGMEMA-DTX using ^{1}H NMR revealed successful copolymerization of MA-GFLG-DTX and OEGMEMA, as was evident from the proton resonances around 8.12 and 8.14 ppm due to the phenyl group of DTX, the proton resonances around 3.39 ppm due to the terminal methyl ether group of OEGMEMA and the disappearance of proton resonances around 5.77 and 5.42 ppm due to the terminal alkenyl group of MA-GFLG-DTX. Varying the feed ratio of monomers resulted in POEGMEMA-DTX conjugates with different molecular weights, 50 kDa and 85 kDa. Full ^{1}H NMR (CD_3OD) spectrum of POEGMEMA-DTX conjugates (50 kDa and 85 kDa) are given in Figure 5.3 and Figure 5.4, respectively. The experimentally obtained monomer compositions of the copolymers show that the incorporation of the MA-GFLG-DTX monomer is lower than aimed in the feed. The weight percent of DTX in POEGMEMA-DTX conjugates was calculated by comparison of integration of the proton resonance at 3.39 ppm due to the terminal methyl ether group of the OEGMEMA monomer with proton resonances around 8.12 and 8.14 ppm due to the phenyl group of DTX. Drug contents for POEGMEMA-DTX (50 kDa) and POEGMEMA-DTX (85 kDa) were calculated as 8.17 % and 4.41 % by weight, respectively. Polymerization conditions and properties of POEGMEMA-DTX conjugates are given in Table 5.1.

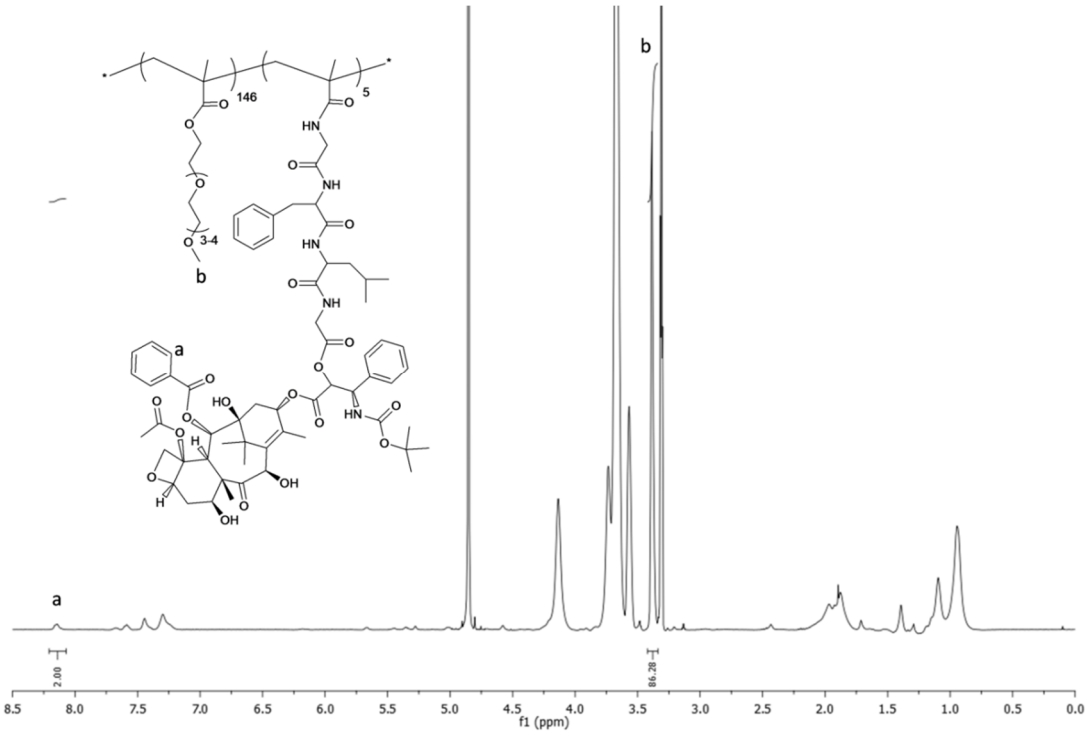


Figure 5.3. ^{1}H NMR spectrum of POEGMEMA-DTX (50 kDa).

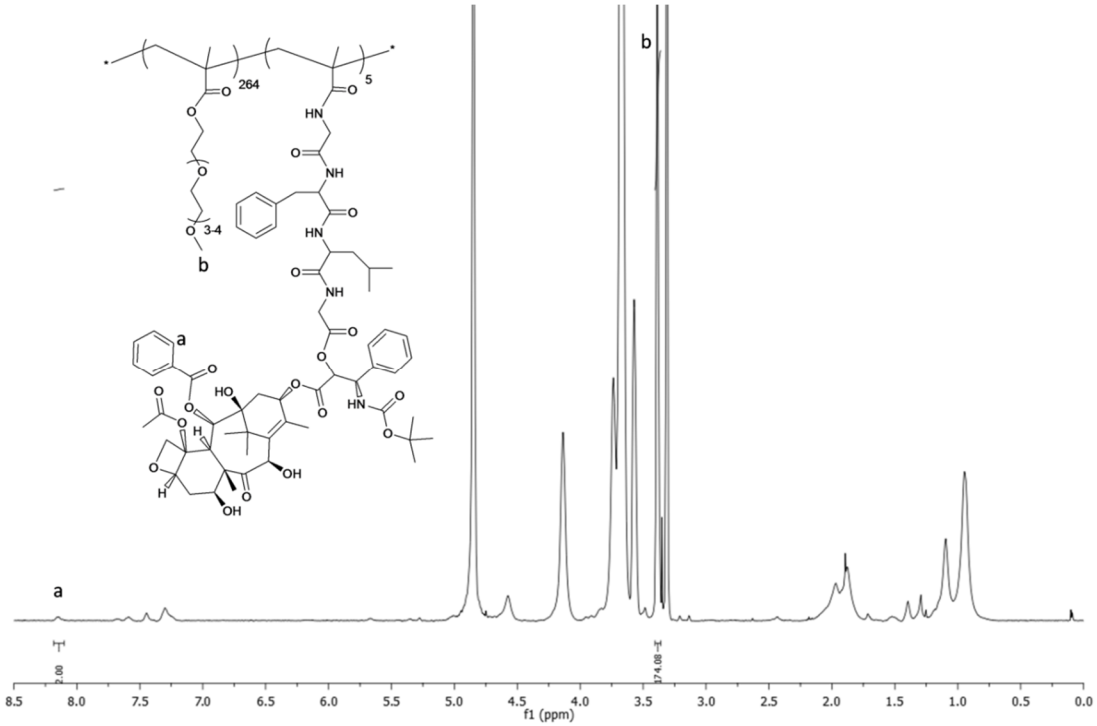


Figure 5.4. ^{1}H NMR spectrum of POEGMEMA-DTX (85 kDa).

5.3.3. Synthesis of HPMA-DTX Conjugates

HPMA and MA-GFLG-DTX monomers were polymerized via free radical copolymerization under AIBN initiation. Polymerization reaction is shown in Figure 5.5.

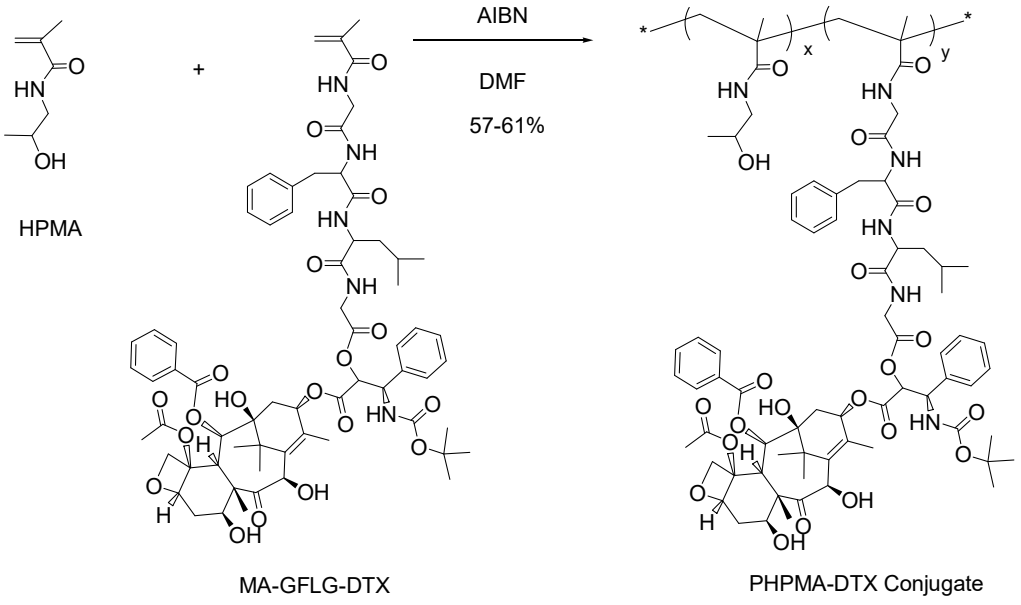


Figure 5.5. Synthesis of PHPMA-DTX polymer drug conjugates.

Analysis of PHPMA-DTX using ^{1}H NMR revealed successful copolymerization of MA-GFLG-DTX and HPMA monomers, as was evident from the proton resonances around 8.12 and 8.14 ppm due to the phenyl group of DTX, the proton resonances around 3.89 ppm due to the specific hydrogen atom of HPMA monomer labeled in Figure 5.6 and Figure 5.7 and the disappearance of proton resonances around 5.77 and 5.42 ppm due to the terminal alkenyl group of MA-GFLG-DTX. Varying the feed ratio of monomers resulted in HPMA-DTX conjugates with different molecular weights, 52 kDa and 85 kDa. Full ^{1}H NMR (CD_3OD) spectrum of HPMA-DTX conjugates (52 kDa and 85 kDa) are given in Figure 5.6 and Figure 5.7. The experimentally obtained monomer compositions of the copolymers show that the incorporation of the MA-GFLG-DTX monomer is lower than aimed in the feed. The weight percent of DTX in PHPMA-DTX conjugates was calculated by comparison of integration of the proton resonance at 3.89 ppm due to the specific hydrogen atom of HPMA monomer with proton resonances around 8.12 and 8.14 ppm due to the phenyl group of DTX. Drug contents for PHPMA-DTX (52 kDa) and PHPMA-DTX (85 kDa) were calculated as 9.14 % and 5.21 % by weight, respectively. Polymerization conditions and properties of PHPMA-DTX conjugates are given in Table 5.1.

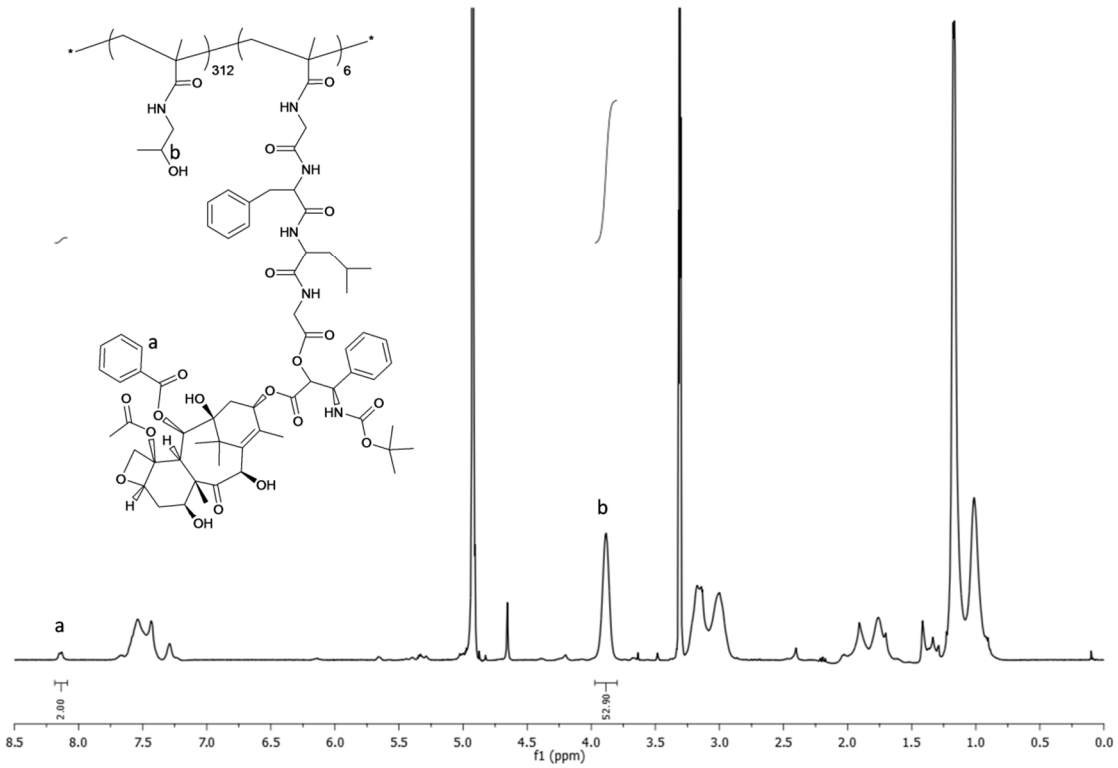


Figure 5.6. ^{1}H NMR spectrum of PHPMA-DTX (52 kDa).

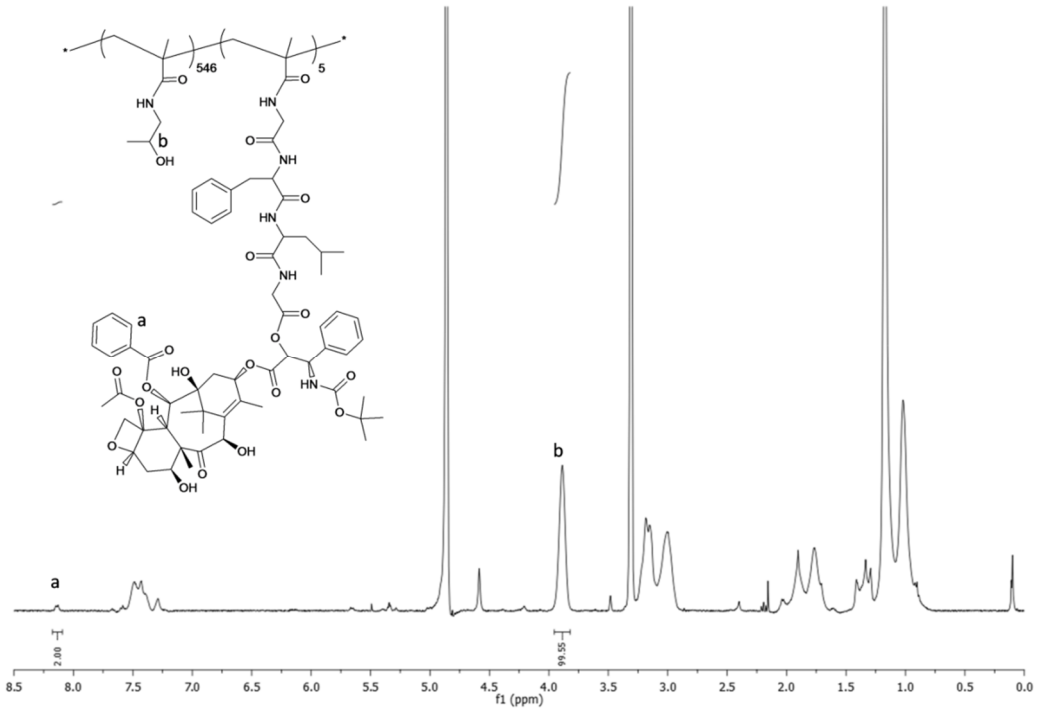


Figure 5.7. ^{1}H NMR spectrum of PHPMA-DTX (85 kDa).

Table 5.1. Polymerization conditions for POEGMEMA-DTX and PHPMA-DTX conjugates.

Mole Feed Ratio					Monomer /DMF (mg/mL)	t (˚C)/(h)*	Mn**	PDI**	Yield (%)
item	OEGMEMA	HPMA	MA-GFLG-DTX	AIBN					
1	120	-	12	1	575 mg/ 3 mL	80/1 +50/47	50 K	2.38	67
2	240	-	24	1	575 mg/ 3 mL	80/1 +50/47	85 K	2.32	70
3		320	20	1	575 mg/ 3 mL	80/1 +50/71	52 K	2.72	57
4		740	20	1	575 mg/ 3 mL	80/1 +50/71	85 K	2.75	61

*Polymerization of OEGMEMA and HPMA was initiated at 80 ºC for 1 h and then MA-GFLG-DTX monomer was added to the reaction mixture. **Mn and PDI values were obtained by SEC.

The weight percentages of DTX in polymer drug conjugates and schematic illustration of polymer drug conjugates are shown in Figure 5.8. As a result of conjugation with water soluble polymers, solubility of DTX in water increased dramatically and only PBS and saline based polymer drug solutions used for all *in vitro* and *in vivo* experiments. Very similar molecular weight values obtained for both POEGMEMA-DTX and PHPMA-DTX conjugates to make a successful comparison in terms of low and high molecular weights (Table 5.1). ^{1}H NMR analysis showed that relatively similar drug content was achieved to make a comparison between polymer drug conjugates with low molecular weights (4.41 % and 5.21 %) and high molecular weights (8.17 % and 9.14 %).

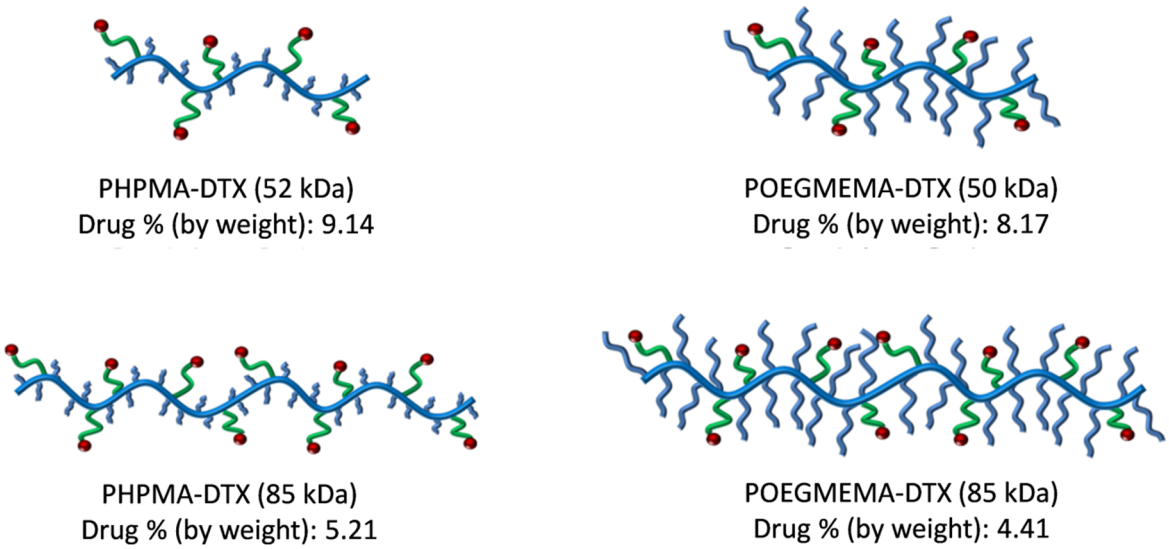


Figure 5.8. Schematic illustration of polymer drug conjugates with drug contents. Where blue for polymer backbone and side chains, green for GFLG linker and red for DTX.

5.3.4. Enzymatic Release Profiles of POEGMEMA-DTX and PHPMA-DTX conjugates

The GFLG linker between polymer backbones and DTX were cleaved by papain enzyme according to procedure as mentioned above. In both cases, where low molecular and high molecular weight polymer conjugates were compared, POEGMEMA-DTX conjugates showed slow release profiles due to branching effect compared to PHPMA-DTX conjugates. The release profiles of the conjugates are shown in Figure 5.9 and Figure 5.10.

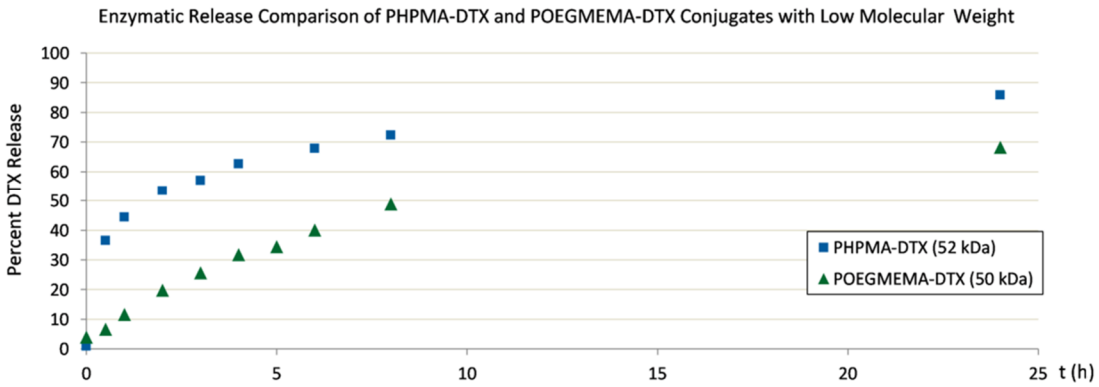


Figure 5.9. Enzymatic release profiles of conjugates with low molecular weights.

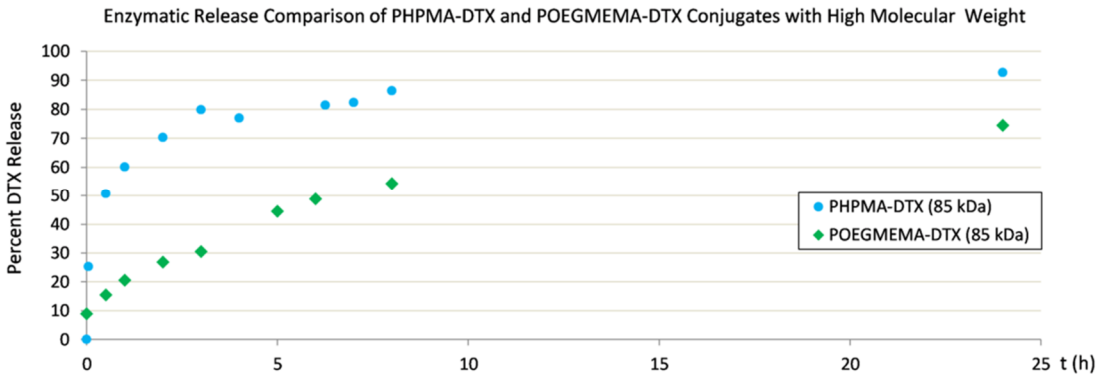


Figure 5.10. Enzymatic release profiles of conjugates with high molecular weights.

5.3.5. Cytotoxicity of POEGMEMA-DTX, PHPMA-DTX Conjugates

Cytotoxicity of synthesized polymer drug conjugates and free DTX were evaluated using MDA-MB-231 and BxPC3 cell lines (Figure 5.11 and 5.12). It is known that polymer drug conjugates usually show different cytotoxicity behavior compared to free drugs due to their different cellular entry routes and the requirement of linker degradation between the polymer backbone and a drug [168]. POEGMEMA-DTX and PHMA-DTX conjugates showed lower cytotoxicity compared to free DTX for both cell lines. BxPC3 cells were more sensitive to DTX compared to MDA-MB-231 cells. POEGMEMA-DTX conjugates showed lower cytotoxicity compared their PHPMA-DTX counterparts with same molecular weights due retarded release of DTX thanks to the branched structure.

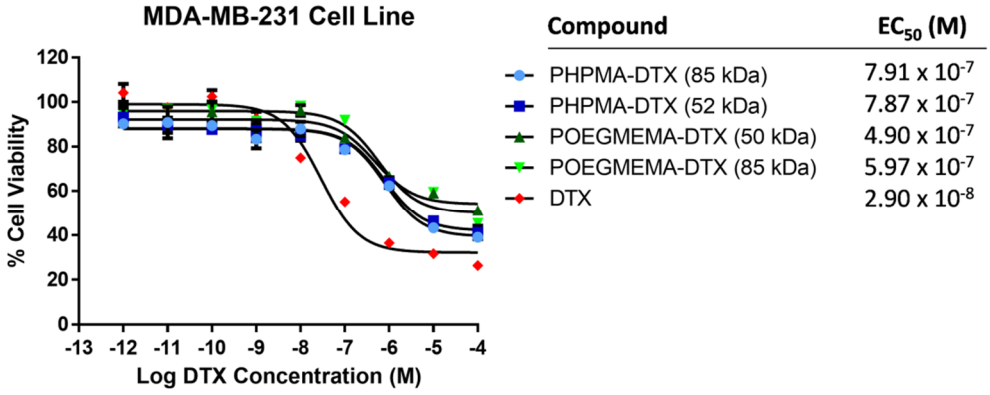


Figure 5.11. Cytotoxicity of polymer drug conjugates and free DTX for MDA-MB-231 cell line. EC_{50} values calculated by Graph-Pad prism, non-linear regression mode.

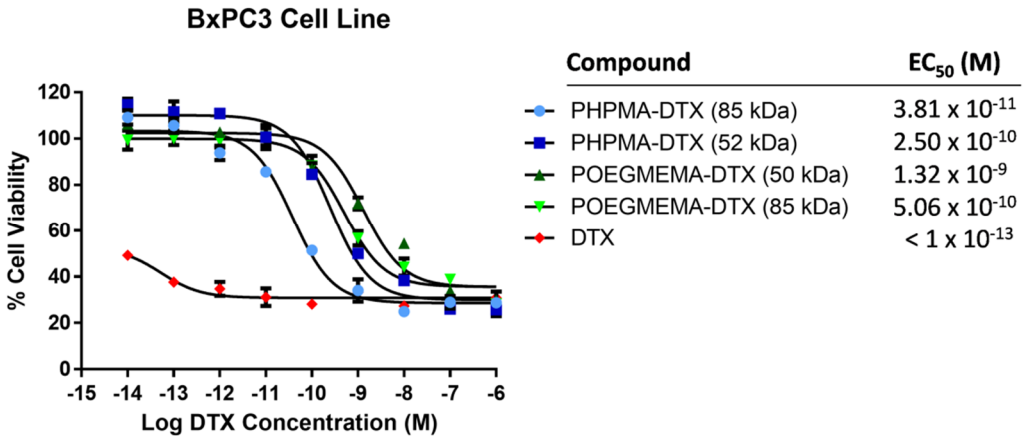


Figure 5.12. Cytotoxicity of polymer drug conjugates and free DTX for BxPC3 cell line. EC_{50} values calculated by Graph-Pad prism, non-linear regression mode.

5.3.6. Blood Toxicity of POEGMEMA-DTX, PHPMA-DTX Conjugates and Free DTX

Blood samples (200 µL) were collected just before and after 24 h of the injection. Whole blood counter was used to measure the hemogram values of the samples. The relative change after 24 h of the injection compared to before injection values were presented in Figure 5.13. White Blood Cell (WBC) Red Blood Cell (RBC) and Hemoglobin (HGB) and Hematocrit (HCT) values were evaluated. Low molecular weight conjugates had lower toxicity compared to high molecular weight ones on WBC. All conjugates showed less toxicity on RBC compared with free DTX. These results were also validated with HGB and HCT.

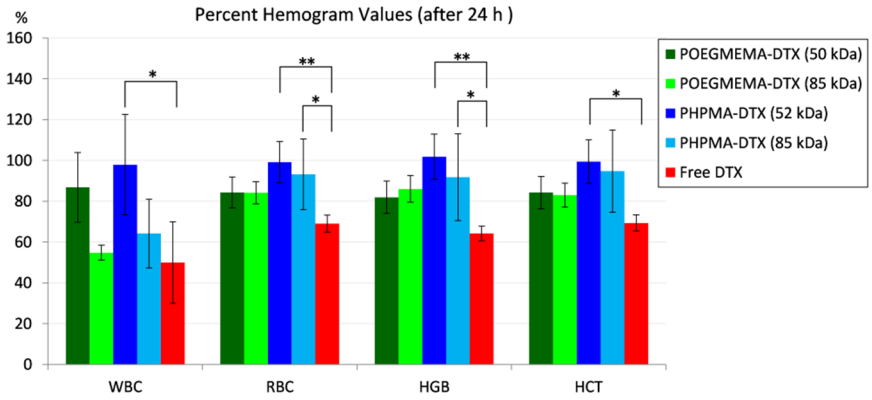


Figure 5.13. Percent change in hemogram values of the rats treated with polymer drug conjugates and DTX. Values represent mean ± SD (n = 3 - 4). * represents $p < 0.05$, ** $p < 0.01$.

5.3.7. Body Weight Change

Body weights of the rats were measured before, after 24 and 48 h of the injection. The relative change in hemogram values after 24 and 48 h of the injection were compared to values the before injection and presented in Figure 11. All conjugates showed less body weight loss compared with free DTX. Body weight change after 24 and 48 h of the injection is shown in Figure 5.14.

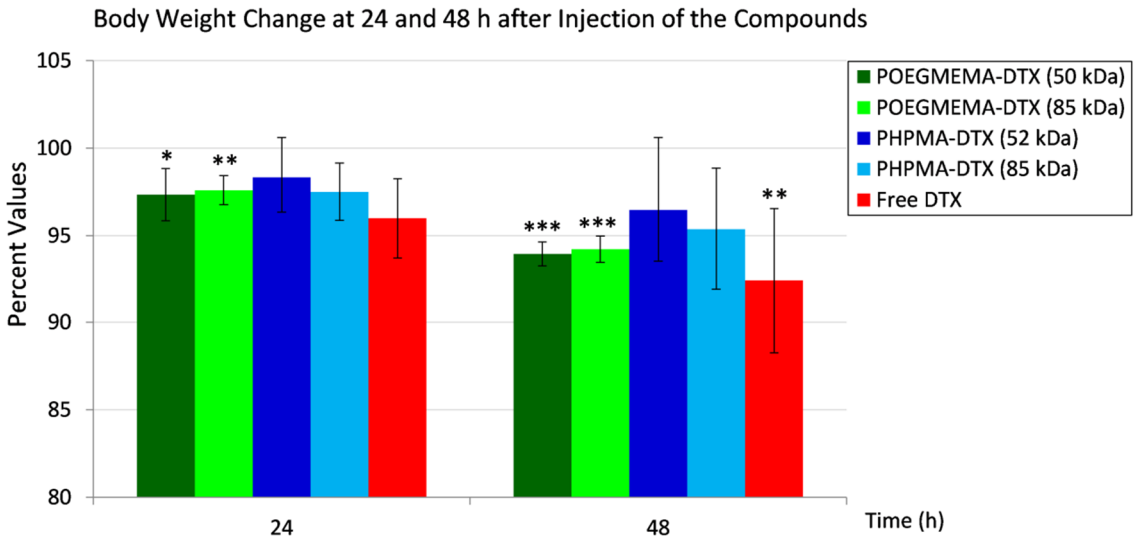


Figure 5.14. Body weight change values of polymer drug conjugates and DTX. Values represent mean ± SD (n = 3 - 4). * represents $p < 0.05$, ** $p < 0.01$, *** $p < 0.001$. cf. initial body weights for each group.

5.3.8. Plasma Free DTX Concentration Values of POEGMEMA-DTX, PHPMA-DTX Conjugates and DTX

We measured free DTX content in POEGMEMA-DTX, PHPMA-DTX conjugates and DTX treated rats' plasma using LC-MS to understand the effects of polymer conjugation. Four polymer drug conjugates with different molecular weights, namely POEGMEMA-DTX (50 kDa), POEGMEMA-DTX (85 kDa), PHPMA-DTX (52 kDa), PHPMA-DTX (85 kDa) and free DTX were evaluated in this study. Free DTX plasma concentration values of polymer drug conjugates and DTX are shown in Figure 5.15. Pharmacokinetic parameters including β half-life, volume of distribution ($V_D\beta$), clearance

(CL), total area under the curve (AUC total) and maximum concentration (Cmax) values were obtained using these values and given in Table 5.2.



Figure 5.15. Plasma free DTX concentrations of polymer drug conjugates.

Table 5.2. Pharmacokinetic parameters of free DTX for polymer drug conjugates and DTX.

	β Half-life (h)	**V_Dβ (mL)**	**CL (mL / h)**	**AUC total (ug / mL.h)**	**Cmax (µg / mL)**
Free DTX	3.12 ± 0.88	664.1 ± 258.1	140.4 ± 42.1	10 ± 3	11.8 ± 5.3
PHPMA-DTX (52kDa)	12.50 ± 3.33	1119.5 ± 173.8	58.3 ± 10.6	26 ± 7	3.5 ± 1.7
PHPMA-DTX (85kDa)	57.01 ± 20.66	1912.5 ± 83.8	19.4 ± 1.8	61 ± 12	1.5 ± 0.4
POEGMEMA-DTX (50kDa)	16.41 ± 0.83	383.4 ± 16.0	16.2 ± 1.5	80 ± 10	5.7 ± 0.6
POEGMEMA-DTX (85kDa)	11.05 ± 2.42	552.9 ± 147.3	38.5 ± 6.3	32 ± 11	3.1 ± 2.2

Higher AUC values of free DTX were obtained for all polymer conjugates compared to DTX confirming the presence of polymer drug conjugates in blood stream and sustained release of DTX from the backbone of polymer drug conjugates. Polymer drug conjugates also showed lower CL values for free DTX as a result of increased half-life. More importantly, this study showed that Cmax value of free DTX for polymer drug conjugates didn't reach the Cmax value for DTX treated rats. Cmax value for free DTX is desired to be lower than the case of DTX treated rats to eliminate possible acute blood toxicity due to higher free DTX concentration. POEGMEMA-DTX and PHPMA-DTX conjugates have demonstrated different release profiles because of branching effect as mentioned by

enzymatic release study. Moreover, there is a simultaneous release and clearance mechanism of DTX to and from the blood stream in the case of polymer drug conjugates, which makes it hard to do an assumption about the content of polymer drug conjugates in plasma using only free DTX pharmacokinetic parameters.

5.3.9. Plasma Total DTX Concentration Values of POEGMEMA-DTX, PHPMA-DTX Conjugates and DTX

We also measured total DTX content in POEGMEMA-DTX, PHPMA-DTX conjugates and DTX treated rats' plasma to evaluate the content of polymer drug conjugate and total drug in the blood stream. Total DTX plasma concentration values of polymer drug conjugates and DTX are shown in Figure 5.16. Pharmacokinetic parameters including β half-life, V_Dβ, CL, AUC and Cmax values were obtained using these values and given in Table 5.3. Total DTX content represents both cleaved and non-cleaved DTX amount from polymer backbone. It should be taken into consideration that there is a huge difference between free and total DTX content in rat plasma for polymer drug conjugates (Figure 5.15 and Figure 5.16). For example; AUC values of free DTX and total DTX for POEGMEMA-DTX (85 kDa) are 32 and 2370 ug / mL.h, respectively. So it is reasonable to ignore the free DTX amount and consider the total DTX content to evaluate the pharmacokinetic parameters for polymer drug conjugates.

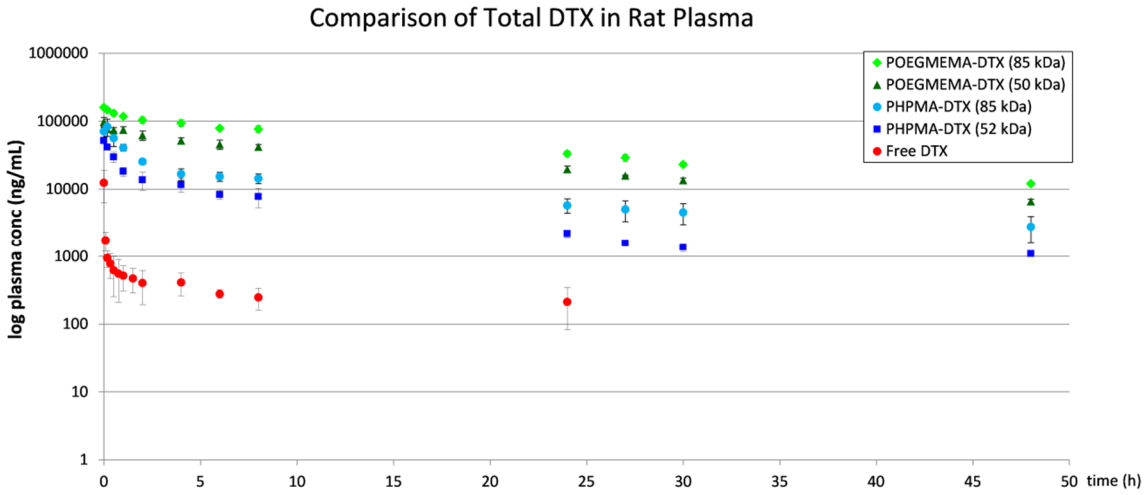


Figure 5.16. Plasma total DTX concentrations of polymer drug conjugates.

Table 5.3. Pharmacokinetic parameters of total DTX for polymer drug conjugates and DTX.

		β Half-life (h)	V_Dβ (mL)	CL (mL/h)	AUC total (ug/mL.h)	Cmax (µg/mL)
a	Free DTX	3.12 ± 0.88	664.1 ± 258.1	140.4 ± 42.1	10 ± 3	11.8 ± 5.3
b	PHPMA-DTX (52kDa)	11.99 ± 0.37 (a)***	102.5 ± 13.8 (a)***	5.9 ± 0.7 (a)***	241 ± 32 (a)**, (d)***	51.8 ± 5.4 (a)**, (d)**
c	PHPMA-DTX (85kDa)	16.24 ± 4.40 (a)***	60.2 ± 11.1 (a)***	2.6 ± 0.2 (a)***	525 ± 57 (a)***, (e)***	83.5 ± 23.6 (a)***, (e)***
d	POEGMEMA-DTX (50kDa)	14.62 ± 0.54 (a)***	20.2 ± 1.9 (a)***	1.0 ± 0.1 (a)***	1357 ± 109 (a)***, (b)***	97.7 ± 16.1 (a)***, (b)**
e	POEGMEMA-DTX (85kDa)	12.10 ± 0.35 (a)***	10.0 ± 0.2 (a)***	0.6 ± 0.0 (a)***	2370 ± 106 (a)***, (e)***	159.8 ± 2.3 (a)***, (e)***

Polymer drug conjugates were compared DTX and their counterparts having same molecular weight. Values represent mean ± SD (n = 3 - 4). ** represents $p < 0.01$, *** $p < 0.001$.

Longer β half-life values of total DTX (between 12 and 16 h) obtained for all polymer drug conjugates compared to DTX, which confirms long circulation of polymer drug conjugates in the blood stream. AUC values of the free drug increased by 24 and 52 times in the case of PHPMA-DTX conjugates, whereas 140 and 240 fold increases were obtained by POEGMEMA-DTX conjugates. When we compare free DTX and total DTX values of each polymer drug conjugates, it is shown that AUC values of free DTX for polymer drug conjugates varies between 26 and 80 ug/mL.h, where this value varies between 241 and 2370 ug/mL.hr in the case of total DTX. AUC values of free and total DTX for polymer drug conjugates provides us to make an assumption about release of DTX from polymer backbone and clearance of the polymer drug conjugates from the blood stream. Considering obtained similar β half-life values of polymer drug conjugates for total DTX, AUC values demonstrate that cleavage of GFLG linker and clearance from blood stream was affected by branching and length of the polymer backbone. For example; where there is a 74 fold difference between AUC values of free DTX and total DTX for PEGMEMA-DTX (85 kDa), there is an only 8.6 fold difference in the case of HPMA-DTX (85 kDa). The difference between AUC values of free DTX and total DTX for POEGMEMA-DTX (50 kDa) is 17 fold. Lower V_Dβ and CL, and higher AUC and Cmax values were obtained with high molecular weight conjugates compared to their counterparts having low molecular weights. These results show that having higher

molecular weights improved pharmacokinetic profiles of polymer drug conjugates. Similarly, POEGMEMA-DTX conjugates with branched structure obtained lower $V_D\beta$ and CL, and higher AUC and Cmax values compared to HPMA-DTX conjugates, demonstrating that branching has also another parameter which improves pharmacokinetic profile of DTX compared to linear polymer drug conjugates. On the other hand, $V_D\beta$ value for DTX (664 mL) significantly decreased in the case of POEGMEMA based polymer drug conjugates (20 and 10 mL). When considering the total blood volume of a rat (around 20 mL for 300 g rat), it can be say that POEGMEMA based polymer drug conjugates more likely present in the blood stream whereas DTX is distributed through all the body in a subcellular way.

5.3.10. Free and Total DTX Biodistribution of POEGMEMA-DTX, PHPMA-DTX Conjugates and DTX

Liver, spleen, kidneys, lung, heart and pancreas organs and muscle tissue samples were collected at 48th h following injection of polymer drug conjugates and DTX. Free DTX biodistribution values of polymer drug conjugates and DTX are given in Figure 5.17.

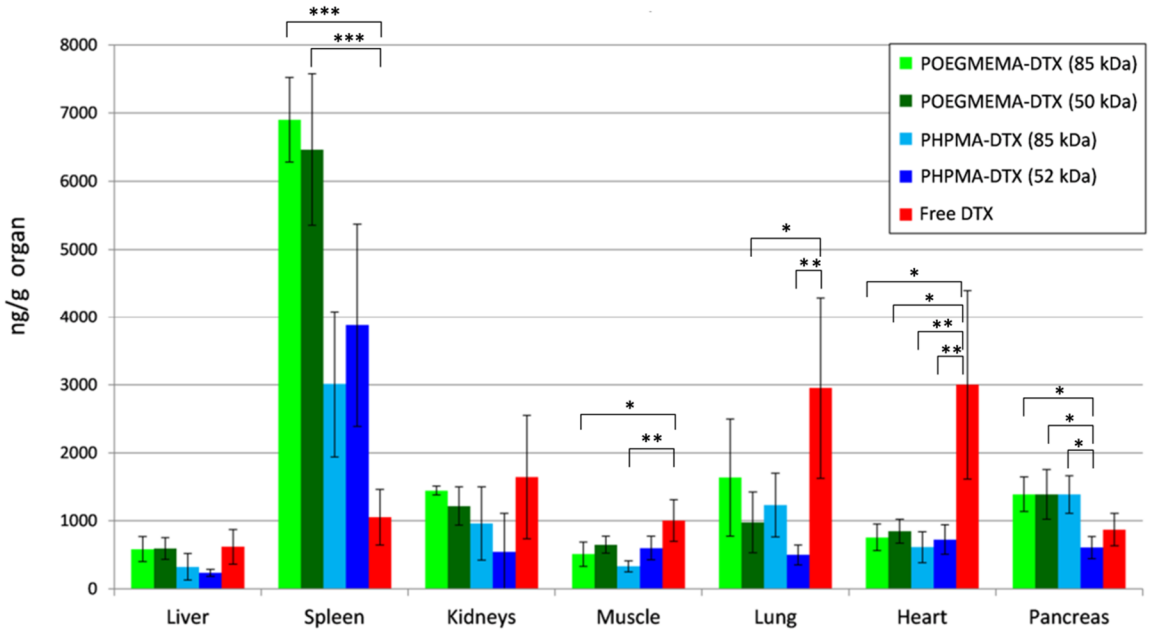


Figure 5.17. Free DTX biodistribution values of polymer drug conjugates and DTX. Values represent mean ± SD (n = 3 - 4). * represents $p < 0.05$, ** $p < 0.01$, *** $p < 0.001$.

Organ and tissue samples were homogenized using homogenizer after addition of acetonitrile and the samples were prepared as mentioned in experimental part. The free DTX content in supernatant was evaluated by LC-MS to calibration standards of DTX prepared using serial dilutions. The accumulation of DTX in organ and tissue samples was expressed as ng DTX in g organ (ng DTX/g organ). Free DTX content in organ and tissue samples represents both accumulation of DTX released from polymer backbone in the blood stream and released DTX from polymer backbone in the organs and muscle tissue. Higher accumulation of free DTX was observed in spleen in the case of polymer drug conjugates compared to DTX treated rats. Relatively lower accumulation of free DTX in muscle, heart and lung tissues was observed for polymer drug conjugates compared to DTX group. To evaluate the amount of polymer drug conjugates in organ and tissue samples we also measured total DTX values as mentioned in the experimental section. Obtained total DTX biodistribution values of polymer drug conjugates and DTX are given in Figure 5.18.

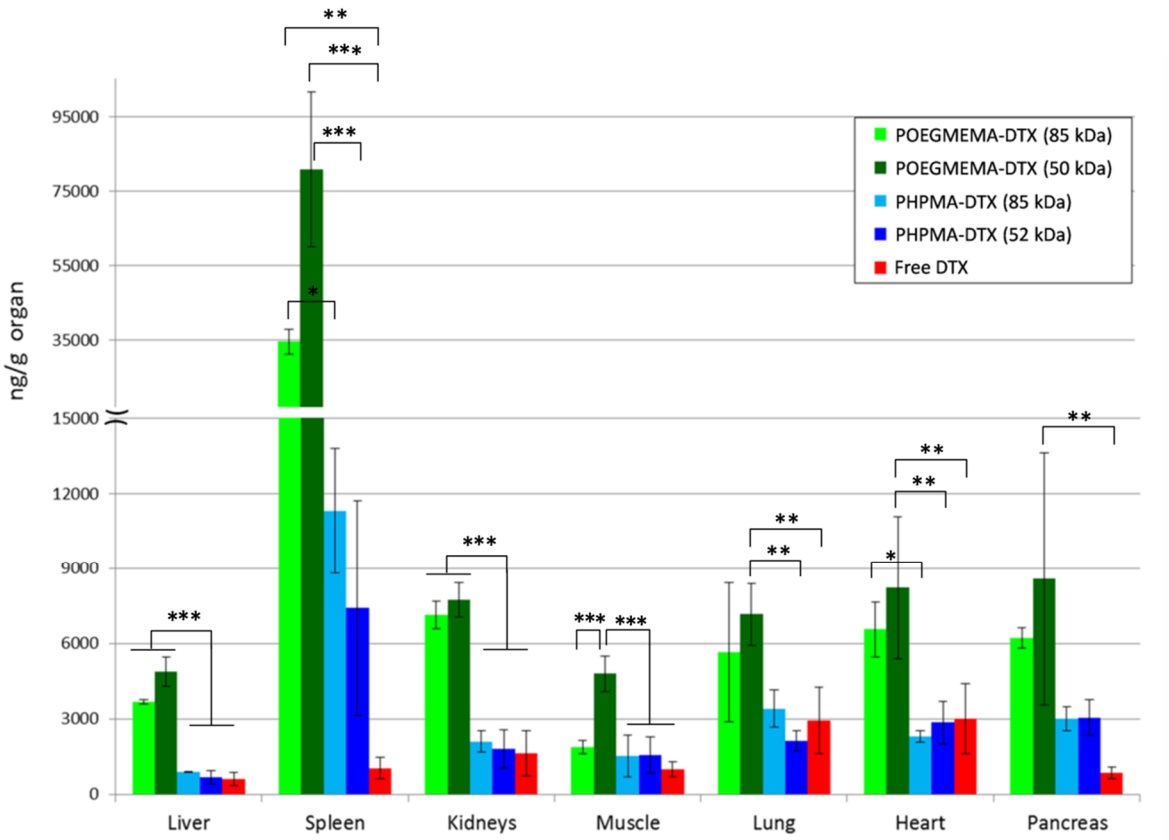


Figure 5.18. Total DTX biodistribution values of polymer drug conjugates and DTX. Values represent mean ± SD (n = 3 - 4). * represents $p < 0.05$, ** $p < 0.01$, *** $p < 0.001$.

Biodistribution of DTX in organ and tissue samples revealed that there is an important difference between free and total DTX values of POEGMEMA-DTX conjugates. It is correlated with free and total DTX values in plasma for branched polymer drug conjugates. However, relatively lower difference was achieved for PHPMA-DTX conjugates between free and total DTX values in organ and tissue samples. That can be explained by slow release of DTX from POEGMEMA-DTX conjugates due to branching effect which also confirmed by enzymatic release study. Higher accumulation of total DTX in spleen was found for polymer drug conjugates compared to other organs. However, the liver accumulation of polymer drug conjugates found to be lower compared to conventional biodistribution of macromolecules. Lower liver accumulation is an important parameter for a drug delivery system to eliminate Hepatic clearance, which generally cause a decrease in blood concentration values of drug carrying macromolecules. On the other hand, total DTX accumulation in all organ and tissue samples were found to be higher in the case of POEGMEMA-DTX conjugates, which confirms higher AUC and lower VDβ and CL values of these branched structures.

5.3.11. Maximum Tolerated Dose (MTD) Study for POEGMEMA-DTX (50 kDa)

We performed a MTD study for POEGMEMA-DTX (50 kDa) polymer drug conjugate because of its lower blood toxicity and the suitable size which around the renal threshold for further studies.

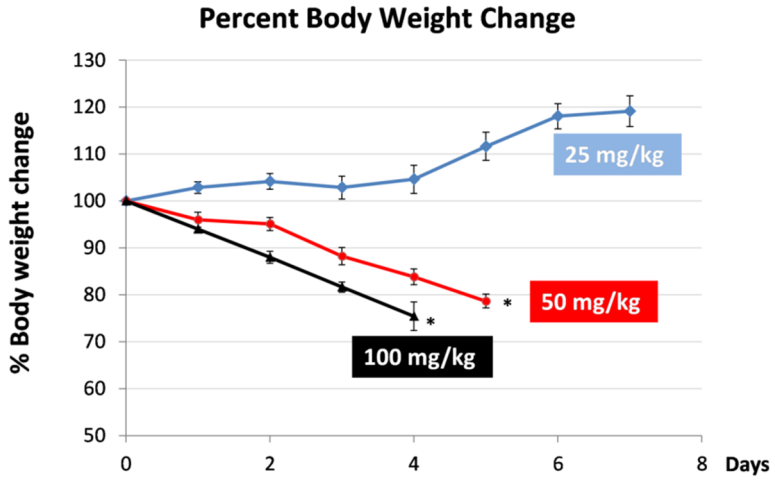


Figure 5.19. Normalized body weight change of POEGMEMA-DTX (50 kDa) injected mice with different dosages. *Animals were sacrificed when weight loss reached 20 % of initial body weight.

Briefly, male Balb-C mice separated into three groups (n=3 for each group) and injected with POEGMEMA-DTX (50 kDa) polymer drug conjugate with different DTX equivalent dosages (25, 50 and 100 mg/kg drug equivalent). The doses, 50 and 100 mg/kg drug equivalent were not tolerated by mice whereas the dose 25 mg/kg quite well-tolerated by mice according to data obtained for % body weight chance as a function of time (Figure 5.19). Mice loosed 20 % of their initial body weight when administered 50 and 100 mg/kg drug equivalent polymer drug conjugate at the fifth and fourth days, respectively.

We also compared liver and spleen based toxicity at the dose administered to the mice. Data obtained when mice were sacrificed (day 7 for 25 mg/kg, day 5 for 50 mg/kg and day 4 for 100 mg/kg). Results showed that spleen/body weight ratio was decreased by the dose increase as can be seen in Figure 5.20. Lower liver/body weight ratio was observed for the 50 and 100 mg/kg drug equivalent POEGMEMA-DTX (50 kDa) administrations compared the dose at 25 mg/kg (Figure 5.20).

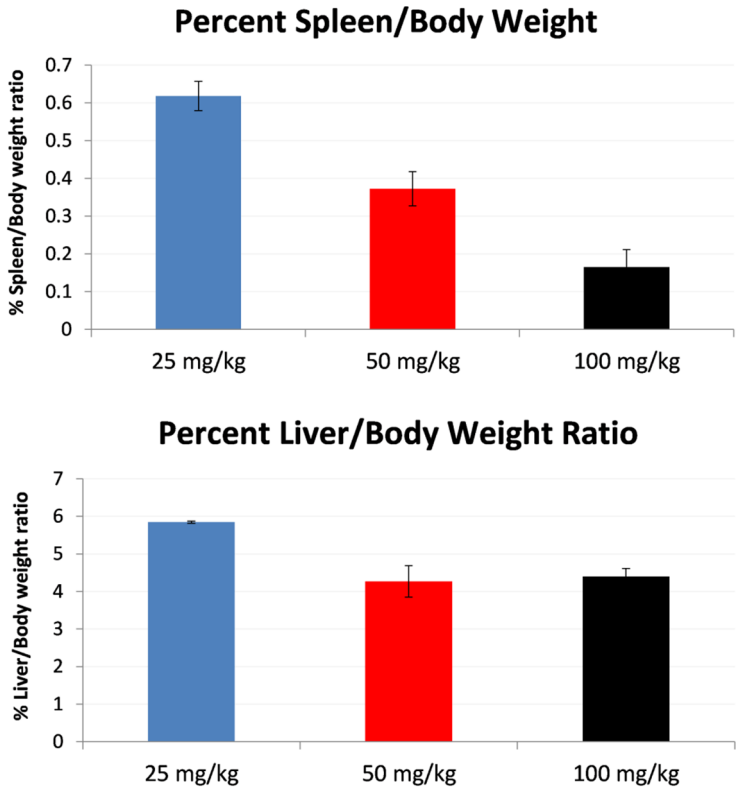


Figure 5.20. Changes in liver/body weight and spleen/body weight ratio of the mice injected with POEGMEMA-DTX (50 kDa).

Blood samples of the mice were collected before conjugate administration, at second day and the day they sacrificed to evaluate the changes in whole blood count during MTD study. White blood cell (WBC) count analysis showed that the mice injected with 100 mg/kg drug equivalent POEGMEMA-DTX (50 kDa) conjugate did not tolerate the dose. Although, WBC values of the ones injected with 50 mg/kg drug equivalent dose decreased at the day second, the values normalized at the day fifth they sacrificed. No dose dependent change was observed for red blood cell (RBC) count values of the mice (Figure 5.21).

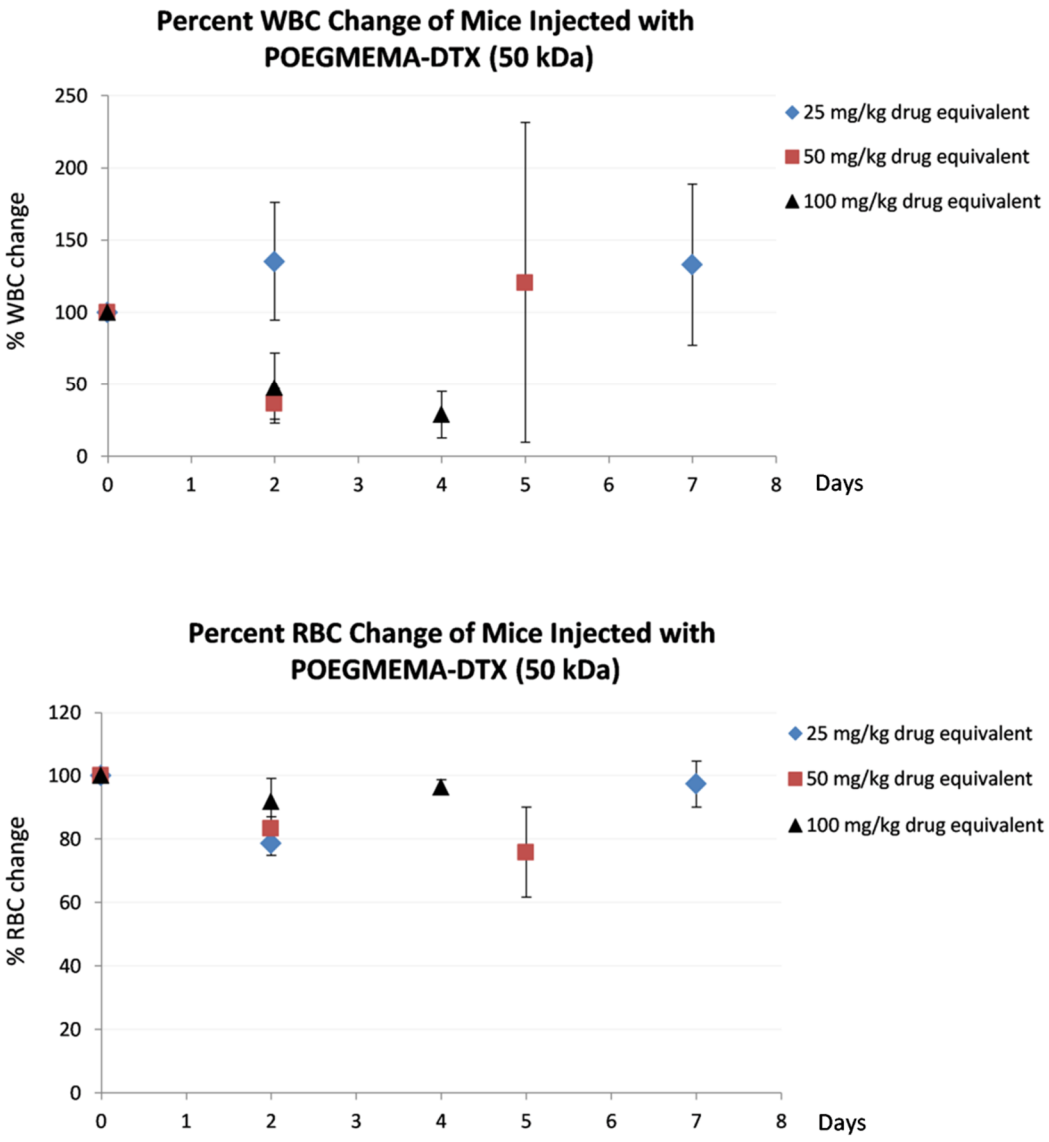


Figure 5.21. Normalized WBC and RBC count change values of the mice injected with POEGMEMA-DTX (50 kDa) polymer drug conjugate.

5.4. Conclusion

In this project, linear and branched polymer-drug conjugates were obtained by using water-soluble methacrylate monomers and hydrophobic drug monomer with a peptide linker (GFLG) via free radical polymerization. Low (50 kDa) and high (85 kDa) molecular weight conjugates were prepared, to assess the molecular weight effect on the pharmacokinetic profile in addition to branching effect. Enzymatic release study and cytotoxicity experiments for MDA-MB-231 and BxPC3 cancer cell lines were carried out. Polymer drug conjugates were compared in terms of pharmacokinetic profile against free DTX in Albino Wistar rats. The synthesized polymer drug conjugates increased the half-life of the free drug from 3 h to between 12 and 16 h AUC value of the DTX increased between 24 and 240 times by the polymer conjugation. Branching and having high molecular weight polymer drug conjugates resulted in greater AUC and Cmax, and lower CL and VDβ values compared to linear and low molecular weight polymer drug conjugates. Pharmacokinetic and biodistribution values of polymer drug conjugates demonstrated that branching in polymer backbone provided aimed slow release profiles in blood stream and major organs which is also confirmed by enzymatic release studies. For further anti-tumor studies we determined a MTD range between 25 and 50 mg/kg DTX equivalent POEGMEMA-DTX (50 kDa) polymer drug conjugate.

6. ANTI-TUMOR EFFECT OF POEGMEMA BASED POLYMER DRUG CONJUGATES

6.1. Introduction

Superiority of branched polymer backbone over linear ones in terms of pharmacokinetic profile as proved in previous chapter encouraged us to perform an anti-tumor study using POEGMEMA based polymer drug conjugates. For designing better prodrug formulations with low dispersities we preferred reversible addition-fragmentation chain transfer (RAFT) polymerization [169,170] for the synthesis of polymer drug conjugates. An enzymatically cleavable peptide linker, GFLG (Gly-Phe-Lys-Gly) was used to achieve blood stability and efficient release dynamics in enzyme-rich tumor tissue. GFLG is known to be released by Cathepsin B, an enzyme over expressed in malignant tumor tissues and premalignant lessions [171]. Additionally, methacrylic acid N-hydroxysuccinimide ester (NHSMA) monomer was introduced to polymer backbone for ligand attachment via post-polymerization modification. Peptide directed active targeting is an efficient strategy for prodrug design and cyclic Arg-Gly-Asp (cRGD) is a commonly used peptide ligand targets αvβ3 and αvβ5 integrins which are highly upregulated in various tumor tissues such as lung, prostate, breast and brain carcinomas [172]. We introduced cRGD moiety to the prodrug formulation using N-hydroxysuccinimide (NHS) group at the polymer backbone to achieve a targeting moiety. *In vivo* therapeutic effects of POEGMEMA based targeted and non-targeted polymer DTX conjugates were evaluated compared to free DTX in human lung carcinoma model.

6.2. Experimental

6.2.1. Materials

Oligo(ethylene glycol) monomethyl ether methacrylate (OEGMEMA, Mn= 300g/mol), 4-cyanopentanoic acid dithiobenzoate (CPADB), 2,2′-azobisisobutyronitrile (AIBN), methacryloyl chloride, *N*,*N*-Diisopropylethylamine (DIPEA), *N*-hydroxysuccinimide (NHS) and amino-2-propanol were purchased from Aldrich. All other solvents were HPLC grade, obtained from Merck and used without further purification. Methacrylic acid *N*-hydroxysuccinimide ester (NHSMA) was synthesized and

characterized according to previously described methods [173]. Cyclo (Arg-Gly-Asp-D-Phe-Lys) (cRGDfK) was synthesized using standard solid phase synthesis. The monomer and copolymer characterizations involved ^{1}H NMR spectroscopy (Varian 400 MHz NMR spectrometer), fourier transform infrared (ATR-FTIR) spectroscopy (Nicolet 380, Thermo Scientific, USA) and gel permeation chromatography GPC (Shimadzu, Japan) with a mobile phase solution of 0.05 M lithium bromide in dimethylaceteamide (DMAc). GPC measurements of copolymers were carried out with PSS WinGPC Unity software. PSS Gram (length/ID 300 mm × 8 mm, 10 µm particle size) column was calibrated with polymethyl methacrylate standards, using refractive index detector (RID-10A). Docetaxel concentration in plasma was characterized by liquid chromatography-mass spectrometry (LC-MS) analysis using a LCMS-2020-Mass Spectrometer System (Shimadzu, Japan) equipped with an C-18 5 µm 150 × 4.6 mm column. Whole blood count analyses were performed using Mindray BC-2800 blood counter.

6.2.2. Synthesis of POEGMEMA-DTX-NHS Conjugate

POEGMEMA-DTX-NHS polymer drug conjugate was synthesized via Reversible addition–fragmentation chain transfer (RAFT) copolymerization of OEGMEMA, NHSMA and MA-GFLG-DTX monomers in anhydrous DMF using AIBN initiator. Briefly, OEGMEMA (650 mg, 2.16 mmol) and NHSMA (27.2 mg, 0.15 mmol) mixture including AIBN (0.44 mg, 0.0027 mmol) in DMF (4.0 mL) were sealed in a round bottom flask under nitrogen and stirred at 80 ºC for 1 h. Then these reaction mixtures were transferred into another oil bath at 50 ºC and MA-GFLG-DTX (371 mg, 0.30 mmol) in 1.5 mL anhydrous DMF was added under nitrogen and stirred for 47 h to give POEGMEMA-DTX-NHS conjugate (710 mg, 67 % yield). DMF was removed under reduced pressure. The crude product was dissolved in dichloromethane (DCM) and precipitated in diethyl ether. The precipitated copolymers were dried under vacuum and characterized using gel permeation chromatography (GPC) and ^{1}H NMR. FTIR spectra of POEGMEMA- DTX-NHS conjugate is given in Figure A.17.

6.2.3. cRGDfK Conjugation for Targeted Polymer Drug Conjugate

Briefly, POEGMEMA-DTX-NHS conjugate (350 mg, 0,008 mmol), cRGDfK (24.6 mg, 0.040 mmol) and DIPEA (26 mg, 0.200 mmol) in DMF (1.25 mL) were sealed in a round bottom flask under nitrogen and stirred at 30 ºC for 24 h to give POEGMEMA-

DTX-cRGDfK conjugate (330 mg, 88 % yield). Then to inactivate unreacted NHS groups, POEGMEMA-DTX-cRGDfK conjugate (320 mg, 0.0074 mmol) reacted with amino-2-propanol (28 mg, 0.372 mmol) in 1.3 mL DMF at RT for 24 h to give 300 mg final product. FTIR spectra of POEGMEMA- DTX-cRGDfK conjugate is given in Figure A.18.

6.2.4. Inactivation of NHS Groups for Non-targeted Polymer Drug Conjugate

POEGMEMA- DTX- NHS conjugate (350 mg, 0,008 mmol) reacted with amino-2-propanol (30 mg, 0.4 mmol) in 1.3 mL DMF at RT for 24 h to give 315 mg POEGMEMA-DTX conjugate. FTIR spectra of POEGMEMA- DTX conjugate is given in Figure A.19.

6.2.5. Plasma Release Study

Briefly, 2.5 mg polymer drug conjugates were dissolved in DCM (500 μL) and separated into 10 eppendorf tubes (50 μL) to each. DCM was evaporated at open atmosphere overnight. Rat plasma (100 μL) was added to each eppendorf tube. Samples were shortly vortexed and incubated at 37 ºC. Acetonitrile (400 μL) was added at the end of incubation times (t_0, 1, 2, 3, 4, 8, 24, and 48 h) for each sample, and then samples were vortexed and spinned down. The DTX content in supernatant was evaluated by LC-MS to calibration standards of DTX prepared using serial dilutions.

6.2.6. Enzymatic Release Study

The released DTX amount from polymer drug conjugates was measured by LC-MS. Briefly, 0.10 mg polymer drug conjugates were dissolved in 10 μL DMSO separately. 100 μL buffer solution (0.1 M citric acid/0.2 M Na_2HPO_4, 2 mM EDTA, 10 mM GSH, pH: 5.0) was added to these polymer drug conjugate solutions. Finally enzyme solution (20 μL, 0.1 M citric acid/0.2 M Na_2HPO_4, 0.2 mM papain, pH: 5.0) was added to the solution mixtures and final solution was shortly vortexed and incubated at 37 ºC. 370 μL acetonitrile was added at the end of incubation times (t_0, 2, 4, 8, 24 and 48 h) for each sample, and then samples were vortexed and spinned down. The DTX content in supernatant was evaluated by LC-MS to calibration standards of DTX prepared using serial dilutions.

6.2.7. Cell Lines

Human lung carcinoma (A549) cell line was obtained from Lonza. Cells were grown in 75 cm^2 flasks in F12/DMEM medium with with 10 % FBS and 1 % penicillin-streptomycin, 1 % sodium pyruvate, 1 % non-essential amino acids in a humidified atmosphere of 5 % CO_2 and at 37 °C. Cells were passaged 1:6 using 0.25 % trypsin-EDTA 3 times per week.

6.2.8. In Vitro Cell Viability Assay

Cell viabilities were determined by Cell Counting Kit-8 (CCK-8, Fluka). Cells were seeded in 100 μL of culture medium at a density of 5000 cells / well into 96-well plates in quadruplicates for each drug concentration. After overnight incubation to let cells to adhere, cell media was replaced with fresh medium containing various concentrations of polymer drug conjugates, free drug, or controls. To increase the water solubility of Docetaxel, stock solution was prepared in 10 % dimethyl sulfoxide (DMSO) in growth medium (V/V) and subsequently diluted where the final DMSO concentration was below 0.5 % (V/V). Polymer drug conjugate solutions are prepared via sonication without any organic solvent addition. Cells were incubated continuously for 48 h in the presence of the polymer drug conjugates. Following the treatment, cell media containing the conjugates was removed, wells were washed with 1× PBS. For the determination the cell viability, 100 μL of culture medium together with 10 μL of CCK-8 solution was added into each well. After 4h incubation the absorbance values of three replicates per treatment at 450 nm were measured with a plate reader (Multiscan FC, Thermo Scientific, USA). Viability of treated cells was expressed as percentage of control cells (cell media only). Half maximal effective concentration (EC_{50}) values were obtained from concentration response curves by nonlinear regression analysis.

6.2.9. Animals

Male athymic nude mice (25-30 g, 7-8 weeks old) and Balb-C mice (25-30 g, 8 weeks old) were obtained from Boğazici University Experimental Animal Production and Maintenance Unit and maintained in a controlled environment with a 12 h light/dark cycle. Water and food was provided ad libitum all the times. Animal experimentations were

approved by the Boğaziçi University Animal Experiments Local Ethics Committee (08.06.2015).

6.2.10. Tolerability Study for Polymer Drug Conjugates at 40 mg/kg DTX Equivalent Dose.

According to MTD data obtained in previous chapter a tolerability study for polymer drug conjugates was planned and Balb-C mice separated into 2 groups. The mice in the first group were injected with POEGMEMA-DTX (40 mg/kg DTX equivalent) and the second group was injected with POEGMEMA-DTX-cRDGfK (40 mg/kg DTX equivalent) via tail vein. Body weights were measured every day. The dosing day (just prior dosing), 48 h and 120 h after dosing blood samples were collected from the orbital sinus or by cardiac puncture under anesthesia and blood count values were obtained using a whole blood counter. Animals were sacrificed following the last blood sampling.

6.2.11. Tumor Study

For solid tumor induction in athymic nude mice, A-549 cells were passaged using trypsin-EDTA, washed once in PBS and resuspended in Matrigel with a final volume of 12 × 10^7 cells/1.5 mL Matrigel. A 50 µL suspension of A-549 cells (4× 10^6 cells in total) was then injected into the right flank of mice (n=24) using a 25G needle. Body weights were measured every 3 days. Tumor growth was monitored with a caliper every 3 days by the equation, Tumor volume (mm^3) = $4/3\pi ab^2$, where a = longest radius (mm), b = shortest radius (mm). When tumor volumes reached approximately 50 mm^3 (approximately 4 weeks after cell injection) mice were separated into 4 groups (n=6 for each group) and injected with targeted and non-targeted polymer drug conjugates, free DTX and saline. The mice in the first group were injected with POEGMEMA-DTX (40 mg/kg DTX equivalent) and the ones in the second group were injected with POEGMEMA-DTX-cRGDfK (40 mg/kg DTX equivalent) in a final volume of 50 µL of sterile saline. The mice in the third group were injected with 40 mg free DTX in a final volume of 50 µL polysorbate 80 (12.5 %, v/v) and ethanol (13 %, v/v) including saline solution. The mice in the last group were injected with saline (50 µL). All injections were applied intravenously via the tail vein using a 27G needle under anesthesia (1.5 % isoflurane) and repeated in every 10 days following first injection (total of 3 injections).

6.2.12. Statistics

One-way ANOVA test was used for the statistical analysis of tumor volume change. Statistical significance was identified at a level of $p < 0.05$.

6.3. Results and Discussion

6.3.1. Synthesis of POEGMEMA-DTX-NHS Conjugate

OEGMEMA, MA-GFLG-DTX and NHSMA monomers were polymerized via RAFT copolymerization using AIBN as initiator in anhydrous DMF. Analysis of POEGMEMA-DTX-NHS using ^{1}H NMR revealed successful copolymerization of the monomers used, as was evident from the proton resonances around 8.12 and 8.14 ppm due to the phenyl group of DTX, the proton resonances around 3.39 ppm due to the terminal methyl ether group of OEGMEMA, the proton resonances around 2.81 ppm due to the succinimide group of NHSMA and the disappearance of proton resonances of the terminal alkenyl groups of the monomers used. Full ^{1}H NMR ($CDCl_3$) spectrum of POEGMEMA-DTX-NHS conjugate is given in Figure 6.1.

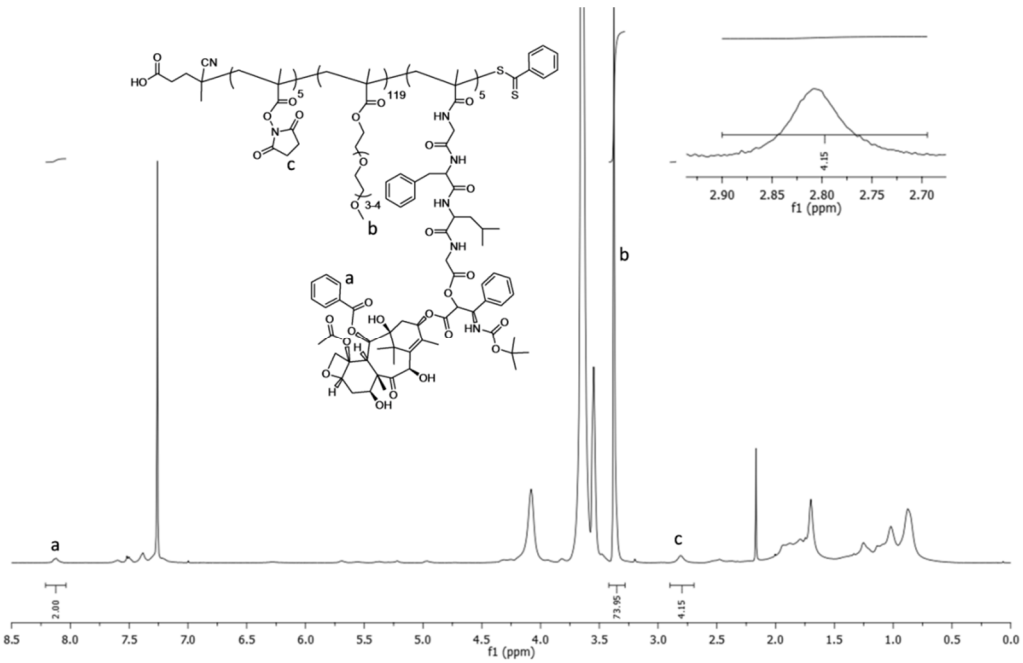


Figure 6.1. ^{1}H NMR spectra of POEGMEMA-DTX-NHS conjugate.

The weight percent of DTX in POEGMEMA-DTX conjugates was calculated by comparison of integration of the above mentioned proton resonances of the monomers and the mass of the CTA fragments. Drug content for POEGMEMA-DTX-NHS was calculated as 8.8 % by weight. Molecular weight (Mn) and PDI values of the POEGMEMA-DTX-NHS conjugate was recorded as 42.6 kDa and 1.30 respectively by using gel permeation chromatography.

6.3.2. Synthesis of POEGMEMA-DTX-cRGDfK Polymer Drug Conjugate

For the synthesis of POEGMEMA-DTX-cRGDfK conjugate, POEGMEMA DTX-NHS conjugate and cRGDfK were reacted in the presence of DIPEA in DMF. Conjugation efficiency is evaluated using ^{1}H NMR spectroscopy. ^{1}H NMR spectroscopy results showed that 1 of 5 NHS group on the polymer backbone of POEGMEMA DTX-NHS conjugate reacted with cRGDfK which is determined by the decrease in proton resonances around 2.81 ppm due to succinimide group of NHS functionality. Full ^{1}H NMR ($CDCl_3$) spectrum of POEGMEMA-DTX-cRGDfK conjugate is given in Figure 6.2.

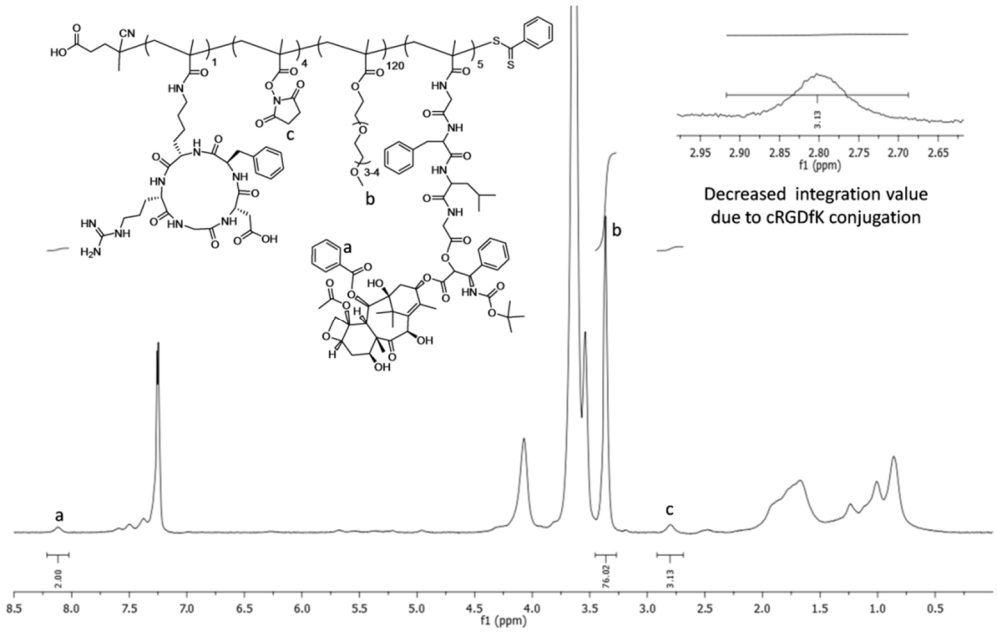


Figure 6.2. ^{1}H NMR spectra of POEGMEMA-DTX-cRGDfK conjugate.

We also provide another proof for the conjugation using bicinchoninic acid (BCA) analysis using BCA protein assay kit (thermo fisher scientific) according to suggested protocols [174]. Presence of cRGDfK group after conjugation is demonstrated by the

protein content increase (Figure 6.3). The reason of protein content in POEGMEMA-DTX conjugate is due to the peptide linker (GFLG).

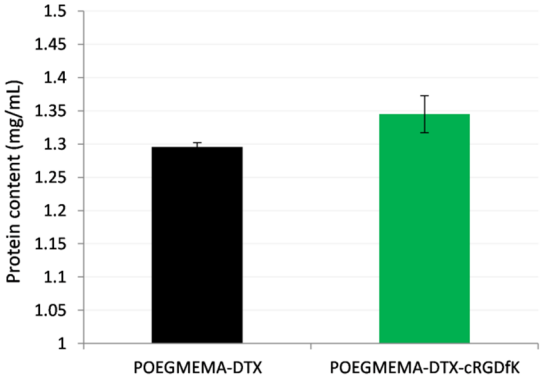


Figure 6.3. BCA protein assay for polymer drug conjugates.

POEGMEMA- DTX- cRGDfK conjugate was further reacted with amino-2-propanol in DMF for inactivation of unreacted NHS groups. Deactivation of NHS groups proved by disappearance of the proton resonances around 2.81 ppm due to succinimide group of NHS functionality. Full ^{1}H NMR ($CDCl_3$) spectrum of POEGMEMA-DTX-cRGDfK conjugate after NHS inactivation is given in Figure 6.4. Molecular weight (Mn) and PDI values of the POEGMEMA-DTX-cRGDfK conjugate was recorded as 43.2 kDa and 1.29 respectively by using gel permeation chromatography.

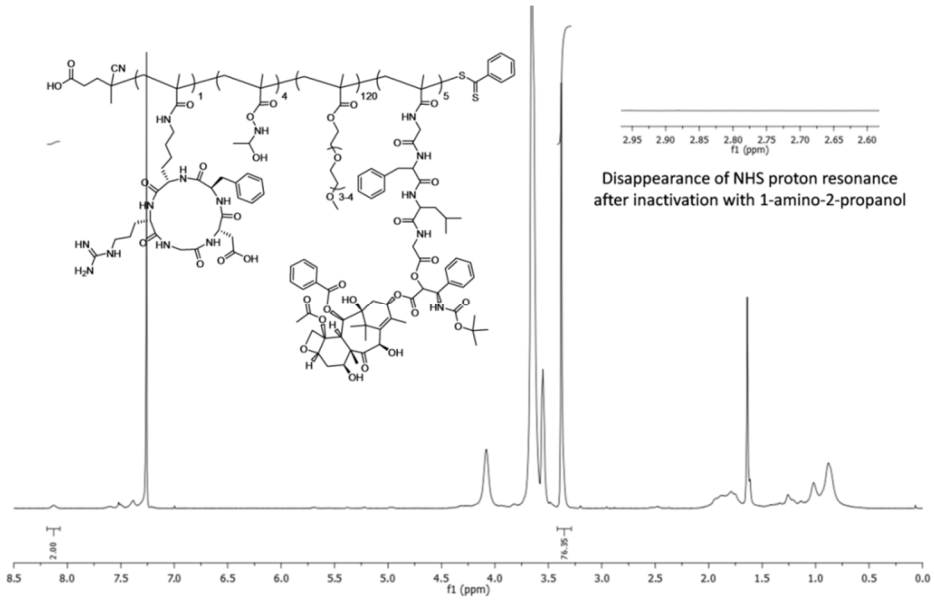


Figure 6.4. ^{1}H NMR spectra of POEGMEMA-DTX-cRGDfK conjugate after NHS deactivation.

6.3.3. Synthesis of POEGMEMA-DTX Polymer Drug Conjugate

POEGMEMA- DTX- NHS conjugate was reacted with amino-2-propanol in DMF for inactivation of unreacted NHS groups for the synthesis of non-targeted polymer drug conjugate, POEGMEMA- DTX. Deactivation of NHS groups proved by disappearance of the proton resonances around 2.81 ppm due to succinimide group of NHS functionality. Full ^{1}H NMR ($CDCl_3$) spectrum of POEGMEMA-DTX conjugate after NHS inactivation is given in Figure 6.5. Molecular weight (Mn) and PDI values of the POEGMEMA-DTX conjugate was recorded as 43.1 kDa and 1.31 respectively by using gel permeation chromatography.

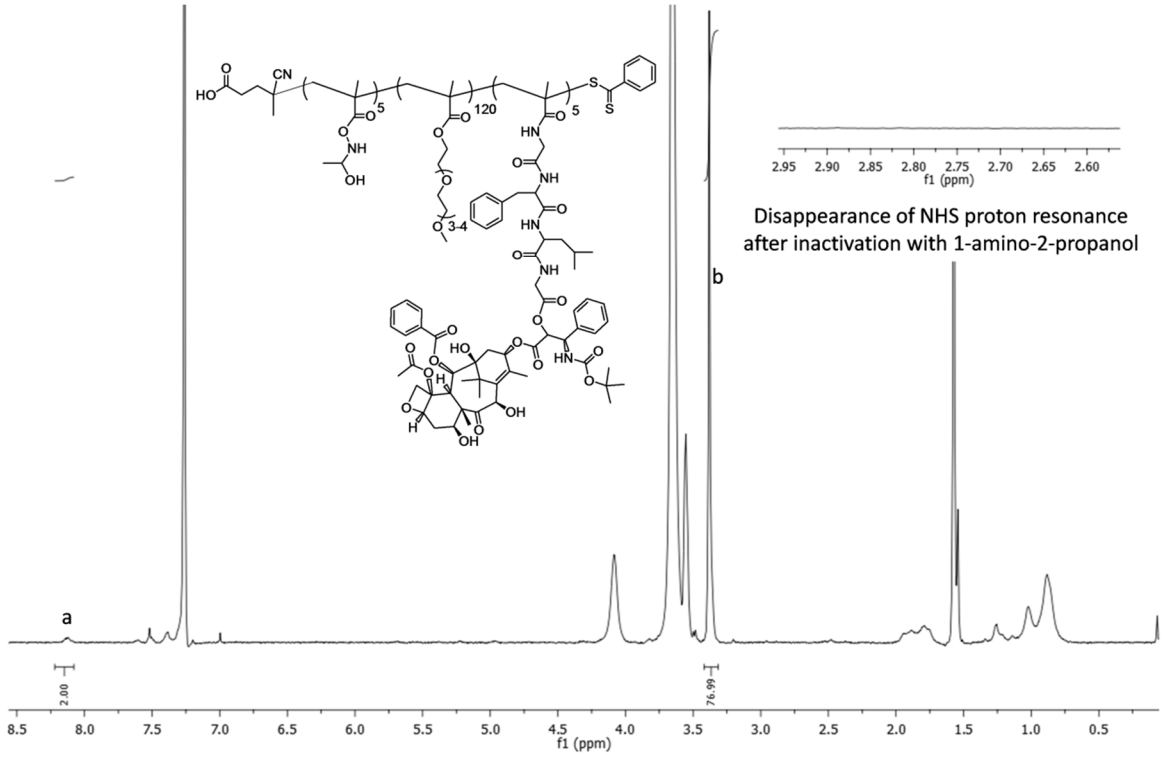


Figure 6.5. ^{1}H NMR spectra of POEGMEMA-DTX conjugate after NHS deactivation.

6.3.4. Enzymatic and Plasma Release profiles of Polymer Drug Conjugates

Drug release dynamics of targeted and non-targeted polymer drug conjugates were evaluated for understanding their stability in plasma and enzymatic degradation efficiency of the GFLG linker. Papain induced enzymatic DTX release were found to be higher than DTX release in plasma for both polymer drug conjugates. Low DTX release in plasma is a

promising outcome to make inferences for the blood stability of the conjugates. On the other hand, high DTX release in enzymatic conditions shows the cleavability of the GFLG linker in enzyme-rich environments such as tumor tissues. Figure 6.6 shows enzymatic and plasma release profiles of DTX for polymer drug conjugates.

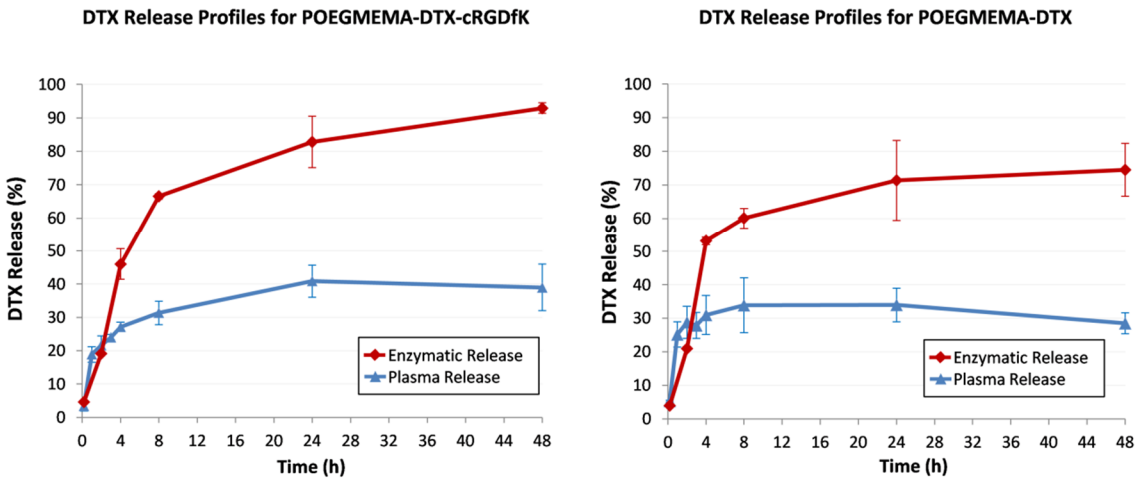


Figure 6.6. Enzymatic and plasma release profiles of DTX for POEGMEMA-DTX-cRGDfK and POEGMEMA-DTX conjugates.

6.3.5. Cytotoxicity of Polymer Drug Conjugates

Cytotoxicity of targeted and non-targeted polymer drug conjugates and free DTX were evaluated using A-549 (human lung carcinoma) cell line.

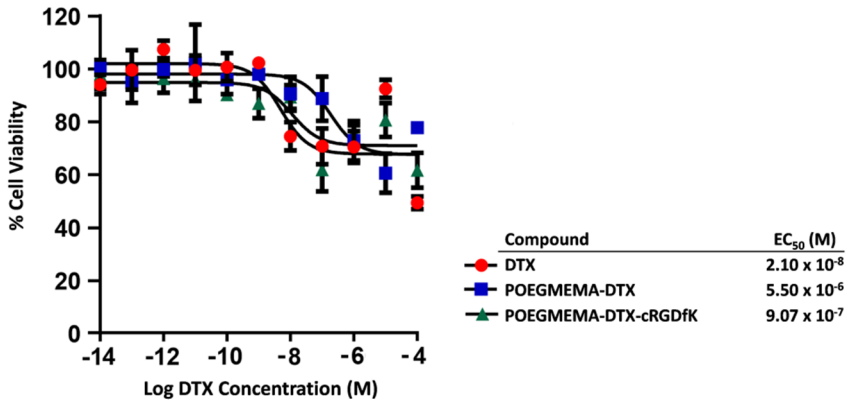


Figure 6.7. Cytotoxicity of polymer drug conjugates and free DTX for A-549 cell line. EC_{50} values calculated by Graph-Pad prism, non-linear regression mode.

Cell viability diagram as a function of concentration and EC_{50} values of the tested compounds are given in Figure 6.7. POEGMEMA-DTX and POEGMEMA-DTX-cRGDfK conjugates showed lower cytotoxicity compared to free DTX for A-549 cells. Results showed that cells were more sensitive to POEGMEMA-DTX-cRGDfK, compared to POEGMEMA-DTX.

6.3.6. Tolerability of POEGMEMA-DTX and POEGMEMA-DTX-cRGDfK Conjugates at 40 mg/kg DTX Equivalent Dose

We designed a tolerability study for polymer drug conjugates by considering obtained results of MTD study for POEGMEMA-DTX (50 kDa) in the previous chapter. Briefly, male Balb-C mice separated into three groups (n=3 for each group) and injected with POEGMEMA-DTX and POEGMEMA-DTX-cRGDfK at 40 mg/kg DTX equivalent doses. We observed that both conjugates were tolerated by mice at tested dose according to data obtained for % body weight chance as a function of time (Figure 6. 8). Mice loosed only about 2 % of their initial body weight when administered 40 mg/kg DTX equivalent polymer drug conjugates at the fifth day.

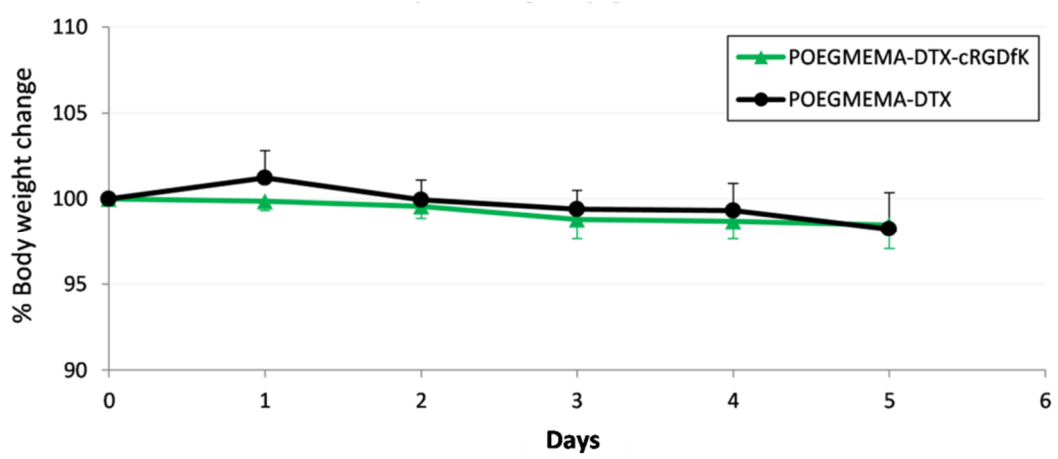


Figure 6.8. Normalized body weight change of mice injected with polymer drug conjugates at dose of 40 mg/kg DTX equivalent.

Polymer drug conjugates showed similar and non-toxic effect at the dose administered to the mice in terms of organ/body weight ratio. Liver/body weight and spleen/body weight ratios of the mice at fifth day are given in Figure 6.9.

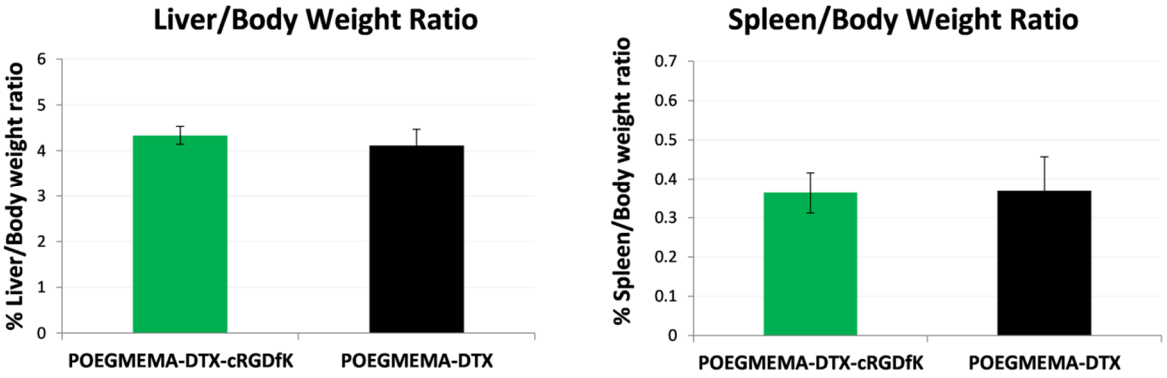


Figure 6.9. Liver/body weight and spleen/body weight ratios of the mice injected with polymer drug conjugates at dose of 40 mg/kg at fifth day.

Blood samples of the mice were collected before conjugate injection, at second and fifth day. WBC and RBC count analysis exhibited that the mice injected with 40 mg/kg drug equivalent polymer drug conjugates tolerated the dose. WBC and RBC count values were found to be in normal range for both polymer drug conjugate administration. Normalized WBC and RBC count change values of mice are given in Figure 6.10.

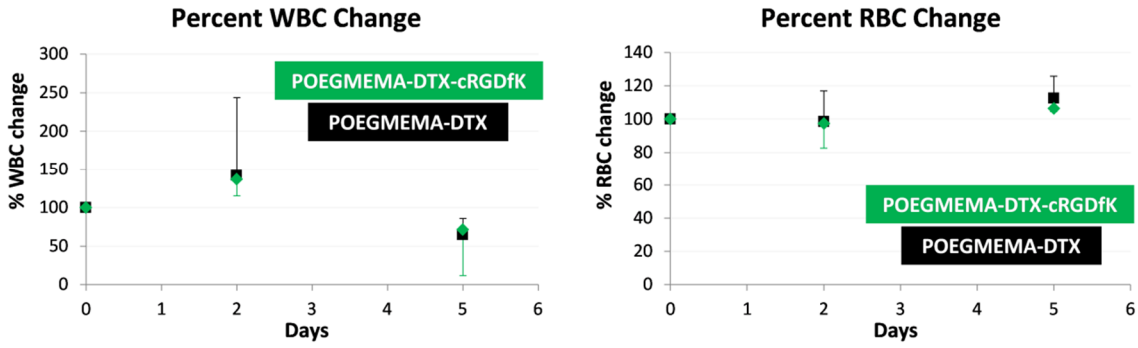


Figure 6.10. Normalized WBC and RBC count change values of the mice injected with polymer drug conjugate at dose of 40 mg/kg DTX equivalent.

At least 3-fold MTD increase (from 13 to 40 mg/kg) was achieved by conjugation of free DTX to POEGMEMA based polymers.

6.3.7. Anti-tumor Efficacy of Polymer Drug Conjugates in Human Lung Carcinoma Model

In vivo anti-tumor activity of polymer drug conjugates were evaluated in human lung carcinoma model. When tumor volumes reached around 50 mm^3 (about 4 weeks after tumor cell transplantation), POEGMEMA-DTX-cRGDfK and POEGMEMA-DTX at dose of 40 mg/kg DTX equivalent and free DTX (13 mg/kg, conventional formulation) were injected to mice (n= 5-6) via tail vein in saline solutions (50 µL). Injections were repeated in every 10 days (total of three injections). Due to slow tumor growth and to achieve better tolerance to dose, long-term treatment schedule was preferred. Saline (50 µL) was injected another group of mice (n= 5) with the same treatment schedule. Body weight and tumor volume parameters were recorded in every 3 days. Body weight measurements revealed that polymer drug conjugates and free DTX were tolerated by the mice at the dose injected. Slightly higher negative body weight change was observed for DTX injected mice compared to other groups. Normalized body weight changes as a function of time is given in Figure 6.11.

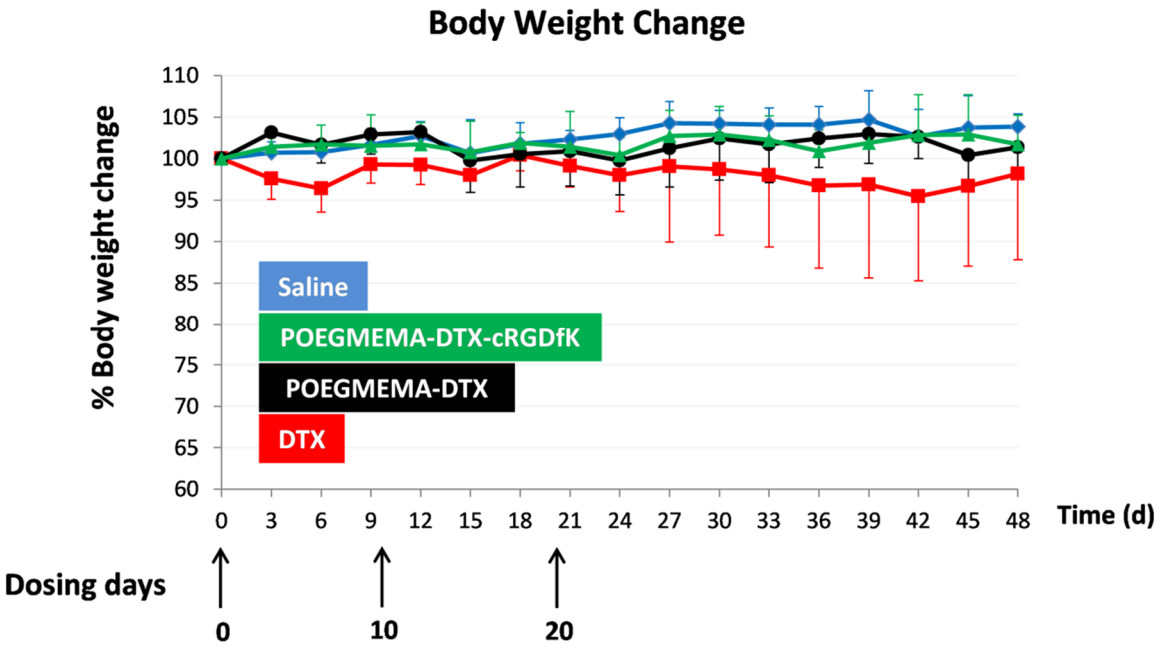


Figure 6.11. Body weight changes of mice at each group during anti-tumor study.

As shown in Figure 6.12, POEGMEMA-DTX and POEGMEMA-DTX-cRGDfK conjugates exhibited superior therapeutic effect compared to free DTX. Targeted polymer

drug conjugate showed slightly higher therapeutic effect compared to non-targeted one as consequence of targeting ligand contribution to EPR effect.

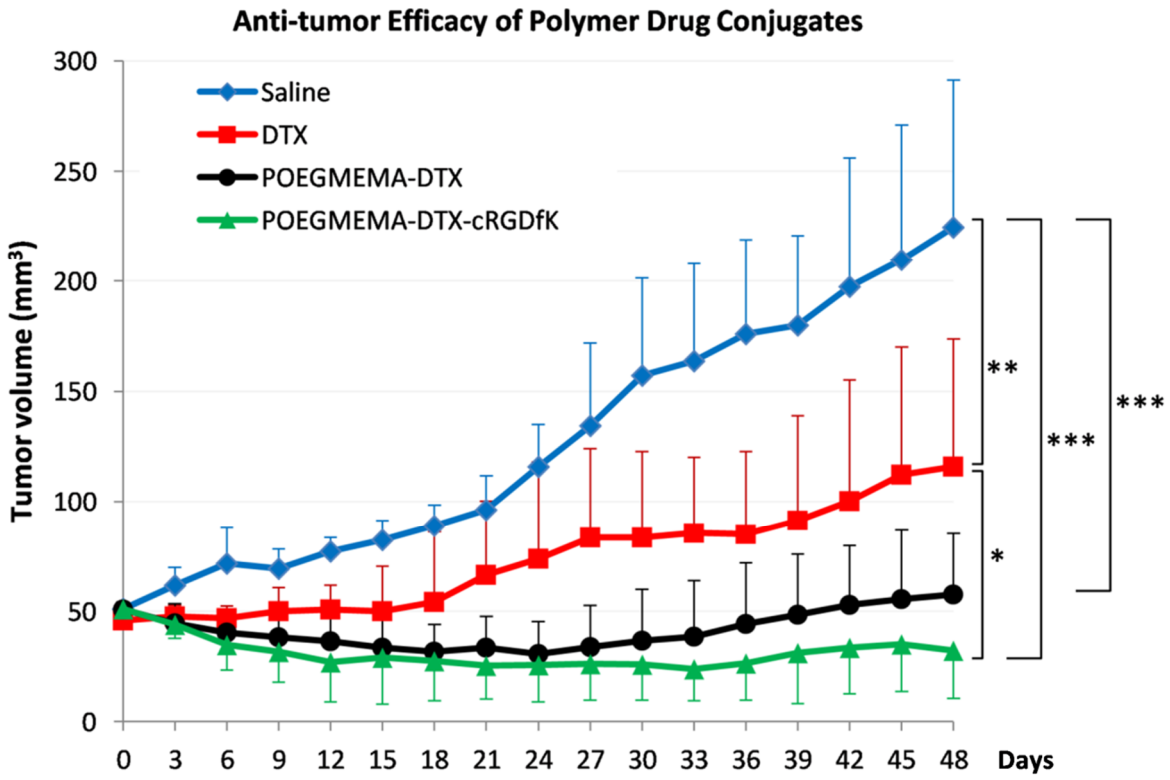


Figure 6.12. Changes in tumor volume of mice at each group during anti-tumor study. Values represent mean ± SD (n = 5 - 6). * represents $p < 0.05$, ** $p < 0.01$, and *** $p < 0.001$.

6.4. Conclusion

POEGMEMA based targeted and non-targeted DTX conjugates with an enzymatically cleavable linker (GFLG) having molecular weights around 43 kDA were successfully synthesized. *In vitro* cytotoxicity results showed effect of targeting ligand over cell proliferation. Blood stability and cleavability of GFLG linker was proved by *in vitro* plasma and enzymatic release experiments. Branched structure of the conjugates due to OEGMEMA monomer provided stability in plasma and sustained enzymatic release profile as also proved in previous chapter. The mice tolerated 40 mg/kg DTX equivalent polymer drug conjugate dose as a result of low drug release in plasma. Anti-tumor efficacy of DTX was improved by conjugation with POEGMEMA based polymers due to the long

blood circulation time of polymer drug conjugates. Introducing targeting ligand contributed to passive targeting (via EPR effect) and improved anti-tumor activity of polymer drug conjugates. These unique polymer drug conjugate design with high therapeutic effect is an attractive and a promising strategy for prodrugs in cancer treatment.

7. BIODISTRIBUTION OF POLYMERIC NANOPARTICLES WITH DIFFERENT SIZE AND MORPHOLOGY GENERATED BY POLYMERIZATION INDUCED SELF ASSEMBLY (PISA)

7.1. Introduction

Reversible addition–fragmentation chain transfer (RAFT) polymerization is a useful technique for the synthesis of block copolymers to end up with polymeric nanoparticles in solution [169,170]. Boyer, Davis and co-workers inspired by initial works of Pan [175,176] and Armes [177,178,179] research groups and used RAFT polymerization for "polymerization induced self-assembly" (PISA). The PISA approach is based on the chain extension of soluble homopolymers with a co-monomer to give insoluble second block forcing self-assembly in polymerization solution. They successfully showed formation and encapsulation of POEGMEMA-*b*-PST block copolymer nanoparticles, spherical micelles, worm-like, rod-like micelles and spherical vesicles generated by PISA concept [180]. In a following study, they prepared POEGMEMA-*b*-P(ST-co-VBA) block copolymer nanoparticles with various morphologies and used aldehyde groups in the cores of nanoparticles for crosslinking or conjugating Doxorubicin via pH-breakable bonds [181]. They demonstrated the significant effect of nanoparticle morphology on cell uptake.

Several research groups have focused on biodistribution of non-spherical polymeric nanoparticles with the diameter range about 5-25 nm [182,183,184]. They all concluded that non-spherical nanoparticles, mainly rod-like and worm like ones, less likely accumulate in major organs (liver, spleen and lung), whereas they more likely accumulate in tumor tissue compared to spherical ones. However biodistribution of non-spherical polymeric particles with larger diameter is unclear. To investigate biodistribution profile of non-spherical polymeric nanoparticles with diameter size around 60 nm compared to spherical ones, we used PISA concept which allows generating non-spherical nanoparticles with desired larger diameters. We synthesized homo polyglycidyl methacrylate (PGMA) using RAFT polymerization as functionalizable segment of nanoparticles. PGMA block which is also the macro chain transfer agent (CTA) copolymerized with oligo(ethyleneglycol) methyl ether methacrylate (OEGMEMA) to give PGMA-*b*-

POEGMEMA copolymer via RAFT polymerization. Chain extension of this block copolymer was performed with styrene (ST) monomer in methanol by RAFT polymerization to yield PGMA-*b*-POEGMEMA-*b*-PST block copolymer. Insolubility of poly styrene (PST) block in methanol enabled self-assembly of this three block copolymer and resulted in nanoparticles with different morphologies such as micelles, rod-like and worm-like nanoparticles. PGMA block provided further functionalization of nanoparticles for biodistribution study via tiritiated 2-amino ethane-1-ol. After radiolabelling of nanoparticles, residual epoxide groups were forced ring opening in acidic conditions for inactivation. Cytotoxicity of inactive nanoparticles tested for HT1080 (human fibrosarcoma cells) cell line. Tumor biodistribution experiments of the radiolabeled and inactivated nanoparticles were performed in tumor-burdened female nude mice. HT1080 cells injected to the flank region of the mice for tumor growth. Tumor and organ samples were collected after 48 h of nanoparticle injections. Liquid scintillation counter was used to measure radioactivity of the samples.

7.2. Experimental

7.2.1. Materials

Glysidyl methacrylate (GMA), styrene (ST) and oligo(ethylene glycol) monomethyl ether methacrylate (OEGMEMA), 4-cyanopentanoic acid dithiobenzoate (CPADB), 2,2′-azobisisobutyronitrile (AIBN) and 12-14K molecular weight cut-off (MWCO) dialysis membrane were purchased from Aldrich. Soluene-350 and Starscint were purchased from Packard Biosciences (Meriden, CT). Heparin (10,000 U/mL) was purchased from Faulding (SA, Australia). Isopropyl alcohol was AR grade and purchased from Mallinckrodt Chemicals (Phillipsburg, NJ). Fetal bovine serum (FBS), Glutamax and 0.25 % trypsin-EDTA were obtained from Invitrogen (VIC, Australia). RPMI and MEM mediums and 3-[4,5-dimethylthiazol-2-yl]-2,5-diphenyltetrazolium bromide (MTT) were purchased from Sigma (NSW, Australia). All other solvents were HPLC grade, obtained from Merck and used without further purification. All polymers were characterized using ^{1}H NMR spectroscopy (Brand-Model, 400 MHz) and gel permeation chromatography GPC (Shimadzu, Japan) with a mobile phase solution of 0.05M lithium bromide in dimethylaceteamide (DMAc). Size and morphology of nanoparticles was determined using Zetasizer (Malvern Zetasizer Nano ZS) and Transmission Electron Microscopy (TEM).

Absorbance values for cytotoxicity assays were measured by Fluorostar microplate reader (Bio-Strategy, Auckland, NZ). Disintegrations per minute (DPM) values of animal samples were measured using liquid scintillation counter (Perkin Elmer Tri-Carb 2800TR).

7.2.2. Cell Culture Conditions

HT1080 (human adenocarcinoma) cell line were purchased from ECACC (Salisbury, UK). HT1080 cells were grown in 75 cm^2 flasks in RPMI medium with with 10 % FBS and 1 % penicillin-streptomycin, 2 mM Glutamax, 1 % non-essential amino acids in a humidified atmosphere of 5 % CO_2 and at 37 °C. Cells were passaged 1:6 using 0.25 % trypsin-EDTA 3 times per week.

7.2.3. Animals

Athymic nude mice (female, 6 weeks of age) were purchased from the Australian Research Centre (Perth, WA) and were housed in microisolators (Australian Research Centre, WA) maintained at 22 °C under cycles of 12-h light/12-h darkness. Mice were fed ad libitum. Animal study was approved by the Victorian College of Pharmacy Animal Ethics Committee (MIPS.2014.28), Monash University (Melbourne, Victoria).

7.2.4. Synthesis of PGMA

RAFT polymerization was used for the synthesis of homo PGMA polymer. To a solution of GMA (2038 mg, 14.33 mmol) and CPADB (200 mg, 0.717 mmol) in toluene (9.5 mL), was added AIBN (11.8 mg, 0.0717 mmol). The mixture was purged with N_2 to remove O_2 and polymerization was allowed for 90 min. at 70 °C. Polymerization was stopped by cooling and air exposure. Just about 3:4 of toluene was evaporated by air flow. PGMA purified by precipitation three times in cold petroleum benzene : diethyl ether (3:1) mixture followed by evaporation in vacuum oven over night (max 30 °C) to give approximately 9 GMA repeating units (30 % yield).

7.2.5. Synthesis of PGMA-*b*-POEGMEMA

PGMA was used as macro chain transfer agent for the synthesis of PGMA-*b*-POEGMEMA block copolymer via RAFT polymerization. To a solution of OEGMEMA (1900 mg, 6.34 mmol) and PGMA (200 mg, 0.127 mmol) in acetonitrile (10 mL), was

added AIBN (2.6 mg, 0.0158 mmol). The mixture was purged with N_2 and polymerization was allowed for 4 h at 70 °C. Polymerization was stopped as above. Just about 3:4 of acetonitrile was evaporated by air flow. PGMA-*b*-POEGMEMA purified by precipitation three times in cold petroleum benzene:diethyl ether (1:2) mixture followed by evaporation in vacuum oven over night (max 30 °C) to give approximately 26 OEGMEMA repeating units (51 % yield).

7.2.6. Nanoparticle Formation by Polymerization Induced Self-Assembly (PISA)

PISA approach was used to generate polymeric nanoparticles. To a solution of ST (19700 mg, 189 mmol) and PGMA-*b*-POEGMEMA (350 mg, 0.0378 mmol) in methanol (27.8 mL), was added AIBN (1.24 mg, 0.00756 mmol). The mixture was purged with N_2. To obtain PGMA-*b*-POEGMEMA-*b*-PST block copolymer nanoparticles with different size and shape, solution samples (5 mL) were collected at different time points under N_2. Additionally 5 mL methanol was gently added to each solution to prevent possible aggregations. Turbid and milky white nanoparticle solution samples were further purified by dialysis membrane (12-14K MWCO) against methanol to remove unreacted ST monomer. Spherical small micelles (30 nm, after 6 h), spherical large micelles (46 nm after 10 h), worm-like micelles (after 24 h) and rod-like micelles (after 46 h) were obtained with the final concentrations of 8, 10.1, 13.4 and 16.5 mg/mL, respectively (Concentration values were calculated by the weight of nanoparticle after evaporation of 1 mL nanoparticle solution).

7.2.7. Radiolabelling of Nanoparticles via Tiritiated 2-amino ethane-1-ol and Inactivation Remaining Epoxide Groups for Biodistribution Study

Tiritiated 2-amino ethane-1-ol solution in 100 µL ethanol was diluted with 900 µL methanol and reacted with purified nanoparticle solutions (2 mL) at RT overnight. Reaction mixtures were then purified by dialysis membrane (12-14K MWCO) in methanol to remove unreacted tiritiated 2-amino ethane-1-ol. Radiolabelled nanoparticle solutions (1 mL) were further reacted with 0.5 mL 0.5 M H_2SO_4 solution for inactivation of unreacted epoxide groups on nanoparticle surfaces. After this reaction nanoparticle solutions were dialyzed by 12-14K MWCO membrane in water and sterile PBS, respectively. Than concentrations of nanoparticles fixed to 2 mg/mL in sterile PBS for biodistribution study and DPM values were measured before injections.

7.2.8. Inactivation of Epoxide Groups for Cytotoxicity Assays

The epoxide groups on unradiolabelled nanoparticle surface were inactivated and the concentration values of nanoparticle solutions fixed to 2 mg/mL in sterile PBS as described above prior to cytotoxicity assays.

7.2.9. Cytotoxicity of Nanoparticles on HT1080 cells

HT1080 cells were seeded in each well of 96 well microplates in of serum free mediums (100 μL) containing supplements as described above at a density of 5,000 cells per well. After 48 h, cell media was exchanged to 100 μL micelle (30 and 46 nm), worm-like or rod-like nanoparticle solutions (1 to 0.00001 mg/mL, nanoparticle/media) was then added to triplicate wells and incubated for 48 h at 37 °C in 5 % CO_2. After 48 h nanoparticle/media solutions was gently removed from cells and reconstructed, sterile filtered MTT solution (100 μL) with a final volume of 0.5 mg/mL MTT/media was added to each well. Plate was covered with foil and incubated at 37 °C in 5 % CO_2 for 2 h. Than MTT solution was removed and DMSO (100 μL) was added to each well. Plates were shaked 5-10 min until all the crystals are dissolved and absorbance was read for three replicates per treatment in a Fluorostar microplate reader (Bio-Strategy, Auckland, NZ) at 540 nm. The equation (As - Ab)/(Ac - Ab) 100 was used to determine the percentage of viable cells relative to untreated control cells. Where As is the absorbance of the nanoparticle treated cell samples, Ab is absorbance of blank cells not treated with MTT solution and Ac is the absorbance of control cells treated with MTT solution.

7.2.10. Biodistribution of Nanoparticles in HT080 Xenografts Tumor Model

HT1080 cells were used between passages 6 and 10 for xenograft tumor model. For solid tumor induction in athymic nude mice, cells were passaged using trypsin-EDTA, washed once in PBS and resuspended in PBS with a final volume of 6×10^7 cells/1 mL PBS. A 50 μL suspension of HT1080 cells (3×10^6 cells in total) was then injected into the right flank of mice (n=17) using a 25G needle. Tumor growth was monitored with a caliper every 2 days by the equation, Tumor volume (mm^3) = $4/3\pi ab^2$, where a = longest radius (mm), b = shortest radius (mm). When tumor volumes reached approximately 100 mm^3 (approximately 8 days after cell injection) mice were anaesthetized with 3 % isoflurane and injected with 0.1 mg of radiolabelled nanoparticle, micelle (30 nm), micelle (46 nm),

worm-like or rod-like nanoparticles (in a final volume of 50 μL of sterile PBS) intravenously via the tail vein using a 27G needle (n=4 for each nanoparticle group). The blank mouse untreated with nanoparticles was killed when tumor volume reached approximately 100 mm^3. The others were killed via intra peritonal (IP) administration of 50 μL lethabarb 48 h after IV dosing of nanoparticles. Blood, tumor, liver, spleen, kidneys, heart, lung, pancreas, muscle (from the left thigh) and fat (from the left dorsal region) were collected for biodistribution analysis. One of the kidneys, approximately 100-150 mg muscle and liver, 50-100 mg fat, 50 mg blood and other organs as whole were put into 20 mL scintillation vials and solubilized in 4 mL of 1:1 soluene : isopropanol by overnight heating at 60 °C. Tissue samples were then bleached with 200 μL 30 % hydrogen peroxide (for blood samples 400 μL) for 30 min. Following bleaching 10 mL Starscint was added to the samples and the samples were vortexed. Samples were kept at 4 °C and dark for 3 days until they were counted using scintillation counter.

7.2.11. Statistics

Biodistribution data within spherical, rod and worm-like nanoparticle groups were compared by one-way ANOVA test using spherical micelle (diameter: 33 nm) as control. Statistical significance was identified at a level of $p < 0.01$.

7.3. Results and Discussion

7.3.1. Nanoparticle Formation with Different Sizes and Morphologies by PISA

Functional polymeric nanoparticles were synthesized by PISA concept using PGMA-*b*-POEGMEMA-*b*-PST block copolymers in methanol. GMA monomer was chosen to form functional segment of the block polymer due to its epoxide groups allowing post modification functionalization with radiolabelled ethanol amine. POEGMEMA as hydrophilic segment of nanoparticles with non-toxic and anti-immunogenic properties and extremely hydrophobic PST segment with high glass transition temperature (Tg) [185,186] ensuring stability of the polymeric nanoparticles and enabling hydrophobic load [180,181] provided an ideal nanoparticle composition for drug delivery with functionalizable PGMA segment. First, the RAFT polymerization of GMA was conducted in toluene at 70 °C using an AIBN initiator and a CPADB chain transfer agent. The homopolymerization of GMA

was stopped at a conversion of about 30 %, yielding PGMA with Mn = 2500 g mol^{-1} and PDI = 1.14. Similar to the approach mentioned in introduction by Boyer, Davis and co-workers [180,181] chain extension was obtained by PST segment to instigate PISA process. PGMA was used as macro chain transfer agent in RAFT polymerization of OEGMEMA using an AIBN initiator at 70 °C to give PGMA-*b*-POEGMEMA copolymer with Mn = 8800 g mol^{-1} and PDI = 1.09 (54 % yield). Chemical structures and ^{1}H NMR spectra of PGMA and PGMA-*b*-POEGMEMA polymers are shown in Figure 7.1.

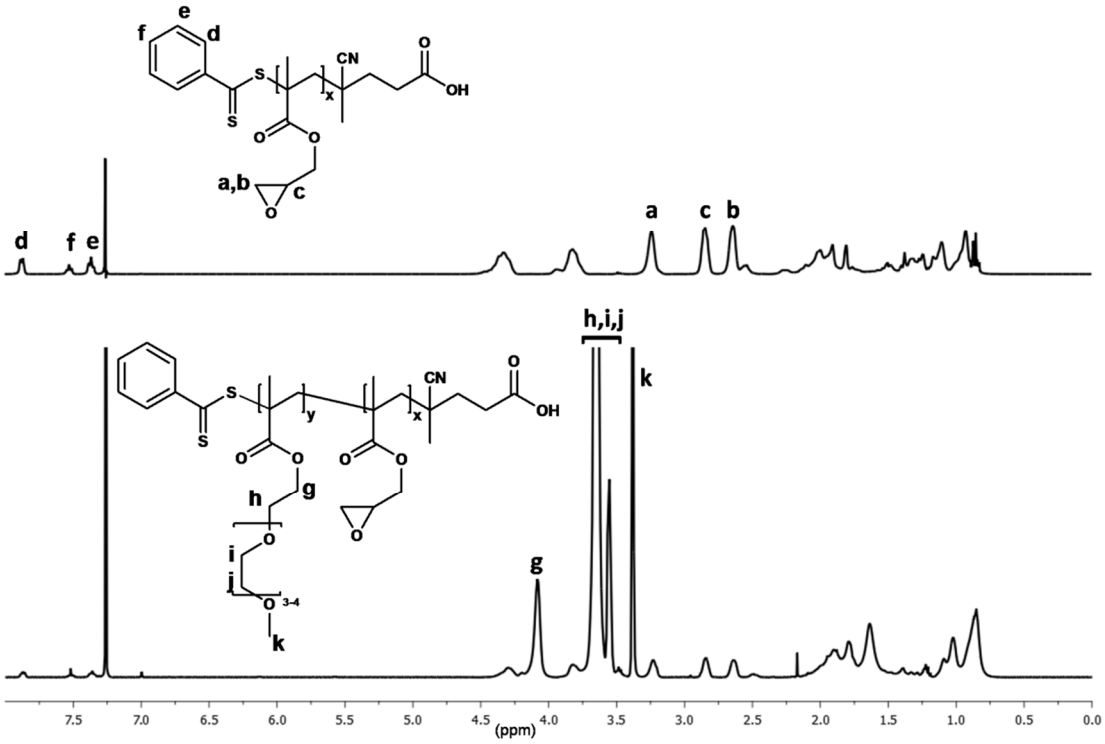


Figure 7.1. Chemical structures and ^{1}H NMR spectra of PGMA and PGMA-*b*-POEGMEMA polymers.

Chain extension of PGMA-*b*-POEGMEMA copolymer with ST resulted in PGMA-*b*-POEGMEMA-*b*-PST copolymer (Figure 7.2, panel a) enabling formation of nanoparticles thanks to the insolubility of PST polymer block in methanol whilst ST is soluble. Proceeding PST polymerization under dispersion conditions during PISA process confirmed by continuous chain extension with ST at different polymerization times. GPC and NMR results showed that the molecular weight linearly increased and low PDI values (< 1.42) were observed throughout PISA process (Figure 7.2, panel b and d).

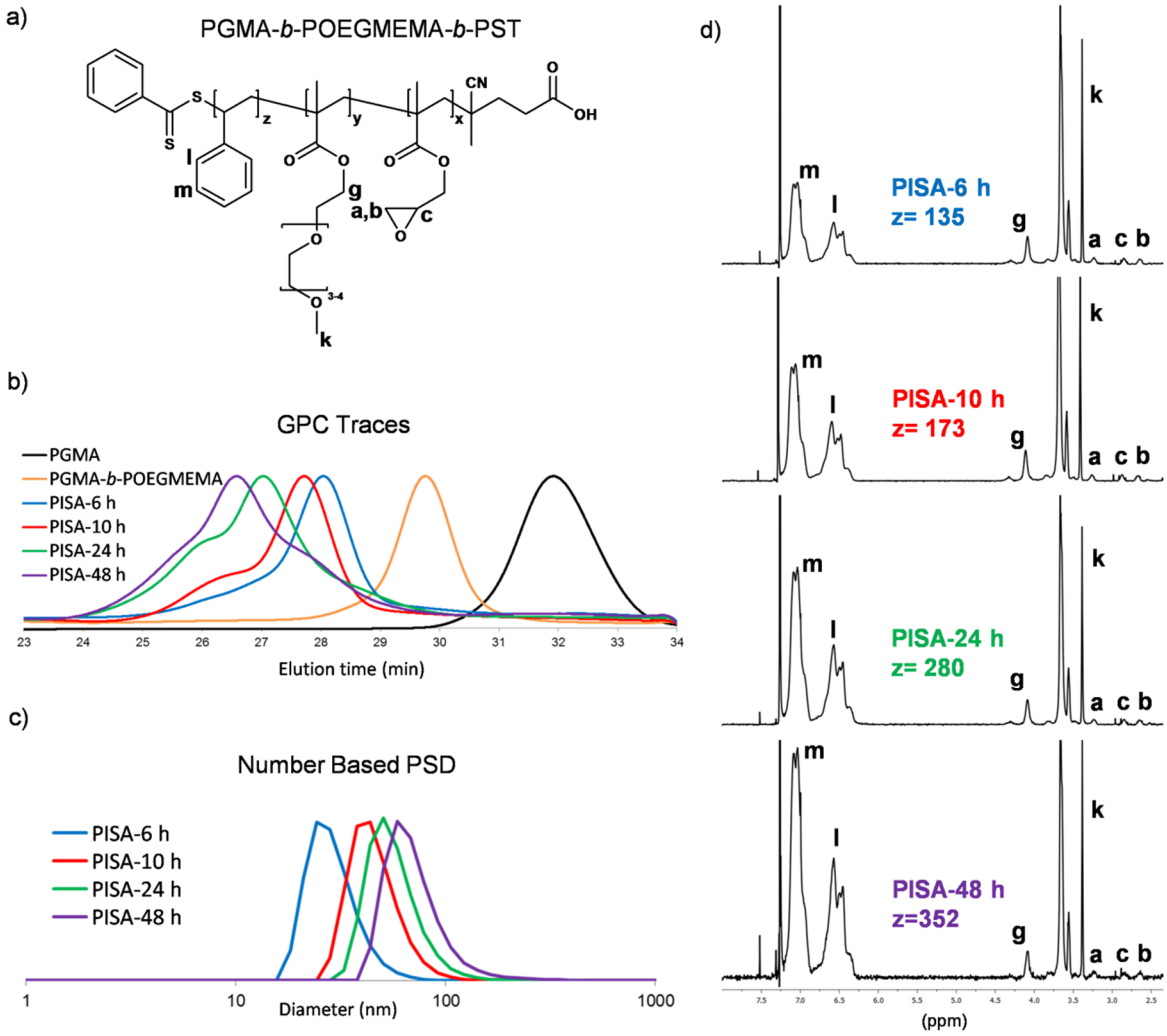


Figure 7.2. Characterization of PGMA-*b*-POEGMEMA-*b*-PST triblock copolymers. (a) Chemical structure of PGMA-*b*-POEGMEMA-*b*-PST; (b) GPC traces of PGMA, PGMA-*b*-POEGMEMA and PGMA-*b*-POEGMEMA-*b*-PST with growing molecular weights; (c) dynamic light scattering (DLS) number mean values showing structural changes during PISA; d) ^{1}H NMR spectra of PGMA-*b*-POEGMEMA-*b*-PST copolymers at different polymerization times, where z is number of repeating unit for PST.

GPC traces showed that possible termination reactions caused small shoulders at low retention times as previously explained by Boyer, Davis and co-workers [180,181]. Transparent polymerization solution turned to turbid and milky white solutions by the time during chain extension, showing the size and morphology change of polymeric nanoparticles. The size of polymeric nanoparticles obtained at different polymerization times measured by DLS. Steadily increased number average sizes of nanoparticles were found from 30 nm to 69 nm. Spherical micelles obtained with low dispersities smaller than

0.14, whereas dispersity values increased up to 0.45 due to morphological transition from spheres to filamentous structures (Figure 7.2, panel c).

Table 7.1 includes all characterization data for synthesized PGMA-*b*-POEGMEMA-*b*-PST copolymers during dispersion polymerization by PISA at different time points.

Table 7.1. Characterization of PGMA-*b*-POEGMEMA-*b*-PST copolymers.

Copolymers	Number of GMA units [a]	Number of OEGMEMA units [a]	Number of ST units [a]	Mw[a] (g/mole)	Mn[b] (g/mole)	PDI[b]	Concentration [c] (mg/mL MeOH)
PISA-6 h	9	26	135	23395	23900	1.27	16.0
PISA-10 h	9	26	173	27352	30900	1.21	20.2
PISA-24 h	9	26	280	38497	36300	1.42	26.8
PISA-46 h	9	26	352	45996	42200	1.37	33.0

Where a, calculated by ^{1}H NMR spectroscopy; b, calculated by GPC (DMAc); c, concentration values were calculated by the weight of nanoparticle after evaporation of 1 mL nanoparticle solution.

Epoxide groups on nanoparticle surfaces enabled covalent attachment of radiolabelled ethanolamine. Sufficient radiolabelling was achieved between the DPM values of 105,000-146,000 for 50 µL injection solutions. Following radiolabelling, remaining epoxide groups were inactivated via ring opening reaction under acidic conditions. Complete inactivation of epoxide groups confirmed by NMR (Figure 7.3).

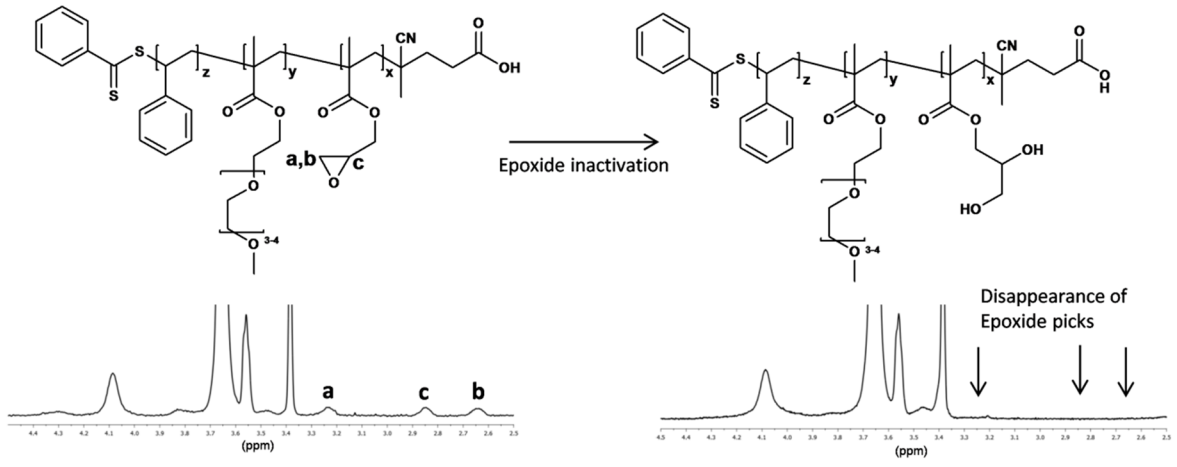


Figure 7.3. Confirmation of successful epoxide inactivation by ^{1}H NMR.

Morphology of purified nanoparticles using dialysis against water was investigated using transition electron microscopy (TEM). TEM images clearly showed the change in size and morphology of nanoparticles during PISA process (Figure 7.4).

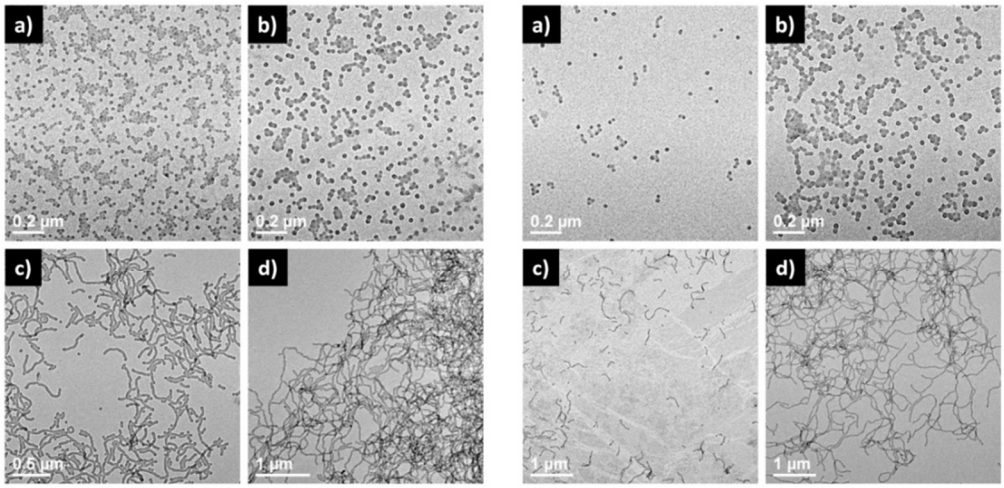


Figure 7.4. TEM images of nanoparticles before and after epoxide inactivation. Small spherical micelles (a), large spherical micelles (b), rod-like micelles (c), and worm-like micelles (d) formed at 6, 10, 24 and 46 h of polymerization times, respectively.

Spherical micelles with the diameter sizes of 33 and 47 nm were obtained when the number of PST repeating units reached 135 and 170, respectively. When this number reached 280, worm-like and 350, rod-like micelles with 63 nm diameter size were formed. TEM images also showed that ring opening reaction did not cause a significant change on the size and morphology of nanoparticles.

Any precipitation was not observed more than 2 months in nanoparticle solutions without any surfactant confirming the stability of these colloidal suspensions in water and methanol. Characterization of polymeric nanoparticles including their diameter, hydrodynamic volume and DPM values were summarized in Table 7.2.

Table 7.2. Characterization of PGMA-*b*-POEGMA-*b*-PST copolymer nanoparticles.

Nanoparticles	Average Diameter[a] (nm)	Morphology[a]	Hydrodynamic volume[b] (nm)	PDI[b]	Zeta Potential[b] (mV)	DPM[c] (for 50 µL)
PISA-6 h	33.05 ± 3.72	Spherical micelle	30.04 ± 0.81	1.140	-0.345 ± 0.103	145421
PISA-10 h	47.32 ± 3.39	Spherical micelle	46.09 ± 0.41	1.118	-0.725 ± 0.232	115195
PISA-24 h	63.44 ± 4.12	Rod-like micelle	55.85 ± 1.49	1.157	-0.342 ± 0.091	105878
PISA-46 h	62.89 ± 3.81	Worm-like micelle	69.22 ± 5.48	1.446	-0.474 ± 0.034	114843

Where a, measured by Transmission Electron Microscopy (TEM); b, average number mean values measured by Dynamic Light Scattering (DLS); c, DPM values measured by Liquid Scintillation Counter.

7.3.2. Cytotoxicity of Nanoparticles

Unradiolabelled and inactivated nanoparticles were tested to evaluate their cytotoxic behaviors. Cytotoxicity of nanoparticles was tested on HT1080 cell line which we used to derive tumor xenografts. Nanoparticles did not show any cytotoxicity on HT1080 cell line at tested concentrations (from 1 to 0.00001 mg/mL), (Figure 7.5).

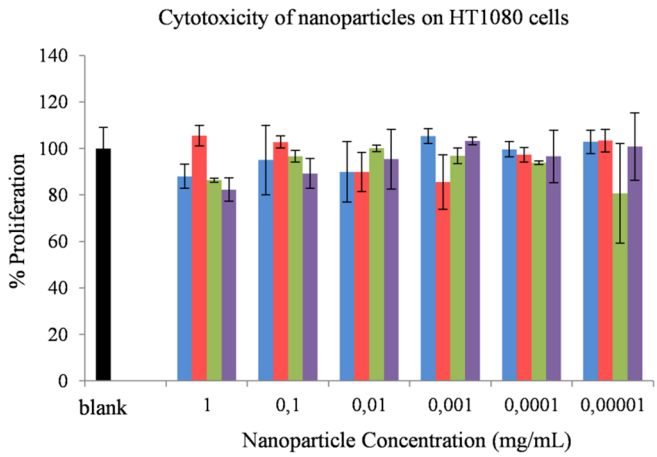


Figure 7.5. Cytotoxicity of polymeric nanoparticles on HT1080 (human adenocarcinoma cell line) cells at different nanoparticle concentrations. (Blue: micelles (diameter: 33 nm), red: micelles (diameter: 47 nm), green: rod-like micelles (diameter: 63 nm), purple: worm-like micelles (diameter: 63nm) treated and black: non-treated cells.)

7.3.3. Biodistribution of Nanoparticles

Four radiolabelled nanoparticle solutions (I: spherical micelles-33 nm diameter, II: spherical micelles-47 nm diameter, III: worm-like micelle-63 nm diameter and IV: rod-like micelle-63 nm diameter) were dosed to athymic nude mice when tumor volumes reached around 100 mm^3 via tail vein (n=4 for each nanoparticle group). Tumor, blood, major organs (hearth, lungs, liver, kidneys, spleen and pancreas) and tissue samples (muscle and fat) of mice were collected 48 h after IV dosing to determine the biodistribution pattern of nanoparticles. Same body samples of blank mouse (not treated with any nanoparticle solution) also collected to measure blank DPM values for each body samples. DPM values of the samples were measured using liquid scintillation counter. The percent injected radiolabel per gram of tissue of injected tritium (^3H) recovered in each body samples at sacrifice are shown in Figure 7.6.

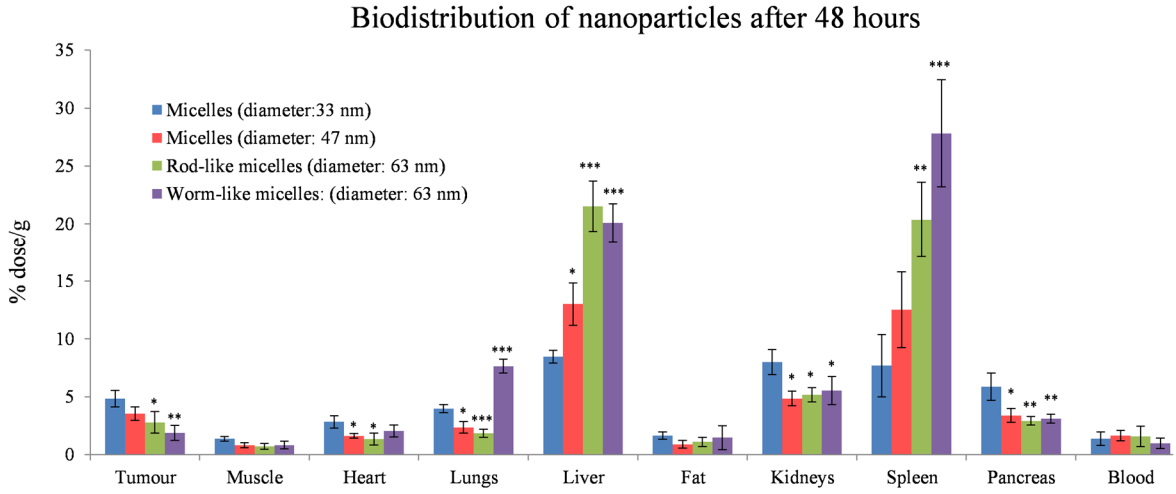


Figure 7.6. Biodistribution of nanoparticles in HT1080 tumor xenografts after sacrifice at 48 h. All data was normalized by tissue mass. Values represent mean ± SD (n = 4). * represents $p < 0.01$, ** $p < 0.001$, and *** $p < 0.0001$ cf. Micelles (33 nm).

One of the main features that predestinate nanoparticles for biodistribution is their size. Blood half-life times of the nanoparticles are known to be heightened by the size increment in a range enabling improved tumor accumulation by EPR effect. However, tumor vascularity and collagen matrix surrounding tumor periphery are the crucial factors which have to be taken into account for designing tumor-targeted nanoparticles [112,187,188]. Kataoka and co-workers [189] have demonstrated that polymeric micelles in range of size between 30-100 nm highly penetrated within permeable tumors, whereas in the case of a poorly permeable tumors, only small size nanoparticles (<50 nm) accumulated in tumors. The fast macrophage uptake of nanoparticles in the major organs (liver, spleen and lung) also affects the tumor accumulation because of reticulo-endothelial system (RES) clearance. Moreover, vascular fenestrations (50-100 nm) in liver, interendothelial cell slits (200-500 nm) in spleen and capillaries in lungs (2-5 μm) increase retention patterns of nanoparticles in these major organs and diminish their blood half-life times which result in poor EPR effect [112,187,188]. Zhang et al. examined biodistribution patterns of PEGylated nanoparticles with the sizes of 20, 40 and 80 nm in tumor-burdened mice and demonstrated that 20 and 40 nm nanoparticles accumulated more slowly in the liver and spleen, and they had higher blood half-life times compared to 80 nm nanoparticles [190] Although, they based these results on higher density of PEG on surface of small nanoparticles which prevents protein binding and thus slowing clearance from the

blood, the effect of issues above mentioned about major organs cannot be ignored. In parallel with the discussed examples, we demonstrated that the penetration of nanoparticles in liver and spleen increased in proportion to the size. Higher accumulation in lungs was measured in the case of worm-like micelles compared to smaller nanoparticles, probably due to long filamentous structure of worms which increased retention in lung capillaries. Higher kidney recovery was observed with micelles with the size of 30 nm compared to larger particles. Micelle (30 nm) accumulation in pancreas through high fibrous tissue content was found to be higher compared to larger particles. Recovery of nanoparticles in blood and, muscle, heart and fat tissues found to be similar. Insignificant accumulation of nanoparticles in muscle, heart and fat tissues was observed when organ blood volumes were considered.

Beside the size of the nanoparticles, their shape has also take a role in determination their biodistribution patterns [112,187,188]. Discher and co-workers prepared polymeric spherical micelles and filomicelles composed of diblock polymers by standard film rehydration techniques to investigate *in vivo* imaging and delivery properties of flexible flaments in A549 tumor xenografts [182]. They demonstrated that while filomicelles showed less permeation into major organs compared to spherical micelles, their accumulation in tumor tissue was higher than spherical ones. Sailor and co-workers designed PEGylated magnetic iron oxide nanoworms to understand tumor imaging and targeting characteristics of these nanoparticles [183]. Their findings showed that cell internalization of nanoworms in MDA-MB-435 cell line was superior to spherical nanoparticles. They also showed that tumor accumulation of these nanoworms in lymph nodes was higher than other organ tissues. In another study, Ghandehari and co-workers prepared PEGylated spherical and rod-shaped gold nanoparticles for testing biodistribution profiles [184]. They showed that accumulation of PEGylated rod-shaped nanoparticles in liver and spleen was relatively low compared to PEGylated spherical nanoparticles, whereas their tumor accumulation was higher than spherical ones. These literature examples [182,183,184] showed that shape of nanoparticles (with diameter range about 5-25 nm) have an important role on biodistribution profiles. Although, they found parallel results demonstrating that worm and rod-like nanoparticles have better accumulation in tumor tissues compared to spherical nanoparticles and low accumulation values in major organs, it is hard to generalize these findings for all nanoparticles, especially for the ones

with larger diameter size. For example, in a study, researchers designed polymer-lipid nanoparticles for testing passive splenotropic drug delivery and showed that spleen accumulation ratio of non-spherical nanoparticles were increased compared to spherical nanoparticles [191]. One another research group evaluated folate decorated cross-linked spherical and worm-like micelles range between 75 and 200 nm for drug delivery [192]. They observed higher accumulation of worm-like micelles in the spleen, liver and kidneys compared to their spherical counterparts. In a more recent study, researchers have developed cylindrical polymer brushes in spherical, rod-like and worm-like structures [193]. Although, their tested spherical particles larger in diameter (≈ 50 nm) compared to rod-like (≈ 25 nm) and worm-like particles (≈40 nm), filamentous, rod-like and worm-like particles accumulated in liver and spleen in an increased manner proportion to their lengths compared to spherical particles, and there was no significant difference between tumor accumulation of spherical and non-spherical particles. Our findings revealed that filamentous particles with larger diameter (about 60 nm) have different biodistribution profiles compared to the ones with smaller diameter values [182,183,184]. Accumulation of rod and worm-like particles in liver and spleen was higher and increased by size increment than spherical ones in a harmonious way with literature examples [191,192,193]. On the other hand, tumor accumulation data showed that increase in diameter together with growing non-sphericity resulted in poor tumor accumulation probably due to improved RES clearance.

7.4. Conclusion

In this study, we successfully showed preparation of stable and functional PGMA-*b*-POEGMEMA-*b*-PST block copolymer nanoparticles using polymerization induced self-assembly. Nanoparticles with different size and morphologies (micelles with 30 and 46 nm size, rod-like micelles and worm-like micelles) were chosen to evaluate the effect of larger diameter on biodistribution profile. Biodistribution study of nanoparticles on HT1080 tumor xenografts showed that spherical micelles disposed highest tumor and relatively low healthy tissue accumulation, whereas less tumor and higher liver and spleen accumulation was observed for the filamentous particles. We suggest that diameter of spherical and non-spherical nanoparticles is a crucial parameter changing biodistribution patterns and it has to

be taken into account while designing nanoparticles for drug delivery and imaging systems as well as other parameters like shape and surface groups.

8. FORMATION OF TARGETED POLYMERIC NANOPARTICLES USING DIBLOCK COPOLYMERS COMPOSED OF POEGMEMA AND POLYMERIC DRUG SEGMENTS

8.1. Introduction

Following the clinical approval of nanoparticles for cancer drug delivery in 1995, a myriad of nanoparticle platforms have been designed and produced to improve the efficacy of anti-cancer drugs by addressing the complex physiological barriers. Drug loading in such polymeric nanoparticles can be achieved by covalent attachment or physical encapsulation via hydrophobic interactions. Considering the very low total volume of these nanoparticles in their colloidal suspensions, high drug loading capacity is one of the crucial factors to achieve effective drug formulations [194]. Low drug loading capacity of polymeric nanoparticles mainly in micellar formulations has still been the major drawback of the issue. This phenomenon was addressed by several researchers who take the advantage of π-π interactions by modifying the drug molecules or using an additive compound [195,196]. However, non-capsulated drug aggregates in the micellar type polymeric nanoparticle formulations is another drawback to provide a safe formulation for their clinical applications. Stenzel and co-workers have utilized drug attachable amphiphilic block copolymers to form hydrophobic segment of the block copolymers for the formation of polymeric nanoparticles [197]. This strategy has the lack of complete conjugation of the drug to the polymer backbone due to steric hindrance which is resulted in not well-defined final structure. Moreover, remaining reactive groups on the polymer backbone due to incomplete conjugation may be the most important drawback of this kind of post-polymerization conjugation strategies due to possible undesirable biological interactions *in vivo*.

Judah Folkman's hypothesis that tumor regression is angiogenesis-dependent and his idea that angiogenesis inhibitors would be used to treat cancer disease have become milestones in anti-cancer therapy [67]. There have been series of anti-angiogenic drugs approved by FDA since he first suggested the anti-angiogenic therapy in 1971. Dual

therapy with anti-mitotic and anti-angiogenic drug molecules would be an efficient strategy and can be achieved by polymer therapeutics [198].

Here we reported formation of micellar type targeted and non-targeted polymeric nanoparticles composed of well-defined amphiphilic block copolymers with high drug content. As a targeting ligand cRGDfK was preferred due to its high affinity towards αvβ3, an integrin overexpressed in human lung tumors [84]. The synthesis of amphiphilic block copolymers was achieved by chain extension of OEGMEMA based hydrophilic segment using a novel anti-angiogenic drug monomer via RAFT polymerization. We also demonstrated encapsulation of a hydrophobic compound into the polymeric micelles to prove the feasibility of these particles for dual anti-cancer therapy. Targeting efficiency of the particles was evaluated by *in vitro* and *in vivo* experiments.

8.2. Experimental

8.2.1. Materials

Oligo(ethylene glycol) monomethyl ether methacrylate (OEGMEMA, Mn= 300g/mol), 4-cyanopentanoic acid dithiobenzoate (CPADB), 2,2′-azobisisobutyronitrile (AIBN), methacryloyl chloride, *N*-Hydroxysuccinimide (NHS), *N,N*-Diisopropylethylamine (DIPEA), dicyclohexylcarbodiimide (DCC) and Nile Red were purchased from Aldrich. All other solvents were HPLC grade, obtained from Merck and used without further purification. 4-cyano-4-((thiobenzoyl)sulfanyl) pentanoic succinimide ester (SCPDB) was synthesized and characterized according to previously described methods. Cyclo (Arg-Gly-Asp-D-Phe-Lys) (cRGDfK) was synthesized using standard solid phase synthesis. The monomer and copolymer characterizations involved ^{1}H NMR spectroscopy (Varian 400 MHz NMR spectrometer) and gel permeation chromatography GPC (Shimadzu, Japan) with a mobile phase solution of 0.05 M lithium bromide in dimethylaceteamide (DMAc). GPC measurements of homopolymers and block copolymers were carried out with PSS WinGPC Unity software. PSS Gram (length/ID 300 mm × 8 mm, 10 µm particle size) column was calibrated with polymethyl methacrylate standards, using refractive index detector (RID-10A). Critical micelle concentration (CMC) calculations were measured with a Varian Cary Eclipse Fluorescence spectrometer (Varian, Agilent, USA). Size of the polymeric nanoparticles was measured via off-line dynamic light scattering (DLS) analysis

using Zetasizer (Malvern Zetasizer Nano ZS). The anhydrous polymeric nanoparticles were visualized by a LVEM5 electron microscope system on transmission electron microscopy (TEM) mode (Delong Instruments, CZ).

8.2.2. Synthesis of Polymerizable Combretastatin-A4 Monomer (CombMA)

Briefly, Combretastatin-A4 (300 mg, 0.95 mmol), triethyl amine (TEA, 191 mg, 1.89 mmol) were dissolved in dry dichloromethane (DCM, 10 mL) under N_2 in a 25 mL round bottom flask. Methacryloyl chloride (198 mg, 1.89 mmol) was added to whole mixture at 0 ºC drop wise in 15 min. Reaction was allowed for 1 h at 0 ºC and 16 h at room temperature. The crude was added 20 mL DCM and extracted with saturated $NaHCO_3$ (20 mL x 2) and distilled water (20 mL x2). Organic layer was dried with Na_2SO_4 and the solvent was evaporated. The CombMA monomer was purified using column chromatography on silica with hexane and EtOAc (4:1, v/v) to give final product. (318 mg, 87 % yield). ^{1}H NMR ($CDCl_3$) δ (ppm): 7.13 (dd, *J*= 8.5, 1.8 Hz, 1H); 7.04 (d, *J*= 1.9 Hz, 1H); 6.86 (d, *J*= 8,3 Hz, 1H); 6.52 (s, 1H); 6.45 (d, *J*= 3.2 Hz, 2H); 6.30 (s, 1H); 5.72 (s, 1H); 3.83 (s, 3H); 3.80 (s, 3H); 3.71 (s, 6H); 2.03 (s, 3H). ^{13}C NMR ($CDCl_3$) δ (ppm): 165.5, 153.1, 150.6, 139.8, 137.4, 135.7, 132.6, 130.2, 129.8, 125.7, 127.8, 127.4, 123.4, 112.2, 106.1, 61.1, 59.1, 25.6, 25.1, 15.6. Anal. Calcd. [$C_{22}H_{24}O_6$]: C, 68.74; H, 6.29; N; O, 24.97. Exact mass: 384.16, molecular weight: 384.42. ^{1}H NMR and ^{13}C NMR spectra of CombMA is given in Figure A.20 and Figure A.21. An IR spectrum of CombMA is given in Figure A.22.

8.2.3. Synthesis of SCPDB

SCPDB was synthesized according to literature protocol [199]. Briefly, CPADB (200 mg, 0.72 mmol) and N-hydroxysuccinimide (125 mg, 1.07 mmol) were dissolved in anhydrous DCM (4 mL). Dicyclohexylcarbodiimide (DCC) (177 mg, 0.86 mmol) was dissolved in anhydrous DCM (1 mL). Two solution mixtures were then mixed and the reaction mixture was stirred at room temperature in the dark for 16 h. The insoluble white by-product dicyclohexylurea (DCU) was removed by filtration. Obtained solution was evaporated by a rotary evaporator, and the crude product was purified by column chromatography on silica with hexane and EtOAc (4:1, v/v) to give final product in the form of red solid (195 mg, 72 % yield). ^{1}H NMR ($CDCl_3$) δ (ppm): 7.39-7.74 (m, 5H); 2.95-3.05 (m, 2H); 2.86 (s, 4H); 2.71-2.78 (m, 1H); 2.53-2.62 (m, 1H); 1.96 (s, 3H). Anal.

Calcd. [$C_{17}H_{16}N_2O_4S_2$]: C, 68.74; H, 6.29; N; O, 24.97. Exact mass: 376.06, molecular weight: 376.45. ^{1}H NMR spectra of SCPDB is given in Figure A.23. An IR spectrum of SCPDB is given in Figure A.24.

8.2.4. Synthesis of POEGMEMA and NHS-POEGMEMA Homopolymers

Reversible addition–fragmentation chain transfer (RAFT) polymerization was used for the synthesis of POEGMEMA and NHS activated POEGMEMA (NHS-POEGMEMA) homopolymers. For the synthesis of POEGMEMA polymer, to a solution of OEGMA (600 mg, 2.0 mmol) and CPADB (20.12 mg, 0.072 mmol) in DMF (3 mL), was added AIBN (1.31 mg, 0.008 mmol). The mixture was purged with N_2 to remove O_2 and polymerization was allowed for 16 h at 70 °C. Polymerization was stopped by cooling and air exposure. Just about 1:3 of DMF was evaporated by a rotary evaporator. POEGMEMA polymer was purified by precipitation three times in cold diethyl ether. The polymer precipitate was dried under reduced pressure to give approximately 35 OEGMEMA repeating units (460 mg, 77 % yield). For the synthesis of NHS-POEGMEMA homopolymer same procedure was applied using SCPDB (27.10 mg, 0.072 mmol) as chain transfer agent to give approximately 35 OEGMEMA repeating units (480 mg, 80 % yield). FTIR spectra of POEGMEMA and NHS-POEGMEMA polymer are given in Figure A.25 and Figure A.26.

8.2.5. Synthesis of POEGMEMA-co-CombMA and NHS-POEGMEMA-co-CombMA Block Copolymers

RAFT polymerization was used for the synthesis of POEGMEMA-*b*-PCombMA and NHS-POEGMEMA-*b*-PCombMA block copolymers. To a solution of CombMA (100 mg, 0.26 mmol) and POEGMEMA polymer as macro chain transfer agent (50 mg, 0.005 mmol) in DMF (0.75 mL), was added AIBN (0.15 mg, 0.00092 mmol). The mixture was purged with N_2 to remove O_2 and polymerization was allowed for 16 h at 65 °C. Polymerization was stopped by cooling and air exposure. DMF was evaporated by a rotary evaporator. The crude was dissolved with 0.25 mL dichloromethane and precipitated three times in cold diethyl ether. The polymer precipitate was dried under reduced pressure to give approximately 32 CombMA repeating units (98 mg, 65 % yield). Same procedure was applied for the synthesis of NHS-POEGMEMA-*b*-PCombMA block copolymer using NHS-POEGMEMA (50 mg, 0.005 mmol) as macro chain transfer agent to give approximately 33 CombMA repeating units (105 mg, 70 % yield). FTIR spectra of

POEGMEMA-*b*-PCombMA and NHS-POEGMEMA-*b*-PCombMA block copolymers are given in Figure A.27 and Figure A.28.

8.2.6. Synthesis of cRGDfK-POEGMEMA-*b*-PCombMA Block Copolymer

NHS-POEGMEMA-*b*-PCombMA (50 mg, 0.002 mmol) and cRGDfK (6.4 mg, 0.01 mmol) were co-dissolved in DMF (0.25 mL) and *N,N*-Diisopropylethylamine (6.5 mg, 0.05 mmol) was added to this reaction mixture. The reaction mixture was stirred at 30 °C for 24 h. DMF was evaporated by a rotary evaporator. The crude was dissolved with minimum amount of dichloromethane and precipitated in cold diethyl ether two times. The polymer precipitate was dried under reduced pressure to give cRGDfK-POEGMEMA-*b*-PCombMA (41 mg, 82 % yield). FTIR spectra of cRGDfK-POEGMEMA-*b*-PCombMA is given in Figure A.29.

8.2.7. Formation of Targeted and Non-targeted Polymeric Nanoparticles

Two solutions were prepared to obtain targeted and non-targeted nanoparticles. For the formation of non-targeted nanoparticles 2.3 mg POEGMEMA-*b*-PCombMA block copolymer was dissolved in 500 µL THF in a glass vial and 3 mL water was added to this solution. THF in the vials was then evaporated at room temperature for 24 h at open atmosphere to give micelles. Targeted nanoparticles were prepared in the same manner using cRGDfK-POEGMEMA-*b*-PCombMA and POEGMEMA-*b*-PCombMA mixture (1/5, w/w).

8.2.8. Critical Micelle Concentration (CMC) Measurements

The fluorescence probe method was utilized for the determination of CMC values of targeted and non-targeted nanoparticles. Block copolymer solutions (450 µL) were prepared in THF using serial dilution in vials as above. Nile Red solution (50 µL) in THF (0.03 mg/mL) and then 3 mL 1× PBS was added to each vial. THF was evaporated completely at open atmosphere and final concentration values for 16 samples ranging between 1×10^{-9} and 1×10^{-5} M in PBS (3 mL) were obtained. Fluorescence measurements were recorded by fluorescence spectrophotometer at an excitation wavelength of 550 nm and the emission was monitored from 580 to 660 nm.

8.2.9. Nile Red Internalization in HUVECs.

Targeted and non-targeted nanoparticle stock solutions with concentration of 1 μM were prepared in 1× PBS in the presence of Nile Red solution (50 μL) in DMSO (0.03 mg/mL) as described above and dialyzed against 1× PBS to remove undoped Nile Red. The control sample was prepared simultaneously without block copolymer addition using same amount of Nile Red. Human umbilical vein endothelial cells (HUVECs) were seeded as 3×10^4 cells per well into 24-well plates in triplicates for each time point and Nile Red doped targeted and non-targeted nanoparticles were added into the wells with a final block copolymer concentration of 100 nM in complete EBM-2 cell media. Cells were incubated for 1 and 4 h at 37 °C and fixed using 4% formaldehyde after 4',6-diamidino-2-phenylindole (DAPI) staining. The images were collected for three replicates per treatment via an inverted fluorescence microscope (Zeiss Observer A1 equipped with AxioCam MRc5) and processed with AxioVision software.

8.2.10. Endothelial Cell Tube Formation Assay on HUVECs

Targeted and non-targated polymeric nanoparticle solutions with concentration of 1 μM were prepared in 1× PBS and dialyzed against 1× PBS. The micelle solutions were added with final concentrations of 100, 500, and 2000 nM in EBM-2 cell media. Tube formation experiment using Matrigel (BD Biosciences, USA) was performed as previously reported with minor changes [200]. Briefly, Matrigel was poured as triplicates for each concentration into 96-well plates. The gels were let to solidify at 37 °C for 30 min, 1×10^4 HUVECs were seeded per well. The cells were incubated for 12 h at 37 °C, and pictures of the formed tubes were collected via bright field microscopy for of three replicates per treatment. The collected images were processed using Angiogenesis Analyzer tool of ImageJ software.

8.2.11. Animals

Male athymic nude mice (25-30 g, 7-8 weeks old) were obtained from Boğazici University Experimental Animal Production and Maintenance Unit and maintained in a controlled environment with a 12 h light/dark cycle. Water and food was provided ad libitum all the times. Animal experimentations were approved by the Boğaziçi University Animal Experiments Local Ethics Committee (08.06.2015).

8.2.12. Fluorescence Based Biodistribution of Targeted and Non-targeted Nanoparticles

Targeted and non-targeted nanoparticle stock solutions with concentration of 3 µM were prepared in 1× PBS in the presence of Cyanine 5.5 (Cy5.5) solution (50 µL) in DMSO (0.1 mg/mL) as described above. THF was evaporated completely at open atmosphere and solutions were dialyzed against 1× PBS solution to remove undoped Cy5.5. Human lung carcinoma xenograft model was generated using athymic nude mice transplanted with 4 × 10^6 A549 cells to right flank region. Targeted and non-targeted nanoparticles doped with Cy5.5 were intravenously injected to the mice (n=2) when tumor volumes reached about 250 mm^3. Lateral fluorescence images of mice were obtained after 15 m, 24 h, 48 h, 72 h and 96 h using Caliper IVIS Lumina III multispectral imaging system. Following sacrification *ex vivo* images of tumor, tissue, blood and organ samples were obtained and analyzed with Living Image® Software.

8.3. Results and Discussion

Overall synthesis of homopolymers, block copolymers and cRGDfK conjugated block copolymer was illustrated in Figure 8.1.

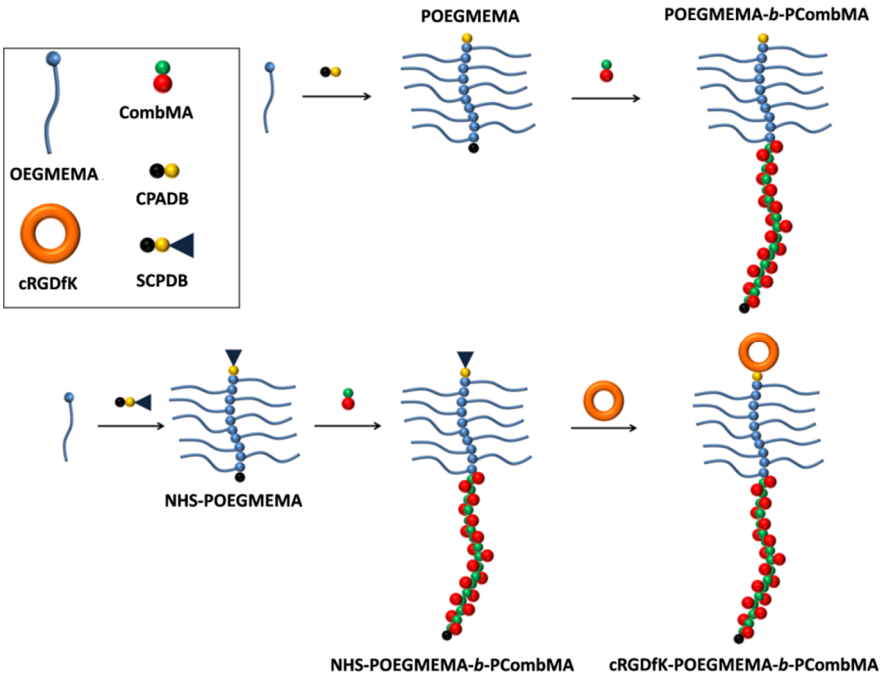


Figure 8.1. Overall scheme for the synthesis of the polymers.

8.3.1. Synthesis of POEGMEMA and NHS-POEGMEMA Homopolymers

For the synthesis of homopolymers RAFT polymerization was used to achieve macro CTAs. Same polymerization conditions were used for the synthesis of the polymers using CPADB and SCPDB chain transfer agents. Although different CTAs used for the polymerizations very similar molecular weight and PDI values were obtained. Analysis of POEGMEMA and NHS-POEGMEMA polymers using ^{1}H NMR revealed successful polymerization of OEGMEMA, as was evident from the proton resonances around 7.36-7-87 ppm due to the of aromatic group of the CTAs, the proton resonances around 3.39 ppm due to the terminal methyl ether group of OEGMEMA and the proton resonances around 2.84 ppm due to succinimide protons (Figure 8.2 and Figure 8.3).

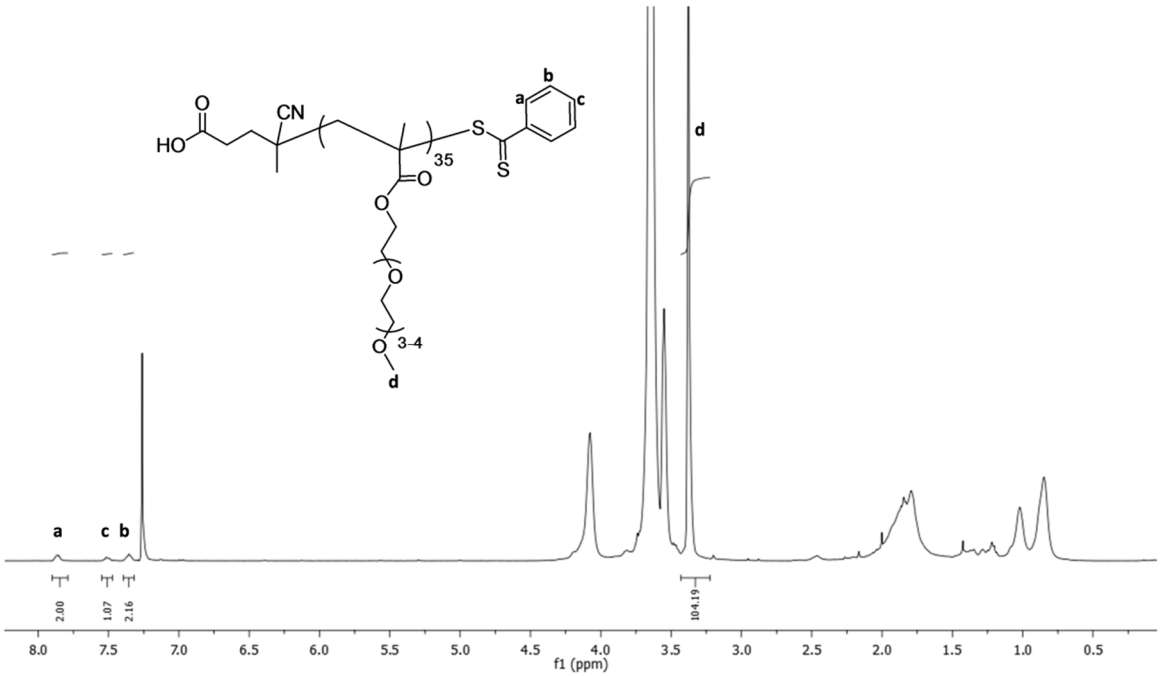


Figure 8.2. ^{1}H NMR spectrum of POEGMEMA.

The number of OEGMEMA repeating units was calculated by comparison of integration of the proton resonance of the terminal methyl ether group of OEGMEMA and aromatic group of the CTAs. In both cases 35 OEGMEMA repeating unit was calculated. Molecular weight (Mn) and PDI values for the POEGMEMA and NHS-POEGMEMA polymers were found to be 7.7 kDa, 1.27 and 7.1 kDa, 1.23, respectively.

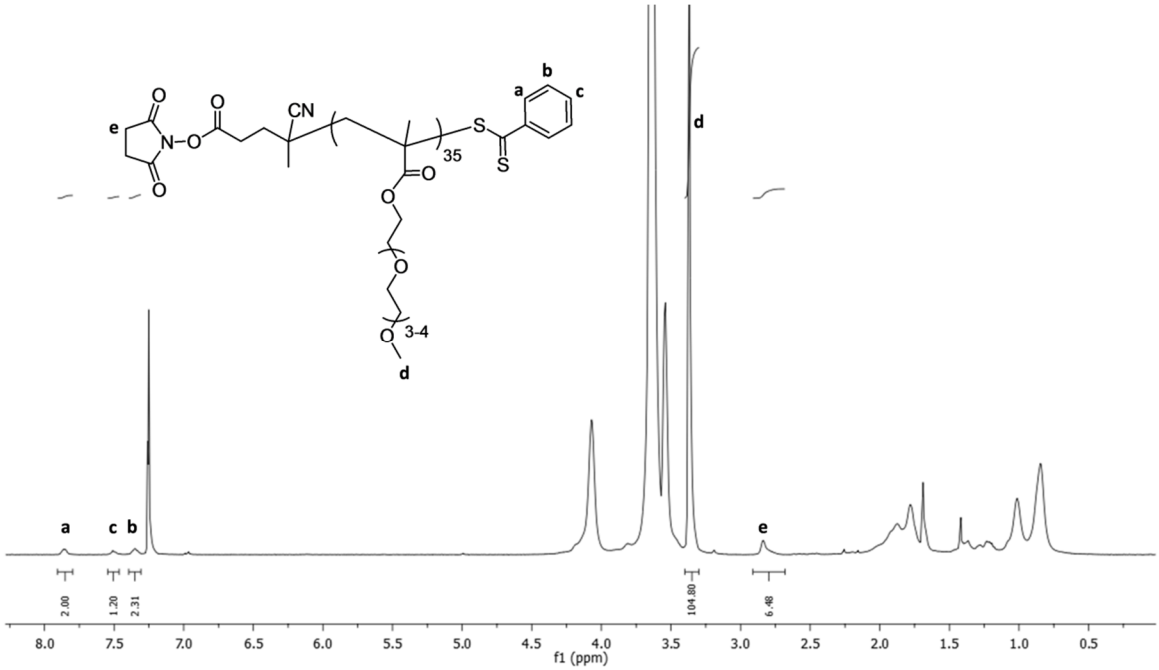


Figure 8.3. ^{1}H NMR spectrum of NHS-POEGMEMA.

8.3.2. Synthesis of POEGMEMA-*b*-PCombMA and NHS-POEGMEMA-*b*-PCombMA Block Copolymers

RAFT polymerization was used for the synthesis of block copolymers. Synthesized POEGMEMA and NHS-POEGMEMA homopolymers were used as macro chain transfer agents for the synthesis of POEGMEMA-*b*-PCombMA and NHS-POEGMEMA-*b*-PCombMA block copolymers, respectively. Same polymerization conditions were used for the synthesis of the copolymers. Analysis of POEGMEMA-*b*-PCombMA and NHS-POEGMEMA-*b*-PCombMA block copolymers using ^{1}H NMR revealed successful polymerization of OEGMEMA, as was evident from the proton resonances around 6.54-7-07 ppm due to one of the aromatic group of the CombMA, the proton resonances around 3.39 ppm due to the terminal methyl ether group of OEGMEMA (Figure 8.4 and Figure 8.5). Successful purification of the polymers was proved by disappearance of the proton resonances around 5.72 and 6.30 ppm due to allylic protons of CombMA. The repeating unit number for CombMA was determined using interation values of proton resonances around 6.54-7.07 ppm belonging to CombMA and 3.39 ppm belonging to OEGMA. 32 and 33 CombMA repeating units were calculated for POEGMEMA-*b*-PCombMA and NHS-POEGMEMA-*b*-PCombMA, respectively.

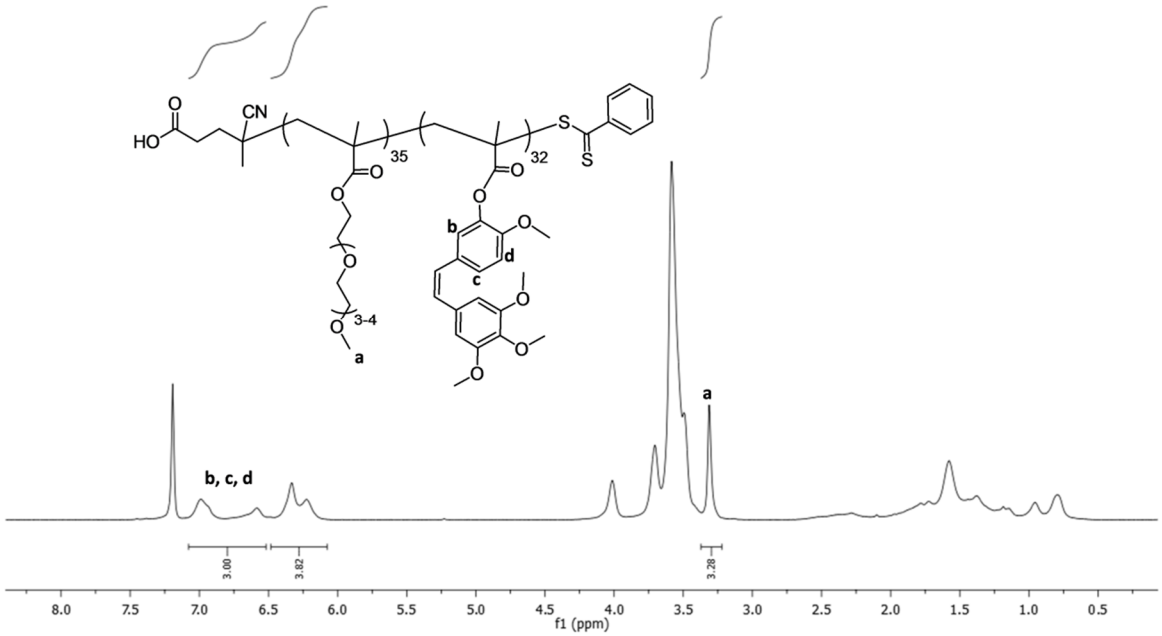


Figure 8.4. ^{1}H NMR spectrum of POEGMEMA-*b*-PCombMA.

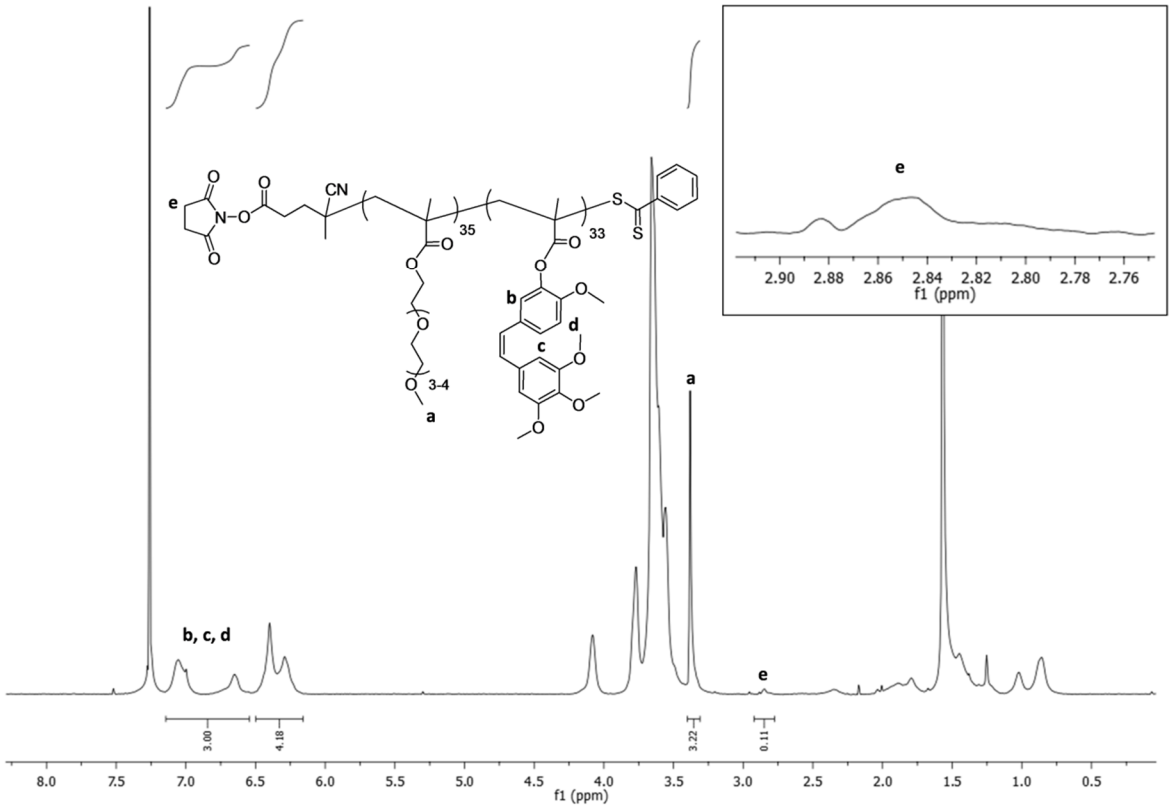


Figure 8.5. ^{1}H NMR spectrum of NHS-POEGMEMA-*b*-PCombMA.

Molecular weight (Mn) and PDI values for the POEGMEMA-*b*-PCombMA and NHS-POEGMEMA-*b*-PCombMA polymers were found to be 11.2 kDa, 1.32 and 11.7 kDa, 1.42, respectively.

8.3.3. Synthesis of cRGDfK-POEGMEMA-*b*-PCombMA Block Copolymer

Amine moiety of the cRGDfK was reacted with terminal NHS activated carboxyl group of the NHS-POEGMEMA-*b*-PCombMA in the presence of DIPEA to give cRGDfK-POEGMEMA-*b*-PCombMA block copolymer. Complete conjugation was proved by the disappearance of the proton resonance around 2.84 ppm due to the succinimide protons belonging to the NHS activated carboxyl group of the NHS-POEGMEMA-*b*-PCombMA (Figure 8.6).

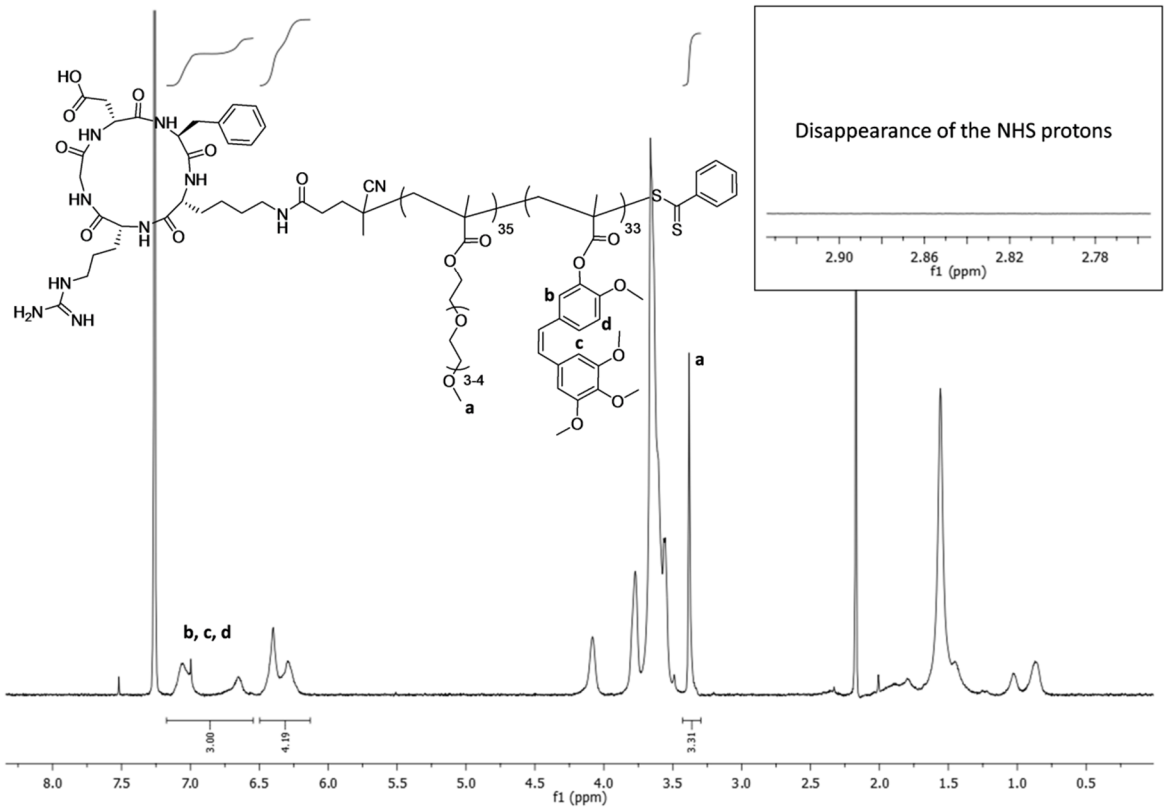


Figure 8.6. ^{1}NMR spectrum of cRGDfK-POEGMEMA-*b*-PCombMA.

To provide another proof for the conjugation we performed bicinchoninic acid (BCA) analysis using BCA protein assay kit (thermo fisher scientific) according to suggested protocols [174]. Presence of cRGDfK moiety after conjugation is demonstrated by the protein content increase (Figure 8.7).

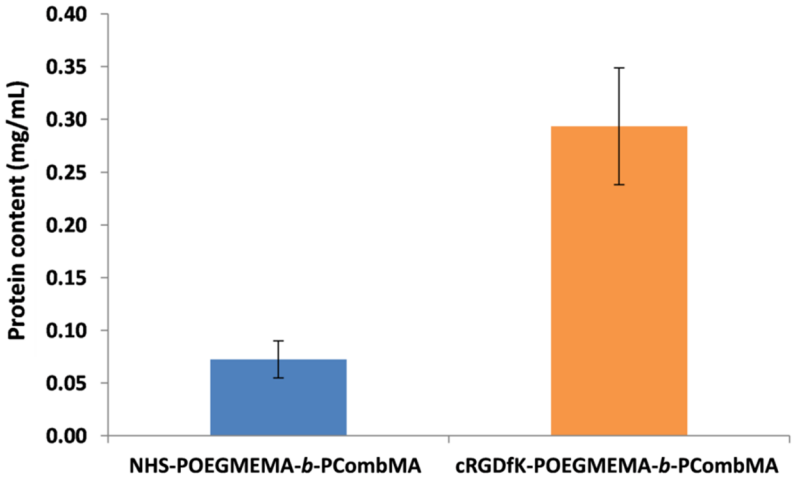


Figure 8.7. Protein content difference due to cRGDfK conjugation.

GPC traces of obtained homopolymers, block copolymers and cRGDfK conjugated block copolymer ware given in Figure 8.8. The GPC measurements of the polymers clearly show the molecular weight increase after copolymerization.

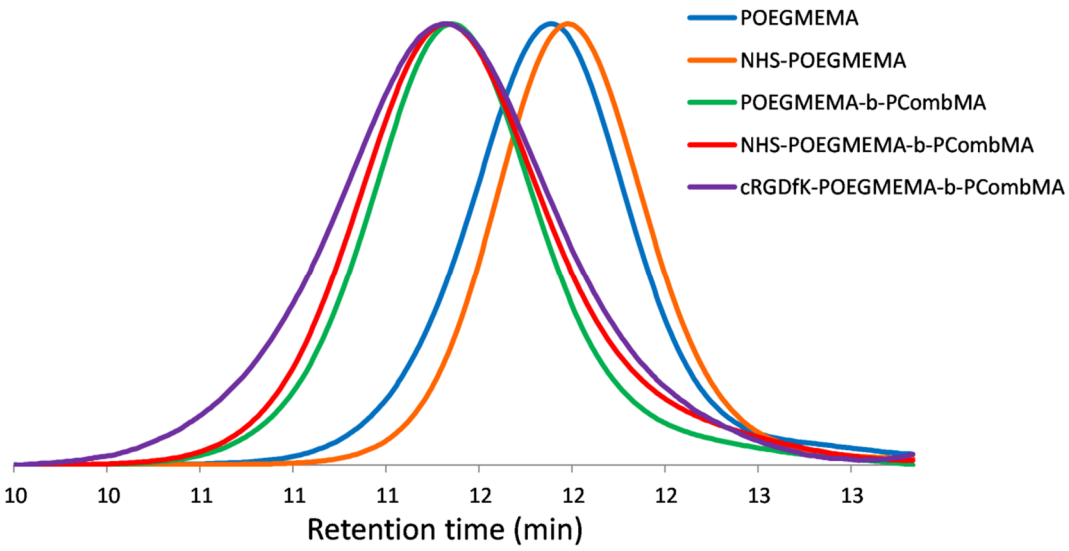


Figure 8.8. GPC traces of obtained homopolymers, block copolymers and copolymer cRGDfK conjugate.

Repeating unit numbers of the OEGMEMA and CombMA monomers on the polymer backbones, molecular weight and PDI values of the polymers were summarized in Table 8.1.

Table 8.1. Repeating unit numbers and molecular weight values of synthesized polymers.

	OEGMEMA Rep. unit	CombMA Rep. unit	Mw* (g/mol)	Mn** (kDa)	PDI**
POEGMEMA	35	-	10779	7.7	1.27
NHS-POEGMEMA	35	-	10876	7.1	1.23
POEGMEMA-*b*-PCombMA	35	32	23079	11.2	1.32
NHS-POEGMEMA-*b*-PCombMA	35	33	23561	11.7	1.42
cRGDfK-POEGMEMA-*b*-PCombMA	35	33	23789	12.5	1.49

* Calculated by ^{1}H NMR spectrum integration values.

** Obtained by gel permeation chromatography (GPC) using poly(methylmethacrylate) standarts.

8.3.4. Formation of Targeted and Non-targeted Polymeric Nanoparticles.

Block copolymers having hydrophilic POEGMEMA segment and hydrophobic polymerized drug segment enabled formation of micelle type polymeric nanoparticles. Water-insoluble polymerized drug block of the block copolymers forced self-assembly in aqueous conditions. Non-targeted nanoparticles were formed by using POEGMEMA-*b*-PCombMA. 1/5 combination of cRGDfK-POEGMEMA-*b*-PCombMA and POEGMEMA-*b*-PCombMA block copolymers was used to form targeted nanoparticles thanks to the introduced cRGDfK moiety on the surface of the nanoparticles. Schematic illustrations of non-targeted and targeted polymeric nanoparticle formation are given in Figure 8.9 and Figure 8.10.

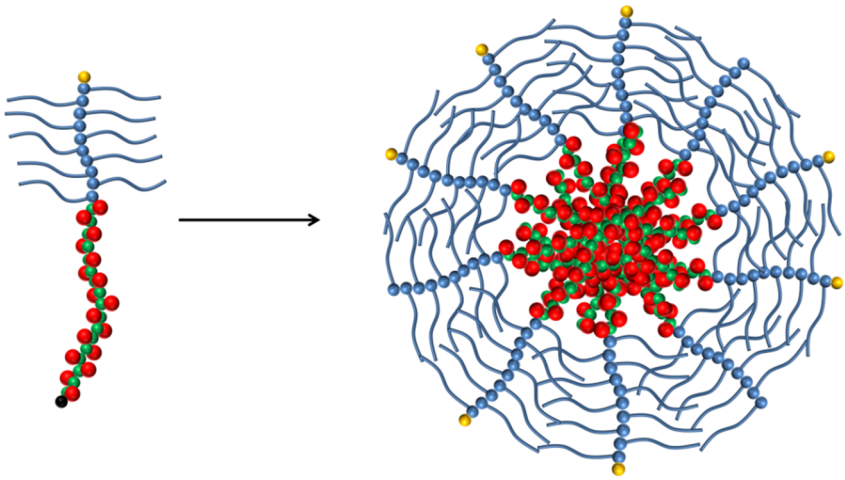


Figure 8.9. Non-targeted polymeric nanoparticle formation.

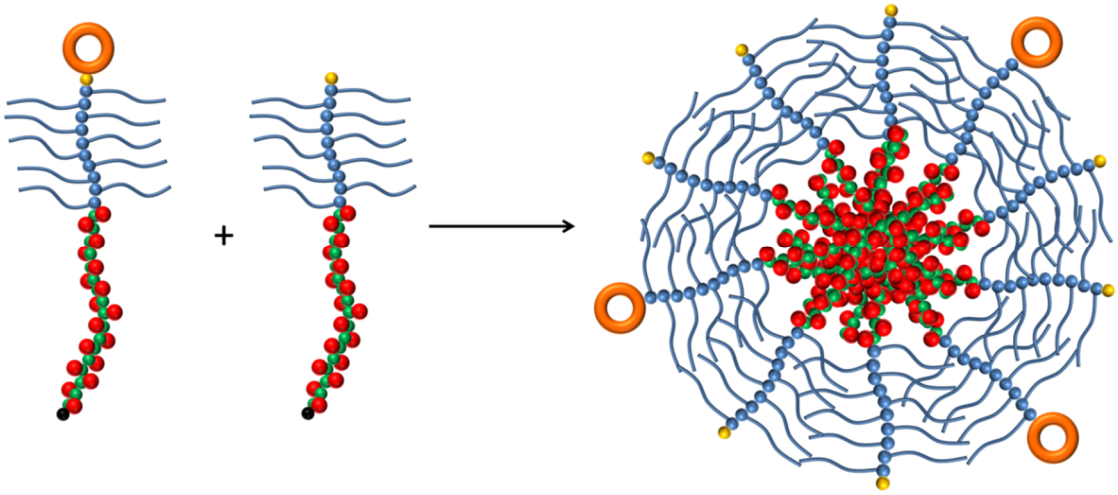


Figure 8.10. Targeted polymeric nanoparticle formation.

The size distribution of the prepared nanoparticles was measured using dynamic light scattering (DLS) analysis. DLS results revealed that using 20 % cRGDfK modified block copolymer in the whole block copolymer mixture to get targeted nanoparticles did not caused a difference compared to non-targeted ones in terms of the size distribution of the obtained nanoparticles. Volume based size distribution data indicates that nanoparticles with average size of around 22 nm were obtained with low poly dispersity index (PDI) values (Figure 8.11).

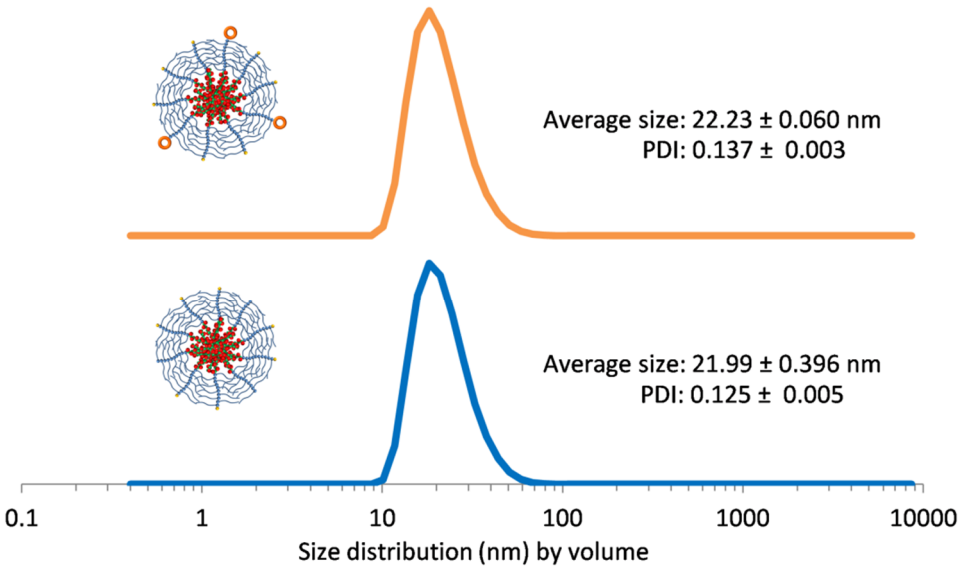


Figure 8.11. Size distribution of targeted (top) and non-targeted (bottom) nanoparticles by volume, average size and PDI values.

8.3.5. Critical Micelle Concentration (CMC) Values for Block Copolymers

For the determination of the minimum required concentration of the amphiphilic polymers to form the micelle type polymeric nanoparticles via self-assembly, the CMC values of the block copolymers were calculated by tracking the fluorescence intensity of Nile Red as function of polymer concentration. Thanks to the distinguishable color of Nile Red in visible light we were able to see the color change due to formation of micelles even with eyes. The photograph images of the prepared CMC samples by increasing concentrations ranging from 1 x 10^{-9} M to 1 x 10^{-5} M for non-targeted and targeted nanoparticle formation are given in Figure 8.12 and Figure 8.13, respectively.

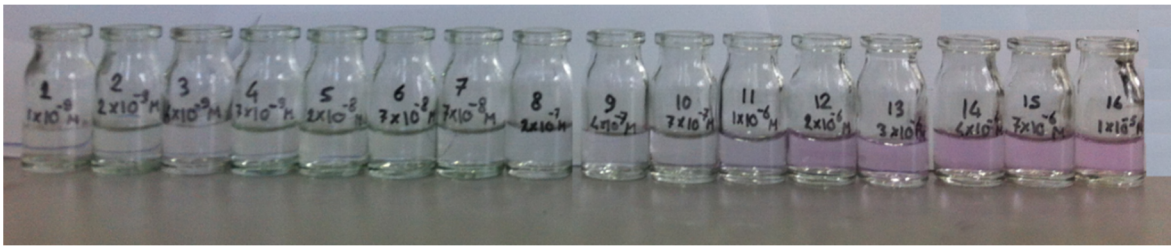


Figure 8.12. CMC analysis samples for non-targeted nanoparticles after THF evaporation.

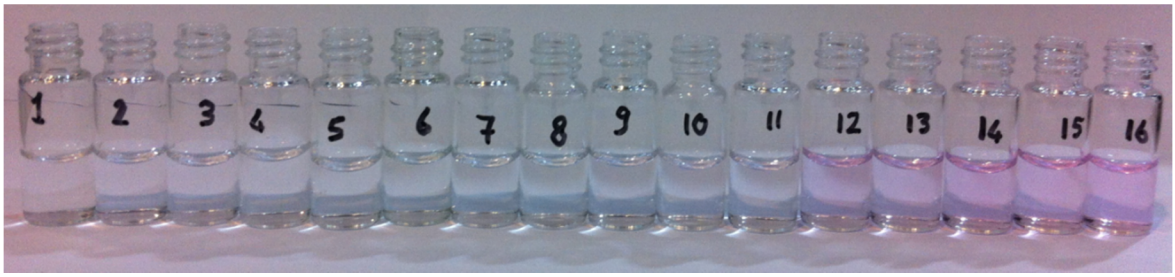


Figure 8.13. CMC analysis samples for targeted nanoparticles after THF evaporation.

Fluorescence emission spectra of Nile Red in non-targeted and targeted nanoparticles were obtained at an excitation wavelength of 550 nm and the emission monitored from 580 to 660 nm (Figure 8.14 and Figure 8.15). For the determination CMC values, plots of the emission intensity at 612 nm versus the log of copolymer concentration were obtained. The CMC values for the non-targeted and targeted nanoparticle formation were calculated by the intersection of the trend lines belonging to intensity ratios with relatively constant values and the rapidly increased intensity ratios.

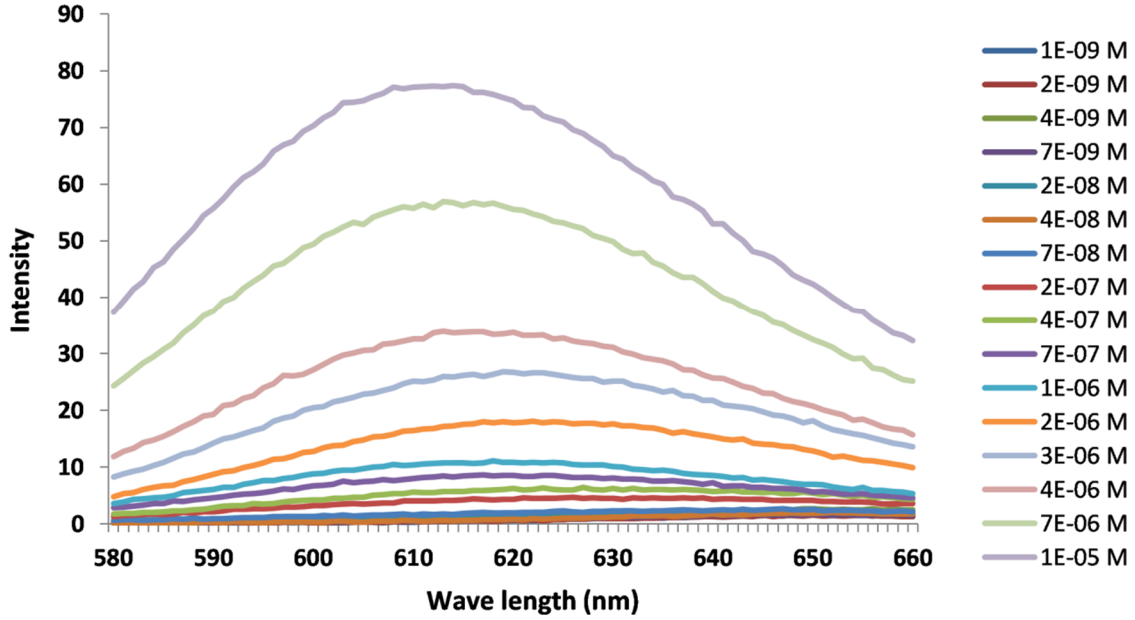


Figure 8.14. Fluorescence emission spectra of Nile Red in non-targeted nanoparticles.

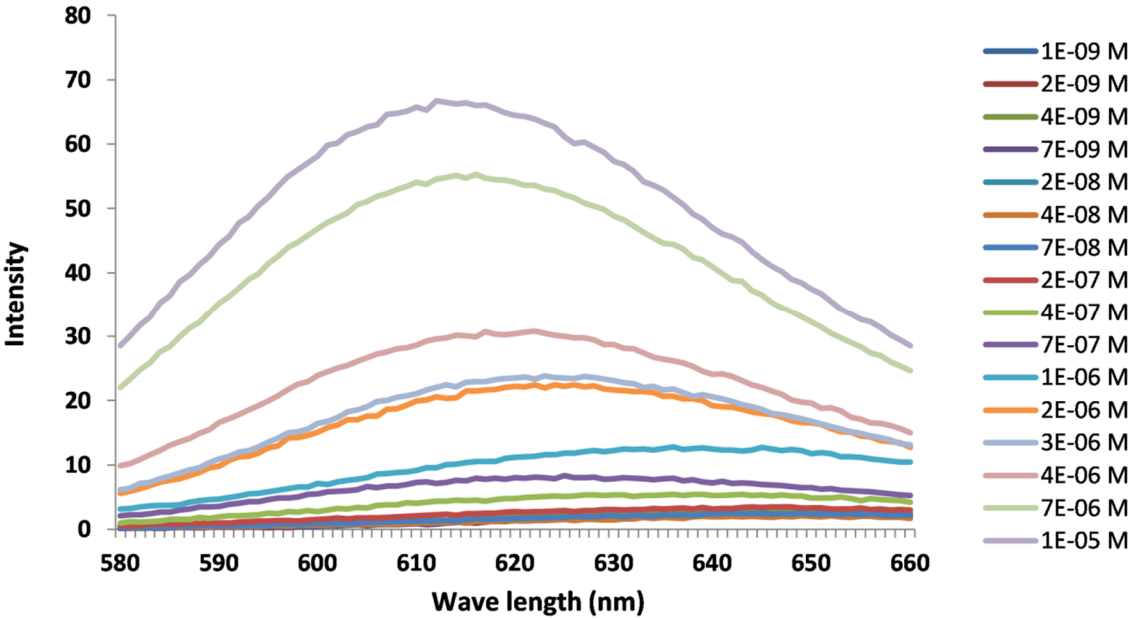


Figure 8.15. Fluorescence emission spectra of Nile Red in targeted nanoparticles.

The CMC values for non-targeted and targeted nanoparticle formation were found to be 1.796 $x10^{-6}$ M and 1.566 $x10^{-6}$ M, respectively. As shown in Figure 8.16 and Figure 8.17 Nile Red exhibits quite low fluorescence intensity below CMC which indicates that the Nile Red was in water and few nanoparticles were present. In the case of

concentrations above CMC, dramatic fluorescence intensity increase was observed upon increasing block copolymer concentration due to encapsulation of Nile Red in the interior of the nanoparticles. Quite similar CMC values obtained for targeted and non-targeted nanoparticle formation probably due to the similar hydrophilic and hydrophobic segment ratios of the used block copolymer.

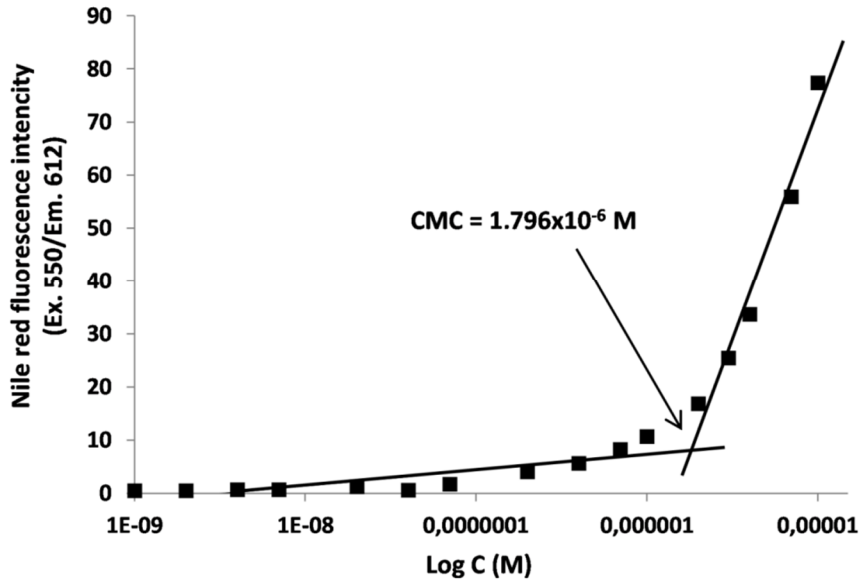


Figure 8.16. Plot of the emission intensity at 612 nm versus the log of POEGMEMA-*b*-PCombMA concentration.

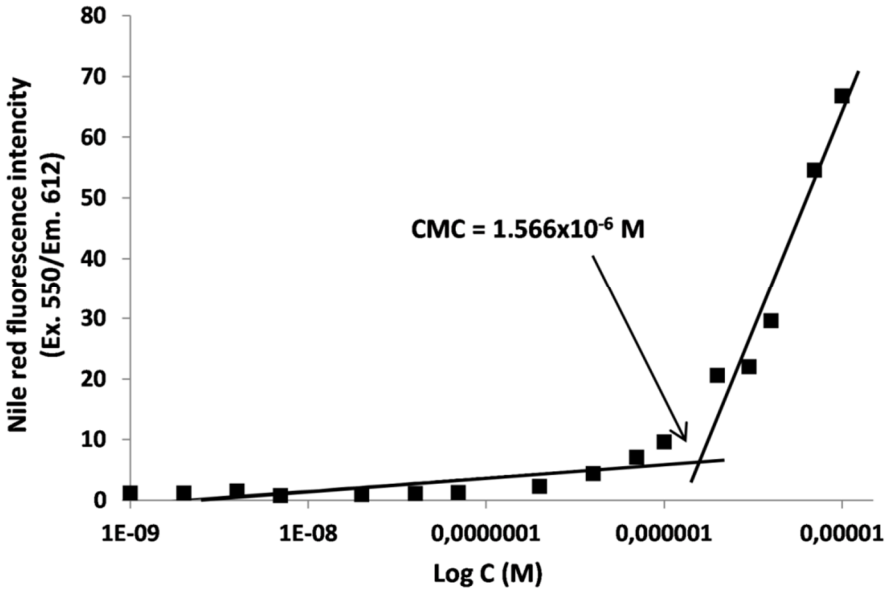


Figure 8.17. Plot of the emission intensity at 612 nm versus the log of total POEGMEMA-*b*-PCombMA and cRGDfK-POEGMEMA-*b*-PCombMA concentration.

The properties of obtained nanoparticles were summarized in Table 8.2.

Table 8.2. Properties of targeted and non-targeted nanoparticles.

	Average size by volume (nm)*	PDI*	CMC (M)	Drug ratio % by weight**
Targeted Nanoparticles	22.23 ± 0.060	0.137 ± 0.003	1.566 x 10^{-6}	44
Non-Targeted Nanoparticles	21.99 ± 0.396	0.125 ± 0.005	1.796 x 10^{-6}	44

* Measured by DLS

** Calculated by the ^{1}H NMR spectra of block copolymers used for nanoparticle formation.

8.3.6. Stability of Nanoparticles upon Addition of Organic Solvent and Serial Dilution with Water

To measure the stabilities of non-targeted and targeted nanoparticles, 1 mL nanoparticle samples with 1 x 10^{-5} M copolymer concentrations subjected to addition of increasing amount of THF as an organic solvent and serial dilution with water (Figure 8.18 and Figure 8.19).

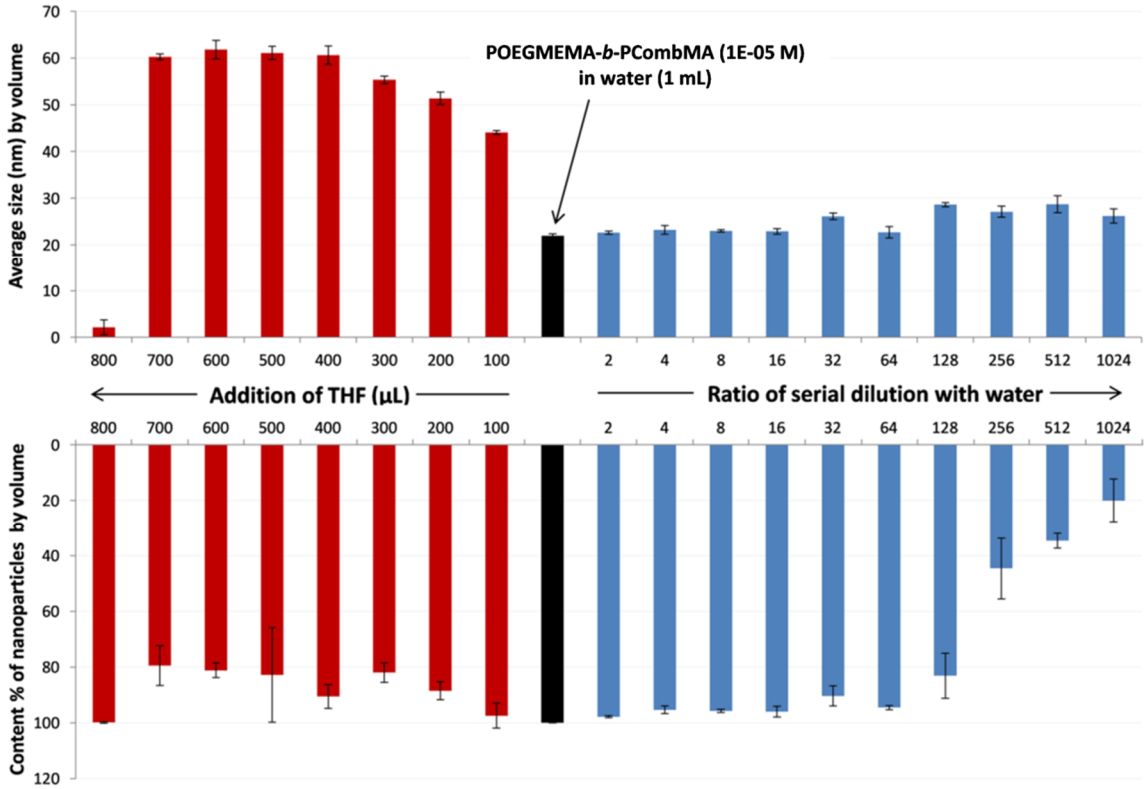


Figure 8.18. Stability of non-targeted particles upon THF addition and ultra-dilution.

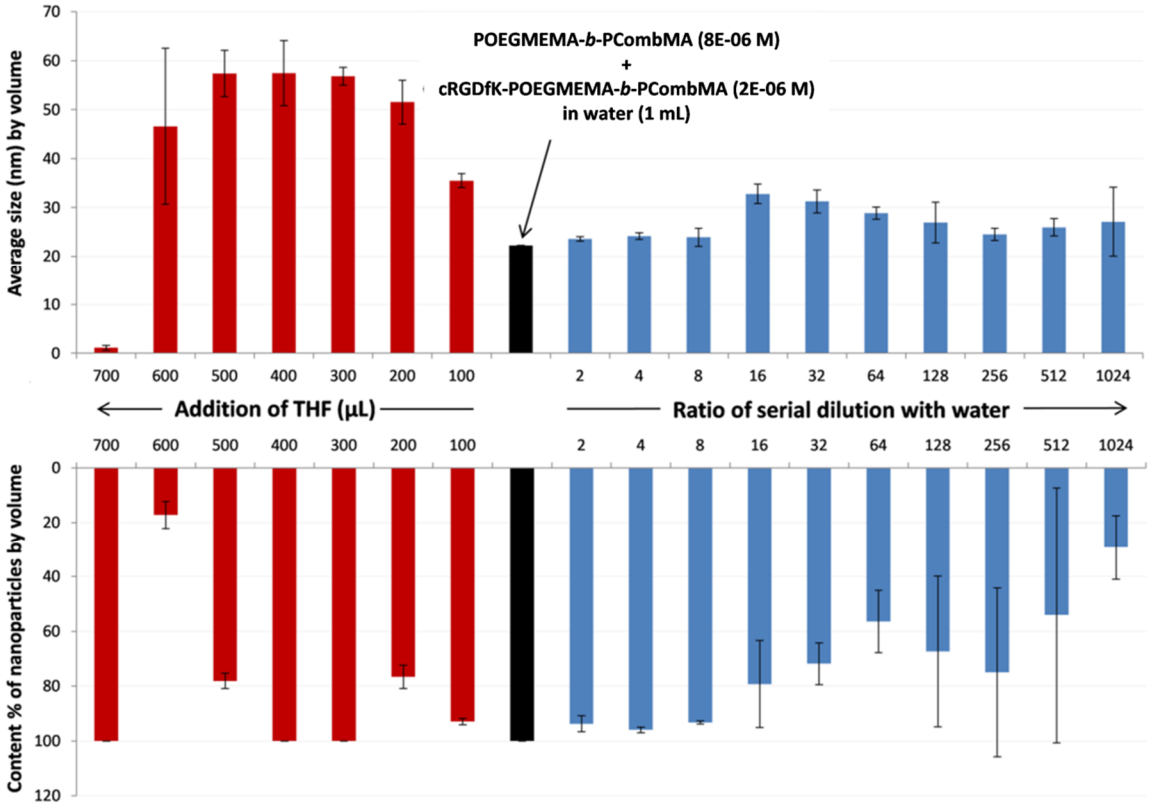


Figure 8.19. Stability of targeted particles upon THF addition and ultra-dilution.

Volume based size change and the ratio of the nanoparticles in overall particulates were measured using DLS. The size of the nanoparticles reached to around 60 nm from around 22 nm upon addition of THF in both cases. The non-targeted nanoparticles dissociated after the addition of 800 µL THF and targeted nanoparticles dissociated after 700 µL THF addition It was observed that percentage of non-targeted nanoparticles was not importantly affected by the THF addition until the dissociation point, whereas the ratio of targeted particles in overall particulates exhibited a fluctuating trend upon THF addition. When dissociation points and percent ratios of nanoparticles considered together, it can be say that the non-targeted nanoparticles stay more stable upon THF addition compared to the targeted ones. Addition of THF was resulted in complete dissociation of nanoparticles to their main components. It was proved by the measured very small particulate size at dissociation point.

The size of the nanoparticles was not affected by serial dilution with water. In addition, the ratio of nanoparticles in overall particulates was not importantly affected till 128 times dilution in both cases. However, the ratio of nanoparticles in overall particulates started to decrease dramatically due to dissociation of the nanoparticles at 256 fold dilution. In the case of serial dilution with water it was accepted that dissociation would not be concluded similar with THF addition due to the insolubility of drug polymer segment of the block copolymers. Irregular aggregate formation is possible in the case of serial dilution. We observed that the main reason in the decrease of nanoparticle ratio upon serial dilution arises from such irregular aggregate formation. Targeted and non-targeted particles showed similar stability behaviors by ultra-dilution studies.

8.3.7. Morphology of the Polymeric Nanoparticles

The size and morphology of the nanoparticles were visualized using transmission electron microscopy (TEM). Figure 8.20 shows the TEM images of the nanoparticles.

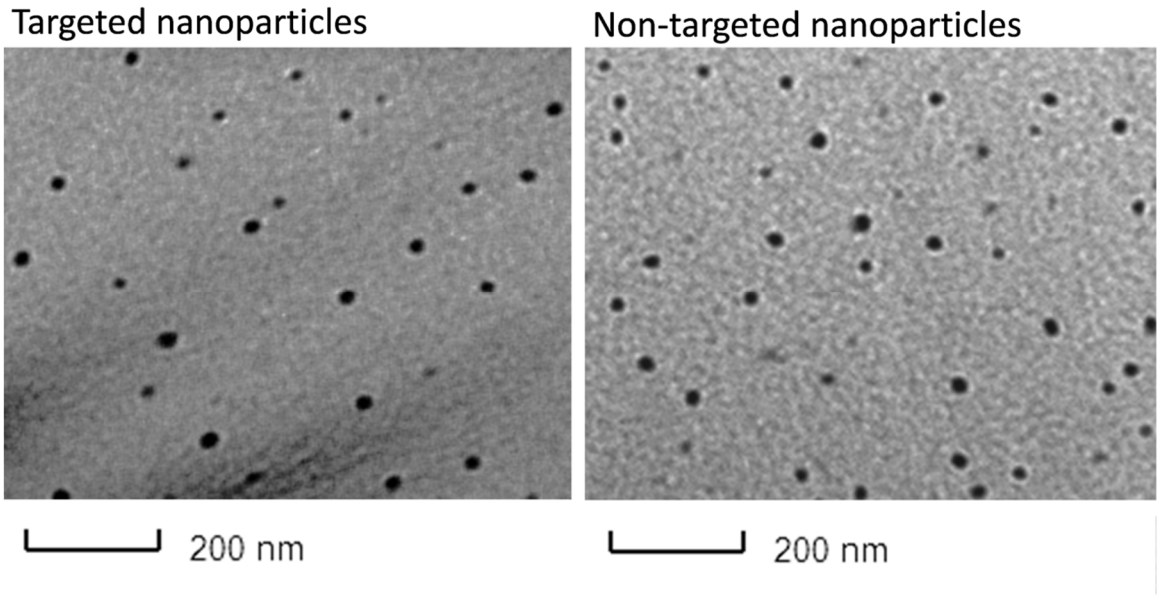


Figure 8.20. TEM images of polymeric nanoparticles.

The anhydrous TEM images revealed that incorporation of cRGDfK moiety as a targeting unit did not affect the size or morphology of the nanoparticles when compared with non-targeted nanoparticles. Spherical micellar type polymeric nanoparticles were obtained in both cases where POEGMEMA-*b*-CombMA used alone or together with

cRGDfK-POEGMEMA-*b*-CombMA in self-assembly. The TEM images also revealed that anhydrous particle size values of particles were not so much affected after drying due to high drug content of block copolymers used in formation of polymeric nanoparticles.

8.3.8. Nile Red Internalization in HUVECs.

The hydrophobic Nile Red dye was doped to the hydrophobic core of the targeted and non-targeted nanoparticles to compare the efficiency of the cell internalization into HUVECs. In HUVECs treated with Nile Red doped targeted nanoparticles red fluorescence intensity was found to be higher than the ones treated with Nile Red doped non-targeted nanoparticles after 1 h incubation. The HUVECs treated with hydrophobic dye alone showed very low fluorescence intensity (Figure 8.20). The results showed Nile Red internalization into the HUVECs due to incorporation of the dye into the hydrophobic core of polymeric nanoparticles. The cRGDfK moiety on the targeted nanoparticles improved the internalization of the nanoparticles as evident from noticeable red fluorescence intensity difference. The number of the HUVECs dropped after 4 h incubation due to the high drug content of the nanoparticles (Figure A.30).

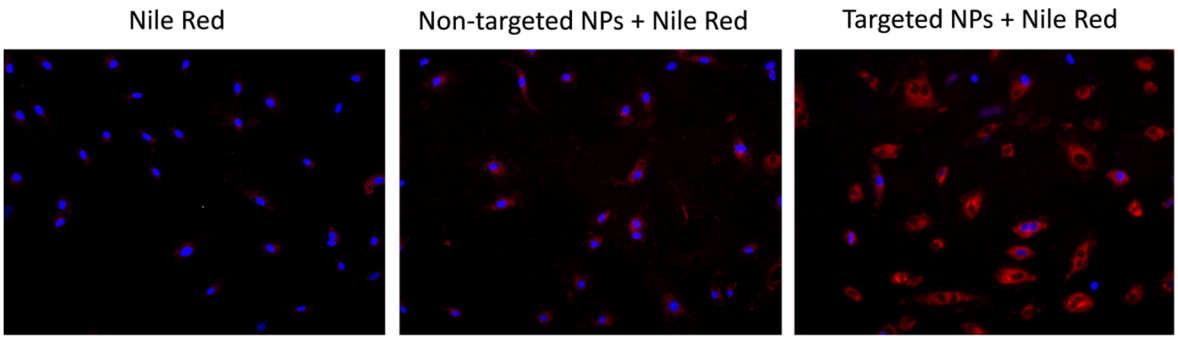


Figure 8.21. Cell internalization of Nile Red doped polymeric nanoparticles and Nile Red dye only into the HUVECs. The resulting images were collected at 1 h. Cell nuclei were stained with DAPI (blue).

8.3.9. Endothelial Cell Tube Formation Assay on HUVECs

In this assay, HUVECs form capillary-like vasculature on the solid Matrigel surface, which is a suitable material for investigation of antiangiogenic agents. Results indicated an inhibition of junction formation as well as a noticeable decrease in total tube length when exposed to 2000 nM Combretastatin A4 (CA4) containing targeted (T) and non-targeted

(NT) polymeric nanoparticle solutions (Figure 8.22, Panel C). Compared to the control samples and 100 nM samples with 24 ± 7.3 and 20.5 ± 0.5 junctions, respectively, the number of junctions for the 2000 nM NT nanoparticle samples decreased, about 7-fold, to 3.3 ± 2.0. In the case of 2000 nM T nanoparticle samples, no junctions were recognized by the ImageJ software. 2000 nM NT and T nanoparticle samples caused about 2-fold and 5 fold decrease in total tube length values, compared to their 100 nM samples, 2159 ± 20 and 2063 ± 32, respectively (Figure 8.22, Panel A and Panel B). The increase of CA4 concentration in nanoparticle solution samples caused a decrease in the tube formation capability of HUVECs. These results showed anti-angiogenic efficacy of T and NT nanoparticles. Moreover, results also proved the contribution of targeting ligand towards anti-angiogenesis.

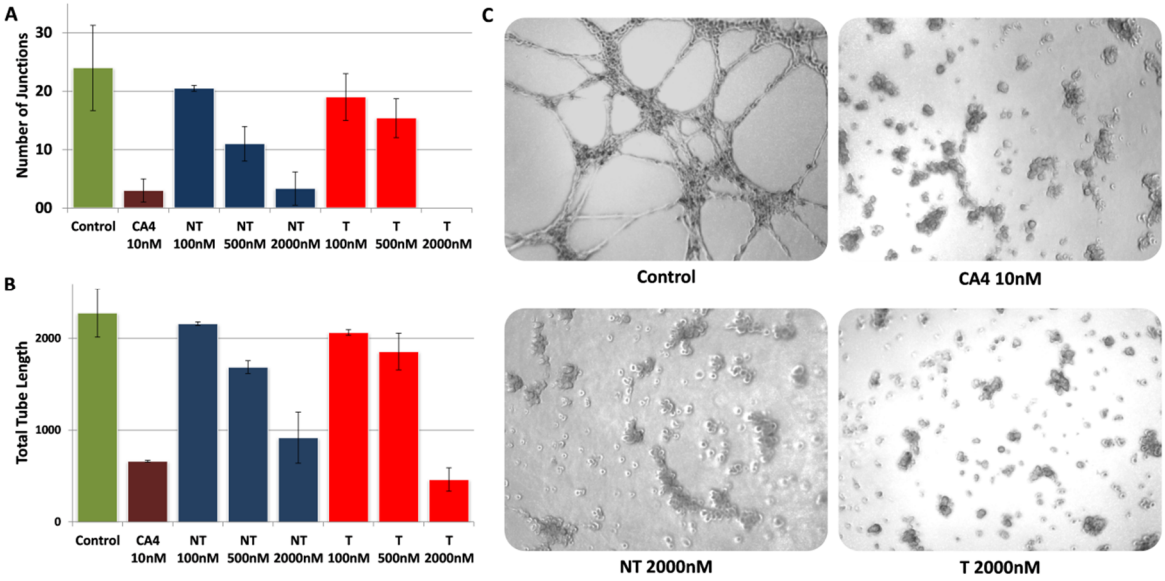


Figure 8.22. Anti-angiogenic assay using HUVECs on Matrigel. (A) Number of junctions and (B) total tube lengths between HUVECs were calculated after 8 h incubation with NT and T polymeric nanoparticles at three different drug concentrations. (C) Representative Matrigel images for control sample, free CA4 and NT and T nanoparticle solutions.

8.3.10. Fluorescence Based Biodistribution of Targeted and Non-targeted Nanoparticles

Cy5.5 doped targeted and non-targeted polymeric nanoparticles were evaluated for their biodistribution profiles with human lung carcinoma xenografts. Time dependent lateral images were collected to demonstrate fluorescence intensity change in tumor tissue

and major organs. Representative black and white photographs and their overlay images with count based fluorescence images are given in Figure 8.23 to show the location of the tumor tissues (right flank region) and relative change in fluorescence as a function of time.

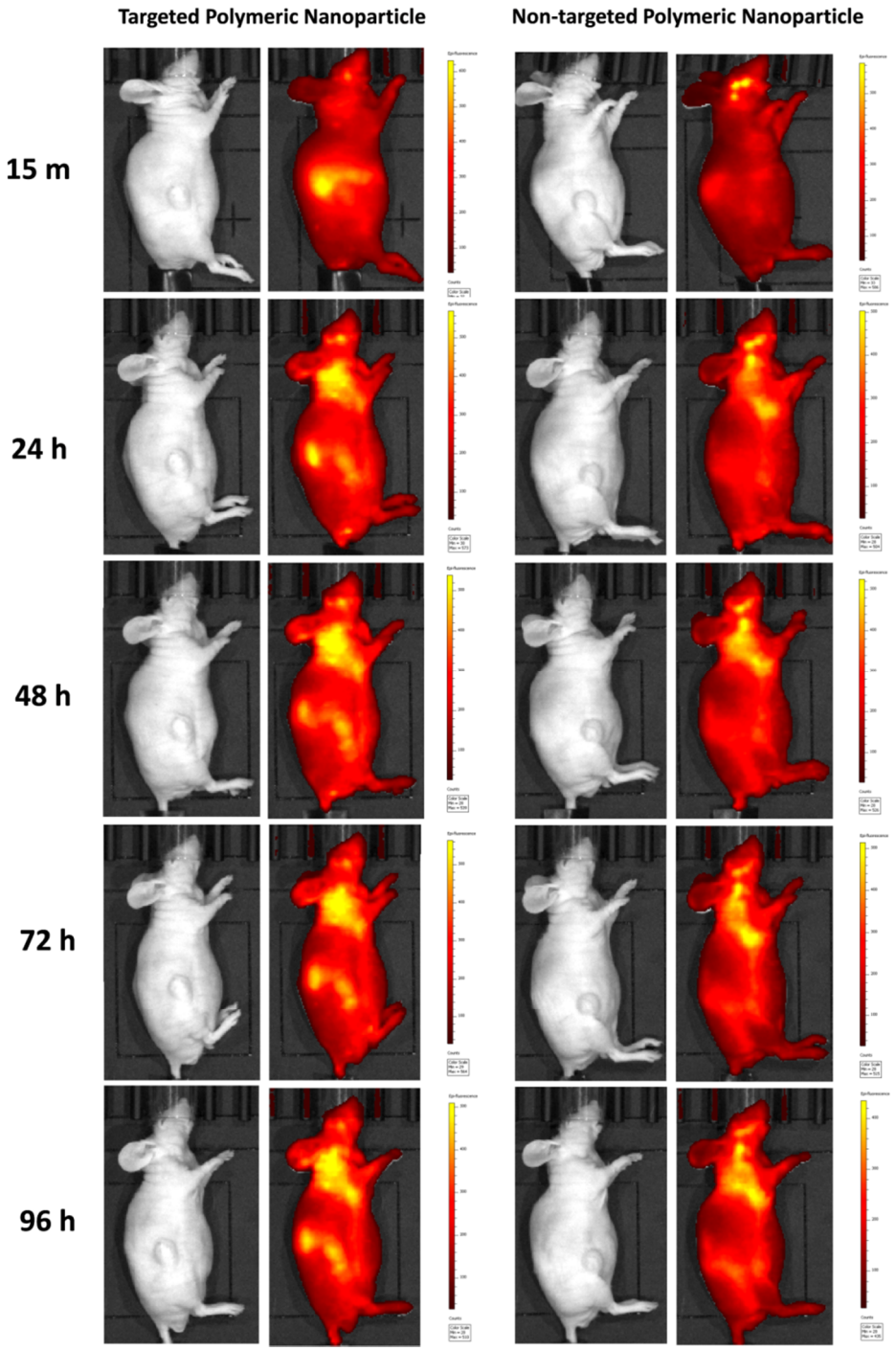


Figure 8.23. Count based lateral IVIS images of mice bearing tumor tissue at right flank site after systemic Cy5.5 doped targeted and non-targeted nanoparticle administration.

The targeted nanocarriers benefit from both passive (due to EPR effect) and active targeting (due to targeting ligand) and show improved accumulation in tumor tissue compared to non-targeted ones [201]. As a result of EPR effect, accumulation of both targeted and non-targeted particles in the tumor tissue was increased by time, proving the stability of Cy5.5 doped micellar type polymeric nanoparticles in blood stream. Targeting ligand, cRGDfK improved the accumulation of nanoparticles in the tumor tissue. Tumor accumulation of targeted polymeric nanoparticles was recognized even within 15 min, whereas no signs of tumor accumulation were observed in the case of non-targeted nanoparticles at the same time point. Moreover, targeted nanoparticles showed relatively higher tumor accumulation compared to non-targeted ones at all the time points. Following the last *in vivo* image collection at 96 h, mice were sacrificed and *ex vivo* tumor, tissue, organ and blood images were obtained (Figure 8.24). The highest accumulation of nanoparticles was found to be in the kidneys. So two representative images; without kidneys (Figure 8.24, panel A) and whole samples (Figure 8.24, panel A) were obtained to get a better visual idea about all samples. Relative fluorescence intensity values belonging to the *ex vivo* images obtained using Living Image® Software and given in Figure 8.25. It has been shown that opsonized nanoparticles are cleared by a receptor-mediated mechanism in a few minutes due to phagocytic cells which found abundantly in the liver and spleen [202]. However, it has been consistently shown that PEGylated nanoparticles with the size below 100 nm reduced plasma protein adsorption and thus reduced hepatic clearance thanks to stealth effect provided by PEG chains [203]. The size of the particles is also a crucial factor that determines tumor penetration efficiency. Kataoka and co-workers have demonstrated that tumor penetration depends on the size of polymeric nanoparticles and the permeability of the tumor vessels. Their results showed that polymeric nanoparticles with size of below 100 nm well penetrated within highly permeable tumors, whereas only smaller polymeric nanoparticles around 30 nm showed higher tumor accumulation for the poorly permeable tumors [189]. Consistent with the suggestions described above, the targeted and non-targeted polymeric nanoparticles fabricated for this study exhibited higher tumor accumulation compared liver, spleen and lungs, the organs responsible for hepatic and reticuloendothelial system (RES) clearance. On the other hand, targeted nanoparticles showed superior tumor accumulation thanks to the targeting moiety.

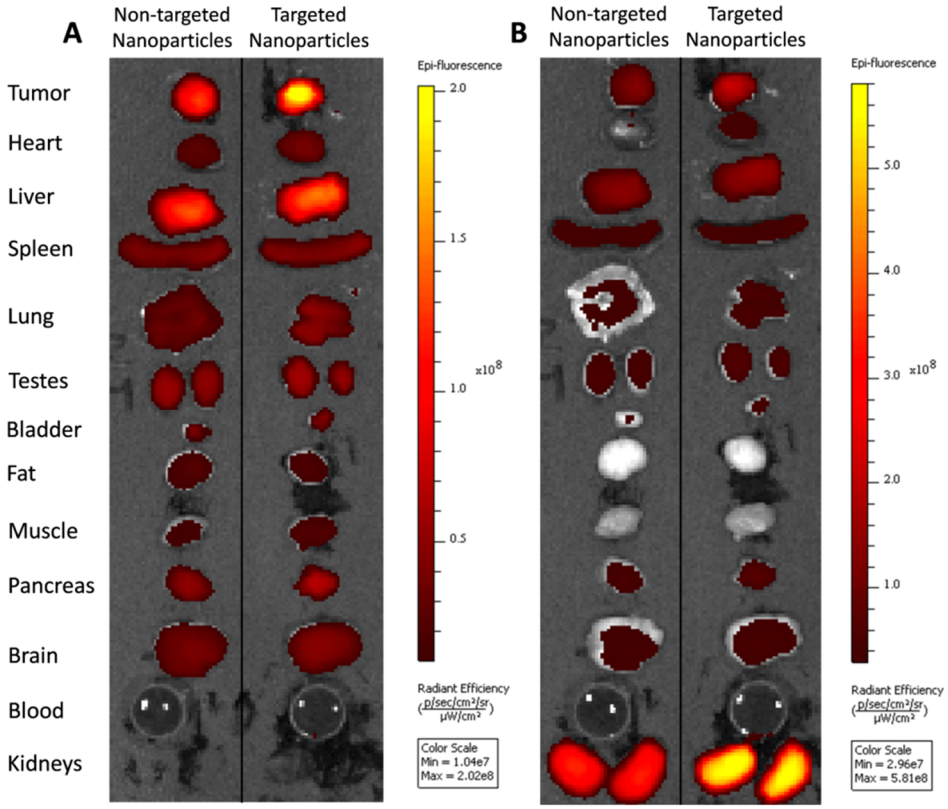


Figure 8.24. *Ex vivo* fluorescence images of tumor, tissue, organ and blood samples. (A) without kidneys 96 h after intravenous injection, (B) whole samples.

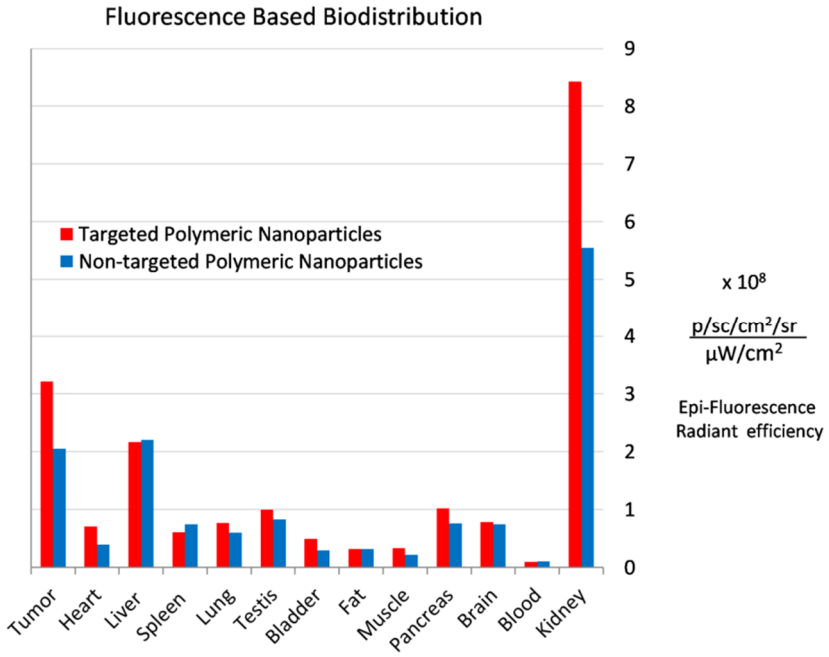


Figure 8.25. Relative fluorescence intensity values belonging to the *ex vivo* images.

Additionally, we observed that both nanoparticles were found to be capable of overcoming blood-brain barrier and showed higher brain accumulation compared to muscle and fat tissues and even spleen and lung. Considering the quick renal filtration threshold for size (hydrodynamic volume = 5.5 nm) [204,205] and molecular weight (40-50 kDa) [205] and tubular secretion process, high kidney accumulation shows the stability of targeted and non-targeted polymeric nanoparticles which have a hydrodynamic volume values around 22 nm and copolymer precursors around 23 kDa. Although fabricated nanoparticles showed high accumulation in kidneys, high fluorescence intensity belonging to bladder in the ventral images of the mice supported that the nanoparticles are also capable of disassembly in the body after a time required for an efficient EPR effect (Figure 8.26). Moreover, ventral images of mice clearly show the removal of both targeted and non-targeted nanoparticles from the liver within 24 h which proves stealth efficiency of such nanoparticle design.

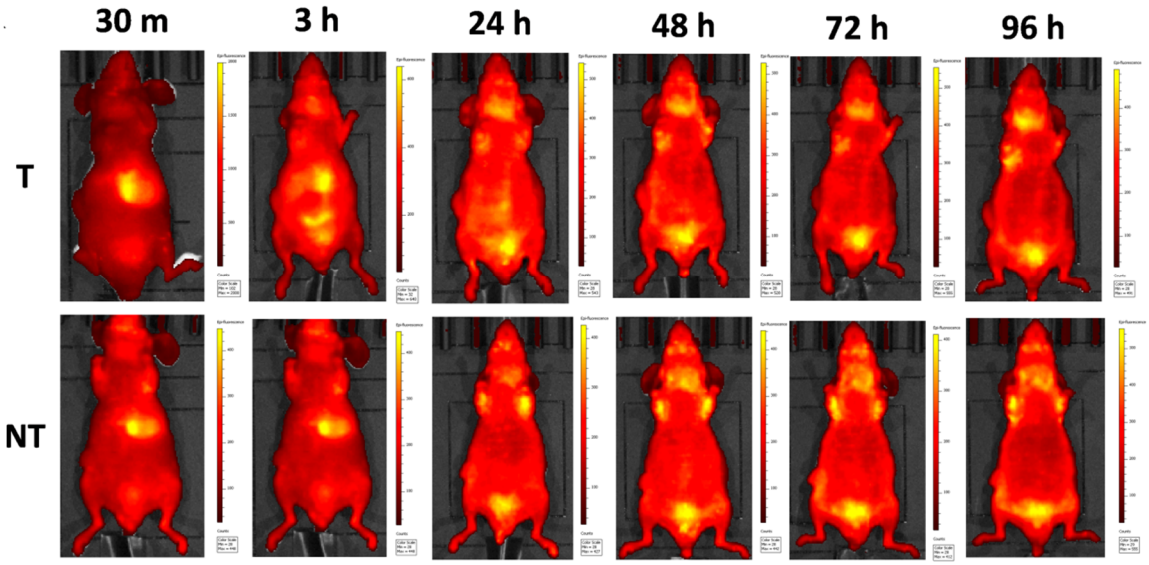


Figure 8.26. Count based ventral IVIS images of mice bearing tumor tissue at right flank site after systemic Cy5.5 doped targeted and non-targeted nanoparticle administration.

8.4. Conclusion

In this study a monomer bearing an anti-angiogenic drug with an ester linkage, CombMA was synthesized successfully. This monomer was used for the chain growth of POEGMEMA homopolymer using RAFT polymerization to obtain an amphiphilic block

copolymer. On the other hand, NHS activated chain transfer agent was utilized to synthesize POEGMEMA and amphiphilic block copolymer with using same approach with similar molecular weights. In both cases, block copolymers having similar POEGMEMA and PCombMA units were obtained. NHS activated amphiphilic block copolymer was further conjugated with cRGDfK to give an amphiphilic block copolymer with a targeting moiety. Targeted and non-targeted polymeric nanoparticles were formed via self-assembly of amphiphilic copolymers in aqueous conditions. To form targeted nanoparticles a mixture of amphiphilic block copolymers were used, whereas the non-targeted ones were obtained only using the block copolymer which doesn't have cRGDfK moiety. High drug content (44 %, w/w) was achieved in the composition of nanoparticles due to the copolymers used bearing high number of CombMA units. DLS results revealed that the size of nanoparticles was not affected by introducing cRGDfK moiety on the nanoparticle surface. Targeted and non-targeted polymeric nanoparticles were obtained around 22 nm with low dispersities. TEM images proved formation of spherical micellar type polymeric nanoparticle formation. High stable behavior was observed upon organic solvent addition and ultra-dilution conditions as non-cross-linked materials which is probably caused by the π-π interactions of the CombMA monomer in the interior of the nanoparticles. Targeting efficiency of cRGDfK moiety was proved by the *in vitro* cell internalization and anti-angiogenic assays and *in vivo* fluorescence based biodistribution study. Higher tumor accumulation was achieved by targeted nanoparticles and biodistribution study proved stability of nanoparticles. Biodistribution of these targeted and non-targeted nanoparticles also showed their capability of overcoming biological barriers such as hepatic and RES clearance and blood-brain barrier. Although biodistribution results are very promising, radiotracing or mass based biodistribution experiments are required to get decisive results. These unique targeted polymeric nanoparticles with high covalently attached anti-angiogenic drug content may be an ideal tool for targeted drug delivery systems. Moreover, it is possible to load a second drug molecule into the hydrophobic core of the nanoparticles during nanoparticle formation which is also proved by the encapsulation of Nile Red in CMC experiments. High anti-angiogenic drug content, availability of loading an anti-mitotic drug molecule and promising biodistribution profile makes these nanoparticles feasible for the dual-therapy of several cancer diseases.

9. CONCLUSIONS

This dissertation covers design and fabrication of functionalizable hydrogels for biosensing applications and synthesis and formation of smart polymeric prodrug formulations for drug delivery. Various type 'click' reactions and formation strategies were utilized for the fabrication of the hydrogels. Different polymerization techniques and architecture designs were used for the synthesis and formation of polymeric drug formulations. Advanced characterization techniques and *in vitro* and *in vivo* studies were performed for obtained prodrug formulations.

In the first part of this dissertation two projects were successfully completed. The first project involved the synthesis of functionalizable hydrogels using ABA type dendron-polymer conjugates constructed with polyester dendrons and PEG. A small library of ABA type dendron-polymer conjugates was synthesized to compare the effect of PEG length and dendron generation on physical and functional properties of the hydrogels. Sequential thiol-ene "click" reaction were utilized in the formation and functionalization of the hydrogels via functional alkene groups at the periphery of the dendron segment. Physical characteristics such as swelling and morphology were evaluated using obtained bulk hydrogels. The available alkene groups allowed post-gelation modification of the hydrogels with a thiol-bearing dye molecule via radical thiol-ene reaction. Control over the degree of functionalization was achieved by altering PEG length and dendron generation and showed by the hydrogel samples prepared by micromolding technique.

The second project belonging to the first part of the thesis related to design of well-defined functionalizable hydrogels using orthogonally functionalized bow-tie polyester dendrons and azide functional telechelic PEGs for biosensing applications. Huisgen type of [3+2] cycloaddition was utilized in the formation of hydrogels thanks to the alkyne units of dendron at the one edge. Hydrogels were prepared with high yields thanks to efficient cross-linking. The alkene units at the opposite site of bow-tie dendrons were used for post-gelation modification. Hydrogels were designed to have same amount of alkene groups, but location of the alkene groups were oriented differently through the heterofunctional nature of the dendrons. Thiol containing carbohydrate and dye molecules were covalently

attached to the alkene groups via radical thiol-ene reaction Carbohydrate modified hydrogels were further used for immobilization of carbohydrate binding protein, Con A. Although, no difference was measured in the fluorescence intensities of the hydrogels modified with small fluorescent dye, immobilization of Con A increased by using high generation dendron and shorter PEG chain as a result of cluster effect.

In the second part of this dissertation we designed POEGMEMA based smart polymeric prodrugs for drug delivery applications. The first project of this second part is related to the synthesis and pharmacokinetic evaluation of polymer drug conjugates with different molecular weights. Polymer drug conjugates were synthesized via random polymerization of OEGMEMA and a drug monomer having a GFLG linker using free radical polymerization. Thanks to the OEGMEMA monomer a branched architecture were obtained. Additionally PHPMA based polymer drug conjugates were synthesized in the same molecular weights using HPMA and same drug monomer to understand the effect of branched structure over pharmacokinetic and biodistribution properties. Sustained drug release profiles were obtained for POEGMEMA based polymer drug conjugates compared to linear PHPMA based ones. This sustained release was also proved by cytotoxicity experiments over different cancer cell lines. *In vivo* pharmacokinetic results clearly showed that for both polymer drugs conjugate types the increase in molecular weight resulted in improved pharmacokinetic parameters such as Cmax, AUC, VDβ and CL and all polymer drug conjugates increased the half-life of free drug in the same manner. However, POEGMEMA based polymer drug conjugates exhibited improved pharmacokinetic parameters compared to linear PHPMA based ones.

After understanding pharmacokinetic properties of POEGMEMA based polymer drug conjugates we performed another project to evaluate anti-tumor efficiency of this prodrugs. In this project POEGMEMA based prodrugs were synthesized using RAFT polymerization to achieve lower poly dispersity. Besides the EPR effect, to explore the difference between targeted and non-targeted POEGMEMA based polymer drug conjugates we also synthesized cRGDfK functionalized prodrugs. NHSMA monomer was introduced to polymer backbone for post-polymerization modification of polymer drug conjugates. Amine functional cRGDfK ligand was reacted with POEGMEMA based polymer drug conjugate having NHS groups and targeted prodrug was synthesized. Prior to

anti-tumor study targeted and non-targeted prodrugs were compared in terms of their cytotoxicity and result proved the targeting efficiency of the prodrugs. At least 3-fold dose tolerability was achieved using POEGMEMA based prodrugs compared to free drug according to performed MTD study. Tumor xenografts were generated using human lung carcinoma cells for anti-tumor study. Both targeted and non-targeted polymer drug conjugates exhibited higher anti-tumor compared to free drug. On the other hand, better therapeutic effect was obtained when using targeted prodrug. This smart polymer drug design is attractive and a promising for targeted drug delivery applications.

In the scope of the second part, besides polymer drug conjugates, polymeric micellar type nanoparticles were also fabricated using different approaches. In the third project of the second part we explored biodistribution characteristics of micellar type OEGMEMA, GMA and ST based polymeric nanoparticles. This project was performed in The Monash Institute of Pharmaceutical Sciences (MIPS) and ARC Centre of Excellence in Convergent Bio-Nano Science & Technology laboratories in Melbourne, Australia. PISA approach was utilized to generate particles with different size and morphology. Obtained spherical, rod-like and worm-like micellar type polymeric nanoparticles were further radiolabelled using tritiated amino ethanol thanks to the glycidyl groups at the polymer backbone. Polymeric nanoparticles were characterized using DLS, NMR, GPC, and TEM. Human sarcoma cell line was used for generation of tumor xenografts. The size and morphological properties affected biodistribution of nanoparticles. The best tumor accumulation was achieved by spherical small (30 nm) nanoparticles. The size increment and the change in morphology towards longer filamentous structures resulted in poor tumor accumulation and increased RES clearance. This project brightens the effect of size (above 30 nm) and morphology of nanoparticles on biodistribution profiles.

As a last and fourth project of the second part of this dissertation, novel polymeric micellar type polymeric nanoparticles were designed composed of OEGMEMA and an anti-angiogenic drug monomer (CombMA). To address the low drug content of nanoparticle drug formulations we synthesized block copolymers having OEGMEMA based hydrophilic block and a hydrophobic block which was completely formed by drug monomer. RAFT polymerization was utilized in the formation block copolymers and different CTAs were used to achieve block copolymers with a targeting moiety or not. As a

targeting moiety cRGDfK was attached to block copolymer thanks to the NHS group of the one of the CTAs used. Nanoparticles were fabricated via self-assembly of hydrophobic segments of block copolymers in aqueous conditions and high drug content was achieved (44 %). CMC experiments were performed using Nile Red and the values for targeted and non-targeted particle formation were found to be similar. CMC experiments also proved hydrophobic drug encapsulability of the nanoparticles. Cell internalization experiments proved targeting efficiency of the particles with cRGDfK moiety. Anti-angiogenic effects of the particles on HUVECs demonstrated by *in vitro* experiments. *In vivo* biodistribution experiments revealed that targeted particles selectively and highly accumulated in tumor tissue compared to non-targeted ones by overcoming biological barriers. These nanoparticles with high drug content and availability of second drug encapsulation possess an effective prodrug design for targeted drug delivery applications.

In the scope of this dissertation a total of six projects were successfully completed. Functionalizable hydrogels for biosensing applications and smart polymeric prodrugs for targeted drug delivery applications were generated, characterized and evaluated in terms of their feasibility.

REFERENCES

1. Tan, H., and K. G. Marra, “Injectable, Biodegradable Hydrogels for Tissue Engineering Applications”, *Materials*, Vol. 3, pp. 1746–1767, 2010.

2. Zhu, J., and R. E. Marchant, “Design Properties of Hydrogel Tissue-engineering Scaffolds”, *Expert Review of Medical Devices*, Vol. 8, pp. 607–26, 2011.

3. Vashist, A., A. Vashist, Y. K. Gupta, and S. Ahmad, “Recent Advances in Hydrogel Based Drug Delivery Systems for the Human Body”, *Journal of Materials Chemistry B*, Vol. 2, pp. 147, 2014.

4. Buenger, D., F. Topuz, and J. Groll, “Hydrogels in Sensing Applications”, *Progress in Polymer Science*, Vol. 37, pp. 1678–1719, 2012.

5. Slaughter, B. V, S. S. Khurshid and O. Z. Fisher, A. Khademhosseini, N. A. Peppas. “Hydrogels in regenerative medicine”, *Advanced Materials*, Vol. 21, pp. 3307–3329, 2009.

6. Yigit, S., R. Sanyal, and A. Sanyal, “Fabrication and Functionalization of Hydrogels Through ‘Click’ Chemistry”, *Chemistry - An Asian Journal*, Vol. 6, pp. 2648–2659, 2011.

7. Altin, H., I. Kosif, and R. Sanyal, “Fabrication of ‘clickable’ hydrogels via Dendron-polymer Conjugates”, *Macromolecules*, Vol. 43, pp. 3801–3808, 2010.

8. Wu, P., M. Malkoch, J. N. Hunt, R. Vestberg, E. Kaltgrad, M. G. Finn, V. V Fokin, K. B. Sharpless, and C. J. Hawker, “Multivalent, Bifunctional Dendrimers Prepared by Click Chemistry”, *Chemical Communications*, pp. 5775, 2005.

9. Acikgoz, S., G. Aktas, and M. N. Inci, “FRET Between BODIPY Azide Dye Clusters within PEG-based Hydrogel: A Handle to Measure Stimuli

Responsiveness", *The Journal of Physical Chemistry B*, Vol. 114, pp. 10954–10960, 2010.

10. Hed, Y., K. Oberg, S. Berg, A. Nordberg, H. von Holst, and M. Malkoch, "Multipurpose Heterofunctional Dendritic Scaffolds as Crosslinkers Towards Functional Soft Hydrogels and Implant Adhesives in Bone Fracture Applications", *Journal of Materials Chemistry B*, Vol. 1, pp. 6015, 2013.

11. Bi, X., J. Amie Luckanagul, A. Allen, M. Ramaboli, E. Campbell, D. West, P. Maturavongsadit, K. Brummett, and Q. Wang, "Synthesis of PAMAM Dendrimer-based Fast Cross-linking Hydrogel for Biofabrication", *J. Biomater. Sci. Polym. Ed.*, Vol. 26, pp. 669–682, 2015.

12. Mongkhontreerat, S., O. C. J. Andren, A. Boujemaoui, and M. Malkoch, "Dendritic Hydrogels: From Exploring Various Crosslinking Chemistries to Introducing Functions and Naturally Abundant Resources", *Journal of Polymer Science, Part A: Polymer Chemistry*, Vol. 53, pp. 2431–2439, 2015.

13. Oberg, K., Y. Hed, I. J. Rahmn, J. Kelly, P. Löwenhielm, and M. Malkoch, "Dual-purpose PEG Scaffolds for the Preparation of Soft and Biofunctional Hydrogels: The Convergence between CuAAC and Thiol-ene Reactions", *Chemical Communications (Cambridge, England)*, Vol. 49, pp. 6938–40, 2013.

14. Fischer, M., and F. Vogtle, "From Design to Application Dendrimers : A Progress Report", *Angewandte Chemie International Edition*, Vol. 38, pp. 884–905, 1999.

15. Carnahan, M. A., C. Middleton, J. Kim, T. Kim, and M. W. Grinstaff, "Hybrid Dendritic-linear Polyester-ethers for in situ Photopolymerization", *Journal of the American Chemical Society*, Vol. 124, pp. 5291–5293, 2002.

16. Sontjens, D. L. Nettles, M. A. Carnahan, L. A. Setton, and M. W. Grinstaff, "Biodendrimer-based Hydrogel Scaffolds for Cartilage Tissue Repair", *Biomacromolecules*, Vol. 7, pp. 310–316, 2006.

17. Degoricija, L., P. N. Bansal, S. H. M. Sontjens, N. S. Joshi, M. Takahashi, B. Snyder, and M. W. Grinstaff, "Hydrogels for Osteochondral Repair Based on Photocrosslinkable Carbamate Dendrimers", *Biomacromolecules*, Vol. 9, pp. 2863–2872, 2008.

18. Oelker, A.M., and M.W. Grinstaff, "Synthesis, Characterization, and In Vitro Evaluation of a Hydrogel-Based Corneal Onlay", *IEEE Transactions on Nanobioscience*, Vol. 11, pp. 37–45, 2012.

19. Kaga, S., S. Yapar, E. M. Gecici, and R. Sanyal, "Photopatternable 'Clickable' Hydrogels: 'Orthogonal' Control over Fabrication and Functionalization", *Macromolecules*, Vol. 48, pp. 5106–5115, 2015.

20. Desai, P. N., Q. Yuan, and H. Yang, "Synthesis And Characterization of Photocurable Polyamidoamine Dendrimer Hydrogels as a Versatile Platform for Tissue Engineering and Drug Delivery", *Biomacromolecules*, Vol. 11, pp. 666–673, 2010.

21. Holden, C. A., P. Tyagi, A. Thakur, R. Kadam, G. Jadhav, U. B. Kompella, and H. Yang, "Polyamidoamine Dendrimer Hydrogel for Enhanced Delivery of Antiglaucoma Drugs", *Nanomedicine: Nanotechnology, Biology, and Medicine*, Vol. 8, pp. 776–783, 2012.

22. Yang, H., P. Tyagi, R. S. Kadam, C. A. Holden, and U. B. Kompella, "Hybrid Dendrimer Hydrogel/PLGA Nanoparticle Platform Sustains Drug Delivery for One Week and Antiglaucoma Effects for Four Days Following One-time Topical Administration", *ACS Nano*, Vol. 6, pp. 7595–7606, 2012.

23. Amrite, A. C., S. P. Ayalasomayajula, N. P. S. Cheruvu, and U. B. Kompella, "Single Periocular Injection Of Celecoxib-PLGA Microparticles Inhibits Diabetes-induced Elevations in Retinal PGE2, VEGF, and Vascular Leakage", *Investigative Ophthalmology and Visual Science*, Vol. 47, pp. 1149–1160, 2006.

24. Wang, Y., Q. Zhao, H. Zhang, S. Yang, and X. Jia, "A Novel Poly(amido Amine)-dendrimer-based Hydrogel as a Mimic for the Extracellular Matrix", *Advanced Materials*, Vol. 26, pp. 4163–4167, 2014.

25. Wathier, M., P. J. Jung, M. a Carnahan, T. Kim, and M. W. Grinstaff, "Dendritic Macromers as in situ Polymerizing Biomaterials for Securing Cataract Incisions", *Journal of the American Chemical Society*, Vol. 126, pp. 12744–12745, 2004.

26. Wathier, M., C. S. Johnson, T. Kim, and M. W. Grinstaff, "Hydrogels Formed by Multiple Peptide Ligation Reactions to Fasten Corneal Transplants", *Bioconjugate Chemistry*, Vol. 17, pp. 873–876, 2006.

27. Oelker, A. M., J. A. Berlin, M. Wathier, and M. W. Grinstaff, "Synthesis and Characterization of Dendron Cross-linked Peg Hydrogels as Corneal Adhesives", *Biomacromolecules*, Vol. 12, pp. 1658–1665, 2011.

28. Ghobril, C., K. Charoen, E. K. Rodriguez, A. Nazarian, and M. W. Grinstaff, "A Dendritic Thioester Hydrogel Based on Thiol-thioester Exchange as a Dissolvable Sealant System for Wound Closure", *Angewandte Chemie - International Edition*, Vol. 52, pp. 14070–14074, 2013.

29. Villa-Camacho, J. C., C. Ghobril, L. Anez-Bustillos, M. W. Grinstaff, E. K. Rodriguez, and A. Nazarian, "The Efficacy of A Lysine-based Dendritic Hydrogel Does Not Differ from Those of Commercially Available Tissue Sealants and Adhesives: An ex vivo Study", *BMC musculoskeletal disorders*, Vol. 16, pp. 116, 2015.

30. Gitsov I., and C. Zhu, "Amphiphilic Hydrogels Constructed by Poly (Ethylene Glycol) and Shape-Persistent Dendritic Fragments", *Macromolecules*, Vol. 35, pp. 8418–8427, 2002.

31. Zhu, C., C. Hard, C. Lin, and I. Gitsov, "Novel Materials for Bioanalytical and Biomedical Applications: Environmental Response and Binding/release Capabilities

of Amphiphilic Hydrogels with Shape-persistent Dendritic Junctions", *Journal of Polymer Science, Part A: Polymer Chemistry*, Vol. 43, pp. 4017–4029, 2005.

32. Unal, B., and R. C. Hedden, "Gelation and Swelling Behavior of End-linked Hydrogels Prepared from Linear Poly(ethylene Glycol) and Poly(amidoamine) Dendrimers", *Polymer*, Vol. 47, pp. 8173–8182, 2006.

33. Navath, R. S., A. R. Menjoge, H. Dai, R. Romero, S. Kannan, and R. M. Kannan, "Injectable PAMAM Dendrimer-PEG Hydrogels for the Treatment of Genital Infections: Formulation Aand in vitro and in vivo Evaluation", *Molecular Pharmaceutics*, Vol. 8, pp. 1209–1223, 2011.

34. Tong, N. A. N., T.H. Nguyen, D. H. Nguyen, C. K. Nguyen, and N. Q. Tran, "Preparation of the Cationic Dendrimer-Based Hydrogels for Controlled Heparin Release", *Journal of Macromolecular Science, Part A*, Vol. 52, pp. 830–837, 2015.

35. Wang, Y., Q. Zhao, Y. Luo, Z. Xu, H. Zhang, S. Yang, Y. Wei, and X. Jia, "A High Stiffness Bio-inspired Hydrogel from the Combination of a Poly(amido Amine) Dendrimer with DOPA", *Chemical communications (Cambridge, England)*, Vol. 51, pp. 16786–16789, 2015.

36. Du, X., J. Zhou, J. Shi, and B. Xu, "Supramolecular Hydrogelators and Hydrogels: from Soft Matter to Molecular Biomaterials", *Chemical Reviews*, Vol. 115, pp. 13165–13307, 2015.

37. Newkome, G. R., G. R. Baker, S. Arai, M. J. Saunders, P. S. Russo, K. J. Theriot, C. N. Moorefield, L. E. Rogers, J. E. Miller, T. R. Lieux, M. E. Murray, B. Phillips, and L. Pascal, "Cascade Molecules. Part 6. Synthesis and Characterization of Two-Directional Cascade Molecules and Formation of Aqueous Gels", *Journal of the American Chemical Society*, Vol. 112, pp. 8458–8465, 1990.

38. G. R. Newkome G. R., C. N. Moorefield, G. R. Baker, R. K. Beheru, G. H. Escamillia, and M. J. Saunder, "Supramolecular Self-Assemblies of Two-Directional

Cascade Molecules: Automorphogenesis", *Angewantde Chemie International Edition*, Vol.31, pp. 917-919, 1992.

39. Zeng, F., and S. C. Zimmerman, "Dendrimers in Supramolecular Chemistry: From Molecular Recognition to Self-Assembly", *Chemical reviews*, Vol. 97, pp. 1681–1712, 1997.

40. Jorgensen, M. and K. Bechgaard, "Synthesis and Structural Characterization of a Bis-arborol-Tetrathiafulvalene Gel: Toward a Self-Assembling "Molecular" Wire", *Journal of Organic Chemistry*, Vol. 59, pp. 5877-5882, 1994.

41. McWatt, M., and G. J. Boons, "Parallel Combinatorial Synthesis of Glycodendrimers and Their Hydrogelation Properties", *European Journal of Organic Chemistry*, pp. 2535–2545, 2001.

42. Marmillon, C., F. Gauffre, T. Gulik-Krzywicki, C. Loup, A. M. Caminade, J. P. Majoral, J. P. Vors, and E. Rump, "Organophosphorus Dendrimers as New Gelators for Hydrogels", *Angewandte Chemie - International Edition*, Vol. 40, pp. 2626–2629, 2001.

43. El Ghzaoui, A., F. Gauffre, A. M. Caminade, J. P. Majoral, and H. Lannibois-Drean, "Self-assembly of Water-soluble Dendrimers into Thermoreversible Hydrogels and Macroscopic Fibers", *Langmuir*, Vol. 20, pp. 9348–9353, 2004.

44. Dasgupta, A., J. H. Mondal, and D. Das, "Peptide Hydrogels", *RSC Advances*, Vol. 3, pp. 9117, 2013.

45. Duan, P., L. Qin, X. Zhu, and M. Liu, "Hierarchical Self-assembly of Amphiphilic Peptide Dendrons: Evolution of Diverse Chiral Nanostructures Through Hydrogel Formation over a Wide PH Range", *Chemistry - A European Journal*, Vol. 17, pp. 6389–6395, 2011.

46. Qin, L., P. Duan, F. Xie, L. Zhang, and M. Liu, "A Metal Ion Triggered Shrinkable

Supramolecular Hydrogel and Controlled Release by an Amphiphilic Peptide Dendron.", *Chemical Communications*, Vol. 49, pp. 10823–5, 2013.

47. Qin, L., F. Xie, P. Duan, and M. Liu, "A Peptide Dendron-based Shrinkable Metallo-hydrogel for Charged Species Separation and Stepwise Release of Drugs", *Chemistry - A European Journal*, Vol. 20, pp. 15419–15425, 2014.

48. Sako, Y., and Y. Takaguchi, "A Photo-responsive Hydrogelator Having Gluconamides at Its Peripheral Branches.", *Organic & biomolecular chemistry*, Vol. 6, pp. 3843–7, 2008.

49. Xie, F., L. Qin, and M. Liu, "A Dual Thermal and Photo-switchable Shrinking–swelling Supramolecular Peptide Dendron Gel", *Chemical Communications*, Vol. 52, pp. 930–933, 2016.

50. Nummelin, S., V. Liljestrom, E. Saarikoski, J. Ropponen, A. Nykanen, V. Linko, J. Seppala, J. Hirvonen, O. Ikkala, L. M. Bimbo, and M. A. Kostiainen, "Self-Assembly of Amphiphilic Janus Dendrimers into Mechanically Robust Supramolecular Hydrogels for Sustained Drug Release", *Chemistry - A European Journal*, Vol. 21, pp. 14433–14439, 2015.

51. Namazi, H., and M. Adeli, "Novel Linear-globular Thermoreversible Hydrogel ABA Type Copolymers from Dendritic Citric Acid as the A Blocks and Poly(ethyleneglycol) as the B Block", *European Polymer Journal*, Vol. 39, pp. 1491–1500, 2003.

52. Namazi, H., and M. Adeli, "Dendrimers of Citric Acid and Poly (Ethylene Glycol) as the New Drug-delivery Agents", *Biomaterials*, Vol. 26, pp. 1175–1183, 2005.

53. Wang, Q., J. L. Mynar, M. Yoshida, E. Lee, M. Lee, K. Okuro, K. Kinbara, and T. Aida, "High-water-content Mouldable Hydrogels by Mixing Clay and a Dendritic Molecular Binder", *Nature*, Vol. 463, pp. 339–343, 2010.

54. Suwandi, J. S., R. E. M. Toes, T. Nikolic, and B. O. Roep, “Inducing Tissue Specific Tolerance in Autoimmune Disease with Tolerogenic Dendritic Cells”, *Clinical and Experimental Rheumatology*, Vol. 33, pp. 97–103, 2015.

55. Crompton, K. E., J. D. Goud, R. V. Bellamkonda, T. R. Gengenbach, D. I. Finkelstein, M. K. Horne, and J. S. Forsythe, “Polylysine-functionalised Thermoresponsive Chitosan Hydrogel for Neural Tissue Engineering”, *Biomaterials*, Vol. 28, pp. 441–449, 2007.

56. Tamesue, S., M. Ohtani, K. Yamada, Y. Ishida, J. M. Spruell, N. A. Lynd, C. J. Hawker, and T. Aida, “Linear Versus Dendritic Molecular Binders for Hydrogel Network Formation with Clay Nanosheets: Studies with ABA Triblock Copolyethers Carrying Guanidinium Ion Pendants”, *Journal of the American Chemical Society*, Vol. 135, pp. 15650–15655, 2013.

57. Seelbach, R. J., P. Fransen, M. Peroglio, D. Pulido, P. Lopez-Chicon, F. Duttenhoefer, S. Sauerbier, T. Freiman, P. Niemeyer, C. Semino, F. Albericio, M. Alini, M. Royo, A. Mata, and D. Eglin, “Multivalent Dendrimers Presenting Spatially Controlled Clusters of Binding Epitopes in Thermoresponsive Hyaluronan Hydrogels”, *Acta Biomaterialia*, Vol. 10, pp. 4340–4350, 2014.

58. Wu, X.Y., S.W. Huang, J. T. Zhang, and R. X. Zhuo, “Preparation and Characterization of Novel Physically Cross-linked Hydrogels Composed of Poly(vinyl Alcohol) and Amine-terminated Polyamidoamine Dendrimer”, *Macromolecular Bioscience*, Vol. 4, pp. 71–75, 2004.

59. World Health Organization, “Global Status Report On Noncommunicable Diseases 2010”, *World Health Organization*, pp. 176, 2010.

60. Stewart, B. W., Wild, C. P., “World Cancer Report 2014”, *World Health Organization*, 2014.

61. Jiang, Y., and P. E. Marszalek, “Detecting DNA Damage at a Single-molecule Level

by Atomic Force Microscopy", *Microscoy: Science, Technology, Applications and Education*, pp. 459–469, 2010.

62. Hanahan, D. and R. A. Weinberg "Hallmarks of Cancer: The Next Generation", *Cell,* Vol. 144, pp. 646–674, 2011.

63. Pommier, Y., and D. Robert, "Pharmacological and Therapeutics Agents That Target DNA Replication", *DNA Replication in Eukaryotic Cells (2nd Edition)*, Vol. 26, pp. 1–28, 2001.

64. Van Vuuren, R. J., M. H. Visagie, A. E. Theron, and A. M. Joubert, "Antimitotic Drugs in the Treatment of Cancer", *Cancer Chemotherapy and Pharmacology*, Vol. 76, pp. 1101–1112, 2015.

65. Kavallaris, M., "Microtubules and Resistance to Tubulin-binding Agents", Vol. 10, pp. 1–12, 2010.

66. Giuliano, S., and G. Pages, "Mechanisms of Resistance to Anti-angiogenesis Therapies", *Biochimie*, Vol. 95, pp. 1110–1119, 2013.

67. Folkman, J., "Tumor Angiogenesis: Therapeutic Implications", *The New England journal of medicine*, Vol. 285, pp. 1182–1186, 1971.

68. Zetter, B. R., "The Scientific Contributions of M. Judah Folkman to Cancer Research", *Nature reviews. Cancer*, Vol. 8, pp. 647–54, 2008.

69. Samant, R. S., and L. A. Shevde, "Recent Advances in Anti-Angiogenic Therapy of Cancer", *Oncotarget*, Vol. 2, pp. 122–134, 2011.

70. Vasudev, N. S., and A. R. Reynolds, "Anti-angiogenic Therapy for Cancer: Current Progress, Unresolved Questions and Future Directions", *Angiogenesis*, Vol. 17, pp. 471–494, 2014.

71. Yanasarn, N., B. R. Sloat, and Z. Cui, "Nanoparticles Engineered from Lecithin-in-water Emulsions as a Potential Delivery System for Docetaxel", *International Journal of Pharmaceutics*, Vol. 379, pp. 174–180, 2009.

72. Zhang, W., Y. Shi, Y. Chen, S. Yu, J. Hao, J. Luo, X. Sha, and X. Fang, "Enhanced Antitumor Efficacy by Paclitaxel-loaded Pluronic P123/F127 Mixed Micelles Against Non-small Cell Lung Cancer Based on Passive Tumor Targeting and Modulation of Drug Resistance", *European Journal of Pharmaceutics and Biopharmaceutics*, Vol. 75, pp. 341–353, 2010.

73. Maeda, H., J. Wu, T. Sawa, Y. Matsumura, and K. Hori, "Tumor Vascular Permeability and the EPR Effect in Macromolecular Therapeutics: A Review", *Journal of Controlled Release*, Vol. 65, pp. 271–284, 2000.

74. Polyak, D., A. Eldar-Boock, H. Baabur-Cohen, and R. Satchi-Fainaro, "Polymer Conjugates for Focal and Targeted Delivery of Drugs", *Polymers for Advanced Technologies*, Vol. 24, pp. 777–790, 2013.

75. Leriche, G., L. Chisholm, and A. Wagner, "Cleavable Linkers in Chemical Biology", *Bioorganic and Medicinal Chemistry*, Vol. 20, pp. 571–582, 2012.

76. Ulbrich, K., T. Etrych, P. Chytil, M. Pechar, M. Jelinkova, and B. Rihova, "Polymeric Anticancer Drugs with PH-controlled Activation", *International Journal of Pharmaceutics*, Vol. 277, pp. 63–72, 2004.

77. Zhang, L., S. Zhu, L. Qian, Y. Pei, Y. Qiu, and Y. Jiang, "RGD-modified PEG-PAMAM-DOX Conjugates: in vitro and in vivo Studies for Glioma", *European Journal of Pharmaceutics and Biopharmaceutics*, Vol. 79, pp. 232–240, 2011.

78. Yang, Y., H. Aloysius, D. Inoyama, Y. Chen, and L. Hu, "Enzyme-mediated Hydrolytic Activation of Prodrugs", *Acta Pharmaceutica Sinica B*, Vol. 1, pp. 143–159, 2011.

79. Sun, Q., J. Wang, M. Radosz, and Y. Shen, "Polymer-Based Prodrugs for Cancer Chemotherapy", *Functional Polymers for Nanomedicine*, pp. 245–260, 2013.

80. Bertrand, N., J. Wu, X. Xu, N. Kamaly, and O. C. Farokhzad "Cancer Nanotechnology: The Impact of Passive and Active Targeting in The Era of Modern Cancer Biology", *Advanced Drug Delivery Reviews*. Vol. 66, pp. 1–25, 2014.

81. Pasqualini, R., W. Arap, and D. M. McDonald, "Probing The Structural And Molecular Diversity of Tumor Vasculature", *Trends in Molecular Medicine*, Vol. 8, pp. 563–571, 2002.

82. Domingo-Espin, J., V. Petegnief, N. de Vera, O. Conchillo-Sole, P. Saccardo, U. Unzueta, E. Vazquez, J. Cedano, L. Negro, X. Daura, H. Peluffo, A. M. Planas, A. Villaverde, and N. Ferrer-Miralles, "RGD-based Cell Ligands for Cell-targeted Drug Delivery Act as Potent Trophic Factors", *Nanomedicine: Nanotechnology, Biology, and Medicine*, Vol. 8, pp. 1263–1266, 2012.

83. Miura, Y., T. Takenaka, K. Toh, S. Wu, H. Nishihara, M. R. Kano, Y. Ino, T. Nomoto, Y. Matsumoto, H. Koyama, H. Cabral, N. Nishiyama, and K. Kataoka, "Cyclic RGD-linked Polymeric Micelles for Targeted Delivery of Platinum Anticancer Drugs to Glioblastoma Through the Blood-brain Tumor Barrier", *ACS Nano*, Vol. 7, pp. 8583–8592, 2013.

84. Danen, E. H. J., "Integrin Signaling as a Cancer Drug Target", *ISRN Cell Biology*, Vol. 2013, pp. 1–14, 2013.

85. Ringsdorf, H., "Structure and Properties of Pharmacologically Active Polymers", *Journal of Polymer Science: Polymer Symposia*, Vol. 51, pp. 135–153, 1975.

86. Gros, B. L., H. Ringsdorf, H. Schupp, and E. Kastner, "Polymeric Antitumor Agents On A Molecular And On A Cellular Level?", *Angewandte Chemie International Edition*, Vol. 20, pp. 305–325, 1981.

87. Drobnik, J., J. Kopecek, J. Labsky, P. Rejmanova, J. Exner, V. Saudek, and J. Kalal, "Enzymatic Cleavage of Side-Chains of Synthetic Water-Soluble Polymers", *Macromolecular Chemistry and Physics*, Vol. 177, pp. 2833–2848, 1976.

88. Duncan, R., L. W. Seymour, K. Ulbrich and J. Kopecek, "Soluble Synthetic Polymers for Targeting and Controlled Release of Anticancer Agents, Particularly Anthracycline Antibiotics", *Journal of Bioactive and Compatible Polymers*, Vol. 3, pp. 4–15, 1988.

89. Rohini, N. Agrawal, A, Joseph, and A. Mukerji, "Polymeric Prodrugs: Recent Achievements and General Strategies", *Journal of Antivirals & Antiretrovirals*, S15, 2013.

90. Pang, X., H. L. Du, H. Q. Zhang, Y. J. Zhai, and G. X. Zhai, "Polymer-drug Conjugates: Present State of Play and Future Perspectives", *Drug Discovery Today*, Vol. 18, pp. 1316–1322, 2013.

91. Yamaoka, T., Y. Tabata, and Y. Ikada, "Distribution and Tissue Uptake of Poly(ethylene Glycol) with Different Molecular Weights After Intravenous Administration to Mice", *Journal of Pharmaceutical Sciences*, Vol. 83, pp. 601–606, 1994.

92. Mehvar, R., "Modulation of the Pharmacokinetics and Pharmacodynamics of Proteins by Polyethylene Glycol Conjugation", *Journal of Pharmacy & Pharmaceutical sciences.* Vol. 3, pp. 125–136, 2000.

93. Tomlinson, R., J. Heller, S. Brocchini, and R. Duncan, "Polyacetal-Doxorubicin Conjugates Designed for PH-Dependent Degradation", *Bioconjugate Chemistry*, Vol. 14, pp. 1096–1106, 2003.

94. Yoo, H. S., and T. G. Park, "Folate-receptor-targeted Delivery of Doxorubicin Nano-aggregates Stabilized by Doxorubicin-PEG-folate Conjugate", *Journal of Controlled Release*, Vol. 100, pp. 247–256, 2004.

95. Veronese, F. M., O. Schiavon, G. Pasut, R. Mendichi, L. Andersson, A. Tsirk, J. Ford, G. Wu, S. Kneller, J. Davies, and R. Duncan, "PEG-doxorubicin Conjugates: Influence of Polymer Structure on Drug Release, in vitro Cytotoxicity, Biodistribution, and Antitumor Activity", *Bioconjugate Chemistry*, Vol. 16, pp. 775–784, 2005.

96. Pasut, G., and F. M. Veronese, "PEG Conjugates in Clinical Development or Use as Anticancer Agents: An Overview", *Advanced Drug Delivery Reviews*, Vol. 61, pp. 1177–1188, 2009.

97. Ray, A., N. Larson, D. B. Pike, M. Gruner, S. Naik, H. Bauer, A. Malugin, K. Greish, and H. Ghandehari, "Comparison of Active and Passive Targeting of Docetaxel for Prostate Cancer Therapy by HPMA Copolymer-RGDfK Conjugates", *Molecular Pharmaceutics*, Vol. 8, pp. 1090–1099, 2011.

98. Etrych, T., M. Sirovae, L. Starovoytova, B. Riehovae, and K. Ulbrich, "HPMA Copolymer Conjugates of Paclitaxel and Docetaxel with PH-controlled Drug Release", *Molecular Pharmaceutics*, Vol. 7, pp. 1015–1026, 2010.

99. Singer, J. W., "Paclitaxel Poliglumex (XYOTAX, CT-2103): A Macromolecular Taxane", *Journal of Controlled Release*, Vol. 109, pp. 120–126, 2005.

100. Matsumura, Y., and H. Maeda, "A New Concept for Macromolecular Therapeutics in Cancer Chemotherapy: Mechanism of Tumoritropic Accumulation of Proteins and the Antitumor Agent Smancs", *Cancer Research*, Vol. 46, pp. 6387–6392, 1986.

101. Cho, H. K., I. W. Cheong, J. M. Lee, and J. H. Kim, "Polymeric Nanoparticles, Micelles and Polymersomes from Amphiphilic Block Copolymer", *Korean Journal of Chemical Engineering*, Vol. 27, pp. 731–740, 2010.

102. Jawahar, N., and S. Meyyanathan, "Polymeric Nanoparticles for Drug Delivery and Targeting: A Comprehensive Review", *International Journal of Health & Allied Sciences*, Vol. 1, pp. 217, 2012.

103. Anselmo, A. C., and S. Mitragotri, "Nanoparticles in the Clinic", *Bioengineering & Translational Medicine*, Vol. 55, pp. 10-29, 2016.

104. Zhang, L., and A. Eisenberg, "Multiple Morphologies and Characteristics of 'Crew-Cut' Aggregates of Polystyrene-*B*-poly (acrylic Acid) Block Copolymers", *Science*, Vol. 268, pp. 1728–1731, 1995.

105. Zhang, L., and A. Eisenberg, "Morphogenic Effect of Added Ions on Crew-Cut Aggregates of Polystyrene-*B*-poly (acrylic Acid) Block Copolymers in Solutions", *Macromolecules*, Vol. 29, pp. 8805–8815, 1996.

106. Mai, Y., and A. Eisenberg, "Self-assembly of Block Copolymers.", *Chemical Society Reviews*, Vol. 41, pp. 5969, 2012.

107. Blanazs, A., S. P. Armes, and A. J. Ryan, "Self-assembled Block Copolymer Aggregates: From Micelles to Vesicles and Their Biological Applications", *Macromolecular Rapid Communications*, Vol. 30, pp. 267–277, 2009.

108. Rao, J. P., and K. E. Geckeler, "Polymer Nanoparticles: Preparation Techniques and Size-control Parameters", *Progress in Polymer Science (Oxford)*, Vol. 36, pp. 887–913, 2011.

109. Nagavarma, B. V. N., H. K. S. Yadav, A. Ayaz, L. S. Vasudha, and H. G. Shivakumar, "Different Techniques for Preparation of Polymeric Nanoparticles", *Asian Journal of Pharmaceutical and Clinical Research*, Vol. 5, pp. 16–23, 2012.

110. Sumer Bolu, B., E. Manavoglu Gecici, and R. Sanyal, "Combretastatin A-4 Conjugated Antiangiogenic Micellar Drug Delivery Systems using Dendron-Polymer Conjugates", *Molecular Pharmaceutics*, Vol. 13, pp. 1482–1490, 2016.

111. Liu, H., R. Zhang, Y. Niu, Y. Li, and C. Qiao, "Development of Hypoxia-triggered Prodrug Micelles as Doxorubicin Carriers For Tumor Therapy", *RSC Advances*, Vol. 5, pp. 20848–20857, 2015.

112. Blanco, E., H. Shen, and M. Ferrari, "Principles of Nanoparticle Design for Overcoming Biological Barriers to Drug Delivery", *Nature biotechnology*, Vol. 33, pp. 941–951, 2015.

113. Karagoz, B., L. Esser, H. T. Duong, J. S. Basuki, and T. P. Davis, "Polymerization-Induced Self-Assembly (PISA) – Control Over the Morphology of Nanoparticles for Drug Delivery Applications", *Polymer Chemistry,* Vol. 5, pp. 350–355, 2014.

114. Beria, L., T. N. Gevrek, A. Erdog, R. Sanyal, D. Pasini, and A. Sanyal, "'Clickable' Hydrogels for All: Facile Fabrication and Functionalization", *Biomaterials Science*, Vol. 2, pp. 67–75, 2014.

115. Zheng, J., L. A. Smith Callahan, J. Hao, K. Guo, C. Wesdemiotis, R. A. Weiss, and M. L. Becker, "Strain-promoted Cross-linking of PEG-based Hydrogels via Copper-Free Cycloaddition", *ACS Macro Letters*, Vol. 1, pp. 1071–1073, 2012.

116. Nimmo, C. M., S. C. Owen, and M. S. Shoichet, "Diels-Alder Click Cross-Linked Hyaluronic Acid Hydrogels for Tissue Engineering", *Biomacromolecules,* Vol. 12, pp. 824–830, 2011.

117. Kirchhof, S., M. Gregoritza, V. Messmann, N. Hammer, A. M. Goepferich, and F. P. Brandl, "Diels-Alder Hydrogels with Enhanced Stability: First Step Toward Controlled Release of Bevacizumab", *European Journal of Pharmaceutics and Biopharmaceutics*, Vol. 96, pp. 217–225, 2015.

118. Azagarsamy, M. A., P. Sokkalingam, and S. Thayumanavan, "Enzyme-triggered Disassembly of Dendrimer-based Amphiphilic Nanocontainers", *Journal of the American Chemical Society*, Vol. 131, pp. 14184–14185, 2009.

119. Cengiz, N., J. Rao, A. Sanyal, and A. Khan, "Designing Functionalizable Hydrogels Through Thiol-epoxy Coupling Chemistry", *Chemical Communications*, Vol. 49, pp. 11191–3, 2013.

120. Arslan, M., T. N. Gevrek, A. Sanyal, and R. Sanyal, "Cyclodextrin Mediated Polymer Coupling Via Thiol–maleimide Conjugation: Facile Access to Functionalizable Hydrogels", *RSC Adv.*, Vol. 4, pp. 57834–57841, 2014.

121. Arslan, M., O. Gok, R. Sanyal, and A. Sanyal, "Clickable Poly (Ethylene Glycol)-Based Copolymers Using Azide – Alkyne Click Polymerization", *Macromolecular Chemistry and Physics*, Vol 215, pp. 2237–2247, 2014.

122. Aimetti, A. A., A. J. Machen, and K. S. Anseth, "Poly(ethylene Glycol) Hydrogels Formed by Thiol-ene Photopolymerization for Enzyme-responsive Protein Delivery", *Biomaterials*, Vol. 30, pp. 6048–6054, 2009.

123. Olofsson, K., M. Malkoch, and A. Hult, "Soft Hydrogels from Tetra-functional PEGs Using UV-induced Thiol-ene Coupling Chemistry: A Structure-to-property Study", *Rsc Advances*, Vol. 4, pp. 30118–30128, 2014.

124. Yang, T., H. Long, M. Malkoch, E. Kristofer Gamstedt, L. Berglund, and A. Hult, "Characterization of Well-defined Poly(ethylene Glycol) Hydrogels Prepared by Thiol-ene Chemistry", *Journal of Polymer Science, Part A: Polymer Chemistry*, Vol. 49, pp. 4044–4054, 2011.

125. Polizzotti, B. D., B. D. Fairbanks, and K. S. Anseth, "Three-dimensional Biochemical Patterning of Click-based Composite Hydrogels via Thiolene Photopolymerization", *Biomacromolecules*, Vol. 9, pp. 1084–1087, 2008.

126. Sawicki, L. A., and A. M. Kloxin, "Design of Thiol–ene Photoclick Hydrogels using Facile Techniques for Cell Culture Applications", *Biomater. Sci.*, Vol. 2, pp. 1612–1626, 2014.

127. Gramlich, W. M., I. L. Kim, and J. A. Burdick, "Synthesis and Orthogonal Photopatterning of Hyaluronic Acid Hydrogels with Thiol-norbornene Chemistry", *Biomaterials*, Vol. 34, pp. 9803–9811, 2013.

128. Shepherd, J. L., A. Kell, E. Chung, C. W. Sinclar, M. S. Workentin, and D. Bizzotto, "Selective Reductive Desorption of A SAM-coated Gold Electrode Revealed using Fluorescence Microscopy", *Journal of the American Chemical Society*, Vol. 126, pp. 8329–8335, 2004.

129. Kose, M. M., S. Onbulak, I. I. Yilmaz, and A. Sanyal, "Orthogonally 'clickable' Biodegradable Dendrons", *Macromolecules*, Vol. 44, pp. 2707–2714, 2011.

130. Gok, O., S. Yigit, M. M. Kose, R. Sanyal, and A. Sanyal, "Dendron-polymer Conjugates via the Diels-alder 'click' reaction of Novel Anthracene-based Dendrons", *Journal of Polymer Science, Part A: Polymer Chemistry*, Vol. 51, pp. 3191–3201, 2013.

131. Altintas, O. B. Yankul, G. Hizal, U. Tunca, "A3-Type Star Polymers via Click Chemistry" *Journal of Polymer Science: Part A: Polymer Chemistry*, Vol. 44, pp. 6458–6465, 2006.

132. Lis, H., and N. Sharon, "Lectins: Carbohydrate-Specific Proteins That Mediate Cellular Recognition", *Chemical Reviews*, Vol. 98, pp. 637–674, 1998.

133. Mortell, K., R. Weatherman, and L. Kiessling, "Recognition Specificity of Neoglycopolymers by Ring-opening Metathesis Polymerization", *Journal of the American Chemical Society*, Vol. 118, pp. 2297–2298, 1996.

134. Lee, Y. C., and R. T. Lee, "Carbohydrate-Protein Interactions: Basis of Glycobiology", *Accounts of Chemical Research*, Vol. 28, pp. 321–327, 1995.

135. Jayaraman, N., "Multivalent Ligand Presentation as a Central Concept to Study Intricate Carbohydrate-protein Interactions", *Chemical Society Reviews*, Vol. 38, pp. 3463–83, 2009.

136. Hudson, H. F., and V. Sharma, "Metabolic Manipulation of Glycosylation Disorders" *Semin Cell. Dev. Biol. Vol*. 21, pp. 655–662, 2010.

137. Lundquist, J. J., and E. J. Toone, “The Cluster Glycoside Effect”, *Chemical Reviews*, Vol. 102, pp. 555–578, 2002.

138. Woller, E. K., and M. J. Cloninger, “The Lectin-binding Properties of Six Generations of Mannose-functionalized Dendrimers”, *Organic Letters*, Vol. 4, pp. 7–10, 2002.

139. Woller, E. K., E. D. Walter, J. R. Morgan, D. J. Singel, and M. J. Cloninger, “Altering the Strength of Lectin Binding Interactions and Controlling the Amount of Lectin Clustering Using Mannose/hydroxyl-functionalized Dendrimers”, *Journal of the American Chemical Society*, Vol. 125, pp. 8820–8826, 2003.

140. Parera Pera, N., H. M. Branderhorst, R. Kooij, C. Maierhofer, M. Van Der Kaaden, R. M. J. Liskamp, V. Wittmann, R. Ruijtenbeek, and R. J. Pieters, “Rapid Screening of Lectins for Multivalency Effects with a Glycodendrimer Microarray”, *ChemBioChem*, Vol. 11, pp. 1896–1904, 2010.

141. Montanez, M. I., Y. Hed, S. Utsel, J. Ropponen, E. Malmström, L. Wagberg, A. Hult, and M. Malkoch, “Bifunctional Dendronized Cellulose Surfaces As Biosensors”, *Biomacromolecules*, Vol. 12, pp. 2114–2125, 2011.

142. Wang, C., Y. L. Zhou, and D. C. Bakerb, “Synthesis of A Mannose-capped Disaccharide with a Thiol Terminus., *Arkivoc*, Vol. 2009, pp. 171–180, 2009.

143. Clarke, S. J., and L. P. Rivory, “Clinical Pharmacokinetics of Docetaxel”, *Clinical Pharmacokinetics*, Vol. 36, pp. 99–114, 1999.

144. Food and Drug Administration (FDA), “Prescribing Information for Taxotere” 2009.

145. Hart, M., and S. Acott, “Physical And Chemical Stability Of Taxotere (Docetaxel) One-vial (20 Mg/ml) Infusion Solution Following Refrigerated Storage”, *Ecancermedicalscience*, Vol. 4, pp. 2–5, 2010.

146. Persohn, E., A. Canta, S. Schoepfer, M. Traebert, L. Mueller, A. Gilardini, S. Galbiati, G. Nicolini, A. Scuteri, F. Lanzani, G. Giussani, and G. Cavaletti, "Morphological and Morphometric Analysis of Paclitaxel and Docetaxel-induced Peripheral Neuropathy in Rats", *European Journal of Cancer*, Vol. 41, pp. 1460–1466, 2005.

147. Ten Tije, A. J., J. Verweij, W. J. Loos, and A. Sparreboom, "Pharmacological Effects of Formulation Vehicles", *Clinical Pharmacokinetics*, Vol. 42, pp. 665–685, 2003.

148. De Oliveira, R., P. Zhao, N. Li, L. C. De Santa Maria, J. Vergnaud, J. Ruiz, D. Astruc, and G. Barratt, "Synthesis and in vitro Studies of Gold Nanoparticles Loaded with Docetaxel", *International Journal of Pharmaceutics*, Vol. 454, pp. 703–711, 2013.

149. Nagesh, P. K. B., N. R. Johnson, V. K. N. Boya, P. Chowdhury, S. F. Othman, V. Khalilzad-Sharghi, B. B. Hafeez, A. Ganju, S. Khan, S. W. Behrman, N. Zafar, S. C. Chauhan, M. Jaggi, and M. M. Yallapu, "PSMA Targeted Docetaxel-loaded Superparamagnetic Iron Oxide Nanoparticles for Prostate Cancer", *Colloids and surfaces. B, Biointerfaces*, Vol. 144, pp. 8–20, 2016.

150. Song, H., H. Geng, J. Ruan, K. Wang, C. Bao, J. Wang, X. Peng, X. Zhang, and D. Cui, "Development of Polysorbate 80/Phospholipid Mixed Micellar Formation for Docetaxel and Assessment of Its in vivo Distribution in Animal Models", *Nanoscale research letters*, Vol. 6, pp. 354, 2011.

151. Wang, Y., L. Chen, L. Tan, Q. Zhao, F. Luo, Y. Wei, and Z. Qian, "PEG-PCL Based Micelle Hydrogels as Oral Docetaxel Delivery Systems for Breast Cancer Therapy", *Biomaterials*, Vol. 35, pp. 6972–6985, 2014.

152. Elsabahy, M., M. E. Perron, N. Bertrand, G. E. Yu, and J. C. Leroux, "Solubilization of Docetaxel in Poly(ethylene Oxide)-block-poly(butylene/styrene Oxide) Micelles",

Biomacromolecules, Vol. 8, pp. 2250–2257, 2007.

153. Immordino, M. L., P. Brusa, S. Arpicco, B. Stella, F. Dosio, and L. Cattel, "Preparation, Characterization, Cytotoxicity and Pharmacokinetics of Liposomes Containing Docetaxel", *Journal of Controlled Release*, Vol. 91, pp. 417–429, 2003.

154. Li, X., X. Tian, J. Zhang, X. Zhao, X. Chen, Y. Jiang, D. Wang, and W. Pan, "In vitro and in vivo Evaluation of Folate Receptor-targeting Amphiphilic Copolymer-modified Liposomes Loaded with Docetaxel", *International Journal of Nanomedicine*, Vol. 6, pp. 1167–1184, 2011.

155. Deeken, J. F., R. Slack, G. J. Weiss, R. K. Ramanathan, M. J. Pishvaian, J. Hwang, K. Lewandowski, D. Subramaniam, A. R. He, I. Cotarla, A. Rahman, and J. L. Marshall, "A Phase I Study of Liposomal-encapsulated Docetaxel (LE-DT) in Patients with Advanced Solid Tumor Malignancies", *Cancer Chemotherapy and Pharmacology*, Vol. 71, pp. 627–633, 2013.

156. Murphy, E. A., B. K. Majeti, R. Mukthavaram, L. M. Acevedo, L. A. Barnes, and D.A. Cheresh, "Targeted Nanogels: A Versatile Platform for Drug Delivery to Tumors" *Mol. Cancer Ther*. Vol. 10, pp. 972-982, 2011.

157. Lu, S., K. G. Neoh, E. T. Kang, R. Mahendran, and E. Chiong, "Mucoadhesive Polyacrylamide Nanogel as a Potential Hydrophobic Drug Carrier for Intravesical Bladder Cancer Therapy", *European Journal of Pharmaceutical Sciences*, Vol. 72, pp. 57–68, 2015.

158. Ray, A., N. Larson, D. B. Pike, M. Gruner, S. Naik, H. Bauer, A. Malugin, K. Greish, and H. Ghandehari, "Comparison of Active and Passive Targeting of Docetaxel for Prostate Cancer Therapy by HPMA Copolymer-RGDfK Conjugates", *Molecular Pharmaceutics*, Vol. 8, pp. 1090–1099, 2011.

159. Xie, Z., T. Lu, X. Chen, Y. Zheng, and X. Jing, "Synthesis, Self-assembly in Water, and Cytotoxicity of MPEG-block-PLLA/DX Conjugates", *Journal of Biomedical*

Materials Research - Part A, Vol. 88, pp. 238–245, 2009.

160. Li, W., P. Zhan, E. De Clercq, H. Lou, and X. Liu, "Current Drug Research on PEGylation with Small Molecular Agents", *Progress in Polymer Science*, Vol. 38, pp. 421–444, 2013.

161. Kopecek, J. and P. Kopeckova, "HPMA copolymers: Origins, Early developments, Present, and Future" *Adv. Drug Deliv. Rev.* Vol. 62, pp. 122–149, 2010.

162. Seymour, L. W., Y. Miyamoto, H. Maeda, M. Brereton, J. Strohalm, K. Ulbrich, and R. Duncan, "Influence of Molecular Weight on Passive Tumour Accumulation of a Soluble Macromolecular Drug Carrier", *European Journal of Cancer*, Vol. 31, pp. 766–770, 1995.

163. Takakura, Y., R. I. Mahato, M. Nishikawa, and M. Hashida, "Control of Pharmacokinetic Profiles of Drug-macromolecule Conjugates", *Advanced Drug Delivery Reviews*, Vol. 19, pp. 377–399, 1996.

164. Noguchi, Y., J. Wu, R. Duncan, J. Strohalm, K. Ulbrich, T. Akaike, and H. Maeda, "Early Phase Tumor Accumulation of Macromolecules: A Great Difference in Clearance Rate Between Tumor and Normal Tissues", *Japanese Journal of Cancer research : Gann*, Vol. 89, pp. 307–314, 1998.

165. Strohalm, J., and J. Kopecek, "Poly [N-(2-hydroxypropyl)methacrylamide] IV. Heterogeneous Polymerization", *Angewandte Macromolecular Chemie* Vol. 70, pp. 109-118, 1978.

166. Ulbrich, K., V. Subr, J. Strohalm, D. Plocova, M. Jelínkova, and B. Ríhova, "Polymeric Drugs Based on Conjugates of Synthetic and Natural Macromolecules. I. Synthesis And Physico-chemical Characterisation", *Journal of Controlled Release*, Vol. 64, pp. 63–79, 2000.

167. Feng, J., Y. Fitz, Y. Li, M. Fernandez, I. Cortes Puch, D. Wang, S. Pazniokas, B.

Bucher, X. Cui, and S.B. Solomon, “Catheterization of the Carotid Artery and Jugular Vein to Perform Hemodynamic Measures, Infusions and Blood Sampling in a Conscious Rat Model”, *Journal of Visualized Experiments*, pp. e51881, 2015.

168. Kopecek, J., and P. Kopeckova, “HPMA Copolymers: Origins, Early Developments, Present, and Future”, *Advanced Drug Delivery Reviews*, Vol. 62, pp. 122–149, 2010.

169. Chiefari, J., Y. K. B. Chong, F. Ercole, J. Krstina, J. Jeffery, T. P. T. Le, R. T. A. Mayadunne, G. F. Meijs, C. L. Moad, G. Moad, E. Rizzardo, S. H. Thang, and C. South, “Living Free-Radical Polymerization by Reversible Addition - Fragmentation Chain Transfer : The RAFT Process”, *Macromolecules*, Vol. 31, pp. 5559–5562, 1998.

170. Moad, G., E. Rizzardo, and S. H. Thang, “Living Radical Polymerization by The RAFT Process”, *Australian Journal of Chemistry*, Vol. 58, pp. 379–410, 2005.

171. Zhong, Y. J., L. H. Shao, and Y. Li, “Cathepsin B-cleavable Doxorubicin Prodrugs for Targeted Cancer Therapy”, *International Journal of Oncology*, Vol. 42, pp. 373–383, 2013.

172. Zhong, Y., F. Meng, C. Deng, and Z. Zhong, “Ligand-directed Active Tumor-targeting Polymeric Nanoparticles for Cancer Chemotherapy”, *Biomacromolecules*, Vol. 15, pp. 1955–69, 2014.

173. Nelson, D. M., Z. Ma, C. E. Leeson, and W. R. Wagner, "Extended and Sequential Delivery of Protein from Injectable Thermoresponsive Hydrogels" *J. Biomed. Mater. Res. A*. Vol. 100, pp. 776–785, 2012.

174. Thermofisher Scientific, “Pierce ® BCA Protein Assay Kit”, *Test*, Vol. 0747, pp. 1–7, 2011.

175. Wan, W. M., X. L. Sun, and C. Y. Pan, “Formation of Vesicular Morphologies via Polymerization Induced Self-assembly and Re-organization”, *Macromolecular Rapid*

Communications, Vol. 31, pp. 399–404, 2010.

176. Huang, C. Q., Y. Wang, C. Y. Hong, and C. Y. Pan, "Spiropyran-based Polymeric Vesicles: Preparation and Photochromic Properties", *Macromolecular Rapid Communications*, Vol. 32, pp. 1174–1179, 2011.

177. Warren, N. J., and S. P. Armes, "Polymerization-induced Self-assembly of Block Copolymer Nano-objects Vvia RAFT Aqueous Dispersion Polymerization", *Journal of the American Chemical Society*, Vol. 136, pp. 10174–10185, 2014.

178. Chambon, P., A. Blanazs, G. Battaglia, and S. P. Armes, "Facile Synthesis of Methacrylic ABC Triblock Copolymer Vesicles by RAFT Aqueous Dispersion Polymerization", *Macromolecules*, Vol. 45, pp. 5081–5090, 2012.

179. Sugihara, S., A. Blanazs, S. P. Armes, A. J. Ryan, and A. L. Lewis, "Aqueous Dispersion Polymerization: A New Paradigm for in situ Block Copolymer Self-assembly in Concentrated Solution", *Journal of the American Chemical Society*, Vol. 133, pp. 15707–15713, 2011.

180. Karagoz, B., C. Boyer, and T. P. Davis, "Simultaneous Polymerization-induced Self-assembly (PISA) and Guest Molecule Encapsulation", *Macromolecular Rapid Communications*, Vol. 35, pp. 417–421, 2014.

181. Karagoz, B., L. Esser, H. T. Duong, J. S. Basuki, C. Boyer, and T. P. Davis, "Polymerization-Induced Self-Assembly (PISA) - Control Over the Morphology of Nanoparticles for Drug Delivery Applications", *Polymer Chemistry*, Vol. 5, pp. 350–355, 2014.

182. Christian, D. A., S. Cai, O. B. Garbuzenko, T. Harada, A. L. Zajac, T. Minko, and D. E. Discher, "Flexible Filaments for in vivo Imaging and Delivery: Persistent Circulation of Filomicelles Opens the Dosage Window for Sustained Tumor Shrinkage", *Molecular Pharmaceutics*, Vol. 6, pp. 1343–1352, 2009.

183. Park, J. H., G. Von Maltzahn, L. Zhang, M. P. Schwartz, E. Ruoslahti, S. N. Bhatia, and M. J. Sailor, “Magnetic Iron Oxide Nanoworms for Tumor Targeting and Imaging”, *Advanced Materials*, Vol. 20, pp. 1630–1635, 2008.

184. Arnida, M.M. Janat-Amsbury, A. Ray, C.M. Peterson, and H. Ghandehari, “Geometry and Surface Characteristics of Gold Nanoparticles Influence Their Biodistribution and Uptake by Macrophages”, *European Journal of Pharmaceutics and Biopharmaceutics*, Vol. 77, pp. 417–423, 2011.

185. Tian, Y., S. Bian, and W. Yang, “A Redox-labile Poly(oligo(ethylene Glycol)methacrylate)-based Nanogel with Tunable Thermosensitivity for Drug Delivery”, *Polym. Chem.*, Vol. 7, pp. 1913–1921, 2016.

186. Rieger, J., “The Glass Transition Temperature Of Polystyrene.”, *Journal of Thermal Analysis*, Vol. 46, pp. 965–972, 1996.

187. Roth, J. A., M. L. Kaeberle, and W. H. Hsu, “Effect of Estradiol and Progesterone on Lymphocyte and Neutrophil Functions in Steers”, *Infection and Immunity*, Vol. 35, pp. 997–1002, 1982.

188. Chen, L.Ts. and L. Weiss, "The Role of the Sinus Wall in the Passage of Eryhtrocytes Through the Spleen", *Blood*, Vol. 41, pp. 529-537, 1973.

189. Cabral, H., Y. Matsumoto, K. Mizuno, Q. Chen, M. Murakami, M. Kimura, Y. Terada, M. R. Kano, K. Miyazono, M. Uesaka, N. Nishiyama, and K. Kataoka, “Accumulation of Sub-100 nm Polymeric Micelles in Poorly Permeable Tumours Depends on Size”, *Nature Nanotechnology*, Vol. 6, pp. 815–823, 2011.

190. Zhang, G., Z. Yang, W. Lu, R. Zhang, Q. Huang, M. Tian, L. Li, D. Liang, and C. Li, “Influence of Anchoring Ligands and Particle Size on The Colloidal Stability and in vivo Biodistribution of Polyethylene Glycol-coated Gold Nanoparticles in Tumor-xenografted Mice”, *Biomaterials*, Vol. 30, pp. 1928–1936, 2009.

191. Taylor, M. J., S. Tanna, and T. Sahota, "In vivo Study of a Polymeric Glucose-sensitive Insulin Delivery System using a Rat Model", *Journal of Pharmaceutical Sciences*, Vol. 99, pp. 4215–4227, 2010.

192. Eliezar, J., W. Scarano, N. R. B. Boase, K. J. Thurecht, and M. H. Stenzel, "In vivo Evaluation of Folate Decorated Cross-linked Micelles for The Delivery of Platinum Anticancer Drugs", *Biomacromolecules*, Vol. 16, pp. 515–523, 2015.

193. Mullner, M., D. Mehta, C. J. Nowell, and C. J. H. Porter, "Passive Tumour Targeting and Extravasation of Cylindrical Polymer Brushes in Mouse Xenografts", *Chem. Commun.*, pp. 9121–9124, 2016.

194. Ho, K. S., and M. S. Shoichet, "Design Considerations of Polymeric Nanoparticle Micelles for Chemotherapeutic Delivery", *Current Opinion in Chemical Engineering*, Vol. 2, pp. 53–59, 2013.

195. Cai, K., X. He, Z. Song, Q. Yin, Y. Zhang, F.M. Uckun, C. Jiang, and J. Cheng, "Dimeric Drug Polymeric Nanoparticles with Exceptionally High Drug Loading and Quantitative Loading Efficiency", *Journal of the American Chemical Society*, Vol. 137, pp. 3458–3461, 2015.

196. Deng, X., Y. Liang, X. Peng, T. Su, S. Luo, J. Cao, Z. Gu, and B. He, "A Facile Strategy to Generate Polymeric Nanoparticles for Synergistic Chemo-photodynamic Therapy", *Chem. Commun.*, Vol. 2000, pp. 2–5, 2015.

197. Huynh, V. T., J. Y. Quek, P. L. De Souza, and M. H. Stenzel, "Block Copolymer Micelles with Pendant Bifunctional Chelator for Platinum Drugs: Effect of Spacer Length on the Viability of Tumor Cells", *Biomacromolecules*, Vol. 13, pp. 1010–1023, 2012.

198. Segal, E., and R. Satchi-fainaro, "Design and Development of Polymer Conjugates as Anti-angiogenic Agents", *Advanced Drug Delivery Reviews*, Vol. 61, pp. 1159–1176, 2009.

199. Warren, N. J., O. O. Mykhaylyk, D. Mahmood, A. J. Ryan, and S. P. Armes, "RAFT Aqueous Dispersion Polymerization Yields Poly(ethylene Glycol)-based Diblock Copolymer Nano-objects with Predictable Single Phase Morphologies", *Journal of the American Chemical Society*, Vol. 136, pp. 1023–1033, 2014.

200. Arnaoutova, I., and H. K. Kleinman, "In vitro Angiogenesis: Endothelial Cell Tube Formation on Gelled Basement Membrane Extract", *Nature Protocols*, Vol. 5, pp. 628–635, 2010.

201. Danhier, F., O. Feron, and V. Preat, "To Exploit the Tumor Microenvironment: Passive and Active Tumor Targeting of Nanocarriers for Anti-cancer Drug Delivery", *Journal of Controlled Release*, Vol. 148, pp. 135–146, 2010.

202. Moghimi, S. M., A. C. Hunter, and J. C. Murray, "Long-Circulating and Target-specific Nanoparticles : Theory To Practice", *Pharmacological Reviews*, Vol. 53, pp. 283–318, 2001.

203. Alexis, F., E. Pridgen, L. K. Molnar, and O. C. Farokhzad, "Factors Affecting the Clearance and Biodistribution of Polymeric Nanoparticles", *Molecular Pharmaceutics*, Vol. 5, pp. 505–515, 2008.

204. Choi, H. S., W. Liu, P. Misra, E. Tanaka, J. P. Zimmer, B. Itty Ipe, M. G. Bawendi, and J. V. Frangioni, "Renal Clearance of Nanoparticles", *Nature Biotechnology*, Vol. 25, pp. 1165–1170, 2007.

205. Pisal, D.S., M.P. Kosloski, and S. V. Balu-Iyler, "Delivery of Therapeutic Proteins", *Journal of Pharmaceutical Sciences*, Vol. 99, pp. 1–33, 2011.

APPENDIX A: SPECTROSCOPY DATA

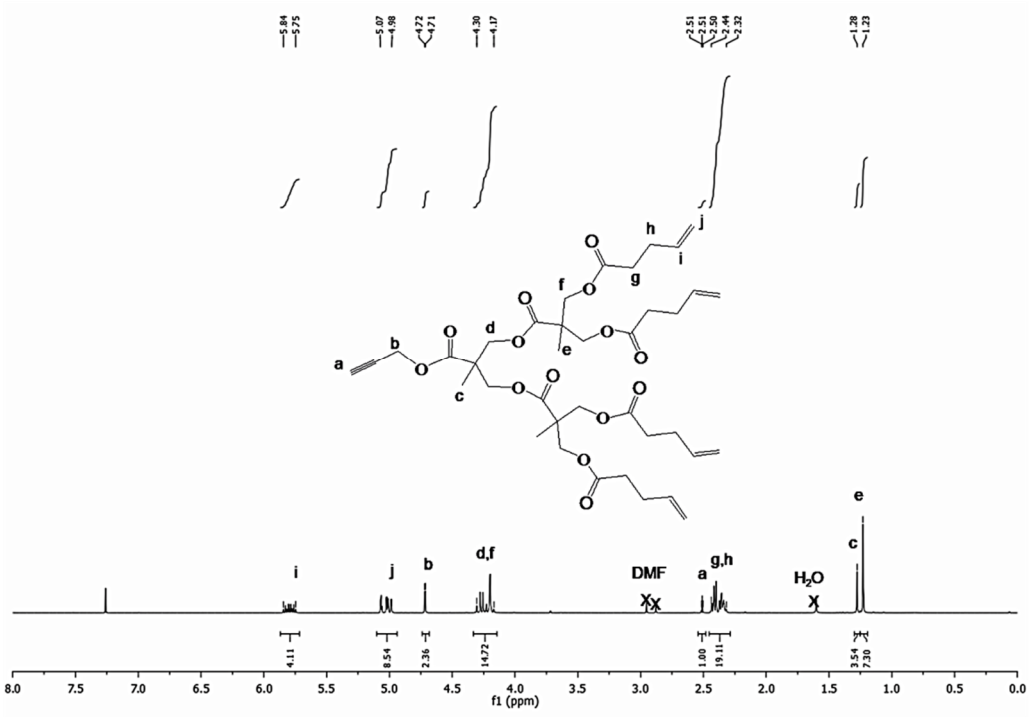


Figure A.1. ^{1}H NMR spectra of alkene functionalized G2 dendron 4.

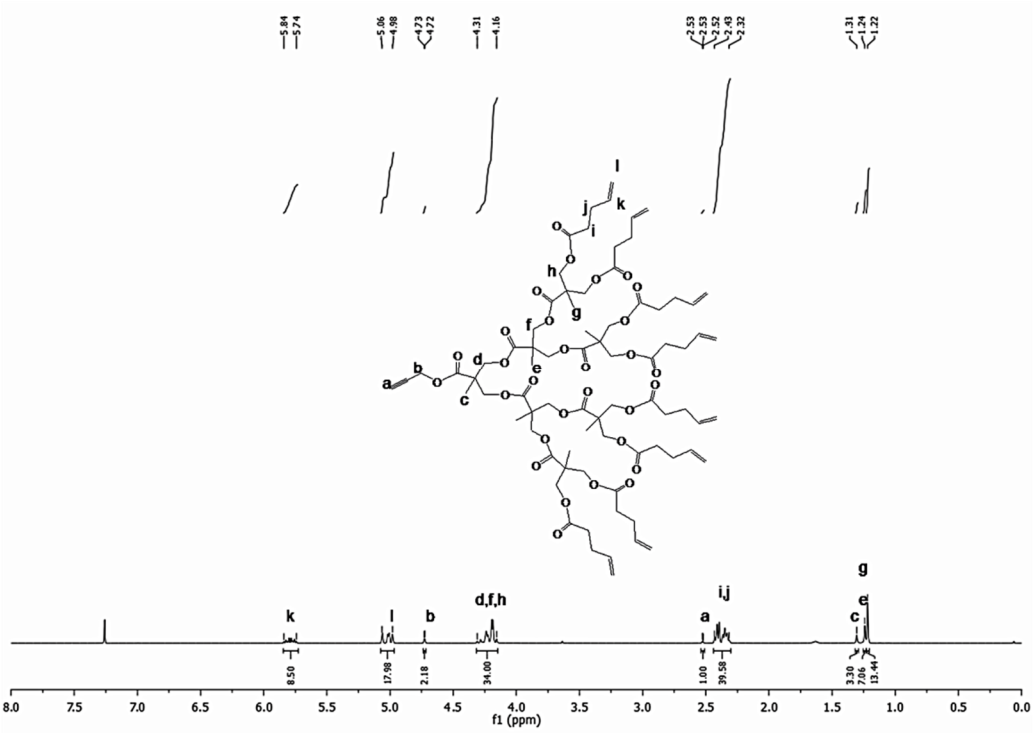


Figure A.2. ^{1}H NMR spectra of alkene functionalized G3 dendron 5.

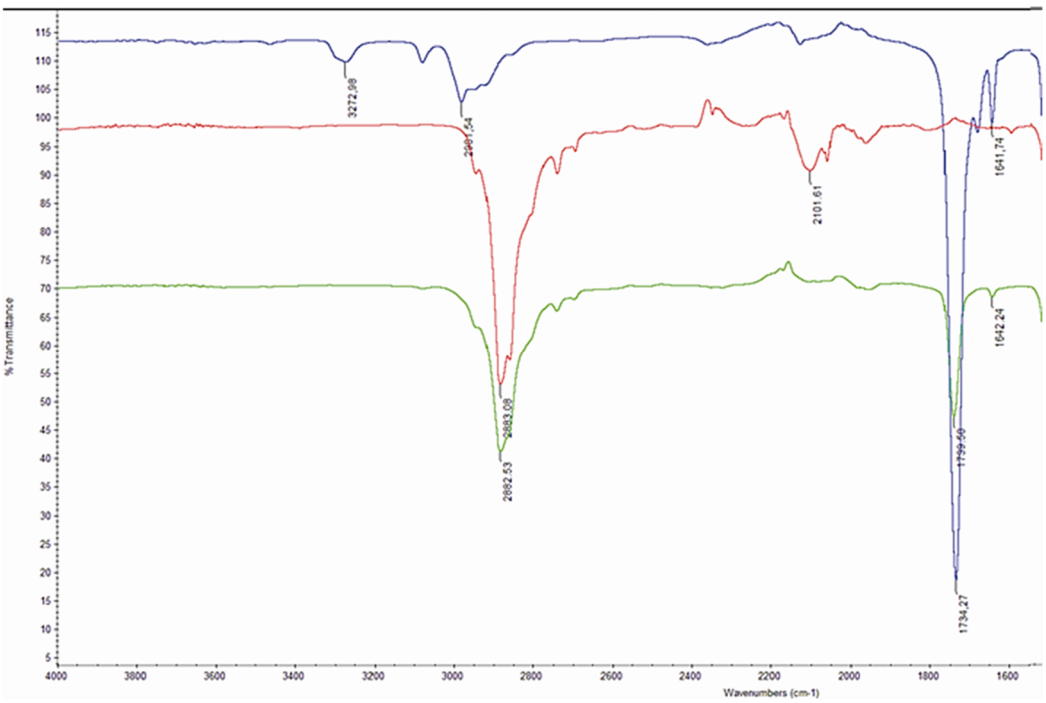


Figure A.3. FTIR spectra of alkene functionalized G2 dendron 4 (blue), PEG-6K bis-azide 6 (red), dendron-polymer conjugate G2PEG6K 8 (green).

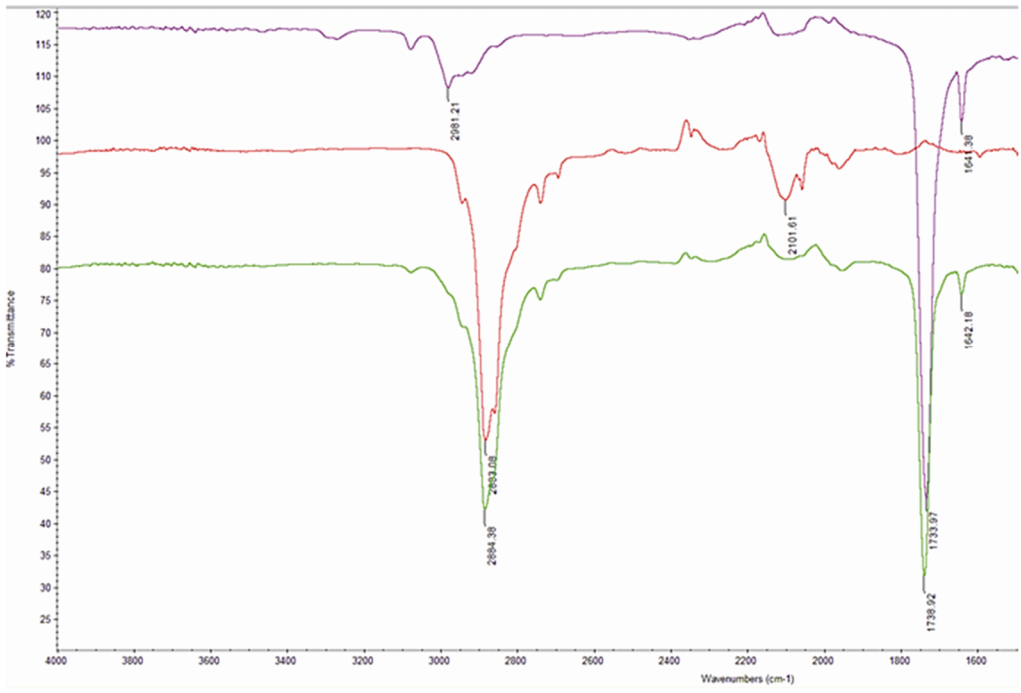


Figure A.4. FTIR spectra of alkene functionalized G3 dendron 5 (purple), PEG-6K bis-azide 6 (red), dendron-polymer conjugate G3PEG6K 9 (green).

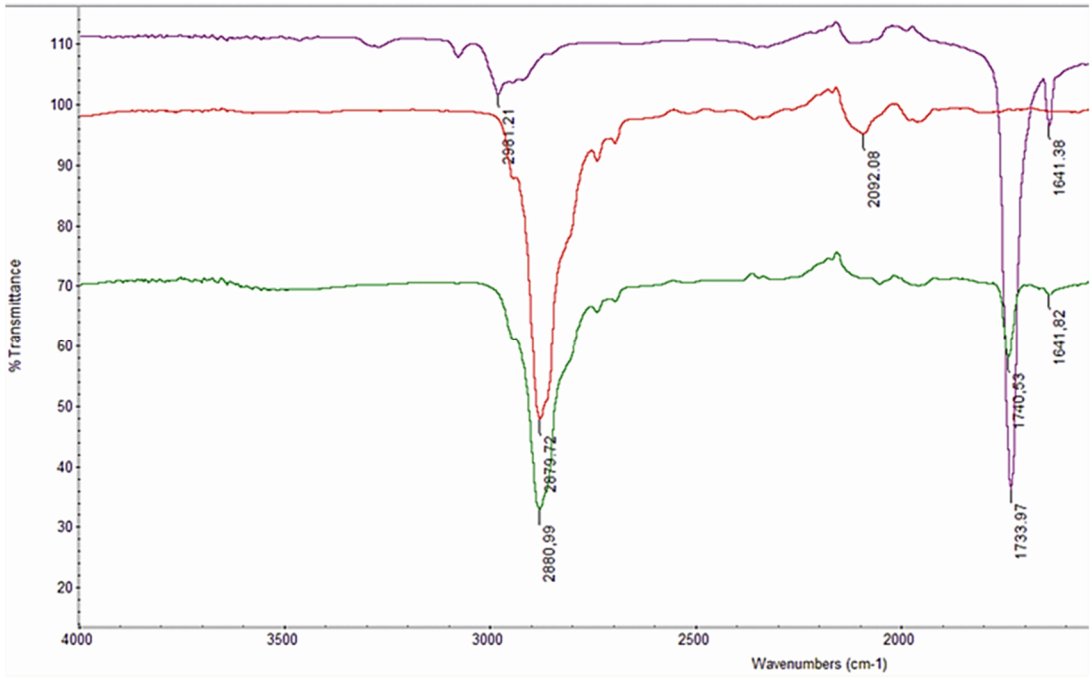


Figure A.5. FTIR spectra of alkene functionalized G3 dendron 5 (purple), PEG-20K bis-azide 7 (red), dendron-polymer conjugate G3PEG20K 10 (green).

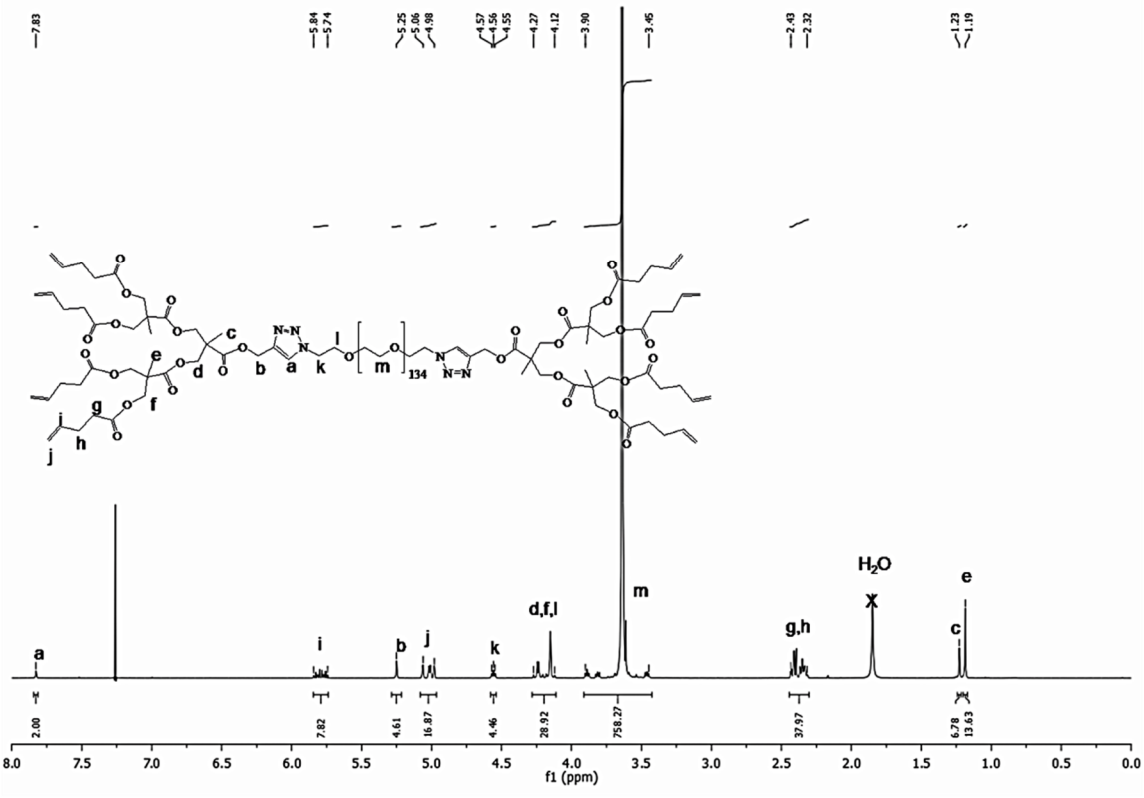


Figure A.6. ^{1}H NMR spectra of dendron-polymer conjugate G2PEG6K 8.

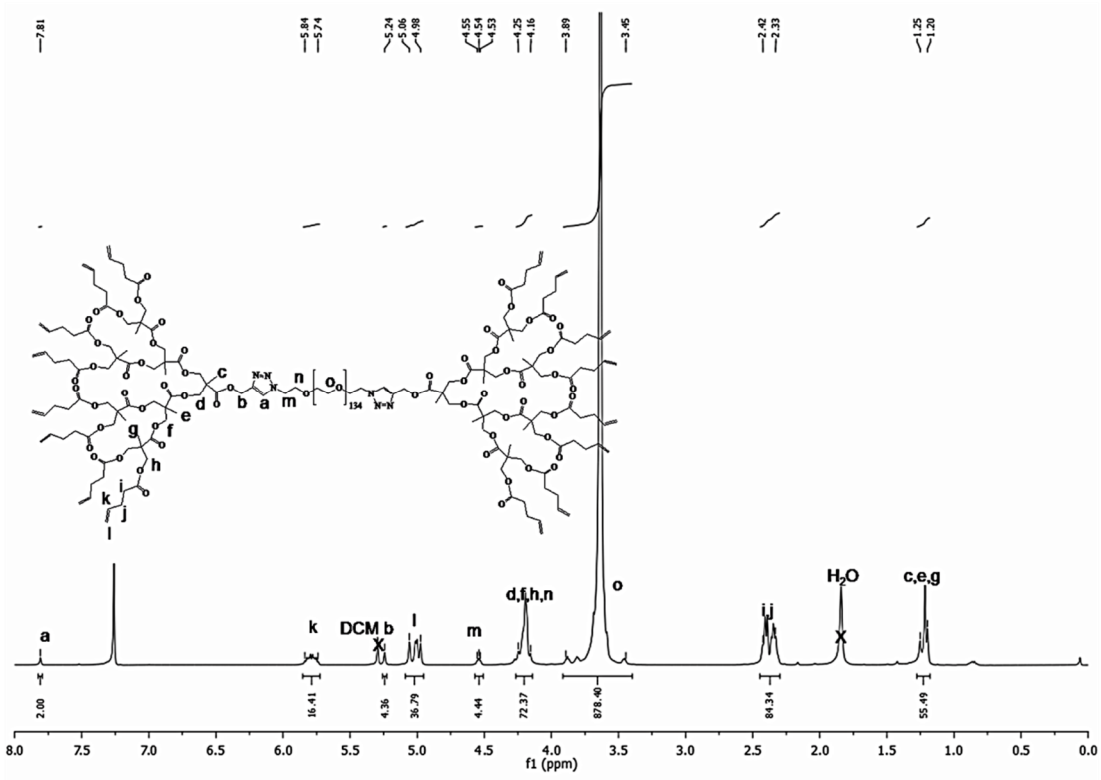


Figure A.7. ^{1}H NMR spectra of dendron-polymer conjugate G3PEG6K 9.

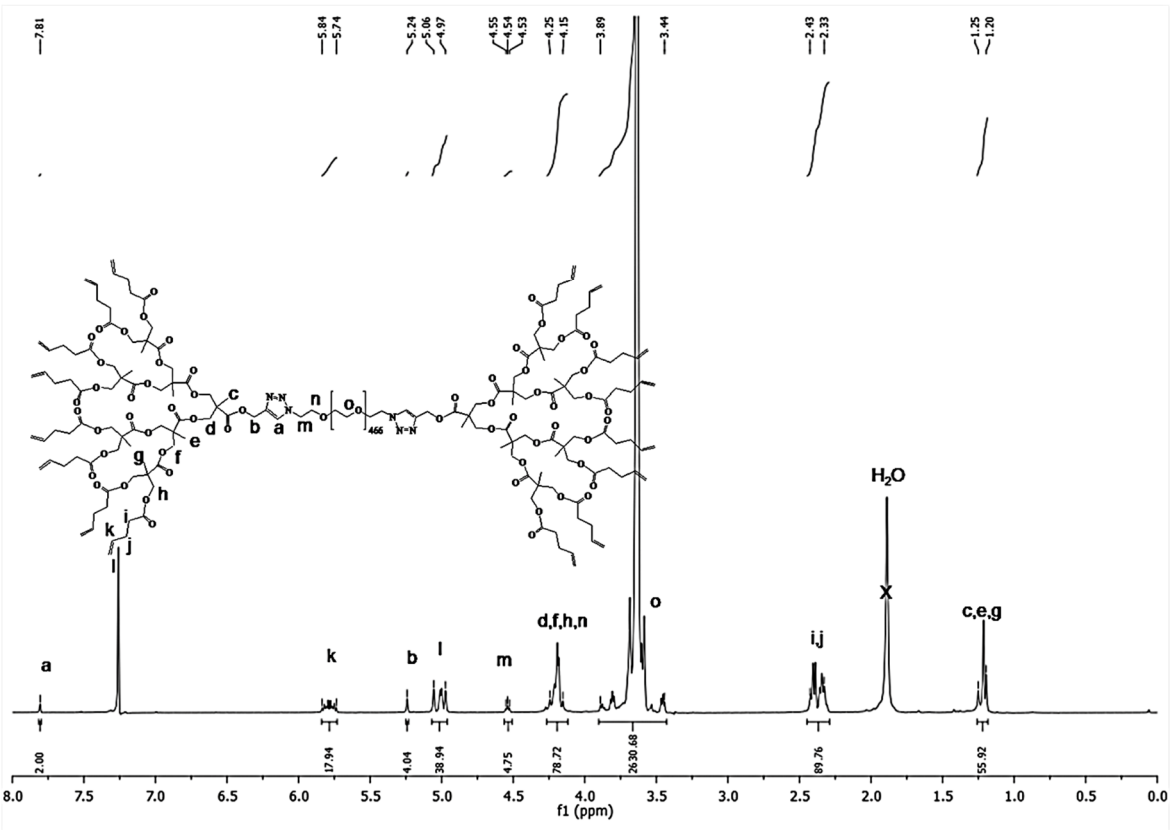
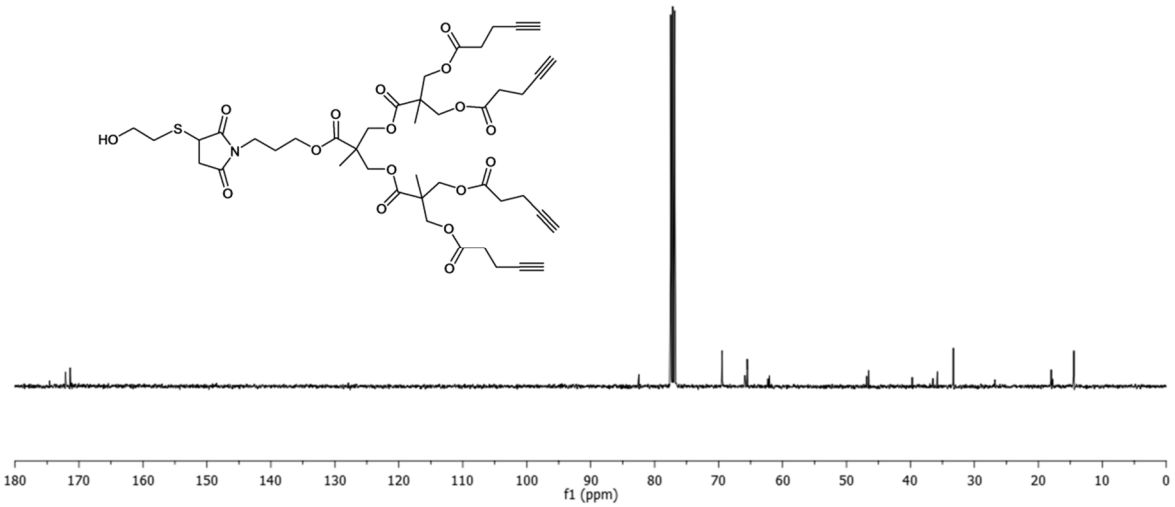


Figure A.8. ^{1}H NMR spectra of dendron-polymer conjugate G3PEG20K 10.


HO
S
N
O
O
O

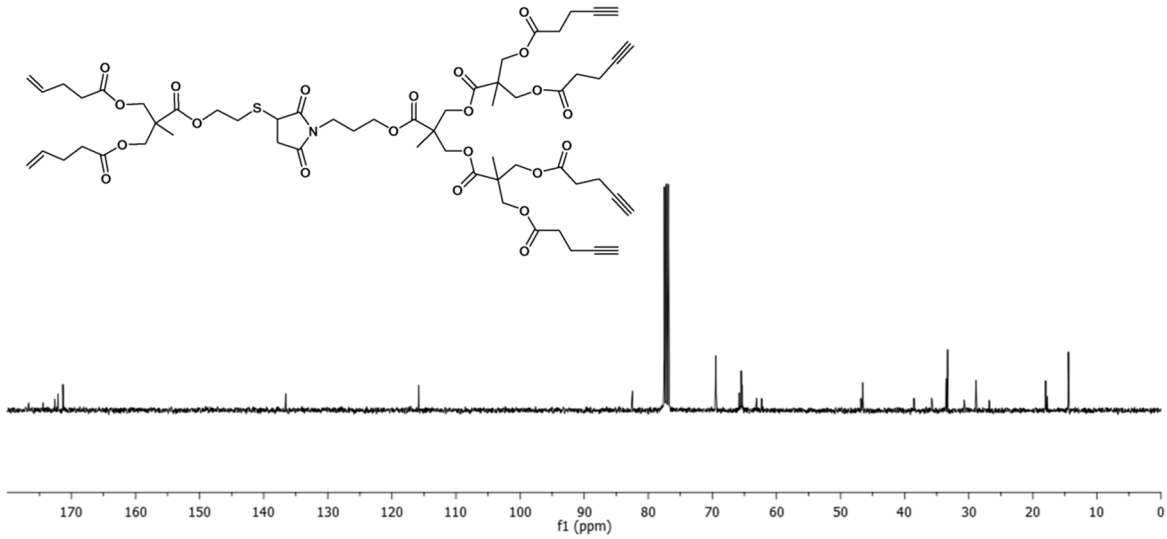


Figure A.11. ^{13}C NMR spectra G2[4 alkyne]-G1[2 alkene].

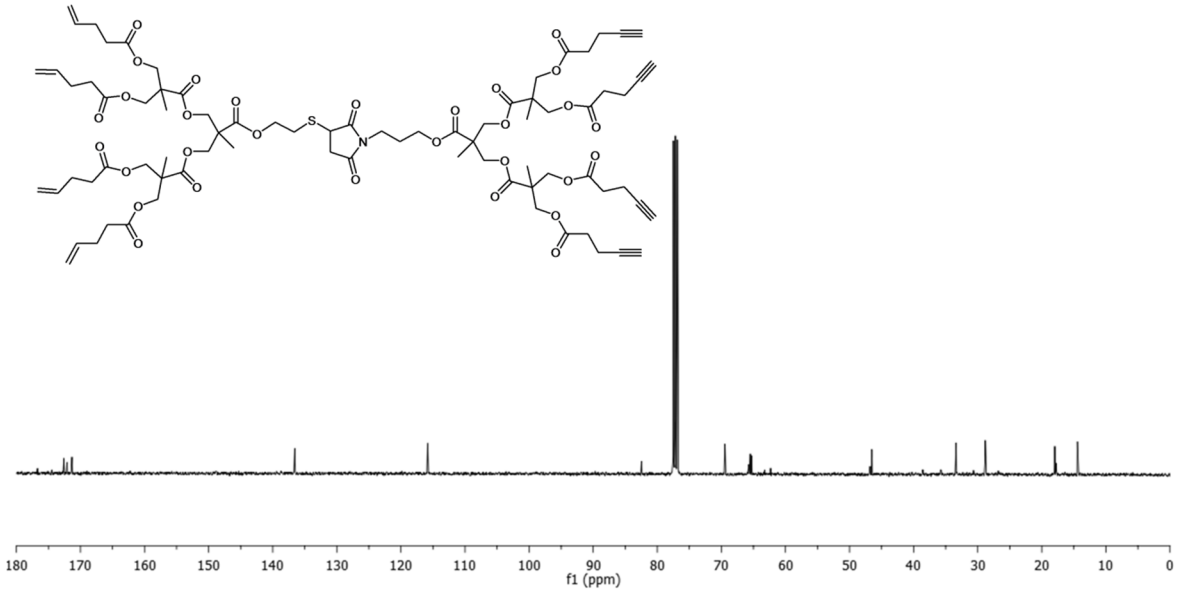


Figure A.12. ^{13}C NMR spectra G2[4 alkyne]-G2[4 alkene].

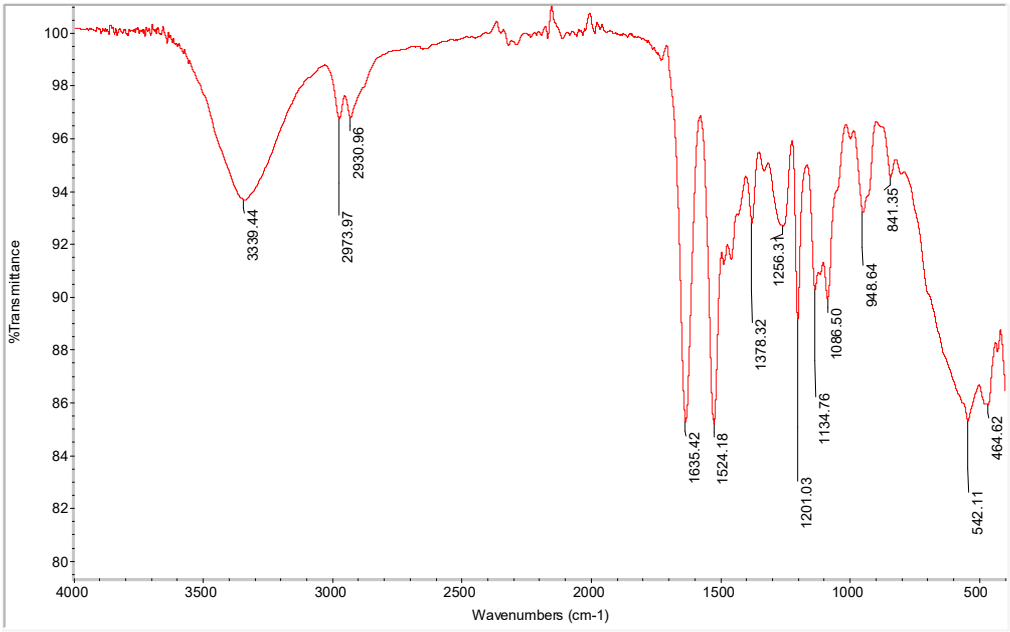


Figure A.13. FTIR spectra of PHPMA-DTX (52 kDa).

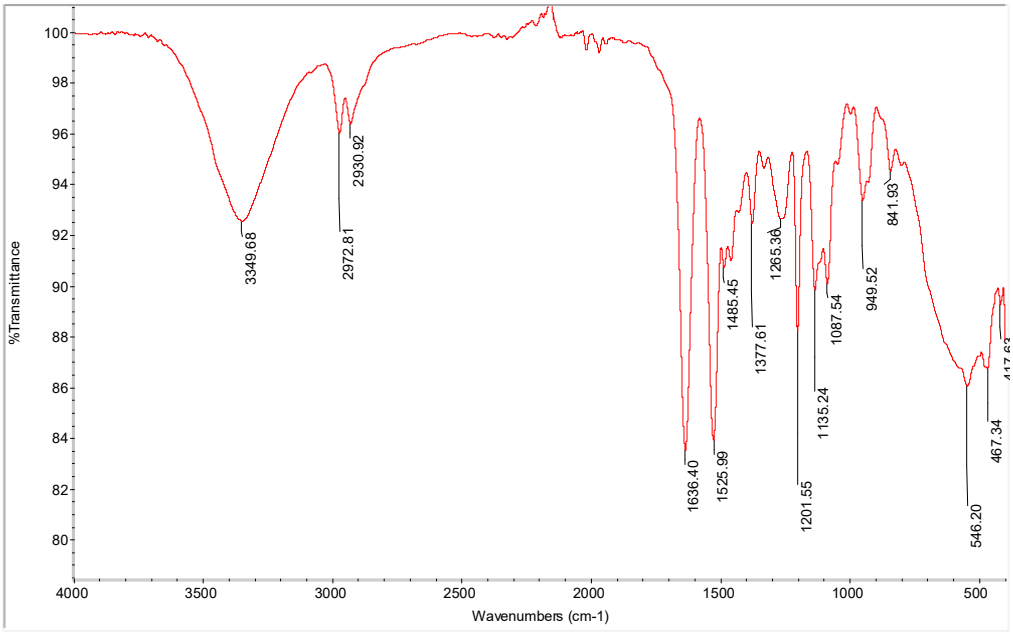


Figure A.14. FTIR spectra of PHPMA-DTX (85 kDa).

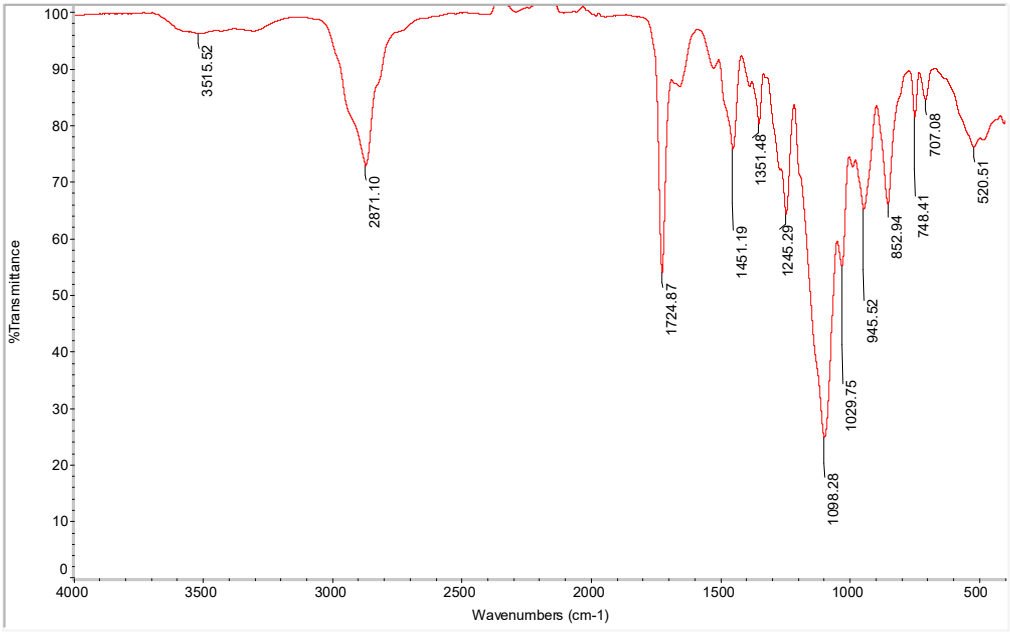


Figure A.15. FTIR spectra of POEGMEMA-DTX (50 kDa).

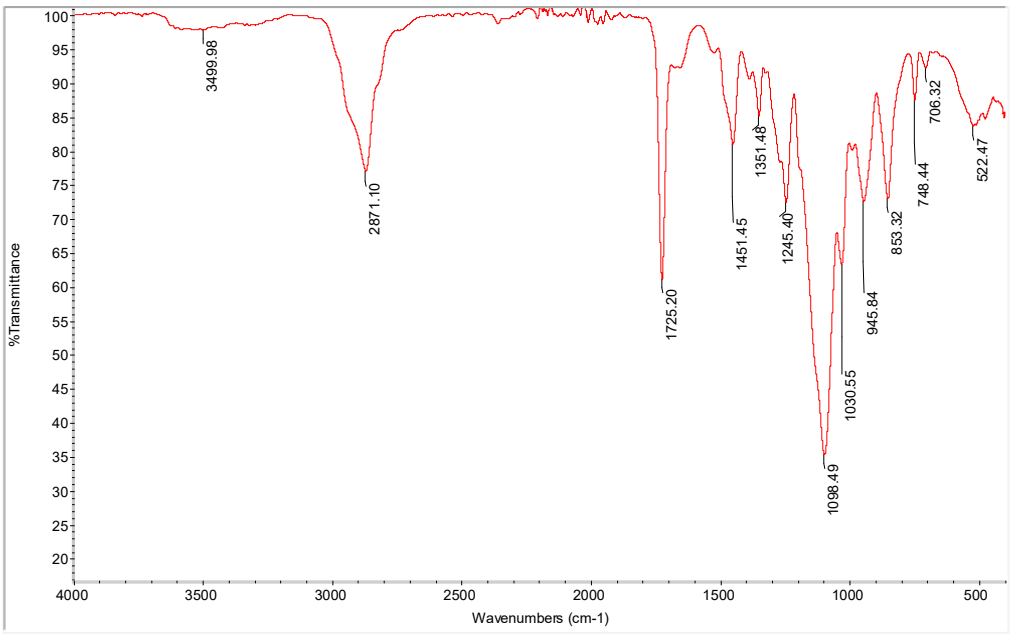


Figure A.16. FTIR spectra of POEGMEMA-DTX (85 kDa).

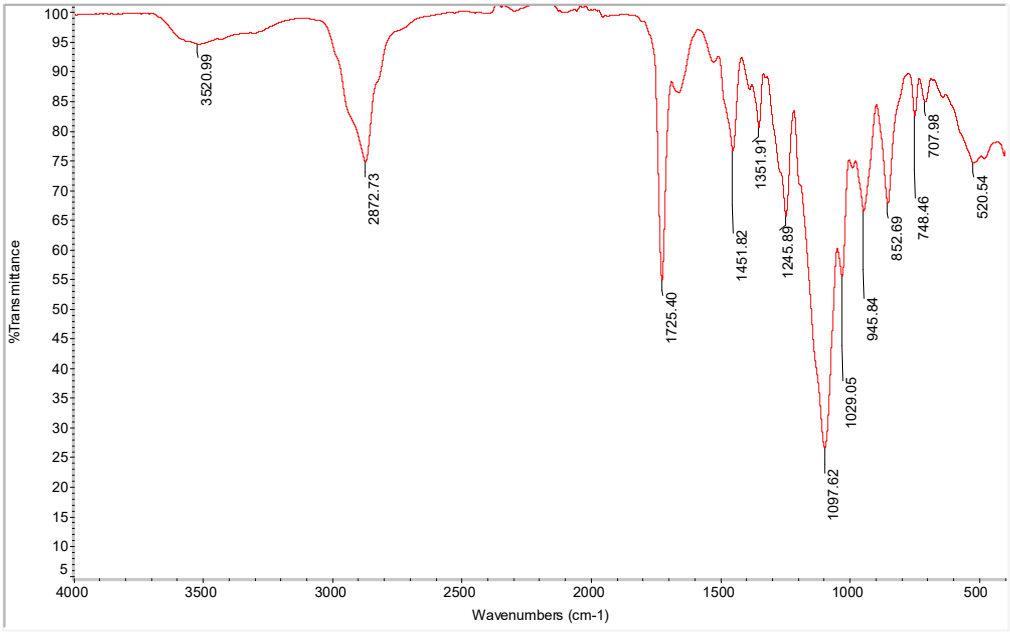


Figure A.17. FTIR spectra of POEGMEMA-DTX-NHS (43 kDa).

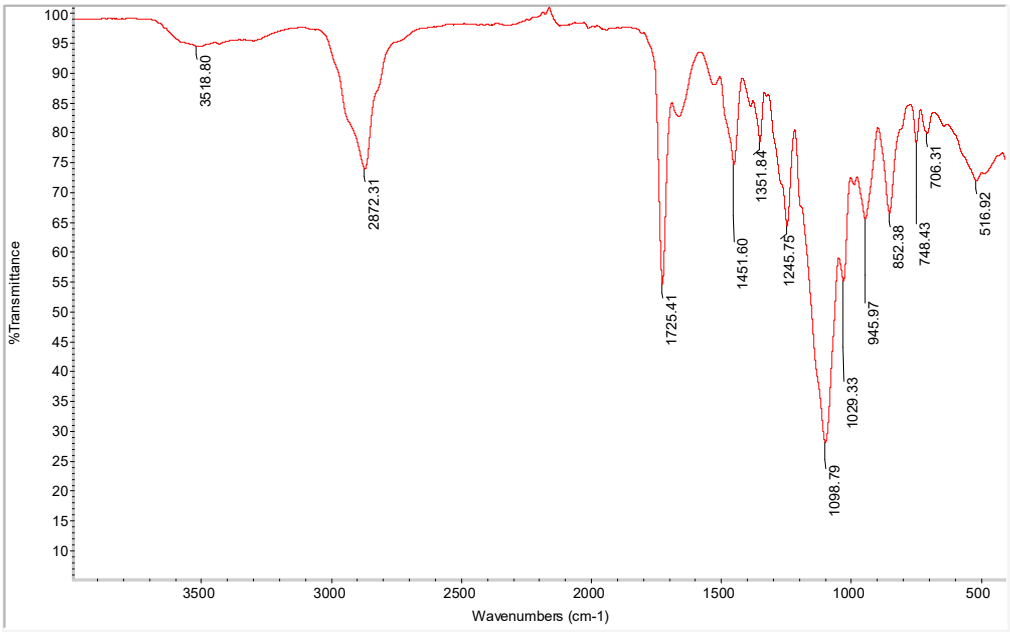


Figure A.18. FTIR spectra of POEGMEMA-DTX-cRGDfK (43 kDa).

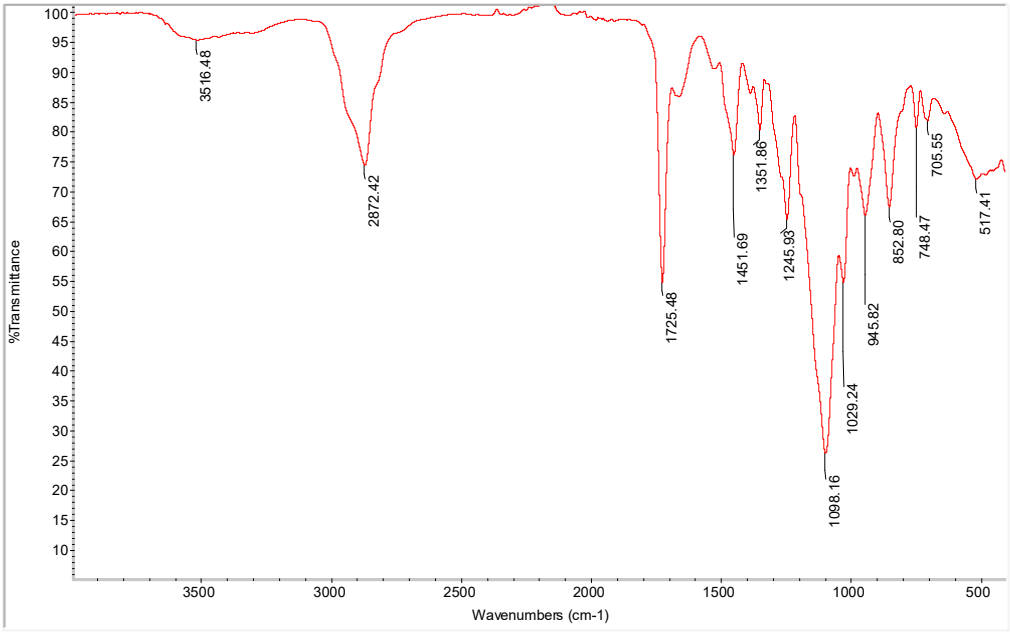


Figure A.19. FTIR spectra of POEGMEMA-DTX (43 kDa).

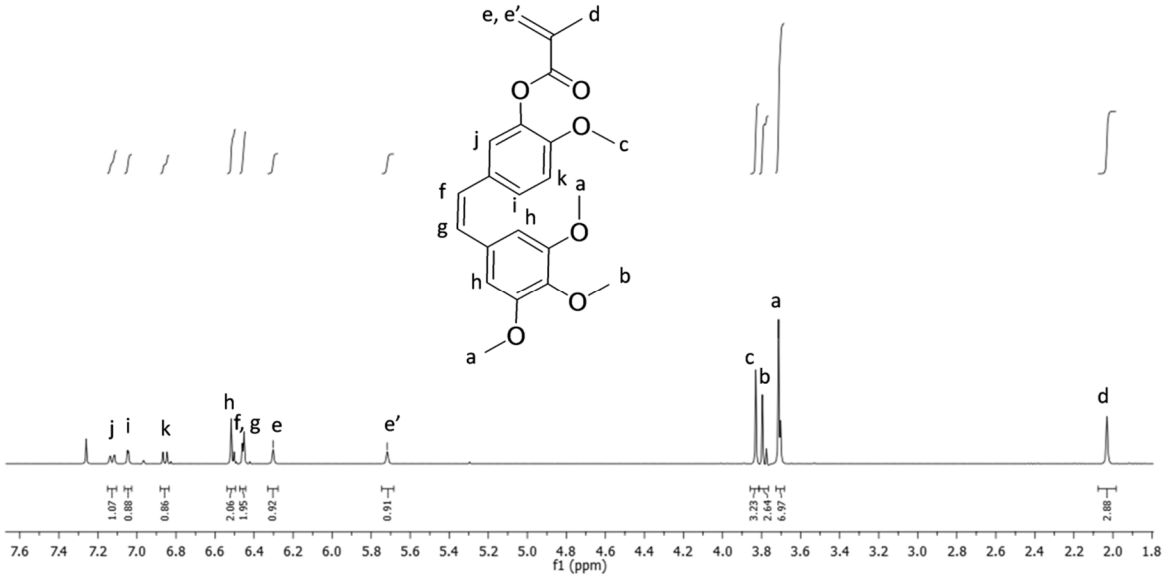


Figure A.20. ^{1}H NMR spectra of CombMA.

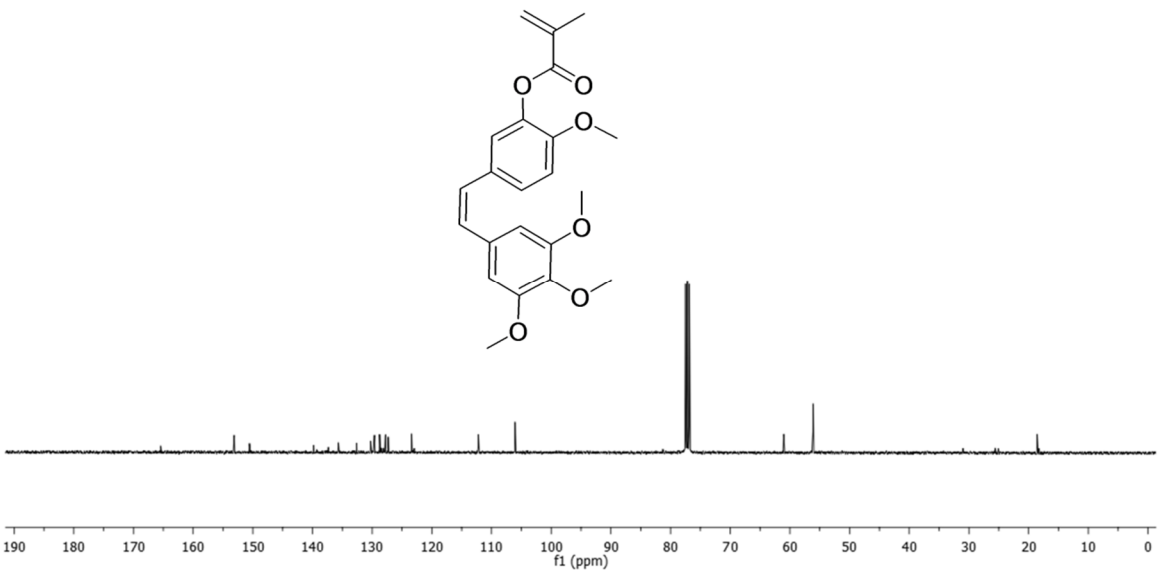


Figure A.21. ^{13}C NMR spectra of CombMA.

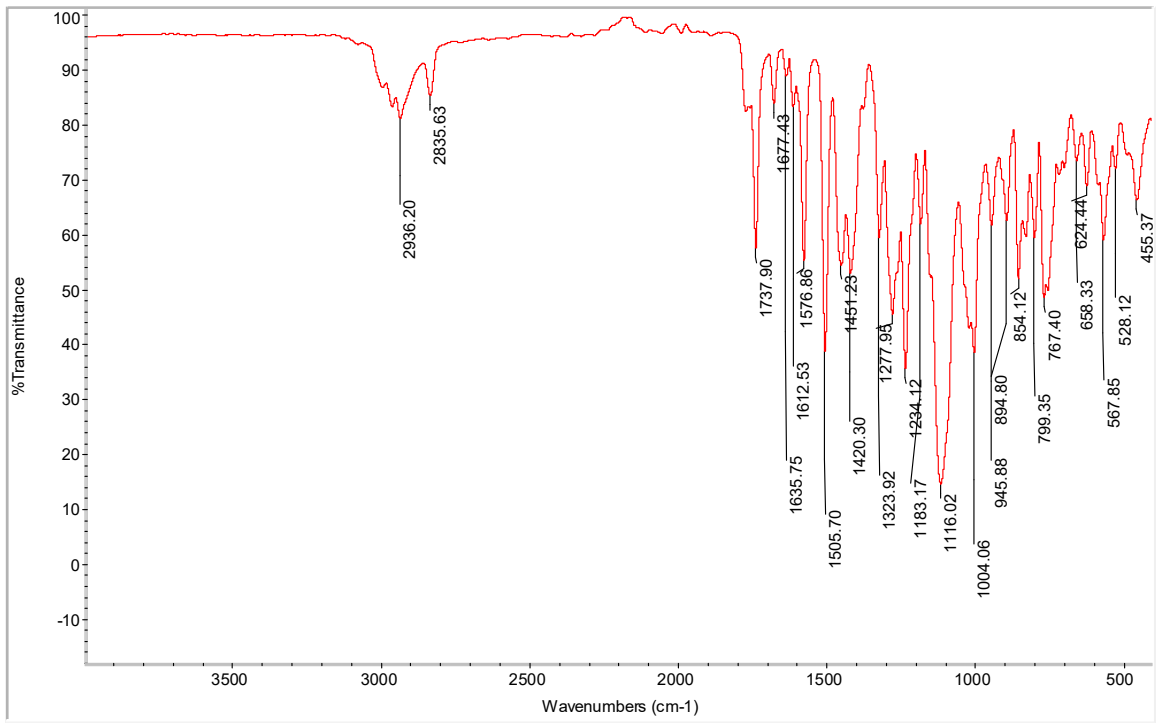


Figure A.22. FTIR spectra of CombMA.

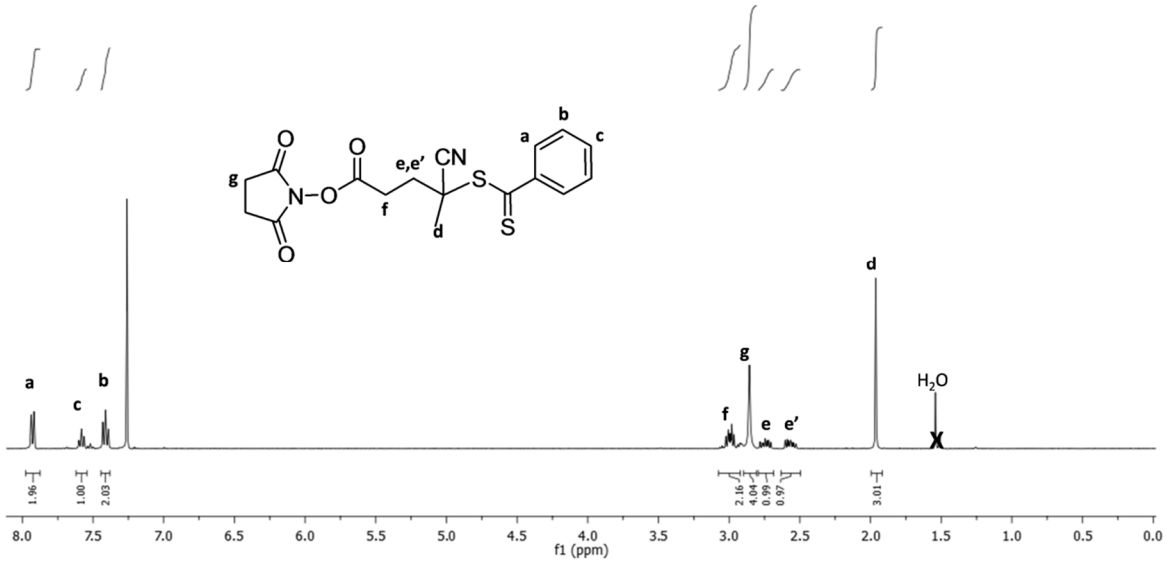


Figure A.23. ^{1}H NMR spectra of SCPDB.

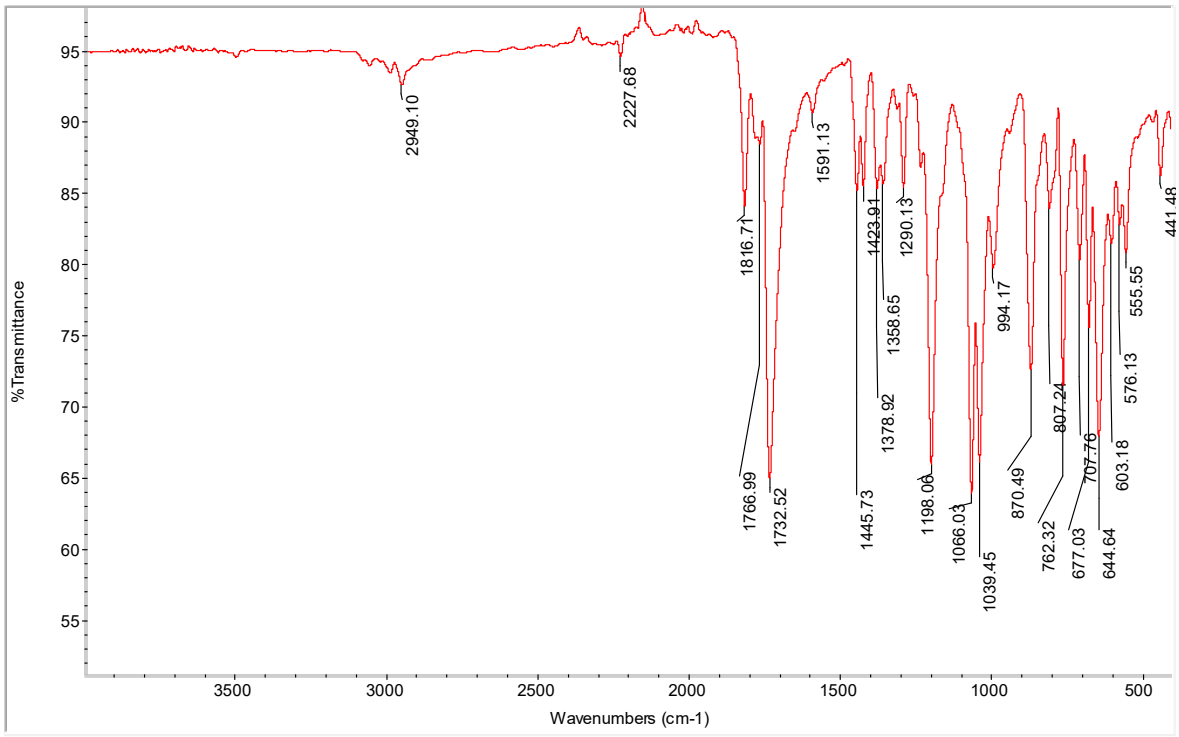


Figure A.24. FTIR spectra of SCPDB.

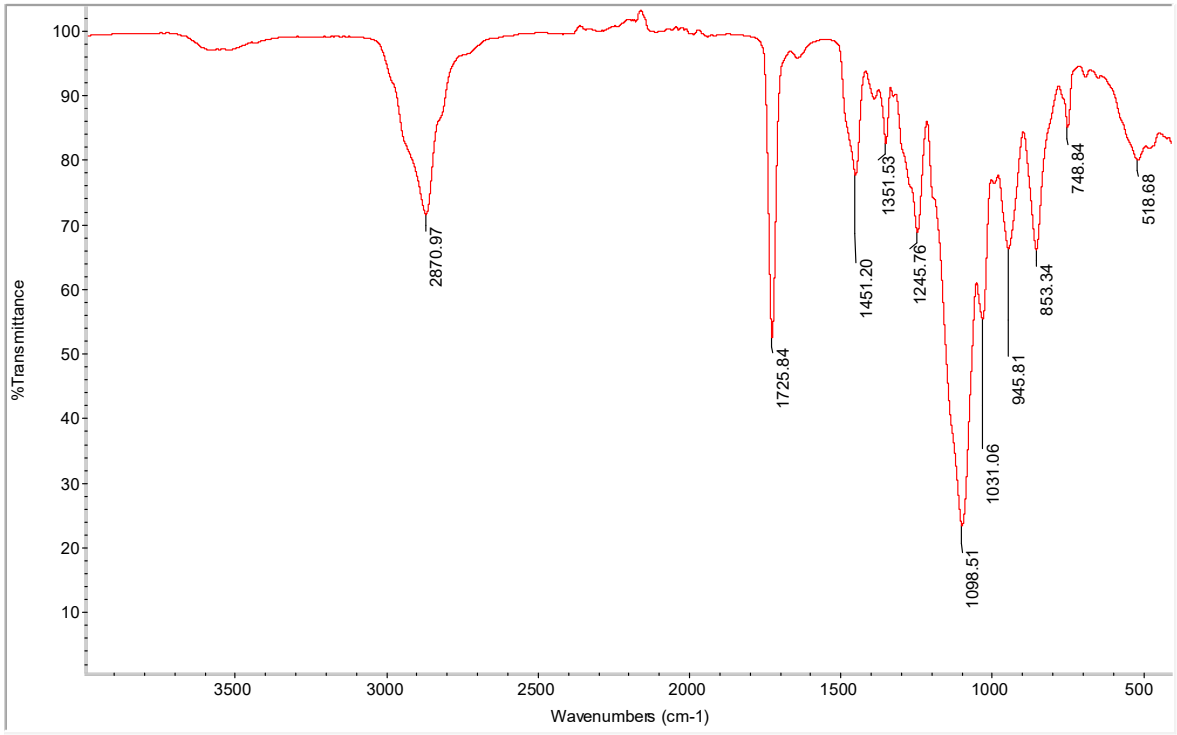


Figure A.25. FTIR spectra of POEGMEMA (7.7 kDa).

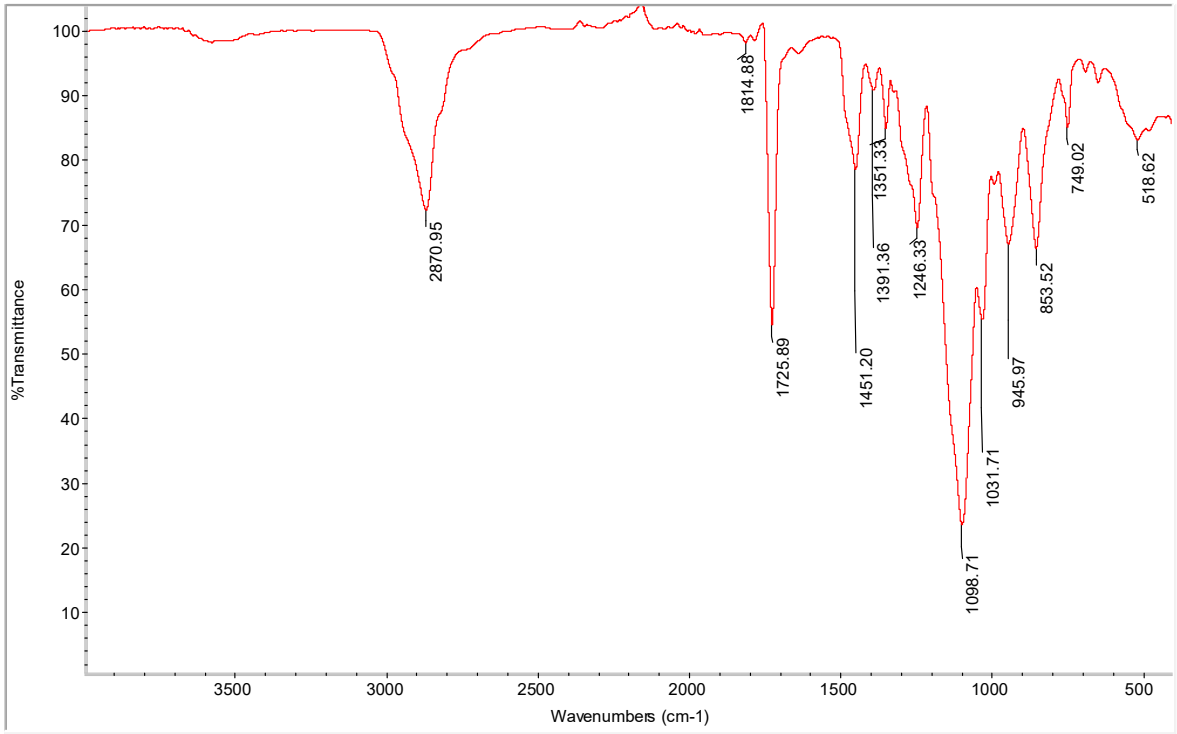


Figure A.26. FTIR spectra of NHS-POEGMEMA (7.1 kDa).

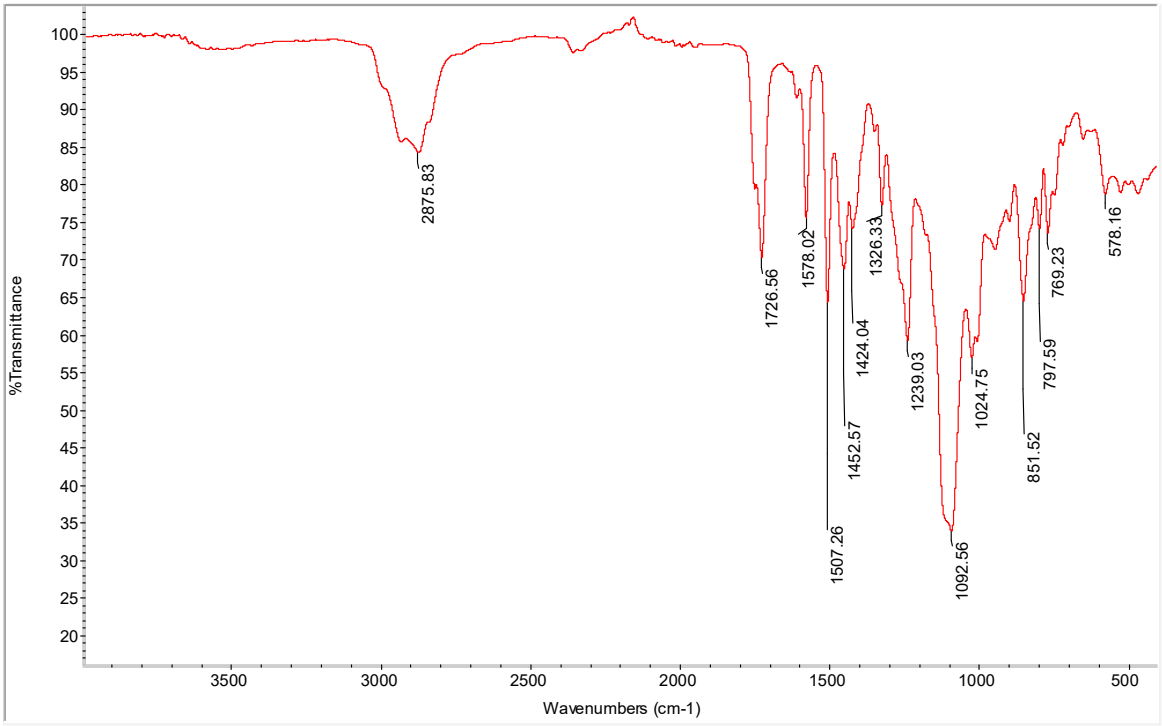


Figure A.27. FTIR spectra of POEGMEMA-*b*-PCombMA (11.2 kDa).

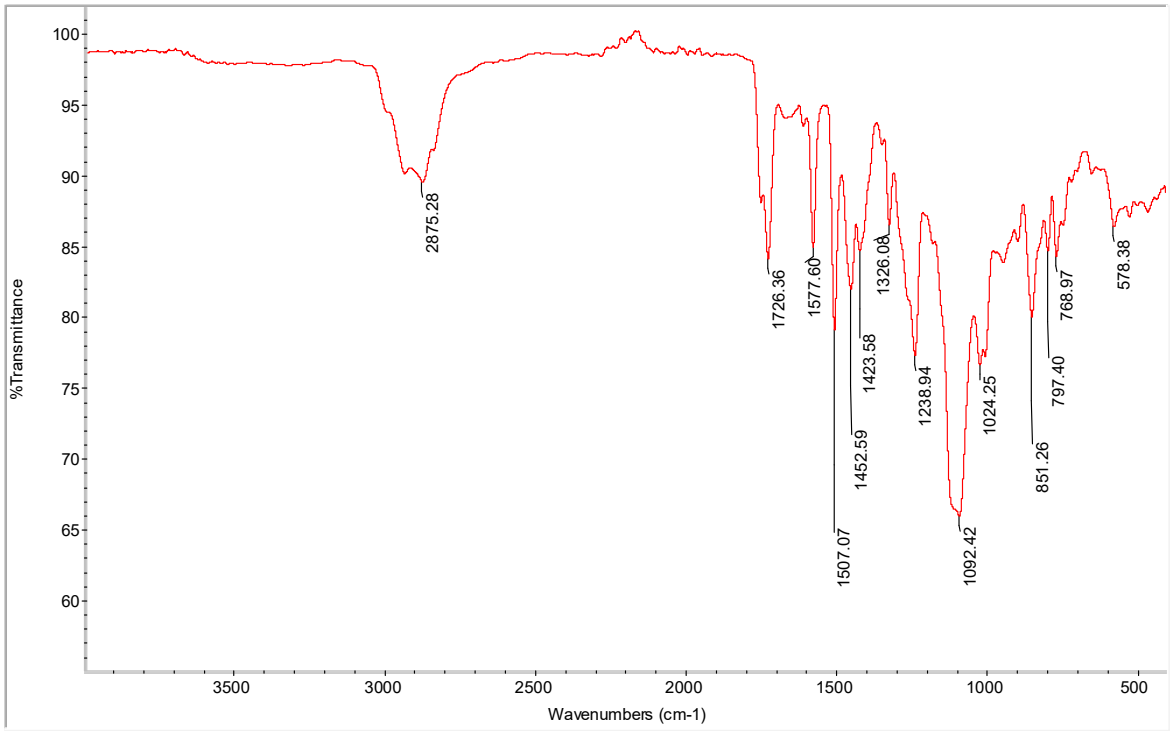


Figure A.28. FTIR spectra of NHS-POEGMEMA-*b*-PCombMA (11.7 kDa).

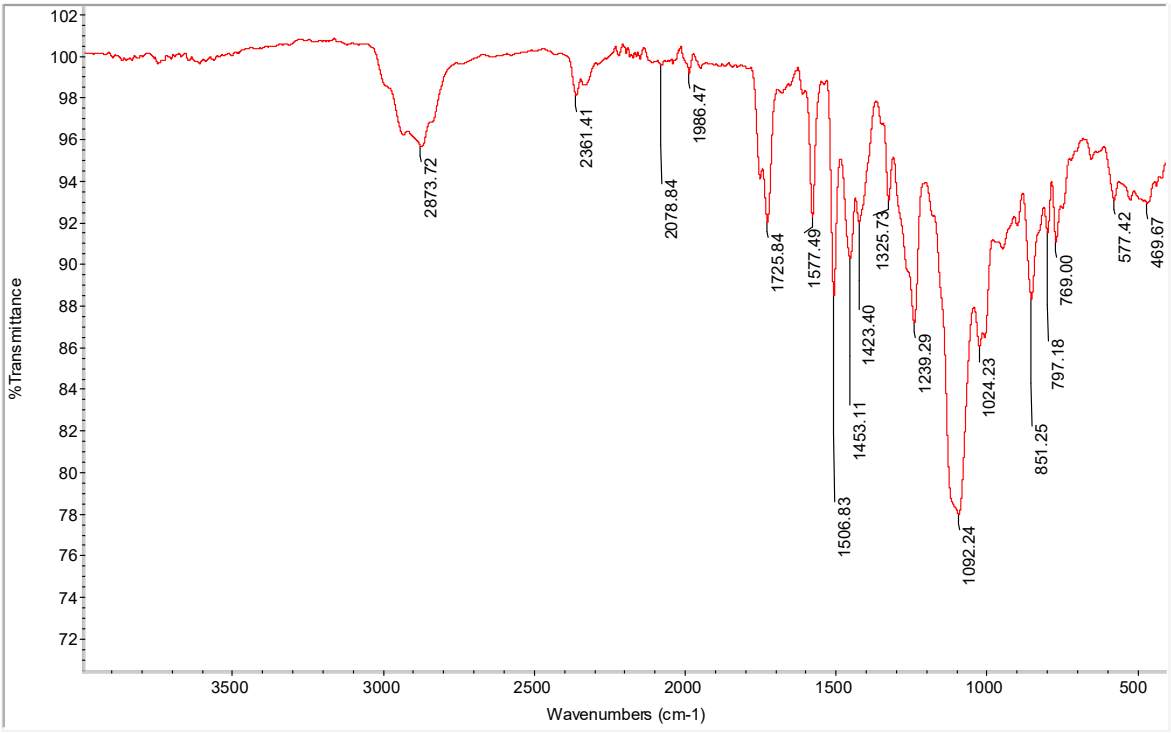


Figure A.29. FTIR spectra of cRGDfK-POEGMEMA-*b*-PCombMA (12.5 kDa).

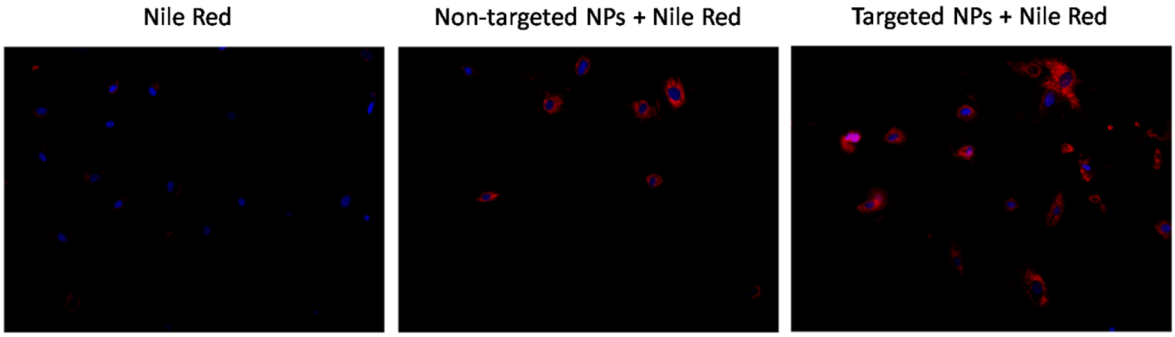


Figure A.30. Cell internalization of Nile Red doped polymeric nanoparticles and Nile Red dye only into the HUVECs. The resulting images were collected at 4 h. Cell nuclei were stained with DAPI (blue).

APPENDIX B: PERMISSIONS FOR FIGURES



23.09.2016 Rightslink® by Copyright Clearance Center

Copyright Clearance Center RightsLink® Home Account Info Help Live Chat

ACS Publications Most Trusted. Most Cited. Most Read.

Title: Fabrication of "Clickable" Hydrogels via Dendron–Polymer Conjugates

Author: Huseyin Altin, Irem Kosif, Rana Sanyal

Publication: Macromolecules

Publisher: American Chemical Society

Date: Apr 1, 2010

Copyright © 2010, American Chemical Society

Logged in as: Sadik Kaga
Account #: 3000999792
LOGOUT

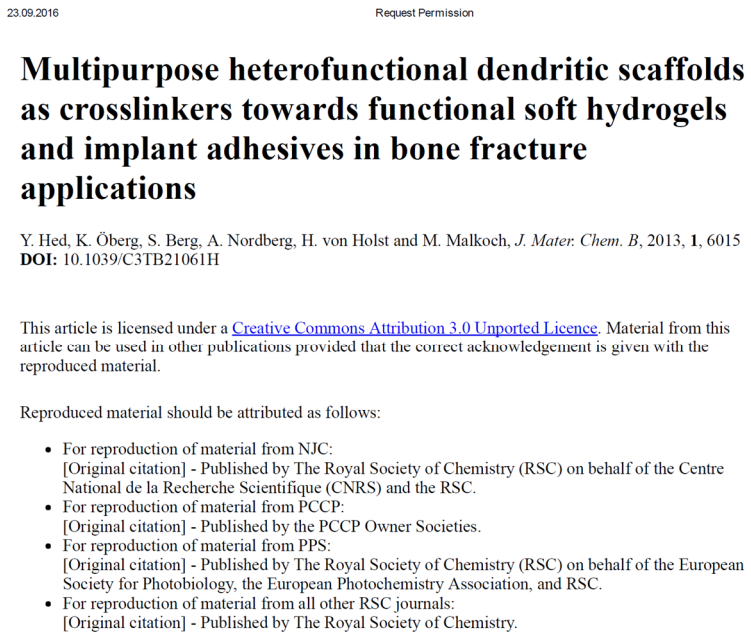
PERMISSION/LICENSE IS GRANTED FOR YOUR ORDER AT NO CHARGE

This type of permission/license, instead of the standard Terms & Conditions, is sent to you because no fee is being charged for your order. Please note the following:

- Permission is granted for your request in both print and electronic formats, and translations.
- If figures and/or tables were requested, they may be adapted or used in part.
- Please print this page for your records and send a copy of it to your publisher/graduate school.
- Appropriate credit for the requested material should be given as follows: "Reprinted (adapted) with permission from (COMPLETE REFERENCE CITATION). Copyright (YEAR) American Chemical Society." Insert appropriate information in place of the capitalized words.
- One-time permission is granted only for the use specified in your request. No additional uses are granted (such as derivative works or other editions). For any other uses, please submit a new request.

If credit is given to another source for the material you requested, permission must be obtained from that source.

Figure B.1. Permission for Figure 1.4.



23.09.2016 Request Permission

Multipurpose heterofunctional dendritic scaffolds as crosslinkers towards functional soft hydrogels and implant adhesives in bone fracture applications

Y. Hed, K. Öberg, S. Berg, A. Nordberg, H. von Holst and M. Malkoch, *J. Mater. Chem. B*, 2013, **1**, 6015
DOI: 10.1039/C3TB21061H

This article is licensed under a Creative Commons Attribution 3.0 Unported Licence. Material from this article can be used in other publications provided that the correct acknowledgement is given with the reproduced material.

Reproduced material should be attributed as follows:

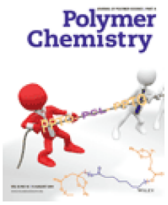
- For reproduction of material from NJC:
  [Original citation] - Published by The Royal Society of Chemistry (RSC) on behalf of the Centre National de la Recherche Scientifique (CNRS) and the RSC.
- For reproduction of material from PCCP:
  [Original citation] - Published by the PCCP Owner Societies.
- For reproduction of material from PPS:
  [Original citation] - Published by The Royal Society of Chemistry (RSC) on behalf of the European Society for Photobiology, the European Photochemistry Association, and RSC.
- For reproduction of material from all other RSC journals:
  [Original citation] - Published by The Royal Society of Chemistry.

Information about reproducing material from RSC articles with different licences is available on our Permission Requests page.

Figure B.2. Permission for Figure 1.5.

23.09.2016 Rightslink® by Copyright Clearance Center

Copyright Clearance Center RightsLink® Home Account Info Help Live Chat



Title: Dendritic hydrogels: From exploring various crosslinking chemistries to introducing functions and naturally abundant resources

Author: Surinthra Mongkhontreerat,Oliver C. J. Andrén,Assya Boujemaoui,Michael Malkoch

Publication: Journal of Polymer Science Part A: Polymer Chemistry

Publisher: John Wiley and Sons

Date: Jul 31, 2015

© 2015 Wiley Periodicals, Inc.

Logged in as:
Sadik Kaga
Account #:
3000999792
LOGOUT

Order Completed

Thank you for your order.

This Agreement between Sadik Kaga ("You") and John Wiley and Sons ("John Wiley and Sons") consists of your license details and the terms and conditions provided by John Wiley and Sons and Copyright Clearance Center.

Your confirmation email will contain your order number for future reference.

Get the printable license.

License Number	3954740107022
License date	Sep 23, 2016
Licensed Content Publisher	John Wiley and Sons
Licensed Content Publication	Journal of Polymer Science Part A: Polymer Chemistry
Licensed Content Title	Dendritic hydrogels: From exploring various crosslinking chemistries to introducing functions and naturally abundant resources
Licensed Content Author	Surinthra Mongkhontreerat,Oliver C. J. Andrén,Assya Boujemaoui,Michael Malkoch
Licensed Content Date	Jul 31, 2015
Licensed Content Pages	9
Type of use	Dissertation/Thesis
Requestor type	University/Academic
Format	Print and electronic
Portion	Figure/table
Number of figures/tables	3
Original Wiley figure/table number(s)	Figure 1, Figure 3, Figure 4
Will you be translating?	No
Title of your thesis / dissertation	Functionalizable Hydrogels and Water Soluble Constructs as Chemotherapy Drug Carriers
Expected completion date	Oct 2016
Expected size (number of pages)	220
Requestor Location	Sadik Kaga Boğaziçi Universitesi Kuzey Campus, Chemistry Department Istanbul, 34342 Turkey Attn: Sadik Kaga
Publisher Tax ID	EU826007151
Billing Type	Invoice
Billing address	

Figure B.3. Permission for Figure 1.6.

23.09.2016 Request Permission

Dual-purpose PEG scaffolds for the preparation of soft and biofunctional hydrogels: the convergence between CuAAC and thiol–ene reactions

K. Öberg, Y. Hed, I. Joelsson Rahmn, J. Kelly, P. Löwenhielm and M. Malkoch, *Chem. Commun.*, 2013, **49**, 6938
DOI: 10.1039/C3CC42084A

This article is licensed under a Creative Commons Attribution 3.0 Unported Licence. Material from this article can be used in other publications provided that the correct acknowledgement is given with the reproduced material.

Reproduced material should be attributed as follows:

- For reproduction of material from NJC:
  [Original citation] - Published by The Royal Society of Chemistry (RSC) on behalf of the Centre National de la Recherche Scientifique (CNRS) and the RSC.
- For reproduction of material from PCCP:
  [Original citation] - Published by the PCCP Owner Societies.
- For reproduction of material from PPS:
  [Original citation] - Published by The Royal Society of Chemistry (RSC) on behalf of the European Society for Photobiology, the European Photochemistry Association, and RSC.
- For reproduction of material from all other RSC journals:
  [Original citation] - Published by The Royal Society of Chemistry.

Information about reproducing material from RSC articles with different licences is available on our Permission Requests page.

Figure B.4. Permission for Figure 1.7.

24.09.2016 Rightslink® by Copyright Clearance Center

Copyright Clearance Center RightsLink® Home Account Info Help Live Chat

ACS Publications Most Trusted. Most Cited. Most Read.

Title: Biodendrimer-Based Hydrogel Scaffolds for Cartilage Tissue Repair
Author: Serge H. M. Söntjens, Dana L. Nettles, Michael A. Carnahan, et al
Publication: Biomacromolecules
Publisher: American Chemical Society
Date: Jan 1, 2006
Copyright © 2006, American Chemical Society

Logged in as: Sadik Kaga
Account #: 3000999792
LOGOUT

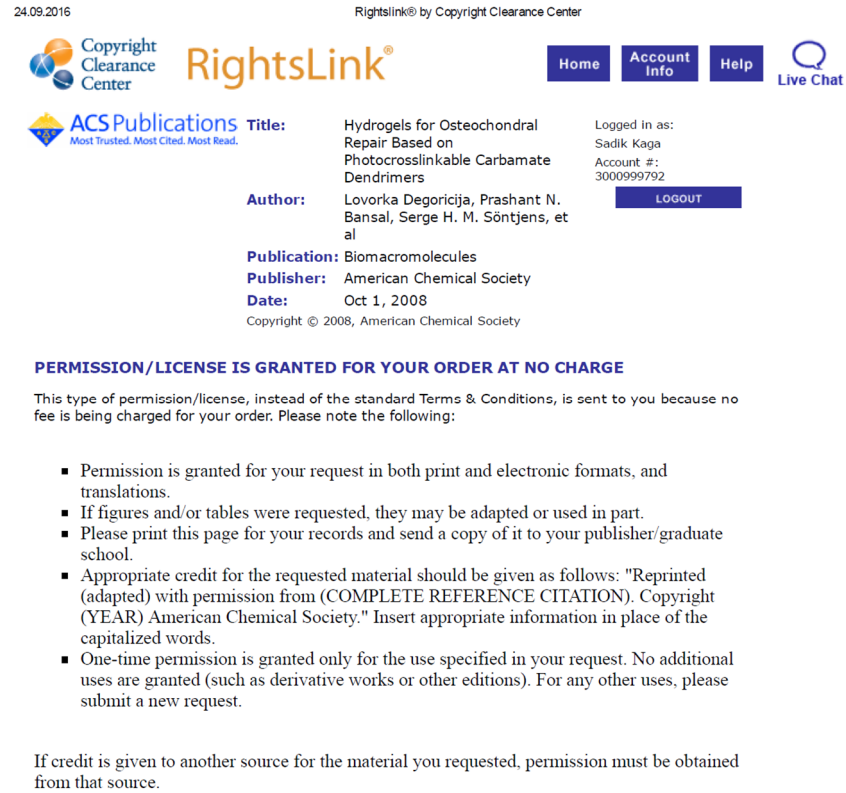
PERMISSION/LICENSE IS GRANTED FOR YOUR ORDER AT NO CHARGE

This type of permission/license, instead of the standard Terms & Conditions, is sent to you because no fee is being charged for your order. Please note the following:

- Permission is granted for your request in both print and electronic formats, and translations.
- If figures and/or tables were requested, they may be adapted or used in part.
- Please print this page for your records and send a copy of it to your publisher/graduate school.
- Appropriate credit for the requested material should be given as follows: "Reprinted (adapted) with permission from (COMPLETE REFERENCE CITATION). Copyright (YEAR) American Chemical Society." Insert appropriate information in place of the capitalized words.
- One-time permission is granted only for the use specified in your request. No additional uses are granted (such as derivative works or other editions). For any other uses, please submit a new request.

If credit is given to another source for the material you requested, permission must be obtained from that source.

Figure B.5. Permission for Figure 1.8.



24.09.2016 Rightslink® by Copyright Clearance Center

Copyright Clearance Center RightsLink® Home Account Info Help Live Chat

ACS Publications Most Trusted. Most Cited. Most Read.

Title: Hydrogels for Osteochondral Repair Based on Photocrosslinkable Carbamate Dendrimers

Author: Lovorka Degoricija, Prashant N. Bansal, Serge H. M. Söntjens, et al

Publication: Biomacromolecules

Publisher: American Chemical Society

Date: Oct 1, 2008

Copyright © 2008, American Chemical Society

Logged in as: Sadik Kaga
Account #: 3000999792
LOGOUT

PERMISSION/LICENSE IS GRANTED FOR YOUR ORDER AT NO CHARGE

This type of permission/license, instead of the standard Terms & Conditions, is sent to you because no fee is being charged for your order. Please note the following:

- Permission is granted for your request in both print and electronic formats, and translations.
- If figures and/or tables were requested, they may be adapted or used in part.
- Please print this page for your records and send a copy of it to your publisher/graduate school.
- Appropriate credit for the requested material should be given as follows: "Reprinted (adapted) with permission from (COMPLETE REFERENCE CITATION). Copyright (YEAR) American Chemical Society." Insert appropriate information in place of the capitalized words.
- One-time permission is granted only for the use specified in your request. No additional uses are granted (such as derivative works or other editions). For any other uses, please submit a new request.

If credit is given to another source for the material you requested, permission must be obtained from that source.

Figure B.6. Permission for Figure 1.9.



23.09.2016 Rightslink® by Copyright Clearance Center

Copyright Clearance Center RightsLink® Home Account Info Help Live Chat

ACS Publications Most Trusted. Most Cited. Most Read.

Title: Photopatternable "Clickable" Hydrogels: "Orthogonal" Control over Fabrication and Functionalization

Author: Sadik Kaga, Serap Yapar, Ece Manavoglu Gecici, et al

Publication: Macromolecules

Publisher: American Chemical Society

Date: Aug 1, 2015

Copyright © 2015, American Chemical Society

Logged in as: Sadik Kaga
Account #: 3000999792
LOGOUT

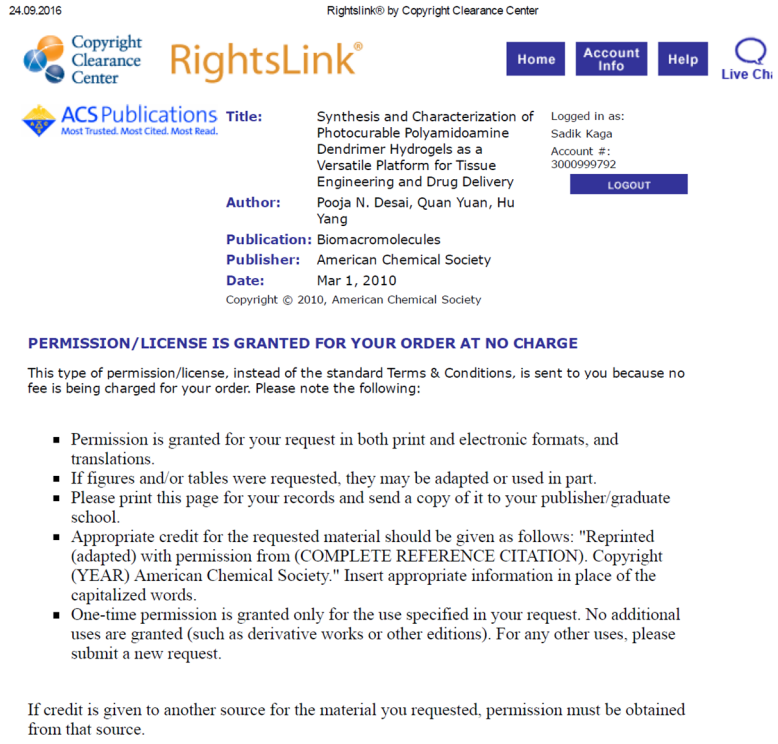
PERMISSION/LICENSE IS GRANTED FOR YOUR ORDER AT NO CHARGE

This type of permission/license, instead of the standard Terms & Conditions, is sent to you because no fee is being charged for your order. Please note the following:

- Permission is granted for your request in both print and electronic formats, and translations.
- If figures and/or tables were requested, they may be adapted or used in part.
- Please print this page for your records and send a copy of it to your publisher/graduate school.
- Appropriate credit for the requested material should be given as follows: "Reprinted (adapted) with permission from (COMPLETE REFERENCE CITATION). Copyright (YEAR) American Chemical Society." Insert appropriate information in place of the capitalized words.
- One-time permission is granted only for the use specified in your request. No additional uses are granted (such as derivative works or other editions). For any other uses, please submit a new request.

If credit is given to another source for the material you requested, permission must be obtained from that source.

Figure B.7. Permission for Figure 1.10.



24.09.2016 Rightslink® by Copyright Clearance Center

Copyright Clearance Center RightsLink® Home Account Info Help Live Chat

ACS Publications Most Trusted. Most Cited. Most Read.

Title: Synthesis and Characterization of Photocurable Polyamidoamine Dendrimer Hydrogels as a Versatile Platform for Tissue Engineering and Drug Delivery

Logged in as: Sadik Kaga
Account #: 3000999792
LOGOUT

Author: Pooja N. Desai, Quan Yuan, Hu Yang

Publication: Biomacromolecules

Publisher: American Chemical Society

Date: Mar 1, 2010

Copyright © 2010, American Chemical Society

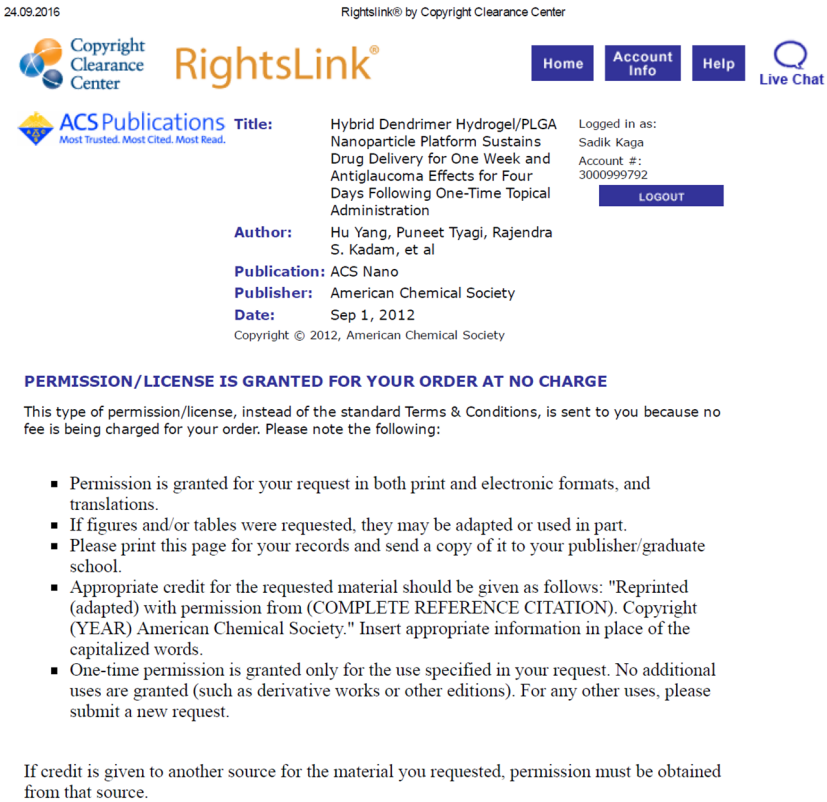
PERMISSION/LICENSE IS GRANTED FOR YOUR ORDER AT NO CHARGE

This type of permission/license, instead of the standard Terms & Conditions, is sent to you because no fee is being charged for your order. Please note the following:

- Permission is granted for your request in both print and electronic formats, and translations.
- If figures and/or tables were requested, they may be adapted or used in part.
- Please print this page for your records and send a copy of it to your publisher/graduate school.
- Appropriate credit for the requested material should be given as follows: "Reprinted (adapted) with permission from (COMPLETE REFERENCE CITATION). Copyright (YEAR) American Chemical Society." Insert appropriate information in place of the capitalized words.
- One-time permission is granted only for the use specified in your request. No additional uses are granted (such as derivative works or other editions). For any other uses, please submit a new request.

If credit is given to another source for the material you requested, permission must be obtained from that source.

Figure B.8. Permission for Figure 1.11.



24.09.2016 Rightslink® by Copyright Clearance Center

Copyright Clearance Center RightsLink® Home Account Info Help Live Chat

ACS Publications Most Trusted. Most Cited. Most Read.

Title: Hybrid Dendrimer Hydrogel/PLGA Nanoparticle Platform Sustains Drug Delivery for One Week and Antiglaucoma Effects for Four Days Following One-Time Topical Administration

Logged in as: Sadik Kaga
Account #: 3000999792
LOGOUT

Author: Hu Yang, Puneet Tyagi, Rajendra S. Kadam, et al

Publication: ACS Nano

Publisher: American Chemical Society

Date: Sep 1, 2012

Copyright © 2012, American Chemical Society

PERMISSION/LICENSE IS GRANTED FOR YOUR ORDER AT NO CHARGE

This type of permission/license, instead of the standard Terms & Conditions, is sent to you because no fee is being charged for your order. Please note the following:

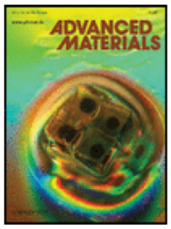
- Permission is granted for your request in both print and electronic formats, and translations.
- If figures and/or tables were requested, they may be adapted or used in part.
- Please print this page for your records and send a copy of it to your publisher/graduate school.
- Appropriate credit for the requested material should be given as follows: "Reprinted (adapted) with permission from (COMPLETE REFERENCE CITATION). Copyright (YEAR) American Chemical Society." Insert appropriate information in place of the capitalized words.
- One-time permission is granted only for the use specified in your request. No additional uses are granted (such as derivative works or other editions). For any other uses, please submit a new request.

If credit is given to another source for the material you requested, permission must be obtained from that source.

Figure B.9. Permission for Figure 1.12.

24.09.2016 Rightslink® by Copyright Clearance Center

Copyright Clearance Center RightsLink® Home Account Info Help Live Chat



Title: A Novel Poly(amido amine)-Dendrimer-Based Hydrogel as a Mimic for the Extracellular Matrix
Author: Yao Wang,Qiang Zhao,He Zhang,Sheng Yang,Xinru Jia
Publication: Advanced Materials
Publisher: John Wiley and Sons
Date: Apr 14, 2014
© 2014 WILEY-VCH Verlag GmbH & Co. KGaA, Weinheim

Logged in as:
Sadik Kaga
Account #: 3000999792
LOGOUT

Order Completed

Thank you for your order.

This Agreement between Sadik Kaga ("You") and John Wiley and Sons ("John Wiley and Sons") consists of your license details and the terms and conditions provided by John Wiley and Sons and Copyright Clearance Center.

Your confirmation email will contain your order number for future reference.

Get the printable license.

License Number	3955270449862
License date	Sep 24, 2016
Licensed Content Publisher	John Wiley and Sons
Licensed Content Publication	Advanced Materials
Licensed Content Title	A Novel Poly(amido amine)-Dendrimer-Based Hydrogel as a Mimic for the Extracellular Matrix
Licensed Content Author	Yao Wang,Qiang Zhao,He Zhang,Sheng Yang,Xinru Jia
Licensed Content Date	Apr 14, 2014
Licensed Content Pages	5
Type of use	Dissertation/Thesis
Requestor type	University/Academic
Format	Print and electronic
Portion	Figure/table
Number of figures/tables	1
Original Wiley figure/table number(s)	Scheme 1.
Will you be translating?	No
Title of your thesis / dissertation	Functionalizable Hydrogels and Water Soluble Constructs as Chemotherapy Drug Carriers
Expected completion date	Oct 2016
Expected size (number of pages)	220
Requestor Location	Sadik Kaga Boğaziçi Universitesi Kuzey Campus, Chemistry Department Istanbul, 34342 Turkey Attn: Sadik Kaga
Publisher Tax ID	EU826007151
Billing Type	Invoice
Billing address	Sadik Kaga Boğaziçi Universitesi Kuzey Campus, Chemistry Department Istanbul, Turkey 34342 Attn: Sadik Kaga
Total	0.00 USD

Figure B.10. Permission for Figure 1.13.



23.09.2016 Rightslink® by Copyright Clearance Center

Copyright Clearance Center RightsLink® Home Account Info Help Live Chat

ACS Publications Most Trusted. Most Cited. Most Read.

Title: Dendritic Macromers as in Situ Polymerizing Biomaterials for Securing Cataract Incisions

Author: Michel Wathier, Pil J. Jung, Michael A. Carnahan, et al

Publication: Journal of the American Chemical Society

Publisher: American Chemical Society

Date: Oct 1, 2004

Copyright © 2004, American Chemical Society

Logged in as: Sadik Kaga
Account #: 3000999792
LOGOUT

PERMISSION/LICENSE IS GRANTED FOR YOUR ORDER AT NO CHARGE

This type of permission/license, instead of the standard Terms & Conditions, is sent to you because no fee is being charged for your order. Please note the following:

- Permission is granted for your request in both print and electronic formats, and translations.
- If figures and/or tables were requested, they may be adapted or used in part.
- Please print this page for your records and send a copy of it to your publisher/graduate school.
- Appropriate credit for the requested material should be given as follows: "Reprinted (adapted) with permission from (COMPLETE REFERENCE CITATION). Copyright (YEAR) American Chemical Society." Insert appropriate information in place of the capitalized words.
- One-time permission is granted only for the use specified in your request. No additional uses are granted (such as derivative works or other editions). For any other uses, please submit a new request.

If credit is given to another source for the material you requested, permission must be obtained from that source.

Figure B.11. Permission for Figure 1.14.



23.09.2016 Rightslink® by Copyright Clearance Center

Copyright Clearance Center RightsLink® Home Account Info Help Live Chat

ACS Publications Most Trusted. Most Cited. Most Read.

Title: Hydrogels Formed by Multiple Peptide Ligation Reactions To Fasten Corneal Transplants

Author: Michel Wathier, C. Starck Johnson, Terry Kim, et al

Publication: Bioconjugate Chemistry

Publisher: American Chemical Society

Date: Jul 1, 2006

Copyright © 2006, American Chemical Society

Logged in as: Sadik Kaga
Account #: 3000999792
LOGOUT

PERMISSION/LICENSE IS GRANTED FOR YOUR ORDER AT NO CHARGE

This type of permission/license, instead of the standard Terms & Conditions, is sent to you because no fee is being charged for your order. Please note the following:

- Permission is granted for your request in both print and electronic formats, and translations.
- If figures and/or tables were requested, they may be adapted or used in part.
- Please print this page for your records and send a copy of it to your publisher/graduate school.
- Appropriate credit for the requested material should be given as follows: "Reprinted (adapted) with permission from (COMPLETE REFERENCE CITATION). Copyright (YEAR) American Chemical Society." Insert appropriate information in place of the capitalized words.
- One-time permission is granted only for the use specified in your request. No additional uses are granted (such as derivative works or other editions). For any other uses, please submit a new request.

If credit is given to another source for the material you requested, permission must be obtained from that source.

Figure B.12. Permission for Figure 1.15.

23.09.2016 Rightslink® by Copyright Clearance Center

Copyright Clearance Center RightsLink® Home Account Info Help Live Chat



Title:	A Dendritic Thioester Hydrogel Based on Thiol–Thioester Exchange as a Dissolvable Sealant System for Wound Closure
Author:	Cynthia Ghobril,Kristie Charoen,Edward K. Rodriguez,Ara Nazarian,Mark W. Grinstaff
Publication:	Angewandte Chemie International Edition
Publisher:	John Wiley and Sons
Date:	Nov 26, 2013

Copyright © 2013 WILEY-VCH Verlag GmbH & Co. KGaA, Weinheim

Logged in as:
Sadik Kaga
Account #:
3000999792
LOGOUT

Order Completed

Thank you for your order.

This Agreement between Sadik Kaga ("You") and John Wiley and Sons ("John Wiley and Sons") consists of your license details and the terms and conditions provided by John Wiley and Sons and Copyright Clearance Center.

Your confirmation email will contain your order number for future reference.

Get the printable license.

License Number	3954800691715
License date	Sep 23, 2016
Licensed Content Publisher	John Wiley and Sons
Licensed Content Publication	Angewandte Chemie International Edition
Licensed Content Title	A Dendritic Thioester Hydrogel Based on Thiol–Thioester Exchange as a Dissolvable Sealant System for Wound Closure
Licensed Content Author	Cynthia Ghobril,Kristie Charoen,Edward K. Rodriguez,Ara Nazarian,Mark W. Grinstaff
Licensed Content Date	Nov 26, 2013
Licensed Content Pages	5
Type of use	Dissertation/Thesis
Requestor type	University/Academic
Format	Print and electronic
Portion	Figure/table
Number of figures/tables	2
Original Wiley figure/table number(s)	Figure 1., Figure 4.
Will you be translating?	No
Title of your thesis / dissertation	Functionalizable Hydrogels and Water Soluble Constructs as Chemotherapy Drug Carriers
Expected completion date	Oct 2016
Expected size (number of pages)	220
Requestor Location	Sadik Kaga Boğaziçi Universitesi Kuzey Campus, Chemistry Department Istanbul, 34342 Turkey Attn: Sadik Kaga
Publisher Tax ID	EU826007151
Billing Type	Invoice
Billing address	Sadik Kaga Boğaziçi Universitesi

Figure B.13. Permission for Figure 1.16 and Figure 1.17.

Villa-Camacho *et al. BMC Musculoskeletal Disorders* (2015) 16:116
DOI 10.1186/s12891-015-0573-7

BMC Musculoskeletal Disorders

RESEARCH ARTICLE Open Access

The efficacy of a lysine-based dendritic hydrogel does not differ from those of commercially available tissue sealants and adhesives: an ex vivo study

Juan C Villa-Camacho[1], Cynthia Ghobril[2], Lorenzo Anez-Bustillos[1], Mark W Grinstaff[2], Edward K Rodríguez[3†] and Ara Nazarian[1*†]

Copyright

© Villa-Camacho et al.; licensee BioMed Central. 2015
This is an Open Access article distributed under the terms of the Creative Commons Attribution License (http://creativecommons.org/licenses/by/4.0), which permits unrestricted use, distribution, and reproduction in any medium, provided the original work is properly credited. The Creative Commons Public Domain Dedication waiver (http://creativecommons.org/publicdomain/zero/1.0/) applies to the data made available in this article, unless otherwise stated.

Figure B.14. Permission for Figure 1.18.

23.09.2016 Rightslink® by Copyright Clearance Center

Copyright Clearance Center RightsLink® Home Account Info Help Live Chat

ACS Publications Most Trusted. Most Cited. Most Read.

Title: Injectable PAMAM Dendrimer–PEG Hydrogels for the Treatment of Genital Infections: Formulation and in Vitro and in Vivo Evaluation
Author: Raghavendra S. Navath, Anupa R. Menjoge, Hui Dai, et al
Publication: Molecular Pharmaceutics
Publisher: American Chemical Society
Date: Aug 1, 2011
Copyright © 2011, American Chemical Society

Logged in as: Sadik Kaga
Account #: 3000999792
LOGOUT

PERMISSION/LICENSE IS GRANTED FOR YOUR ORDER AT NO CHARGE

This type of permission/license, instead of the standard Terms & Conditions, is sent to you because no fee is being charged for your order. Please note the following:

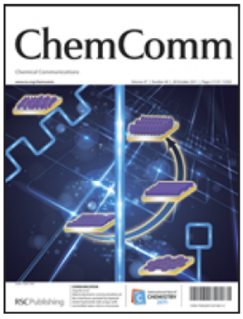
- Permission is granted for your request in both print and electronic formats, and translations.
- If figures and/or tables were requested, they may be adapted or used in part.
- Please print this page for your records and send a copy of it to your publisher/graduate school.
- Appropriate credit for the requested material should be given as follows: "Reprinted (adapted) with permission from (COMPLETE REFERENCE CITATION). Copyright (YEAR) American Chemical Society." Insert appropriate information in place of the capitalized words.
- One-time permission is granted only for the use specified in your request. No additional uses are granted (such as derivative works or other editions). For any other uses, please submit a new request.

If credit is given to another source for the material you requested, permission must be obtained from that source.

Figure B.15. Permission for Figure 1.19.

24.09.2016 Rightslink® by Copyright Clearance Center

Copyright Clearance Center RightsLink® Home Account Info Help Live Chat



Title: A high stiffness bio-inspired hydrogel from the combination of a poly(amido amine) dendrimer with DOPA

Author: Yao Wang,Qiang Zhao,Yiyang Luo,Zejun Xu,He Zhang,Sheng Yang,Yen Wei,Xinru Jia

Publication: Chemical Communications (Cambridge)

Publisher: Royal Society of Chemistry

Date: Sep 21, 2015

Copyright © 2015, Royal Society of Chemistry

Logged in as:
Sadik Kaga
Account #:
3000999792

LOGOUT

Order Completed

Thank you for your order.

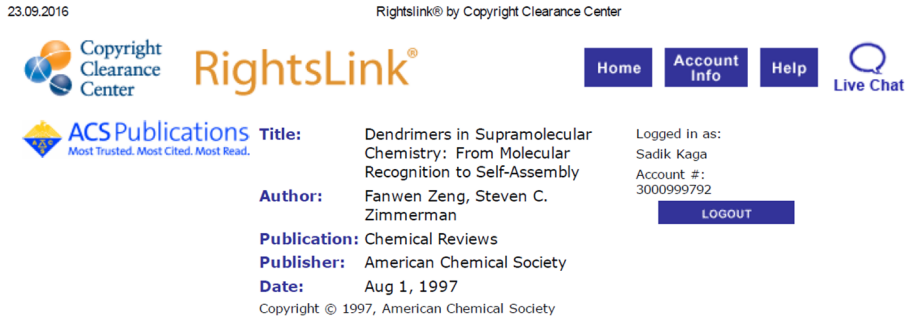
This Agreement between Sadik Kaga ("You") and Royal Society of Chemistry ("Royal Society of Chemistry") consists of your license details and the terms and conditions provided by Royal Society of Chemistry and Copyright Clearance Center.

Your confirmation email will contain your order number for future reference.

Get the printable license.

License Number	3955280786816
License date	Sep 24, 2016
Licensed Content Publisher	Royal Society of Chemistry
Licensed Content Publication	Chemical Communications (Cambridge)
Licensed Content Title	A high stiffness bio-inspired hydrogel from the combination of a poly(amido amine) dendrimer with DOPA
Licensed Content Author	Yao Wang,Qiang Zhao,Yiyang Luo,Zejun Xu,He Zhang,Sheng Yang,Yen Wei,Xinru Jia
Licensed Content Date	Sep 21, 2015
Licensed Content Volume	51
Licensed Content Issue	94
Type of Use	Thesis/Dissertation
Requestor type	non-commercial (non-profit)
Portion	figures/tables/images
Number of figures/tables/images	2
Distribution quantity	10
Format	print and electronic
Will you be translating?	no
Order reference number	
Title of the thesis/dissertation	Functionalizable Hydrogels and Water Soluble Constructs as Chemotherapy Drug Carriers
Expected completion date	Oct 2016
Estimated size	220
Requestor Location	Sadik Kaga Boğaziçi Universitesi Kuzey Campus, Chemistry Department Istanbul, 34342 Turkey Attn: Sadik Kaga
Billing Type	Invoice
Billing address	Sadik Kaga Boğaziçi Universitesi Kuzey Campus, Chemistry Department

Figure B.16. Permission for Figure 1.20.



23.09.2016 Rightslink® by Copyright Clearance Center

Copyright Clearance Center RightsLink® Home Account Info Help Live Chat

ACS Publications Most Trusted. Most Cited. Most Read.

Title: Dendrimers in Supramolecular Chemistry: From Molecular Recognition to Self-Assembly

Author: Fanwen Zeng, Steven C. Zimmerman

Publication: Chemical Reviews

Publisher: American Chemical Society

Date: Aug 1, 1997

Copyright © 1997, American Chemical Society

Logged in as: Sadik Kaga
Account #: 3000999792
LOGOUT

PERMISSION/LICENSE IS GRANTED FOR YOUR ORDER AT NO CHARGE

This type of permission/license, instead of the standard Terms & Conditions, is sent to you because no fee is being charged for your order. Please note the following:

- Permission is granted for your request in both print and electronic formats, and translations.
- If figures and/or tables were requested, they may be adapted or used in part.
- Please print this page for your records and send a copy of it to your publisher/graduate school.
- Appropriate credit for the requested material should be given as follows: "Reprinted (adapted) with permission from (COMPLETE REFERENCE CITATION). Copyright (YEAR) American Chemical Society." Insert appropriate information in place of the capitalized words.
- One-time permission is granted only for the use specified in your request. No additional uses are granted (such as derivative works or other editions). For any other uses, please submit a new request.

If credit is given to another source for the material you requested, permission must be obtained from that source.

Figure B.17. Permission for Figure 1.21.



15.02.2016 Rightslink® by Copyright Clearance Center

Copyright Clearance Center RightsLink® Home Account Info Help Live Chat

ACS Publications Most Trusted. Most Cited. Most Read.

Title: Synthesis and Structural Characterization of a Bis-arborol-Tetrathiafulvalene Gel: Toward a Self-Assembling "Molecular" Wire

Author: Mikkel Joergensen, Klaus Bechgaard, Thomas Bjoernholm, et al

Publication: The Journal of Organic Chemistry

Publisher: American Chemical Society

Date: Oct 1, 1994

Copyright © 1994, American Chemical Society

Logged in as: Sadik Kaga
LOGOUT

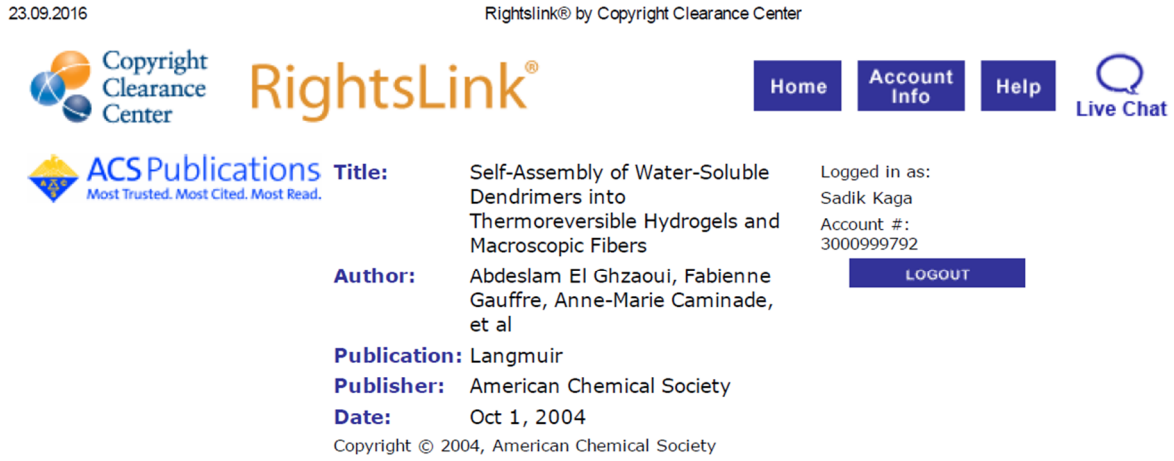
PERMISSION/LICENSE IS GRANTED FOR YOUR ORDER AT NO CHARGE

This type of permission/license, instead of the standard Terms & Conditions, is sent to you because no fee is being charged for your order. Please note the following:

- Permission is granted for your request in both print and electronic formats, and translations.
- If figures and/or tables were requested, they may be adapted or used in part.
- Please print this page for your records and send a copy of it to your publisher/graduate school.
- Appropriate credit for the requested material should be given as follows: "Reprinted (adapted) with permission from (COMPLETE REFERENCE CITATION). Copyright (YEAR) American Chemical Society." Insert appropriate information in place of the capitalized words.
- One-time permission is granted only for the use specified in your request. No additional uses are granted (such as derivative works or other editions). For any other uses, please submit a new request.

If credit is given to another source for the material you requested, permission must be obtained from that source.

Figure B.18. Permission for Figure 1.22.



PERMISSION/LICENSE IS GRANTED FOR YOUR ORDER AT NO CHARGE

This type of permission/license, instead of the standard Terms & Conditions, is sent to you because no fee is being charged for your order. Please note the following:

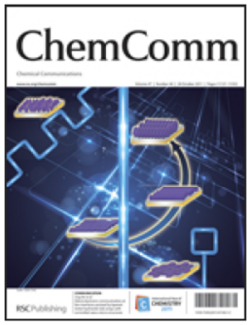
- Permission is granted for your request in both print and electronic formats, and translations.
- If figures and/or tables were requested, they may be adapted or used in part.
- Please print this page for your records and send a copy of it to your publisher/graduate school.
- Appropriate credit for the requested material should be given as follows: "Reprinted (adapted) with permission from (COMPLETE REFERENCE CITATION). Copyright (YEAR) American Chemical Society." Insert appropriate information in place of the capitalized words.
- One-time permission is granted only for the use specified in your request. No additional uses are granted (such as derivative works or other editions). For any other uses, please submit a new request.

If credit is given to another source for the material you requested, permission must be obtained from that source.

Figure B.19. Permission for Figure 1.23.

24.09.2016 Rightslink® by Copyright Clearance Center

Copyright Clearance Center RightsLink® Home Account Info Help Live Chat



Title:	A metal ion triggered shrinkable supramolecular hydrogel and controlled release by an amphiphilic peptide dendron
Author:	Long Qin,Pengfei Duan,Fan Xie,Li Zhang,Minghua Liu
Publication:	Chemical Communications (Cambridge)
Publisher:	Royal Society of Chemistry
Date:	Oct 1, 2013

Copyright © 2013, Royal Society of Chemistry

Logged in as:
Sadik Kaga
Account #:
3000999792
LOGOUT

Order Completed

Thank you for your order.

This Agreement between Sadik Kaga ("You") and Royal Society of Chemistry ("Royal Society of Chemistry") consists of your license details and the terms and conditions provided by Royal Society of Chemistry and Copyright Clearance Center.

Your confirmation email will contain your order number for future reference.

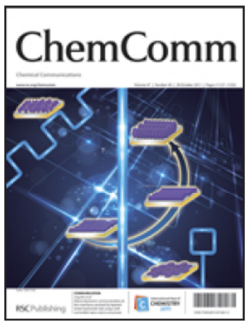
Get the printable license.

License Number	3955290081143
License date	Sep 24, 2016
Licensed Content Publisher	Royal Society of Chemistry
Licensed Content Publication	Chemical Communications (Cambridge)
Licensed Content Title	A metal ion triggered shrinkable supramolecular hydrogel and controlled release by an amphiphilic peptide dendron
Licensed Content Author	Long Qin,Pengfei Duan,Fan Xie,Li Zhang,Minghua Liu
Licensed Content Date	Oct 1, 2013
Licensed Content Volume	49
Licensed Content Issue	92
Type of Use	Thesis/Dissertation
Requestor type	academic/educational
Portion	figures/tables/images
Number of figures/tables/images	1
Distribution quantity	10
Format	print and electronic
Will you be translating?	no
Order reference number	
Title of the thesis/dissertation	Functionalizable Hydrogels and Water Soluble Constructs as Chemotherapy Drug Carriers
Expected completion date	Oct 2016
Estimated size	220
Requestor Location	Sadik Kaga Boğaziçi Universitesi Kuzey Campus, Chemistry Department Istanbul, 34342 Turkey Attn: Sadik Kaga
Billing Type	Invoice
Billing address	Sadik Kaga Boğaziçi Universitesi Kuzey Campus, Chemistry Department

Figure B.20. Permission for Figure 1.24.

24.09.2016 Rightslink® by Copyright Clearance Center

Copyright Clearance Center RightsLink® Home Account Info Help Live Chat



Title: A dual thermal and photo-switchable shrinking–swelling supramolecular peptide dendron gel

Author: Fan Xie,Long Qin,Minghua Liu

Publication: Chemical Communications (Cambridge)

Publisher: Royal Society of Chemistry

Date: Nov 10, 2015

Copyright © 2015, Royal Society of Chemistry

Logged in as:
Sadik Kaga
Account #:
3000999792
LOGOUT

Order Completed

Thank you for your order.

This Agreement between Sadik Kaga ("You") and Royal Society of Chemistry ("Royal Society of Chemistry") consists of your license details and the terms and conditions provided by Royal Society of Chemistry and Copyright Clearance Center.

Your confirmation email will contain your order number for future reference.

Get the printable license.

License Number	3955290383324
License date	Sep 24, 2016
Licensed Content Publisher	Royal Society of Chemistry
Licensed Content Publication	Chemical Communications (Cambridge)
Licensed Content Title	A dual thermal and photo-switchable shrinking–swelling supramolecular peptide dendron gel
Licensed Content Author	Fan Xie,Long Qin,Minghua Liu
Licensed Content Date	Nov 10, 2015
Licensed Content Volume	52
Licensed Content Issue	5
Type of Use	Thesis/Dissertation
Requestor type	academic/educational
Portion	figures/tables/images
Number of figures/tables/images	2
Distribution quantity	10
Format	print and electronic
Will you be translating?	no
Order reference number	
Title of the thesis/dissertation	Functionalizable Hydrogels and Water Soluble Constructs as Chemotherapy Drug Carriers
Expected completion date	Oct 2016
Estimated size	220
Requestor Location	Sadik Kaga Boğaziçi Universitesi Kuzey Campus, Chemistry Department Istanbul, 34342 Turkey Attn: Sadik Kaga
Billing Type	Invoice
Billing address	Sadik Kaga Boğaziçi Universitesi Kuzey Campus, Chemistry Department Istanbul, Turkey 34342 Attn: Sadik Kaga

Figure B.21. Permission for Figure 1.25.

23.09.2016 Rightslink® by Copyright Clearance Center

Copyright Clearance Center RightsLink®

Home | Account Info | Help | Live Chat



Title: Self-Assembly of Amphiphilic Janus Dendrimers into Mechanically Robust Supramolecular Hydrogels for Sustained Drug Release

Author: Sami Nummelin,Ville Liljeström,Eve Saarikoski,Jarmo Ropponen,Antti Nykänen,Veikko Linko,Jukka Seppälä,Jouni Hirvonen,Olli Ikkala,Luis M. Bimbo,Mauri A. Kostiainen

Publication: Chemistry - A European Journal

Publisher: John Wiley and Sons

Date: Jul 1, 2015

© 2015 WILEY-VCH Verlag GmbH & Co. KGaA, Weinheim

Logged in as:
Sadik Kaga
Account #:
3000999792
LOGOUT

Order Completed

Thank you for your order.

This Agreement between Sadik Kaga ("You") and John Wiley and Sons ("John Wiley and Sons") consists of your license details and the terms and conditions provided by John Wiley and Sons and Copyright Clearance Center.

Your confirmation email will contain your order number for future reference.

Get the printable license.

License Number	3954770387581
License date	Sep 23, 2016
Licensed Content Publisher	John Wiley and Sons
Licensed Content Publication	Chemistry - A European Journal
Licensed Content Title	Self-Assembly of Amphiphilic Janus Dendrimers into Mechanically Robust Supramolecular Hydrogels for Sustained Drug Release
Licensed Content Author	Sami Nummelin,Ville Liljeström,Eve Saarikoski,Jarmo Ropponen,Antti Nykänen,Veikko Linko,Jukka Seppälä,Jouni Hirvonen,Olli Ikkala,Luis M. Bimbo,Mauri A. Kostiainen
Licensed Content Date	Jul 1, 2015
Licensed Content Pages	7
Type of use	Dissertation/Thesis
Requestor type	University/Academic
Format	Print and electronic
Portion	Figure/table
Number of figures/tables	1
Original Wiley figure/table number(s)	Figure 1.
Will you be translating?	No
Title of your thesis / dissertation	Functionalizable Hydrogels and Water Soluble Constructs as Chemotherapy Drug Carriers
Expected completion date	Oct 2016
Expected size (number of pages)	220
Requestor Location	Sadik Kaga Boğaziçi Universitesi Kuzey Campus, Chemistry Department Istanbul, 34342 Turkey Attn: Sadik Kaga
Publisher Tax ID	EU826007151

Figure B.22. Permission for Figure 1.26.





Title: High-water-content mouldable hydrogels by mixing clay and a dendritic molecular binder

Author: Qigang Wang, Justin L. Mynar, Masaru Yoshida, Eunji Lee, Myongsoo Lee et al.

Publication: Nature

Publisher: Nature Publishing Group

Date: Jan 21, 2010

Copyright © 2010, Rights Managed by Nature Publishing Group

Logged in as:
Sadik Kaga
Account #: 3000999792
LOGOUT

Order Completed

Thank you for your order.

This Agreement between Sadik Kaga ("You") and Nature Publishing Group ("Nature Publishing Group") consists of your license details and the terms and conditions provided by Nature Publishing Group and Copyright Clearance Center.

Your confirmation email will contain your order number for future reference.

Get the printable license.

License Number	3954770661479
License date	Sep 23, 2016
Licensed Content Publisher	Nature Publishing Group
Licensed Content Publication	Nature
Licensed Content Title	High-water-content mouldable hydrogels by mixing clay and a dendritic molecular binder
Licensed Content Author	Qigang Wang, Justin L. Mynar, Masaru Yoshida, Eunji Lee, Myongsoo Lee et al.
Licensed Content Date	Jan 21, 2010
Licensed Content Volume	463
Licensed Content Issue	7279
Type of Use	reuse in a dissertation / thesis
Requestor type	academic/educational
Format	print and electronic
Portion	figures/tables/illustrations
Number of figures/tables/illustrations	2
High-res required	no
Figures	Figure 1., Figure 2.
Author of this NPG article	no
Your reference number	
Title of your thesis / dissertation	Functionalizable Hydrogels and Water Soluble Constructs as Chemotherapy Drug Carriers
Expected completion date	Oct 2016
Estimated size (number of pages)	220
Requestor Location	Sadik Kaga Boğaziçi Universitesi Kuzey Campus, Chemistry Department Istanbul, 34342 Turkey Attn: Sadik Kaga
Billing Type	Invoice
Billing address	Sadik Kaga Boğaziçi Universitesi Kuzey Campus, Chemistry Department Istanbul, Turkey 34342 Attn: Sadik Kaga

Figure B.23. Permission for Figure 1.27.

23.09.2016 Rightslink® by Copyright Clearance Center

Copyright Clearance Center RightsLink® Home Account Info Help Live Chat

ACS Publications Most Trusted. Most Cited. Most Read.

Title: Linear versus Dendritic Molecular Binders for Hydrogel Network Formation with Clay Nanosheets: Studies with ABA Triblock Copolyethers Carrying Guanidinium Ion Pendants

Author: Shingo Tamesue, Masataka Ohtani, Kuniyo Yamada, et al

Publication: Journal of the American Chemical Society

Publisher: American Chemical Society

Date: Oct 1, 2013

Copyright © 2013, American Chemical Society

Logged in as: Sadik Kaga
Account #: 3000999792
LOGOUT

PERMISSION/LICENSE IS GRANTED FOR YOUR ORDER AT NO CHARGE

This type of permission/license, instead of the standard Terms & Conditions, is sent to you because no fee is being charged for your order. Please note the following:

- Permission is granted for your request in both print and electronic formats, and translations.
- If figures and/or tables were requested, they may be adapted or used in part.
- Please print this page for your records and send a copy of it to your publisher/graduate school.
- Appropriate credit for the requested material should be given as follows: "Reprinted (adapted) with permission from (COMPLETE REFERENCE CITATION). Copyright (YEAR) American Chemical Society." Insert appropriate information in place of the capitalized words.
- One-time permission is granted only for the use specified in your request. No additional uses are granted (such as derivative works or other editions). For any other uses, please submit a new request.

If credit is given to another source for the material you requested, permission must be obtained from that source.

Figure B.24. Permission for Figure 1.28.

21.10.2016 Rightslink® by Copyright Clearance Center

Copyright Clearance Center RightsLink® Home Account Info Help Live Chat

nature publishing group

Title: Microtubules and resistance to tubulin-binding agents
Author: Maria Kavallaris
Publication: Nature Reviews Cancer
Publisher: Nature Publishing Group
Date: Mar 1, 2010
Copyright © 2010, Rights Managed by Nature Publishing Group

Logged in as:
Sadik Kaga
Account #:
3000999792
LOGOUT

Order Completed

Thank you for your order.

This Agreement between Sadik Kaga ("You") and Nature Publishing Group ("Nature Publishing Group") consists of your license details and the terms and conditions provided by Nature Publishing Group and Copyright Clearance Center.

Your confirmation email will contain your order number for future reference.

Get the printable license.

License Number	3973610299045
License date	Oct 21, 2016
Licensed Content Publisher	Nature Publishing Group
Licensed Content Publication	Nature Reviews Cancer
Licensed Content Title	Microtubules and resistance to tubulin-binding agents
Licensed Content Author	Maria Kavallaris
Licensed Content Date	Mar 1, 2010
Licensed Content Volume	10
Licensed Content Issue	3
Type of Use	reuse in a dissertation / thesis
Requestor type	academic/educational
Format	print and electronic
Portion	figures/tables/illustrations
Number of figures/tables/illustrations	2
High-res required	no
Figures	Figure 1, Figure 3
Author of this NPG article	no
Your reference number	
Title of your thesis / dissertation	Functionalizable Hydrogels and Water Soluble Constructs as Chemotherapy Drug Carriers
Expected completion date	Oct 2016
Estimated size (number of pages)	220
Requestor Location	Sadik Kaga Boğaziçi Universitesi Kuzey Campus, Chemistry Department Istanbul, 34342 Turkey Attn: Sadik Kaga
Billing Type	Invoice
Billing address	Sadik Kaga Boğaziçi Universitesi Kuzey Campus, Chemistry Department Istanbul, Turkey 34342 Attn: Sadik Kaga
Total	0.00 USD

Figure B.25. Permission for Figure 1.31 and Figure 1.32.

21.10.2016 Rightslink® by Copyright Clearance Center

Copyright Clearance Center RightsLink® Home Account Info Help Live Chat

nature publishing group

Title: The scientific contributions of M. Judah Folkman to cancer research
Author: Bruce R. Zetter
Publication: Nature Reviews Cancer
Publisher: Nature Publishing Group
Date: Aug 1, 2008
Copyright © 2008, Rights Managed by Nature Publishing Group

Logged in as:
Sadik Kaga
Account #:
3000999792
LOGOUT

Order Completed

Thank you for your order.

This Agreement between Sadik Kaga ("You") and Nature Publishing Group ("Nature Publishing Group") consists of your license details and the terms and conditions provided by Nature Publishing Group and Copyright Clearance Center.

Your confirmation email will contain your order number for future reference.

Get the printable license.

License Number	3973640204668
License date	Oct 21, 2016
Licensed Content Publisher	Nature Publishing Group
Licensed Content Publication	Nature Reviews Cancer
Licensed Content Title	The scientific contributions of M. Judah Folkman to cancer research
Licensed Content Author	Bruce R. Zetter
Licensed Content Date	Aug 1, 2008
Licensed Content Volume	8
Licensed Content Issue	8
Type of Use	reuse in a dissertation / thesis
Requestor type	academic/educational
Format	print and electronic
Portion	figures/tables/illustrations
Number of figures/tables/illustrations	1
High-res required	no
Figures	Figure 3
Author of this NPG article	no
Your reference number	
Title of your thesis / dissertation	Functionalizable Hydrogels and Water Soluble Constructs as Chemotherapy Drug Carriers
Expected completion date	Oct 2016
Estimated size (number of pages)	220
Requestor Location	Sadik Kaga Boğaziçi Universitesi Kuzey Campus, Chemistry Department Istanbul, 34342 Turkey Attn: Sadik Kaga
Billing Type	Invoice
Billing address	Sadik Kaga Boğaziçi Universitesi Kuzey Campus, Chemistry Department Istanbul, Turkey 34342 Attn: Sadik Kaga
Total	0.00 USD

Figure B.26. Permission for Figure 1.33.

19.10.2016 Rightslink® by Copyright Clearance Center

Copyright Clearance Center RightsLink®

Home | Account Info | Help | Live Chat

ACS Publications Most Trusted. Most Cited. Most Read.

Title: PEG–Doxorubicin Conjugates: Influence of Polymer Structure on Drug Release, in Vitro Cytotoxicity, Biodistribution, and Antitumor Activity

Author: Francesco M Veronese, Oddone Schiavon, Gianfranco Pasut, et al

Publication: Bioconjugate Chemistry

Publisher: American Chemical Society

Date: Jul 1, 2005

Copyright © 2005, American Chemical Society

Logged in as: Sadik Kaga

Account #: 3000999792

LOGOUT

PERMISSION/LICENSE IS GRANTED FOR YOUR ORDER AT NO CHARGE

This type of permission/license, instead of the standard Terms & Conditions, is sent to you because no fee is being charged for your order. Please note the following:

- Permission is granted for your request in both print and electronic formats, and translations.
- If figures and/or tables were requested, they may be adapted or used in part.
- Please print this page for your records and send a copy of it to your publisher/graduate school.
- Appropriate credit for the requested material should be given as follows: "Reprinted (adapted) with permission from (COMPLETE REFERENCE CITATION). Copyright (YEAR) American Chemical Society." Insert appropriate information in place of the capitalized words.
- One-time permission is granted only for the use specified in your request. No additional uses are granted (such as derivative works or other editions). For any other uses, please submit a new request.

Figure B.27. Permission for Figure 1.38.

19.10.2016 Rightslink® by Copyright Clearance Center

Copyright Clearance Center RightsLink®

Home | Account Info | Help | Live Chat



Title: PEG conjugates in clinical development or use as anticancer agents: An overview
Author: Gianfranco Pasut,Francesco M. Veronese
Publication: Advanced Drug Delivery Reviews
Publisher: Elsevier
Date: 12 November 2009
Copyright © 2009 Elsevier B.V. All rights reserved.

Logged in as:
Sadik Kaga
Account #:
3000999792
LOGOUT

Order Completed

Thank you for your order.

This Agreement between Sadik Kaga ("You") and Elsevier ("Elsevier") consists of your license details and the terms and conditions provided by Elsevier and Copyright Clearance Center.

Your confirmation email will contain your order number for future reference.

Get the printable license.

License Number	3972140054016
License date	Oct 18, 2016
Licensed Content Publisher	Elsevier
Licensed Content Publication	Advanced Drug Delivery Reviews
Licensed Content Title	PEG conjugates in clinical development or use as anticancer agents: An overview
Licensed Content Author	Gianfranco Pasut,Francesco M. Veronese
Licensed Content Date	12 November 2009
Licensed Content Volume	61
Licensed Content Issue	13
Licensed Content Pages	12
Type of Use	reuse in a thesis/dissertation
Portion	figures/tables/illustrations
Number of figures/tables/illustrations	1
Format	both print and electronic
Are you the author of this Elsevier article?	No
Will you be translating?	No
Order reference number	
Original figure numbers	Figure 3.
Title of your thesis/dissertation	Functionalizable Hydrogels and Water Soluble Constructs as Chemotherapy Drug Carriers
Expected completion date	Oct 2016
Estimated size (number of pages)	220
Elsevier VAT number	GB 494 6272 12
Requestor Location	Sadik Kaga Boğaziçi Universitesi Kuzey Campus, Chemistry Department Istanbul, 34342 Turkey Attn: Sadik Kaga
Total	0.00 USD

Figure B.28. Permission for Figure 1.39.

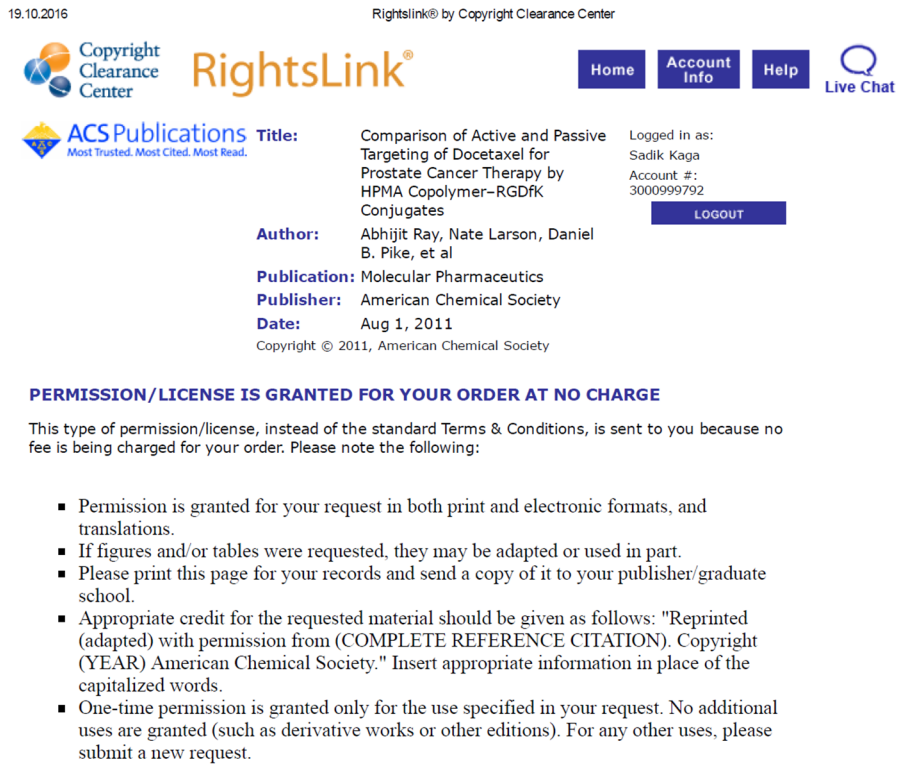


Figure B.29. Permission for Figure 1.40 and Figure 1.41.



Figure B.30. Permission for Figure 1.42 and Figure 1.43.

19.10.2016 Rightslink® by Copyright Clearance Center

Copyright Clearance Center RightsLink® Home Account Info Help Live Chat



Title: Paclitaxel poliglumex (XYOTAX™, CT-2103): A macromolecular taxane
Author: Jack W. Singer
Publication: Journal of Controlled Release
Publisher: Elsevier
Date: 5 December 2005
Copyright © 2005 Elsevier B.V. All rights reserved.

Logged in as:
Sadik Kaga
Account #:
3000999792
LOGOUT

Order Completed

Thank you for your order.

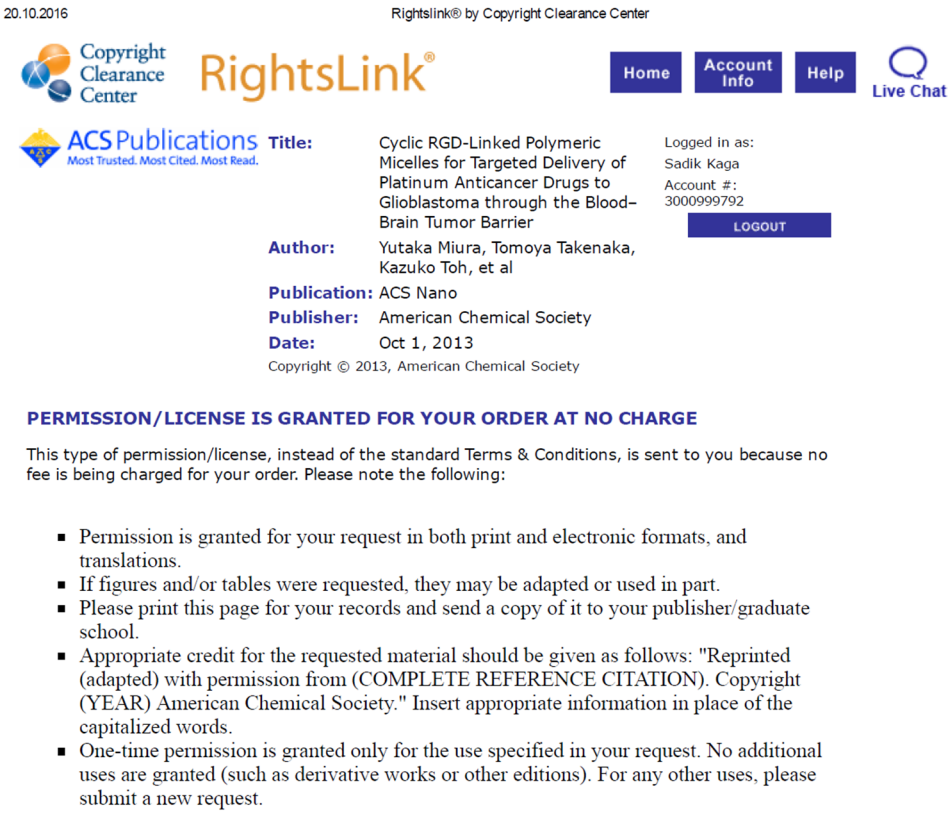
This Agreement between Sadik Kaga ("You") and Elsevier ("Elsevier") consists of your license details and the terms and conditions provided by Elsevier and Copyright Clearance Center.

Your confirmation email will contain your order number for future reference.

Get the printable license.

License Number	3972440797762
License date	Oct 19, 2016
Licensed Content Publisher	Elsevier
Licensed Content Publication	Journal of Controlled Release
Licensed Content Title	Paclitaxel poliglumex (XYOTAX™, CT-2103): A macromolecular taxane
Licensed Content Author	Jack W. Singer
Licensed Content Date	5 December 2005
Licensed Content Volume	109
Licensed Content Issue	1-3
Licensed Content Pages	7
Type of Use	reuse in a thesis/dissertation
Portion	figures/tables/illustrations
Number of figures/tables/illustrations	3
Format	both print and electronic
Are you the author of this Elsevier article?	No
Will you be translating?	No
Order reference number	
Original figure numbers	Figure 1, Figure 2, Figure 3
Title of your thesis/dissertation	Functionalizable Hydrogels and Water Soluble Constructs as Chemotherapy Drug Carriers
Expected completion date	Oct 2016
Estimated size (number of pages)	220
Elsevier VAT number	GB 494 6272 12
Requestor Location	Sadik Kaga Boğaziçi Universitesi Kuzey Campus, Chemistry Department Istanbul, 34342 Turkey Attn: Sadik Kaga
Total	0.00 USD

Figure B.31. Permission for Figure 1.44 and Figure 1.45.



20.10.2016 Rightslink® by Copyright Clearance Center

Copyright Clearance Center RightsLink® Home Account Info Help Live Chat

ACS Publications Most Trusted. Most Cited. Most Read.

Title: Cyclic RGD-Linked Polymeric Micelles for Targeted Delivery of Platinum Anticancer Drugs to Glioblastoma through the Blood–Brain Tumor Barrier

Author: Yutaka Miura, Tomoya Takenaka, Kazuko Toh, et al

Publication: ACS Nano

Publisher: American Chemical Society

Date: Oct 1, 2013

Copyright © 2013, American Chemical Society

Logged in as: Sadik Kaga
Account #: 3000999792
LOGOUT

PERMISSION/LICENSE IS GRANTED FOR YOUR ORDER AT NO CHARGE

This type of permission/license, instead of the standard Terms & Conditions, is sent to you because no fee is being charged for your order. Please note the following:

- Permission is granted for your request in both print and electronic formats, and translations.
- If figures and/or tables were requested, they may be adapted or used in part.
- Please print this page for your records and send a copy of it to your publisher/graduate school.
- Appropriate credit for the requested material should be given as follows: "Reprinted (adapted) with permission from (COMPLETE REFERENCE CITATION). Copyright (YEAR) American Chemical Society." Insert appropriate information in place of the capitalized words.
- One-time permission is granted only for the use specified in your request. No additional uses are granted (such as derivative works or other editions). For any other uses, please submit a new request.

Figure B.32. Permission for Figure 1.47 and Figure 1.48.



20.10.2016 Rightslink® by Copyright Clearance Center

Copyright Clearance Center RightsLink® Home Account Info Help Live Chat

ACS Publications Most Trusted. Most Cited. Most Read.

Title: Combretastatin A-4 Conjugated Antiangiogenic Micellar Drug Delivery Systems Using Dendron–Polymer Conjugates

Author: Burcu Sumer Bolu, Ece Manavoglu Gecici, Rana Sanyal

Publication: Molecular Pharmaceutics

Publisher: American Chemical Society

Date: May 1, 2016

Copyright © 2016, American Chemical Society

Logged in as: Sadik Kaga
Account #: 3000999792
LOGOUT

PERMISSION/LICENSE IS GRANTED FOR YOUR ORDER AT NO CHARGE

This type of permission/license, instead of the standard Terms & Conditions, is sent to you because no fee is being charged for your order. Please note the following:

- Permission is granted for your request in both print and electronic formats, and translations.
- If figures and/or tables were requested, they may be adapted or used in part.
- Please print this page for your records and send a copy of it to your publisher/graduate school.
- Appropriate credit for the requested material should be given as follows: "Reprinted (adapted) with permission from (COMPLETE REFERENCE CITATION). Copyright (YEAR) American Chemical Society." Insert appropriate information in place of the capitalized words.
- One-time permission is granted only for the use specified in your request. No additional uses are granted (such as derivative works or other editions). For any other uses, please submit a new request.

Figure B.33. Permission for Figure 1.49.

21.10.2016 Rightslink® by Copyright Clearance Center

Copyright Clearance Center RightsLink® Home Account Info Help Live Chat



Title: Development of hypoxia-triggered prodrug micelles as doxorubicin carriers for tumor therapy

Author: Hongmei Liu,Ruilong Zhang,Yunwei Niu,Yan Li,Chenmeng Qiao,Jie Weng,Jun Li,Xiaoning Zhang,Zuobing Xiao,Xin Zhang

Publication: RSC Advances

Publisher: Royal Society of Chemistry

Date: Jan 23, 2015

Copyright © 2015, Royal Society of Chemistry

Logged in as:
Sadik Kaga
Account #:
3000999792
LOGOUT

Order Completed

Thank you for your order.

This Agreement between Sadik Kaga ("You") and Royal Society of Chemistry ("Royal Society of Chemistry") consists of your license details and the terms and conditions provided by Royal Society of Chemistry and Copyright Clearance Center.

Your confirmation email will contain your order number for future reference.

Get the printable license.

License Number	3973651403748
License date	Oct 21, 2016
Licensed Content Publisher	Royal Society of Chemistry
Licensed Content Publication	RSC Advances
Licensed Content Title	Development of hypoxia-triggered prodrug micelles as doxorubicin carriers for tumor therapy
Licensed Content Author	Hongmei Liu,Ruilong Zhang,Yunwei Niu,Yan Li,Chenmeng Qiao,Jie Weng,Jun Li,Xiaoning Zhang,Zuobing Xiao,Xin Zhang
Licensed Content Date	Jan 23, 2015
Licensed Content Volume	5
Licensed Content Issue	27
Type of Use	Thesis/Dissertation
Requestor type	academic/educational
Portion	figures/tables/images
Number of figures/tables/images	1
Distribution quantity	10
Format	print and electronic
Will you be translating?	no
Order reference number	
Title of the thesis/dissertation	Functionalizable Hydrogels and Water Soluble Constructs as Chemotherapy Drug Carriers
Expected completion date	Oct 2016
Estimated size	220
Requestor Location	Sadik Kaga Boğaziçi Universitesi Kuzey Campus, Chemistry Department Istanbul, 34342 Turkey Attn: Sadik Kaga
Billing Type	Invoice
Billing address	Sadik Kaga Boğaziçi Universitesi Kuzey Campus, Chemistry Department

Figure B.34. Permission for Figure 1.50.

Copyright Clearance Center RightsLink®

Home | Account Info | Help | Live Chat



Title: Polymerization-Induced Self-Assembly (PISA) – control over the morphology of nanoparticles for drug delivery applications

Author: Bunyamin Karagoz,Lars Esser,Hien T. Duong,Johan S. Basuki,Cyrille Boyer,Thomas P. Davis

Publication: Polymer Chemistry

Publisher: Royal Society of Chemistry

Date: Oct 22, 2013

Copyright © 2013, Royal Society of Chemistry

Logged in as:
Sadik Kaga
Account #:
3000999792
LOGOUT

Order Completed

Thank you for your order.

This Agreement between Sadik Kaga ("You") and Royal Society of Chemistry ("Royal Society of Chemistry") consists of your license details and the terms and conditions provided by Royal Society of Chemistry and Copyright Clearance Center.

Your confirmation email will contain your order number for future reference.

Get the printable license.

License Number	3972811345416
License date	Oct 19, 2016
Licensed Content Publisher	Royal Society of Chemistry
Licensed Content Publication	Polymer Chemistry
Licensed Content Title	Polymerization-Induced Self-Assembly (PISA) – control over the morphology of nanoparticles for drug delivery applications
Licensed Content Author	Bunyamin Karagoz,Lars Esser,Hien T. Duong,Johan S. Basuki,Cyrille Boyer,Thomas P. Davis
Licensed Content Date	Oct 22, 2013
Licensed Content Volume	5
Licensed Content Issue	2
Type of Use	Thesis/Dissertation
Requestor type	academic/educational
Portion	figures/tables/images
Number of figures/tables/images	2
Distribution quantity	10
Format	print and electronic
Will you be translating?	no
Order reference number	
Title of the thesis/dissertation	Functionalizable Hydrogels and Water Soluble Constructs as Chemotherapy Drug Carriers
Expected completion date	Oct 2016
Estimated size	220
Requestor Location	Sadik Kaga Boğaziçi Universitesi Kuzey Campus, Chemistry Department Istanbul, 34342 Turkey Attn: Sadik Kaga
Billing Type	Invoice
Billing address	Sadik Kaga Boğaziçi Universitesi Kuzey Campus, Chemistry Department

Figure B.35. Permission for Figure 1.51 and Figure 1.52.